

University of Groningen

Homologous recombination-deficient cancers: approaches to improve treatment and patient selection

Talens, Francien

DOI:
[10.33612/diss.146371913](https://doi.org/10.33612/diss.146371913)

IMPORTANT NOTE: You are advised to consult the publisher's version (publisher's PDF) if you wish to cite from it. Please check the document version below.

Document Version
Publisher's PDF, also known as Version of record

Publication date:
2020

[Link to publication in University of Groningen/UMCG research database](#)

Citation for published version (APA):

Talens, F. (2020). *Homologous recombination-deficient cancers: approaches to improve treatment and patient selection*. University of Groningen. <https://doi.org/10.33612/diss.146371913>

Copyright

Other than for strictly personal use, it is not permitted to download or to forward/distribute the text or part of it without the consent of the author(s) and/or copyright holder(s), unless the work is under an open content license (like Creative Commons).

The publication may also be distributed here under the terms of Article 25fa of the Dutch Copyright Act, indicated by the "Taverne" license. More information can be found on the University of Groningen website: <https://www.rug.nl/library/open-access/self-archiving-pure/taverne-amendment>.

Take-down policy

If you believe that this document breaches copyright please contact us providing details, and we will remove access to the work immediately and investigate your claim.

Downloaded from the University of Groningen/UMCG research database (Pure): <http://www.rug.nl/research/portal>. For technical reasons the number of authors shown on this cover page is limited to 10 maximum.

Homologous recombination-deficient cancers: approaches to improve treatment and patient selection

Francien Talens

The work described in this thesis was conducted at the Department of Medical Oncology of the University Medical Center Groningen, the Netherlands.

Cover: Hein Talens, gemaakt in 1990 te Groningen
Lay-out design: Francien Talens, Nathalie van den Tempel
Printing: Gildeprint, Enschede

Printing of this thesis was supported by:
- UMCG Graduate School of Medical Sciences
- Stichting Werkgroep Interne Oncologie
- University of Groningen

Copyright © 2020, F.G. Talens

All rights reserved. No part of this thesis may be reproduced, stored or transmitted in any form without permission by the author.



rijksuniversiteit
 groningen

Homologous recombination-deficient cancers: approaches to improve treatment and patient selection

Proefschrift

ter verkrijging van de graad van doctor
aan de Rijksuniversiteit Groningen
op gezag van de
rector magnificus prof. dr. C. Wijmenga
en volgens besluit van het College voor Promoties.

De openbare verdediging zal plaatsvinden op
woensdag 9 december 2020 om 11.00 uur

door

Francien Gesina Talens

geboren op 2 december 1990
te Groningen

Promotores

Prof. dr. M.A.T.M. van Vugt

Prof. dr. J.A. Gietema

Beoordelingscommissie

Prof. dr. J.W.M. Martens

Prof. dr. H.W. Nijman

Prof. dr. C.F. Calkhoven

Paranimfen

Danique Giesen

Nathalie van den Tempel

Contents

Chapter 1	Introduction and outline of the thesis	9
Chapter 2	Inflammatory signaling in genomically unstable cancers <i>Cell Cycle, 2019</i>	17
Chapter 3	Progression through mitosis promotes PARP inhibitor-induced cytotoxicity in homologous recombination-deficient cancer cells <i>Nature Communications, 2017</i>	39
Chapter 4	BRCA2 deficiency instigates cGAS-mediated inflammatory signaling and confers sensitivity to tumor necrosis factor-alpha-mediated cytotoxicity <i>Nature Communications, 2019</i>	71
Chapter 5	MYC promotes immune-suppression in TNBC via inhibition of IFN signaling <i>In preparation</i>	105
Chapter 6	Therapeutic targeting and patient selection for cancers with homologous recombination defects <i>Expert Opinion on Drug Discovery, 2017</i>	141
Chapter 7	Functional RAD51 based assay predicts in vivo PARP inhibitor response in ovarian cancer models beyond BRCA <i>In preparation</i>	167
Chapter 8	Summary, discussion and future perspectives	193
Appendices	Nederlandse samenvatting Over de auteur Dankwoord	211

Introduction and outline of the thesis

Introduction

DNA damage maintenance

In order for cells to proliferate, the genomic material of a cell needs to be copied without errors and subsequently distributed over two daughter cells. However, the DNA in our cells continuously encounters different types of lesions, either from exogenous sources (e.g. UV rays from sunlight) or endogenous sources (e.g. radical species as byproducts of metabolism, and errors during DNA replication). To maintain genomic integrity, cells are therefore equipped with a broad spectrum of pathways that can detect and repair DNA lesions, together called the DNA damage response (DDR)¹.

A very toxic type of DNA lesion that needs to be repaired to maintain genomic integrity and cellular viability, is the DNA double-stranded break (DSB). Cells have two main pathways to repair DSBs, namely non-homologous end-joining (NHEJ) and homologous recombination (HR) (**Figure 1**). NHEJ is able to repair DSBs throughout the cell cycle and directly ligates DNA-ends together². Although NHEJ is very efficient, it is also error-prone and can induce mutations. In contrast, HR is an error-free repair mechanism that is only able to repair DSBs in S- or G2-phase of the cell cycle, as it uses the sister chromatid as a template for DSB repair³. HR is slower and more complex when compared to NHEJ because HR requires more extensive processing of the DNA-ends⁴. Ultimately, HR involves the loading of the recombinase enzyme RAD51 onto single-stranded DNA (ssDNA) stretches that are created around the break site. The formation of RAD51 filaments initiates invasion of the broken DNA ends into the sister chromatid to search for a homologous sequence to repair the break without introducing mutations. The loading of RAD51 onto the ssDNA is frequently used as a readout for functional HR and is explored as a diagnostic tool to identify DNA repair-defective cancers⁵. If DNA lesions are not properly repaired, for instance, due to defects in DNA repair, this may lead to genomic instability, defined as structural alterations in the genome involving the accumulation of mutations or larger genomic rearrangements, with consequent chromosomal defects.

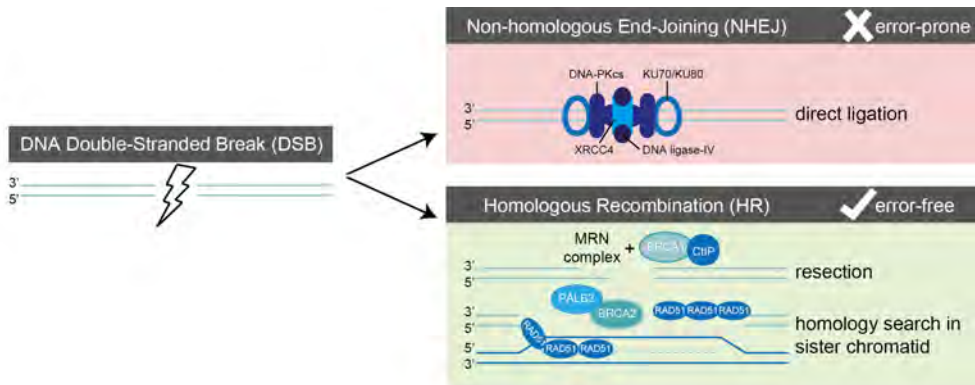


Figure 1. DNA double-strand break repair pathways. For repair of DSBs by NHEJ, breaks are recognized and bound by Ku70-Ku80 heterodimers which activate DNA-PKcs. XRCC4, DNA ligase-IV, and polymerases (μ/λ) are recruited to complete DNA-end joining. During HR repair, DSBs are recognized by the MRN complex, which initiates DNA-end resection in conjunction with CtIP and BRCA1. EXO1 and DNA2 generate extensive ssDNA stretches, which are coated with RPA. In a PALB2-dependent fashion, BRCA2 is recruited, which loads RAD51 onto the ssDNA to invade the sister chromatid and to find sequence homology.

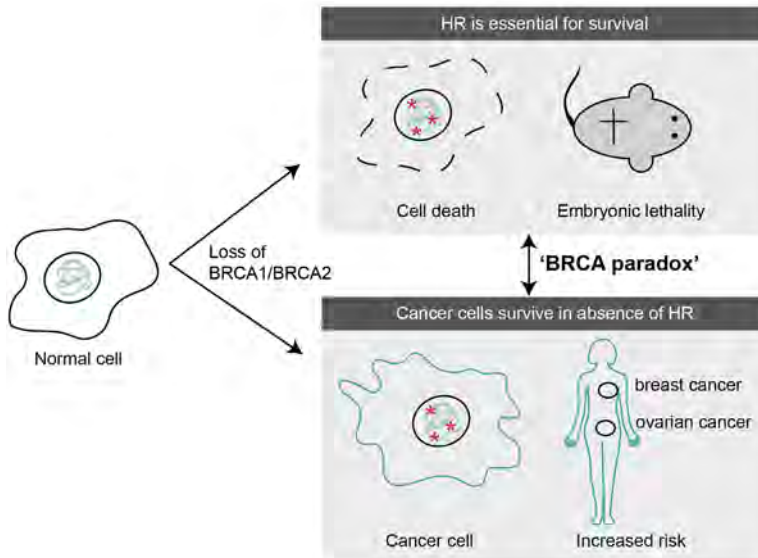


Figure 2. BRCA paradox.

Loss of *BRCA1* or *BRCA2* in normal cells results in cell death and embryonic lethality in mice. Surprisingly, cancer cells are viable in the absence of *BRCA1* or *BRCA2*. Individuals harboring a *BRCA1/2* mutation have an increased lifetime risk to develop breast- or ovarian cancer.

Loss of DNA damage repair in cancer

Genetic defects in DNA repair pathways leading to the accumulation of DNA lesions and have been associated with a range of diseases, including neurological disorders, accelerated aging, and play an important role in the development of cancer¹. A significant subset of cancers has been described to have defects in DNA repair, including HR⁶. In line with this notion, DNA repair deficiencies and the resulting genomic instability has been described as a hallmark of cancer^{7,8}.

A link between defective DNA repair and cancer was first established when specific gene mutations were identified to underlie cancer-predisposing syndromes and hereditary breast cancer, and led to their gene names, for instance, Ataxia Telangiectasia Mutated (*ATM*) and Breast cancer 1, early onset (*BRCA1*)^{9,10}. Individuals who harbor a germline mutation in *BRCA1* or the subsequently identified *BRCA2* gene have an increased lifetime risk of up to 70% to develop breast cancer¹¹. Furthermore, germline *BRCA1/2* mutations are also associated with an increased risk to develop ovarian cancer and a range of other cancer types¹². In the decades that followed the initial discovery of the *BRCA1/2* genes, numerous germline mutations in other HR genes have been associated with cancer predisposition, including *PALB2* and *RAD51C*^{13,14}.

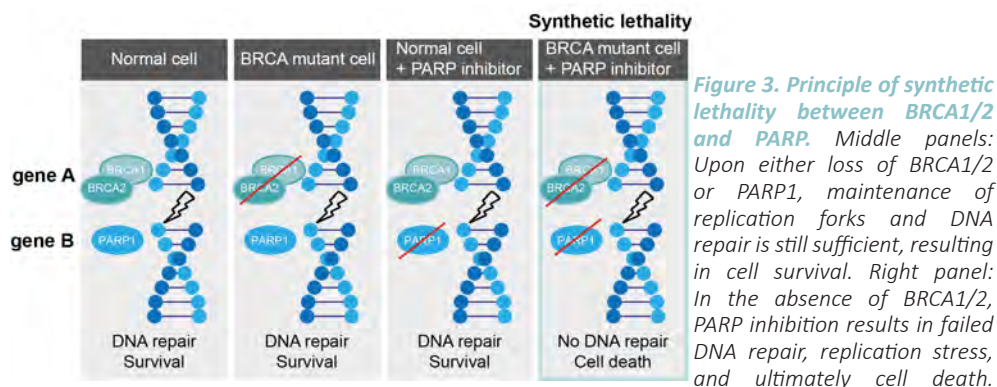
To study *BRCA1/2*-mediated cancers, *Brca1* and *Brca2* genes emerged to be essential for development while developing mouse models, pointing towards HR as an essential process in proliferating normal cells^{15,16}. Additionally, *BRCA1* and *BRCA2* serve important functions in the protection of stalled replication forks to maintain genomic stability¹⁷. These observations formed a clear contrast with the notion that *BRCA1* or *BRCA2* mutant cancer cells are viable in the absence of functional HR and replication fork protection. How cancer cells survive in the absence of *BRCA1/2* is still incompletely understood and is called the 'BRCA paradox'¹⁸ (**Figure 2**). Increasing evidence suggests that secondary (epi)genetic events, such as mutations or overexpression of other genes, might allow these cancer cells to survive in the context of HR deficiency. Also, the role of the immune system is increasingly recognized to play a role in the survival and growth of HR-deficient cancer cells.

Treatment of HR deficient cancer

If cancer is still localized, it is preferably surgically removed. If surgery is not possible, most cancer types are being treated with radiotherapy, chemotherapy, or with a

combination of both. Radiotherapy and most chemotherapeutic agents induce high levels of DNA damage, which kills rapidly dividing cancer cells but is also harmful to normal cells. Furthermore, like normal cells, many cancer cells have residual repair activity and are not properly sensitive to these treatment options or become resistant.

To increase the effectiveness of cancer treatment, strategies are needed that specifically target characteristics that are unique to cancer cells. This treatment strategy is called 'targeted therapy'. A specific type of targeted therapy is based on the principle of 'synthetic lethality' (**Figure 3**). A combination of genes is termed synthetic lethal, when defects in these genes are combined (e.g. simultaneous loss of function of gene A and gene B) and result in cell death, whereas loss of only one of these genes is not enough. The principle of synthetic lethality can be applied to cancer therapy when in cancer cells with a loss-of-function mutation in gene A, gene B is therapeutically targeted¹⁹. Notably, a synthetic lethal interaction between *BRCA1/2* and Poly-(ADP-Ribose)-polymerase 1 (*PARP1*) was discovered and led to the finding that cancers that are deficient for HR can be targeted with PARP inhibitors^{20,21}. Healthy cells still have functional HR and will therefore be less sensitive to PARP inhibitors. Additionally, PARP is trapped onto the DNA during PARP inhibition resulting in replication fork stalling²². In 2014, the first PARP inhibitor olaparib (Lynparza) was approved by the FDA to treat *BRCA1/2*-associated advanced ovarian cancer patients²³. In 2016, rucaparib and niraparib were also approved for the treatment of patients with recurrent *BRCA1/2*-mutated ovarian cancer²⁴. Most recently, olaparib has also been approved for *BRCA1/2* mutant HER2-negative metastatic breast cancers²⁵.



Simultaneous loss of function of gene A (*BRCA*) and gene B (*PARP1*) ultimately results in cell death, defined as synthetic lethality.

Unfortunately, many cancers eventually develop resistance to PARP inhibitor treatment. Resistance might occur when cells restore HR function by deregulation of HR suppressor genes such as *53BP1*, *REV7*, *RIF1*, *JMJD1C*, and *SHLD* components in a *BRCA1*-mutant background^{26–30}. Furthermore, loss of *BRCA1* promoter methylation or secondary mutations can restore *BRCA1/2* function^{31,32}. Finally, the protection of stalled replication forks can be restored in a *BRCA2*-mutant background³³. To prevent resistance, it is important to increase our knowledge of the exact mechanisms of action of PARP inhibitors and to improve their efficacy by developing combination strategies with other drugs. Combination trials have thus far focused on combining PARP inhibitors with chemotherapy, anti-angiogenic agents, and most recently immunotherapy. Unfortunately, dose-limiting toxicity is frequently observed in trials that combine chemotherapy with PARP inhibitors³⁴. To develop tolerable and effective combination therapies, it is imperative to understand the cellular and molecular

consequences of BRCA defects in cancer cells. In this context, the combination of PARP inhibitors with immunotherapy is increasingly studied, as the role of the immune system is recently suggested to play an important role in the survival of HR-deficient cancer cells.

Whereas PARP inhibitors are currently approved to treat *BRCA1/2*-mutated ovarian and breast cancer, HR deficiency can also be caused by mutations in other DNA repair genes, beyond *BRCA1* or *BRCA2*³⁵. These patients are currently not eligible for PARP inhibitor treatment but may benefit from this treatment as has already been shown in clinical trials²⁴. Therefore, the selection of patients that could benefit from PARP inhibitors beyond *BRCA1/2* mutations is needed and tools to do this are currently suboptimal. Such patient selection tools will likely also be relevant for identifying tumors that might have become PARP inhibitor-resistant, to avoid unnecessary treatment.

The overall **aim of this thesis** is to dissect the molecular mechanisms and cellular consequences of HR-deficient cancer cells to improve the effectiveness of treatment modalities and patient selection for PARP inhibitors.

Outline of the thesis

Alterations in the ability of cells to repair their DNA can lead to genomic instability, which occurs frequently in cancer. As a result of genomic instability, DNA can end up in the cytoplasm of cells where it triggers a cell-intrinsic immune response via cGAS/STING signaling. In **chapter 2** of this thesis, several mechanisms are described by which genomic instability leads to cGAS/STING-mediated inflammatory signaling, and how this influences tumor development and interferes with the tumor microenvironment. Tumor cells that are characterized by genomic instability, for example, due to loss of HR, have evolved to escape these innate immune responses to overcome clearance by the immune system. Possible mechanisms by which tumors can adapt to inflammatory signaling are described. Finally, we outline how cGAS/STING-mediated inflammatory signaling can be therapeutically targeted to improve therapy responses.

PARP inhibition is an established treatment strategy for HR-deficient cancers. However, not all tumors respond to PARP inhibitors and many tumors ultimately develop resistance which results in tumor regrowth after an initial response. More insights into how PARP inhibitors kill HR-defective cancer cells are needed to improve therapy responses and to design new combination strategies. In **chapter 3**, we studied the mechanisms of PARP inhibitor cytotoxicity in multiple HR-deficient *in vitro* and *in vivo* cancer models. Using these models, we studied how cells deal with PARP inhibitor-induced replication stress throughout the cell cycle and if HR-defective cells maintain replication fork stability upon PARP inhibitor treatment. Furthermore, we assessed whether progression through mitosis influences PARP inhibitor-induced cytotoxicity.

Loss of HR -for example due to a *BRCA1/2* mutation- is tolerated in cancer cells, while this is lethal to normal cells. In **chapter 4**, we performed a loss-of-function haploid genetic screen to identify gene mutations that can rescue cellular viability upon inactivation of *BRCA2* in *TP53*-mutant tumor cells. We validated whether the loss of the identified genes can indeed rescue the cellular viability upon *BRCA2* depletion in various murine and human cancer *in vitro* models. Furthermore, we studied the molecular mechanisms by which the identified gene mutations influence cell viability in a *BRCA2*-defective context.

Overexpression of oncogenes is described to promote cell proliferation and to activate pathways that are beneficial for the survival and metastasis of cancer cells. Specifically, the *MYC* oncogene is often amplified in genomic unstable tumors, such as triple-negative breast cancer (TNBC), and often co-occurs with a *BRCA1/2* mutation. Based on our results in chapter 4 and other recent findings, *BRCA1/2*-mutant tumor cells were

hypothesized to circumvent cell-intrinsic inflammatory responses to evade clearance by the immune system. In **chapter 5**, we investigated the role of *MYC* in *BRCA1/2*-defective cells using *in vitro* and *in vivo* models for TNBC. Specifically, we assessed how amplification of *MYC* alters cGAS/STING-mediated inflammatory signaling in *BRCA1/2*-depleted cells, and how this subsequently affects the tumor microenvironment and activity of immune cells.

In **chapter 6**, the recent literature is reviewed on how the HR pathway is mechanistically wired, and current treatment options for HR-deficient cancers are represented with a focus on PARP inhibitors. As resistance to PARP inhibitors often occurs, the currently known PARP inhibitor resistance mechanisms are described. To optimally implement PARP inhibitor treatment in the clinic, patients with HR-deficient tumors must be adequately selected. Currently, only patients with germline or somatic *BRCA1/2* mutations are eligible for PARP inhibitor treatment and only a proportion of patients respond. Therefore, we discussed possible new combination therapies with PARP inhibitors and patient selection methods.

It is thought that a large proportion of patients with high-grade serous ovarian cancer (HGSOC) have HR-deficient cancer but do not harbor a *BRCA1/2* mutation. These patients are therefore not eligible for PARP inhibitor treatment, whereas they may benefit from this treatment. To further improve patient selection, in **chapter 7** we determined genomic features, including *BRCA1/2* mutation status and copy number variations (CNVs) profile, in a cohort of 30 patient-derived xenograft (PDX) models of ovarian cancer. In a subset of PDX models, we assessed *ex vivo* HR functionality and replication fork stability and correlated all genomic and functional outcomes with *in vivo* olaparib responses.

In **chapter 8**, the obtained results and conclusions of all previous chapters are summarized and discussed.

References

1. Jackson, S. P. & Bartek, J. The DNA-damage response in human biology and disease. *Nature* 461, 1071–1078 (2009).
2. Lieber, M. R. The mechanism of human nonhomologous DNA End joining. *Journal of Biological Chemistry* 283, 1–5 (2008).
3. Moynahan, M. E. & Jasin, M. Mitotic homologous recombination maintains genomic stability. *Nat Rev Mol Cell Biol.* 11, 196–207 (2010).
4. Sung, P. & Klein, H. Mechanism of homologous recombination: Mediators and helicases take on regulatory functions. *Nature Reviews Molecular Cell Biology* 7, 739–750 (2006).
5. Naipal, K. A. T. et al. Functional Ex vivo assay to select homologous recombination-deficient breast tumors for PARP inhibitor treatment. *Clin. Cancer Res.* 20, 4816–4826 (2014).
6. Helleday, T. Homologous recombination in cancer development, treatment and development of drug resistance. *Carcinogenesis* 31, 955–60 (2010).
7. Hanahan, D. & Weinberg, R. A. Hallmarks of cancer: The next generation. *Cell* 144, 646–674 (2011).
8. Negrini, S., Gorgoulis, V. G. & Halazonetis, T. D. Genomic instability — an evolving hallmark of cancer. *Nat. Rev. Mol. Cell Biol.* 11, 220–228 (2010).
9. Wooster, R. et al. Identification of the breast cancer susceptibility gene BRCA2. *Nature* 378, 789–792 (1995).
10. Miki, Y. et al. A strong candidate for the breast and ovarian cancer susceptibility gene BRCA1. *Science* 266, 66–71 (1994).
11. Kuchenbaecker, K. B. et al. Risks of breast, ovarian, and contralateral breast cancer for BRCA1 and BRCA2 mutation carriers. *JAMA- J. Am. Med. Assoc.* 317, 2402–2416 (2017).
12. Mavaddat, N. et al. Cancer risks for BRCA1 and BRCA2 Mutation carriers: results From Prospective Analysis of EMBRACE. *J Natl Cancer Inst.* 105, 812–22 (2013).
13. Heeke, A. L. et al. Prevalence of Homologous Recombination-Related Gene Mutations Across Multiple Cancer Types. *JCO Precis. Oncol.* 2018, 1–13 (2018).
14. Buys, S. S. et al. A study of over 35,000 women with breast cancer tested with a 25-gene panel of

- hereditary cancer genes. *Cancer* 123, 1721–1730 (2017).
15. Suzuki, A. et al. Brca2 is required for embryonic cellular proliferation in the mouse. *Genes Dev.* 11, 1242–1252 (1997).
 16. Hakem, R. et al. The tumor suppressor gene Brca1 is required for embryonic cellular proliferation in the mouse. *Cell* 85, 1009–23 (1996).
 17. Schlacher, K., Wu, H. & Jasin, M. A distinct replication fork protection pathway connects Fanconi anemia tumor suppressors to RAD51-BRCA1/2. *Cancer Cell* 22, 106–16 (2012).
 18. Elledge, S. J. & Amon, A. The BRCA1 suppressor hypothesis: An explanation for the tissue-specific tumor development in BRCA1 patients. *Cancer Cell* 1, 129–132 (2002).
 19. Kaelin, W. G. The concept of synthetic lethality in the context of anticancer therapy. *Nat. Rev. Cancer* 5, 689–98 (2005).
 20. Bryant, H. E. et al. Specific killing of BRCA2-deficient tumours with inhibitors of poly(ADP-ribose) polymerase. *Nature* 434, 913–917 (2005).
 21. Farmer, H. et al. Targeting the DNA repair defect in BRCA mutant cells as a therapeutic strategy. *Nature* 434, 917–921 (2005).
 22. Murai, J. et al. Trapping of PARP1 and PARP2 by clinical PARP inhibitors. *Cancer Res.* 72, 5588–5599 (2012).
 23. Kim, G. et al. FDA approval summary: Olaparib monotherapy in patients with deleterious germline BRCA-mutated advanced ovarian cancer treated with three or more lines of chemotherapy. *Clin. Cancer Res.* 21, 4257–4261 (2015).
 24. Taylor, K. N. & Eskander, R. N. PARP Inhibitors in Epithelial Ovarian Cancer. *Recent Pat. Anticancer. Drug Discov.* 13, 145–158 (2018).
 25. Robson, M. et al. Olaparib for metastatic breast cancer in patients with a germline BRCA mutation. *N. Engl. J. Med.* 377, 523–533 (2017).
 26. Bunting, S. F. et al. 53BP1 inhibits homologous recombination in brca1-deficient cells by blocking resection of DNA breaks. *Cell* 141, 243–254 (2010).
 27. Xu, G. et al. REV7 counteracts DNA double-strand break resection and affects PARP inhibition. *Nature* 521, 541–544 (2015).
 28. Chapman, J. R. et al. RIF1 Is Essential for 53BP1-Dependent Nonhomologous End Joining and Suppression of DNA Double-Strand Break Resection. *Mol. Cell* 49, 858–871 (2013).
 29. Noordermeer, S. M. et al. The shieldin complex mediates 53BP1-dependent DNA repair. *Nature* 560, 117–121 (2018).
 30. Watanabe, S. et al. JMJD1C demethylates MDC1 to regulate the RNF8 and BRCA1-mediated chromatin response to DNA breaks. *Nat. Struct. Mol. Biol.* 20, 1425–1433 (2013).
 31. Norquist, B. et al. Secondary somatic mutations restoring BRCA1/2 predict chemotherapy resistance in hereditary ovarian carcinomas. *J. Clin. Oncol.* 29, 3008–15 (2011).
 32. Patch, A. M. et al. Whole-genome characterization of chemoresistant ovarian cancer. *Nature* 521, 489–494 (2015).
 33. Sunada, S., Nakanishi, A. & Miki, Y. Crosstalk of DNA double-strand break repair pathways in poly(ADP-ribose) polymerase inhibitor treatment of breast cancer susceptibility gene 1/2-mutated cancer. *Cancer Sci.* 109, 893–899 (2018).
 34. Lord, C. J. & Ashworth, A. PARP inhibitors: Synthetic lethality in the clinic. *Science* (80-.). 355, 1152–1158 (2017).
 35. Konstantinopoulos, P. A., Ceccaldi, R., Shapiro, G. I. & D’Andrea, A. D. Homologous Recombination Deficiency: Exploiting the Fundamental Vulnerability of Ovarian Cancer. *Cancer Discov.* 5, 1137–54 (2015).

Inflammatory signaling in genomically unstable cancers

Francien Talens¹ & Marcel A.T.M. Van Vugt¹

¹Department of Medical Oncology, University Medical Center
Groningen, University of Groningen , Groningen , The Netherlands.

Cell cycle (2019) 18(16):1830-1848

Abstract

Recent studies have shown that genomic instability in tumor cells leads to activation of inflammatory signaling through the cGAS/STING pathway. In this review, we describe multiple ways by which genomic instability leads to cGAS/STING-mediated inflammatory signaling, as well as the consequences for tumor development and the tumor microenvironment. Also, we elaborate on how tumor cells have apparently evolved to escape the immune surveillance mechanisms that are triggered by cGAS/STING signaling. Finally, we describe how cGAS/STING-mediated inflammatory signaling can be therapeutically targeted to improve therapy responses.

Genomic instability in cancer

Cells are equipped with a tightly regulated “DNA damage response” (DDR) to protect their genome from lesions that arise from endogenous and exogenous sources. In this way, different DNA lesions are continuously being detected and repaired to maintain genomic stability. Conversely, alterations in the ability of cells to repair their DNA can lead to genomic instability, which occurs frequently in cancer. Depending on the underlying cause, genomic instability is characterized by the accumulation of mutations, complex genomic rearrangements, and the progressive loss or gain of genomic regions or whole chromosomes.

Genomic instability has been recognized as a hallmark of cancer¹, and various underlying mechanisms have been identified. For instance, germline mutations in DNA repair genes can drive the accumulation of genomic aberrancies and ensuing tumorigenesis. Prototypical examples are mutations in the breast and ovarian cancer susceptibility genes *BRCA1* and *BRCA2*, which result in defective DNA repair of DNA double-strand breaks (DSBs) through homologous recombination (HR)². Alternatively, germline mutations in mismatch repair (MMR) genes, collectively known as Lynch syndrome, lead to cancer predisposition, which mainly involves endometrial and non-polyposis colorectal cancer³⁻⁵. These cancers are characterized by microsatellite instability (MSI), which involves an increased number of somatic mutations at repetitive genomic loci⁶. Of note, HR or MRR are not the only DNA repair pathways in which defects are associated with an increased risk to develop cancer. Notably, besides germ-line mutations, also somatic alterations were shown to underlie cancer-associated DNA repair deficiencies⁷. Interestingly, telomere dysfunction has also been described as an underlying mechanism of genomic instability in cancer cells. Cells that accumulate unprotected chromosome ends may bypass senescence, which can lead to the formation of clones with high levels of genomic instability⁸. Cells that survive a telomere crisis gain various genomic alterations, involving chromothripsis and kataegis^{9,10}.

Another important cause of genomic instability in cancer is oncogene-induced replication stress^{11,12}. Overexpression of specific oncogenes, including *CCND1* (encoding Cyclin D1), *CCNE1* (encoding Cyclin E1), or *MYC* (encoding c-MYC), leads to deregulation of the cell cycle and was shown to induce replication stress via different mechanisms¹¹⁻¹⁴. A common theme in, this context involves elevated CDK activity, notably CDK2, which consequently leads to increased firing of replication origins¹⁵. As a result, oncogene overexpression leads to depletion of the nucleotide pool activity, which limits replication fork progression and triggers genomic instability^{16,17}. Indeed, Cyclin E1 or Cdc25A overexpression was shown to induce reversal and slowing of replication forks¹⁸. In parallel, the elevated levels of origin firing combined with high transcriptional activity lead to frequent collisions between the replication machinery and the transcriptional apparatus¹⁹.

Single-stranded DNA (ssDNA) stretches that are exposed upon replication fork stalling and the DNA breaks that form upon the collapse of stalled replication forks will trigger activation of the ATR and ATM kinases within the DNA damage response (DDR). Under

physiological conditions, DDR activation leads to p53-mediated apoptosis or senescence to clear pre-cancerous cells^{20,21}. The DNA lesion that arises as a consequence of oncogene-induced replication stress or defective DNA repair results in genetic pressure on tumor suppressor genes involved in DNA damage-induced cell cycle checkpoint activation^{22,23}. Indeed, loss of p53 is one of the mechanisms by which transformed cells with high levels of replication stress and DNA damage escape cell cycle checkpoint activation and apoptosis to continue proliferation²⁴. In line with this notion, *TP53* mutations are frequently observed in cancers (~42% of all human cancers), especially in those that are characterized by high levels of genomic instability, such as high-grade serous ovarian cancer (96% with *TP53* alteration) or triple-negative breast cancer (80% with *TP53* alteration)^{25–28}. Although p53-dependent cell cycle checkpoint control is frequently inactivated in genomically unstable cancers, other levels of cell cycle control are typically retained. In fact, genomically unstable cancers increasingly depend on their survival on the remaining cell cycle checkpoint components, including Chk1 and Wee1^{29,30}.

Although residual cell cycle checkpoint control in genomically unstable cancer cells can delay entry into mitosis in situations of DNA damage, we increasingly realize that these checkpoints do not fully prevent damaged cells from entering mitosis. Notably, cancer-associated genomic instability frequently involves DNA lesions that originate during DNA replication and remain unresolved at mitotic entry^{31–34}. As a consequence, such DNA lesions interfere with normal chromosome segregation and lead to breakage-fusion-bridge cycles, ultimately resulting in structural genomic aberrations³⁵.

Aberrant chromosome segregation is not only observed in situations of defective genome maintenance. Defects in spindle assembly checkpoint (SAC) functioning or improper attachment of microtubules to the kinetochore leads to missegregation of entire chromosomes during mitosis. The resulting chromosomal instability (CIN) involves lagging chromosomes and numerical aneuploidies. Importantly, numerical chromosomal defects were shown to induce structural chromosomal abnormalities and vice versa, in good agreement with these phenotypes frequently co-occurring in cancers (**Figure 1**, left panel)^{36–38}.

Micronuclei formation as a source of cytoplasmic DNA

The presence of unresolved mitotic DNA damage or chromosome missegregation often results in the formation of micronuclei upon mitotic exit (**Figure 1**). Micronuclei contain complete chromosomes or chromosome fragments, which are surrounded by a nuclear envelope. However, multiple “non-core” envelope proteins, including nuclear pore complex (NPC) components, cannot be assembled on lagging chromosomes and therefore prevent the formation of a proper nuclear envelope³⁹. As a consequence, multiple “nuclear” processes do not function properly in micronuclei⁴⁰. Among these disturbed processes, micronuclei show defects in nucleo-cytoplasmic transport, which impairs the recruitment of the MCM components of the replicative DNA helicase as well as DNA repair proteins³⁷. Therefore, DNA damage accumulates in micronuclei during S- and G2-phase of the cell cycle and leaves genomic regions under-replicated. Furthermore, chromatids in micronuclei that contain centromeric regions are defective in building a functional kinetochore and do not properly recruit spindle assembly checkpoint proteins⁴¹. Also, the re-integration of damaged chromatin from micronuclei into the main nucleus, which occurs with almost 40% of the micronuclei, triggers replication problems, genomic instability, and extensive genomic rearrangements involving chromotripsis^{37,42,43}. Finally, the surrounding membrane of micronuclei is more fragile when compared to the membrane surrounding the main nucleus. As a consequence, the nuclear membrane of micronuclei is prone to rupture, which results in the release of chromatin into the cytosol⁴⁴.

Inactivation of multiple DNA repair factors has been shown to result in the formation of micronuclei⁴⁵. For instance, inactivation of the HR factors BRCA1, BRCA2, or Rad51 leads

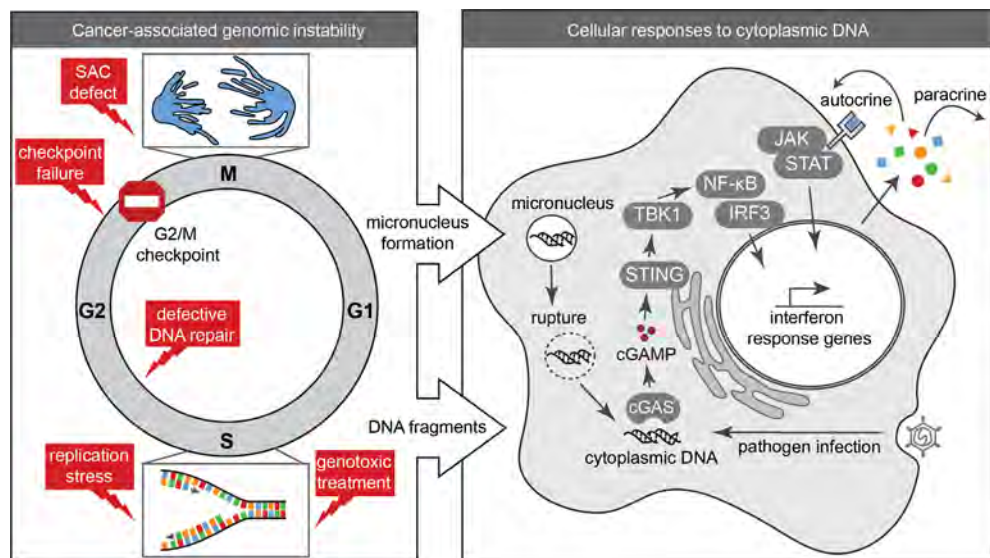


Figure 1. Genomic instability and cGAS/STING signaling in response to cytoplasmic DNA. Left panel: Cells that suffer from oncogene-induced replication stress, DNA repair defects, checkpoint failure, SAC defects, or genotoxic stress progress into mitosis with unrepaired DNA lesions. These unrepaired lesions drive genomic instability and the release of DNA fragments into the cytoplasm and/or micronucleus formation. **Right panel:** Rupture of micronuclei leads to the release of dsDNA into the cytoplasm. Both ssDNA and dsDNA are recognized by cGAS, which in turn activates STING via cGAMP. Upon STING activation, TBK1 is phosphorylated which leads to phosphorylation of IRF3 and NF- κ B. These transcription factors migrate to the nucleus to instigate a Type-I IFN response. Secreted cytokines trigger autocrine and paracrine effects.

to chromosome segregation failure with a range of consequences, including micronucleus formation^{46–48}. These effects are exaggerated when HR-deficient cells are treated with genotoxic agents, including PARP inhibitors³⁴. Similarly, defects in the removal of ribonucleotides from DNA lead to mitotic failures. During normal DNA replication, ribonucleotides may be incorporated into DNA, making DNA more susceptible to mutagenesis and strand breaks⁴⁹. Ribonucleotide excision repair (RER) functions to remove aberrantly incorporated ribonucleotides and thereby maintains genome stability. Conversely, inactivation of the RER nuclease RNaseH2, which also functions in removing RNA:DNA hybrids (R-loops) that arise during transcription, interferes with the maintenance of genome stability^{50,51}. Importantly, inactivating mutations in *RNASEH2A* lead to cytoplasmic DNA, as a result of micronuclei formation⁵⁰.

Of note, because the presence of micronuclei reflects the accumulation of persistent DNA lesions or chromosome missegregation, micronucleus formation is established as a reliable method for toxicological assessment of the clastogenic or aneugenic effects of compounds⁵². In line with DNA repair defects leading to micronuclei that are prone to rupture, increased amounts of cytoplasmic DNA have been observed in various contexts of DNA repair deficiency, including ATM, ERCC1, and BRCA1 deficiency^{53,54}.

Genomic instability can also lead to the release of DNA into the cytoplasm through mitosis-independent mechanisms (**Figure 1**, left panel). At stalled replication forks, the presence of ssDNA activates the checkpoint kinase ATR to prevent entry into mitosis with under-replicated regions⁵⁵. A subsequent restart of stalled replication forks depends on the degradation of nascent DNA by MRE11⁵⁶. However, unsuccessful restoration of replication forks leads to the release of ssDNA parts into the cytosol, a process that is stimulated by the

BLM helicase and EXO1 exonuclease⁵⁷ and can be prevented by binding of RPA and Rad51 to stretches of ssDNA⁵⁸. Recently, the dNTPase SAMHD1 was shown to promote DNA resection capacity, and in conjunction with MRE11 prevents the release of ssDNA into the cytosol^{59–61}. In line with these findings, mutations in *SAMHD1* increase the release of DNA into the cytoplasm that occur during replicating errors⁵⁹.

Response to cytoplasmic DNA: cgas/sting signaling

As soon as double-stranded DNA (dsDNA) or ssDNA enters the cytosol, it is recognized by pattern recognition receptors, including the DNA sensing molecule *cyclic GMP-AMP synthase* (cGAS). This response is part of the innate immune response, the first-line defense against a range of pathogens, including viruses and bacteria. The basis of this innate response is that no free DNA should be present in the cytoplasm (**Figure 1**, right panel)

cGAS can bind various DNA substrates but has the highest affinity for dsDNA, of which the length strongly influences the potential to activate cGAS^{62,63}. Once cGAS is in complex with DNA, it is able to catalyze the synthesis of cyclic GMP-AMP (cGAMP), which in turn binds the ER-membrane adaptor protein *stimulator of interferon genes* (STING)^{64,65}. Activated STING subsequently recruits and activates the TBK1 kinase, which phosphorylates the transcription factor IRF3. STING also leads to the activation of both canonical and non-canonical signaling of the NF- κ B transcription factor by indirect degradation of its inhibitor I κ B^{66,67}. Activation of both IRF3 and NF- κ B transcription results in the expression of type-I interferon (IFN) genes and pro-inflammatory cytokines, which instigates a cell-intrinsic innate immune response^{68,69}. Importantly, positive feedback regulation leads to type-I IFN-induced cGAS expression due to the presence of IFN response elements in the cGAS promoter⁷⁰. This feedback loop is further regulated by cleavage of cGAS and IRF3 by the apoptotic caspase-3⁷¹.

The recognition of cytosolic DNA does not only occur through cGAS. Various other DNA sensors were identified to be present in the cytoplasm; however, their ability to activate STING-dependent IFN responses appears to be limited. Besides cGAS, the most prominent DNA sensors that can induce IFN signaling in response to cytoplasmic DNA appear to be “AIM2-like receptors” (ALRs), including IFI16 and AIM2⁷². In conjunction with ATM and PARP-1, IFI16 forms a complex with STING upon nuclear DNA damage and triggers NF- κ B signaling, independently of cGAS^{73,74}. AIM2 forms an ‘inflammasome; in response to cytoplasmic DNA, and thereby promotes secretion of pro-inflammatory cytokines via caspase-1^{73–76}. Although multiple DNA sensors seem to possess DNA-binding capacities, the downstream activation of STING seems to be crucial to ultimately initiate innate immune responses⁷⁷.

In addition to cytoplasmic DNA, also RNA has been demonstrated to enter the cytoplasm. Cytoplasmic RNA is predominantly recognized by the RNA sensors *Retinoic acid-inducible gene-1 protein* (RIG-I) and *melanoma differentiation-associated protein-5* (MDA5)⁷⁸. Detection of RNA species in the cytoplasm also triggers the production of inflammatory cytokines, including type-I IFN. However, this process depends on the *mitochondrial antiviral-signaling protein* (MAVS) and is independent of cGAS⁷⁹. Although STING was proposed to function in the cellular response to cytoplasmic RNA, this role is not entirely clear⁷⁷. Also, IFN signaling in response to sensing of cytoplasmic RNA appears more relevant for anti-viral responses against RNA virus infections rather than cancer-associated genomic instability⁸⁰.

cGAS/STING activation in situations of genomic instability

Sensing of cytoplasmic DNA as a mechanism to respond to pathogens is based on the premise that the “own” DNA of the cell is retained within the nucleus. Clearly, in situations where cytoplasmic DNA arises due to genomic instability or genotoxic treatment, cGAS/STING signaling will be activated by “self” DNA and leads to a sterile inflammatory response

Indeed, various conditions in which persistent DNA damage is induced have been linked to inflammatory signaling, although the underlying mechanisms initially remained elusive. Irradiation, for instance, was shown to induce pro-inflammatory cytokines secretion^{81,82}. Only recently, the induction of cytosolic DNA after irradiation was shown to trigger cGAS/STING signaling, which was shown to be responsible for the observed inflammatory response^{83,84}. Similarly, DNA damage repair defects, as induced by loss of BRCA1, BRCA2 or ATM lead to micronuclei formation and cGAS/STING-dependent IFN signaling^{46,47,53,85}. Likewise, DNA lesions as a result of telomere erosion^{88,89} or oncogenic stress were shown to activate cGAS/STING signaling⁸⁴. Additionally, aberrant RNA:DNA hybrids were reported to trigger cGAS/STING signaling⁸⁶. Specifically, mutations in genes encoding RNase H2 subunits lead to the autoimmune disorder Aicardi-Goutières syndrome (AGS), which is characterized by increased production of type-I IFN^{87,88}. Of note, the observed inflammatory response in AGS was recently demonstrated to depend on cGAS/STING signaling, which in part may be instigated by micronuclei formation^{50,89}. Defective processing of stalled replication forks can also lead to cGAS/STING-dependent inflammatory signaling. Under physiological conditions, the resection capacity of SAMHD1 prevents the release of ssDNA from stalled replication forks into the cytosol. Conversely, SAMHD1 deficiency leads to the accumulation of cytoplasmic ssDNA and thereby triggers a cGAS/STING-induced cytokine response⁵⁹. Besides resection capacity, SAMHD1 also prevents the induction of a cGAS/STING-induced IFN response upon viral infection, and limits anti-viral T cell responses *in vivo*⁹⁰.

Cells are able to degrade DNA, which has aberrantly reached the cytoplasm. TREX1, a cytoplasmic exonuclease – originally described as DNase-III – can degrade ssDNA in the cytoplasm^{91,92}. As a consequence, TREX1 deficiency, analogous to RNase H2 or SAMHD1 inactivation, triggers a cell-intrinsic inflammatory response, which requires cGAS⁹³. In line with this notion, the cGAS-dependent IFN response triggered by cytoplasmic HIV-1 derived ssDNA is suppressed by TREX1^{94,95}. Clearly, cells with defects in the function of cytoplasmic nucleases fail to clear cytoplasmic DNA, which will result in similar cell-intrinsic inflammatory responses⁹⁶.

Taken together, genomic DNA can trigger pro-inflammatory responses when genome maintenance is defective, while various nucleases, both in the nucleus (e.g. RNase H2 and SAMHD1) and cytoplasm (e.g. TREX1), can prevent the accumulation of cytoplasmic DNA and therefore dampen innate inflammatory responses.

Consequences of inflammatory signaling induced by genomic instability

Early on, the secretion of pro-inflammatory cytokines was recognized as an important feature of senescence, a state of permanent growth arrest. Senescence can be triggered by multiple cues including telomere erosion, in which critical shortening of telomeres instigate DNA damage signaling. The array of cytokines that are secreted by senescent cells – known as the senescence-associated secretory phenotype (SASP) – has been described as a consequence of DNA damage and NF- κ B signaling^{81,97}. The secretion of SASP cytokines facilitates immune cell recruitment, as part of an attempt to eliminate possibly pre-malignant cells, thereby providing a cell-intrinsic surveillance mechanism with tumor-suppressive capacity^{98,99}.

Recently, it was found that the cGAS/STING pathway promotes SASP and regulates senescence both *in vitro* and *in vivo*^{84,100,101}. In good agreement with this notion, different treatments that induce senescence, including irradiation, CDK4/6 inhibition, or oncogene expression, were able to engage the cGAS/STING pathway⁸⁴. Specifically, due to the presence of chromatin fragments in the cytoplasm of senescent cells, activation of cGAS/STING – and thus SASP – maintains paracrine senescence⁸⁴. Indeed, also telomere damage that occurs during a replicative crisis was shown to result in cytosolic DNA fragments, which trigger cGAS/STING-dependent autophagy^{102,103}. The observations that senescence was STING- and cGAS-dependent, suggest that cGAS/STING signaling

plays an important role in regulating SASP and maintenance of a senescence state^{84,100}. Indeed, cells lacking cGAS or STING were able to escape replicative crises and continue proliferation, underscoring the notion that the inability to initiate cell-intrinsic inflammatory signaling may allow the oncogenic transformation of genomically unstable cells¹⁰³.

Instead of apoptotic cell death, cells that undergo replicative crisis show characteristics of autophagy, including vacuolization and lysosomal protein expression¹⁰³. Gui et al. recently showed that cGAMP triggers STING translocation to the endoplasmic reticulum and Golgi, where it supports the formation of autophagosomes. Through these mechanisms, cytosolic DNA is targeted for destruction, independently of the canonical cGAS/STING effector TBK1 and inflammatory cytokine release¹⁰⁴. Similarly, cytosolic DNA originating from micronuclei in RNase H2 mutant cells is targeted by autophagy. Inhibition of autophagy, as a consequence, aggravated the IFN response⁵⁰. These findings illustrate that autophagy plays a role in limiting the amounts of cytoplasmic DNA and through this mechanism determines cell fate in situations of genomic instability.

cGAS/STING signaling in the tumor microenvironment

The secretion of cytokines upon cGAS/STING signaling serves many paracrine functions (**Figure 2**). Type-I IFN plays an important role in shaping the innate immune response towards tumor cells. The impact of IFN in this context is illustrated by the finding that mice in which dendritic cells cannot respond to type-I IFN due to lack of the IFNAR receptor or its downstream signaling molecule STAT1 are unable to clear tumor cells and show defects in antigen cross-presentation towards CD8⁺ T cells^{105,106}. Furthermore, IFN signaling in antigen-presenting cells (APCs) is essential for the accumulation of CD8⁺ dendritic cells in the tumor and tumor cell recognition¹⁰⁶. Also, expression of cytokines that are secreted upon STING activation, including CCL5 and CXCL10, has been shown to correlate with high tumor infiltration of CD8⁺ T cells¹⁰⁷. Conversely, CD8⁺ T cell priming is severely impaired in STING- or IRF3-deficient mice and results in the failure to reject immunogenic tumors¹⁰⁸. Likewise, STING-induced IFN secretion in prostate cancer cells due to loss of the MUS81 endonuclease triggers macrophage-dependent phagocytosis of tumor cells¹⁰⁹. STING activation in tumor cells enhances the expression of several proteins, such as *Suppressor of Cytokine Signaling-1* (SOCS1) in Epstein-Barr virus-associated carcinoma cells and myeloid cells. As a result, the production of GM-CSF and IL-6 is inhibited, leading to a decrease in activation of myeloid-derived suppressor cells (MDSCs) and thereby lowering its immunosuppressive functions¹¹⁰. Also, STING activation in tumor cells as a result of DNA damage and ensuing cytoplasmic DNA triggers the expression of NKG2D receptor ligands, which promotes NK cell-dependent tumor cell killing^{111,112}. Finally, Type I IFNs and STAT1 activation has been described to induce polarization of M1 macrophages^{113,114}, a specific macrophage subtype that is known for its anti-tumor responses¹¹⁵. These findings support an important role of inflammatory signaling and secreted cytokines upon STING activation in tumor cells on infiltration and activation of surrounding immune cells to trigger anti-tumor responses.

cGAS/STING signaling not only originates tumor cell-intrinsically. STING signaling can also be initiated in the tumor microenvironment. Specifically, tumor cell-derived DNA can be taken up by antigen-presenting cells (APCs) in which it triggers STING signaling. Indeed, *in vitro* and *in vivo* data showed that when tumor-derived DNA is taken up by APCs, it enters the cytosol and triggers cGAS, leading to phosphorylation of TBK1, IRF3, and STING-induced IFN β production¹⁰⁸. Indeed, the release of tumor-derived DNA triggered by irradiation led to an uptake of tumor DNA by dendritic cells and resulted in a cGAS/STING type-I IFN response and induction of an adaptive anti-tumor response¹¹⁶.

Based on other studies, cGAMP was shown to exert its function in a paracrine fashion. cGAMP is able to migrate through gap junctions to activate STING in neighboring

cells and thereby provides a soluble “warning signal”¹¹⁷. In a more recent study, NK cells from STING-deficient mice failed to generate effective anti-tumor responses, in contrast to NK cells from cGAS-deficient mice¹¹⁸. Specifically, in cGAS-deficient mice, injection of cGAS-proficient tumor cells that were able to produce cGAMP led to the rejection of tumor cells via STING activation in NK cells¹¹⁸. These findings support the importance of STING activation in response to paracrine cGAMP to trigger anti-tumor responses in the tumor microenvironment (**Figure 2**, left panel)¹¹⁹. In line with these observations, the paracrine actions of cGAMP are being explored as a target for possible treatment strategies.

Tumor-promoting features of cGAS/STING signaling

In contrast to the observed STING-induced anti-tumor responses, cGAS/STING signaling also has tumor-promoting features (**Figure 2**, right panel). For instance, cGAMP produced by cancer cells in the brain and transferred to astrocytes via gap-junctions was shown to promote cancer growth¹²⁰. Specifically, in response to cGAMP, astrocytes activated STING-signaling and produced cytokines, including IFN and TNF, which in turn activated STAT1 and NF- κ B signaling in brain cancer cells to induce growth, chemoresistance and eventually promoted metastasis¹²⁰.

As described above, cGAS/STING signaling elicits secretion of pro-inflammatory cytokines, which facilitate the recruitment of immune cells as part of an innate immune response. However, contradicting observations have been done in this context. Whereas STING signaling was demonstrated to inhibit activation of MDSCs to promote anti-tumor immune activation¹¹⁰, another study reported that STING signaling in response to irradiation promotes tumor infiltration of myeloid-derived suppressor cells, leading to resistance of cancer cells towards irradiation¹²¹. Also, STING activation in tumors characterized by low antigenicity, promoted tumor growth via indoleamine-2,3-dioxygenase (IDO) activation¹²².

Important to realize in this context is that acute and chronic IFN responses lead to differential downstream effects. Whereas early type-I IFN responses promote the elimination of tumor cells¹⁰⁵, persistent inflammation, which is also accompanied by the production of pro-inflammatory cytokines, promotes tumor growth and metastatic properties in established tumors¹²³. In good agreement with these findings, chronic STAT-1-mediated IFN responses trigger immune checkpoint activation and resistance towards anti-PD1, anti-PD-L1 or anti-CTLA4-targeted immune checkpoint blockade due to increased expression of T cell inhibitory receptors and exhausted T cells¹²⁴. Furthermore, genetic or pharmacological interference with tumor-induced IFN signaling through JAK inactivation improved responses of immune checkpoint therapy-resistant tumors¹²⁴. Of note, two CRISPR/Cas9-based genetic screens identified IFN-gamma signaling as a key requirement for successful T cell-based immunotherapies^{125,126}. Based on these latter studies, one would argue against using inhibitors of interferon signaling in combination with immune checkpoint inhibitors.

In line with the observed tumor-promoting effects of a chronic IFN response, chromosomally unstable tumor cells were shown to continuously trigger STING signaling due to their micronuclei, which promoted metastatic capacity¹²⁷. Surprisingly, in these tumor cells, cGAS/STING activation did not result in canonical downstream events, including TBK1/IRF3 phosphorylation, canonical NF- κ B, and activation and type-I IFN secretion. Rather, chronic cGAS/STING activation was found to install non-canonical NF- κ B activation, which was independent of TBK1¹²⁷. In line with these findings, an analysis of TCGA samples revealed a correlation between high chromosomal instability and expression of non-canonical NF- κ B target genes in breast cancer¹²⁷.

The observation that the downstream consequences of cGAS/STING are not generic and can be skewed towards non-canonical pro-tumorigenic effects resembles findings in senescent cells. Whereas cGAS/STING activation in senescent cells leads to the secretion of pro-inflammatory cytokines, p38-MAPK signaling can prevent excretion of

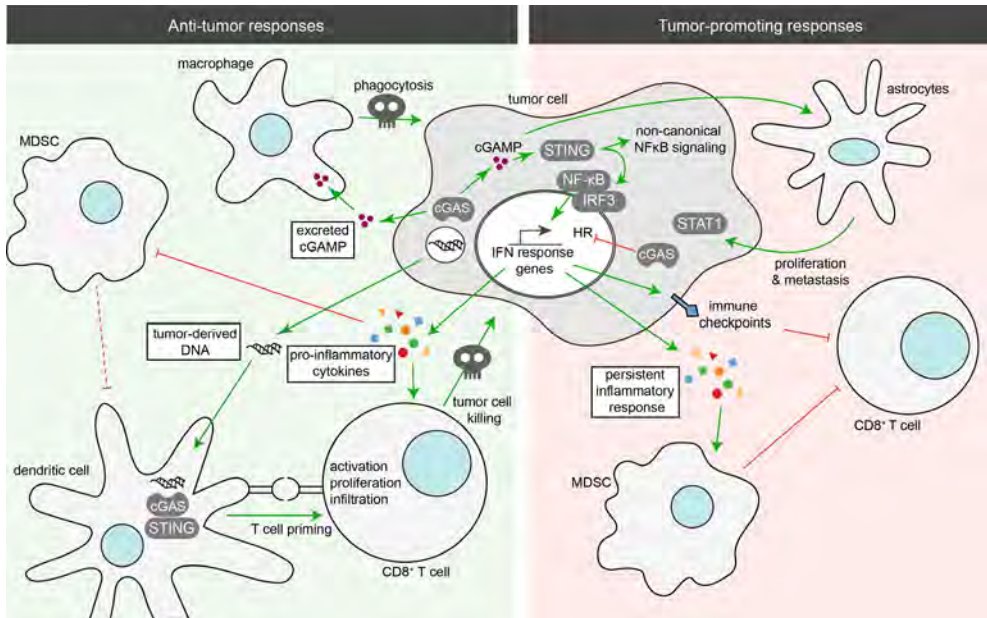


Figure 2. cGAS/STING signaling serves multiple paracrine functions in the tumor microenvironment. **Left panel:** Anti-tumor responses upon cGAS/STING-induced type-I IFN signaling in tumor cells. Type-I IFN leads to the activation of APCs and CD8⁺ T cell priming. Also, type-I IFN signaling promotes the infiltration of dendritic- and CD8⁺ T cells into the tumor microenvironment. IFN secretion triggers macrophage-dependent phagocytosis of tumor cells. STING enhances SOCS1 expression to decrease the activation of MDSCs. Tumor cell-derived DNA can be taken up by APCs to trigger a cGAS/STING-mediated type-I IFN. Finally, cGAMP can migrate through gap junctions to activate STING signaling in neighboring cells. **Right panel:** Tumor promoting responses upon cGAS/STING-induced type-I signaling in tumor cells. STING activation triggers non-canonical NF-κB activation, independent of TBK1. In brain cancer cells, cGAMP is transferred to astrocytes, leading to cytokine production and subsequently STAT1 and NF-κB signaling in brain cancer cells to promote growth, metastasis, and chemo-resistance. Persistent inflammation promotes tumor growth and metastatic properties in tumor cells. STAT1-induced IFN responses trigger immune checkpoint activation. Finally, cGAS has non-canonical functions and inhibits HR.

IFN, altering the SASP¹⁰¹. In line with these findings, senescence has been demonstrated to exert pro-tumorigenic effects, including metalloproteinase-mediated remodeling of the extracellular matrix, which facilitates migration of tumor cells^{128,129}. Also, SASP components, especially CXCL12, have been attributed to attract and promote the survival of cancer-associated fibroblasts (CAFs)¹³⁰. CXCL12, which is also excreted by CAFs, stimulates the proliferation of tumor cells and promotes angiogenesis^{130,131}. Combined, besides leading to permanent cell cycle arrest of damaged cells, the inflamed state of senescent cells promotes aggressive tumor behavior and is associated with poor prognosis^{132,133}.

In summary, cGAS/STING activation can lead to differential downstream effects in tumor cells (**Figure 2**). In general, the induction of an IFN response triggers the immune system to clear tumor cells. In contrast, non-canonical NF-κB activation triggered by chronic IFN responses preferentially leads to tumor growth and metastasis. These dual effects, including tumor-promoting features, might explain why cGAS and/or STING are hardly ever lost or mutated in cancer. Yet, it remains unclear how tumor cells deal with the tumor-eradicating effects of STING signaling. Further complicating these observations, cGAS itself was recently also described to have non-canonical functions in DNA repair, where it inhibits

HR and may promote genomic instability and tumor progression^{134,135}.

How do genomic unstable tumors escape cGAS/STING dependent immune clearance

cGAS/STING signaling plays an important role in anti-tumor immune responses and promotes immune clearance of tumor cells. Yet, genomic instability is a common feature of cancer and a continuous source of cytoplasmic DNA, either through the formation of micronuclei or leakage of DNA fragments from aberrantly processed stalled replication forks^{136,137}. As a consequence, tumor cells continuously produce intrinsic cues that activate cGAS/STING activation and subsequent inflammatory signaling. Indeed, it has been shown that high STING expression correlates with higher expression of pro-inflammatory genes in both cancer cell lines and multiple human cancers from database analyses¹⁰¹.

The notion that tumor cells frequently display cGAS/STING activation implies that during the transformation of normal cells into malignant cells, cells evolve mechanisms to suppress the tumor cell-clearing effects of STING signaling to allow tumor formation (**Figure 3**). How tumor cells achieve this, remains unclear.

Suppression of STING signaling in tumor cells has been demonstrated, for instance in colorectal cancer cell lines and melanoma cells^{138,139}. The level of STING suppression appeared functional since it altered the cellular responses to virus-mediated therapies^{138,139}. Furthermore, database analyses showed that STING signaling may be suppressed in tumors due to loss-of-function mutations in *TMEM173*, the gene encoding STING, or epigenetic silencing of *CGAS/TMEM173*, although the frequencies of these events were low^{139,140}.

In line with cGAS/STING signaling remaining intact in cancer cells, breast cancers with DNA repair defects showed cytoplasmic DNA, constitutive activation of cGAS/STING signaling, and increased T cell infiltration, but did not trigger effective anti-tumor immune responses⁴⁷. The lack of an anti-tumor T cell response in these tumor cells could be explained by DNA damage-induced STING activation and subsequent upregulation of the immune checkpoint component PD-L1^{47,141}. Thus, although cGAS/STING signaling in tumor cells is activated, the consequent anti-tumor immune response can be counterbalanced, for instance, through increased expression of immune-checkpoint proteins.

Suppression of the anti-tumor cGAS/STING signaling cascade might also be achieved by oncogene overexpression. *MYC*, encoding the transcription factor c-MYC, is frequently found amplified in multiple cancer types and is an established oncogene¹⁴². In tumors that are characterized by high genomic instability, e.g. high-grade serous ovarian cancers and triple-negative breast cancers, more than half show amplification of *MYC*^{143,144}. C-MYC overexpression is not only a critical oncogenic driver of tumor growth but also has inflammation modulatory effects. In a *KRAS*-driven tumor model, c-MYC expression was shown to contribute to both immunosuppressive and inflammatory phenotypes in the tumor microenvironment, with the *CCL9* and *IL-23*-mediated tumor-promoting effects¹⁴⁵. Conversely, c-MYC inactivation in models of lymphoma and B cell leukemia lead to alterations in cytokine release and increased numbers of CD4⁺ T cells within the tumor microenvironment, which mediated tumor regression¹⁴⁶. Furthermore, c-MYC inactivation leads to the down-regulation of the PD-L1 immune checkpoint protein on tumor cells, further underscoring a role for c-MYC in shaping immune responses in the tumor microenvironment¹⁴⁷. Similarly, also the *KRAS* oncogene was recently shown to modulate inflammatory responses. Specifically, *KRAS* inhibits *IRF2* and thereby down-regulates IFN responses, resulting in increased resistance towards immune checkpoint inhibition¹⁴⁸. Likewise, expression of the viral HPV oncogenes E1A and E7 in cervical cancer were described to interact with STING to inhibit DNA sensing and prevent activation of the cGAS/STING pathway¹⁴⁹. These combined data support a model in which oncogene activation not only drives proliferation but simultaneously alters the expression of immune checkpoints on tumor cells and the subsequent

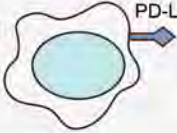


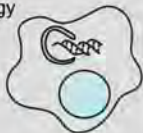

Adaptation mechanisms to cytoplasmic DNA	Consequences	References
Upregulation of immune checkpoint components 	↑ Immune checkpoint activation ↓ Anti-tumor immune response	44, 132
Oncogene expression 	↓ Interferon response ↑ CD4+ T cells ↑ Immune checkpoint proteins	136-140
Somatic copy number alterations (SCNAs) 	↑ Gains/losses of genes ↑ Proteotoxic stress ↑ Immune evasion	141, 142
Upregulation of autophagy 	↓ Cytoplasmic DNA ↑ Bypass of replicative crisis ↑ Interferon response	47, 99, 100
Activation of cytoplasmic nucleases 	↓ Cytoplasmic DNA ↓ Interferon response	88, 93, 145

Figure 3. Mechanisms by which tumor cells can escape the anti-tumor effects of cGAS/STING signaling. Various possibilities are depicted that can be employed by tumor cells to evade the immune-promoting effects of cGAS/STING signaling. The consequences of each mechanism on cGAS/STING-induced responses are described.

presence and activation of immune cells to ultimately escape anti-tumor immunity.

Alternatively, tumors with high levels of genomic instability may evolve karyotypes that go along with immune evasion. Specifically, tumors with high levels of aneuploidy showed a reduction in cytotoxic infiltrating immune cells and conversely, an increased expression of cell proliferation markers¹⁵⁰. Although it remains elusive how aneuploidy results in immune evasion mechanistically, high levels of somatic copy number alterations (SCNAs) were predictive for poor response to CTLA-4-mediated immunotherapy and could serve as a biomarker in this context^{150,151}.

Another mechanism by which tumor cells can adapt to deal with inflammatory signaling that is triggered by cytoplasmic DNA is autophagy upregulation. Autophagy is a catabolic process that involves the self-digestion of organelles and has been shown to affect multiple aspects of tumor cell biology, including tumor suppression^{152,153}. However, elevated levels of autophagy were recently shown to allow the bypass of replicative crisis and enhanced survival of genomically instable cells¹⁰³. Of note, DNA

in the cytoplasm can trigger autophagy to mediate clearance of cytoplasmic DNA in a manner that depends on STING but is independent of IFN secretion¹⁰⁴. In line with these findings, inhibiting autophagy aggravated the IFN response, whereas the induction of autophagy leads to bypass of replicative crisis to continue proliferation^{50,103}.

Finally, multiple nucleases, including TREX1, are able to clear cytoplasmic DNA and thereby prevent cell-intrinsic immunity^{91,96}. Tumor cells utilize this mechanism to dampen the cellular response to cytoplasmic DNA. For instance, TREX1 is induced in tumor cells upon irradiation to degrade irradiation-induced cytoplasmic DNA¹⁵⁴. This response prevents activation of cGAS/STING-induced IFN secretion and subsequent activation of surrounding immune cells. Possibly, tumor cells with high expression levels of such nucleases may be less susceptible to therapies that induce DNA damage and cGAS/STING activation.

Targeting inflammatory signaling in genomically unstable cancers

cGAS/STING signaling as a determinant of anti-cancer therapy response

Similar to other features of cancer cells, the presence of cytoplasmic DNA in tumor cells appears to be a determinant of tumor behavior and treatment outcome and might turn out to be an actionable vulnerability of tumor cells.

The induction of micronuclei has long been recognized as a consequence of radiotherapy as well as genotoxic chemotherapeutics^{155–157}. Treatment-induced micronuclei formation has been linked to adaptation to a G2/M cell cycle arrest. Similarly, treatment with genotoxic chemotherapeutics or radiotherapy was shown to increase IFN signaling^{158,159}. Increasingly, we realize that the treatment-induced interferon response that goes along with micronuclei formation is not merely a bystander effect, but also a determinant of treatment outcome. For instance, irradiation-induced secretion of Type-I IFN triggers both innate and adaptive immune mechanisms that target tumor cells¹⁶⁰. In line with these findings, intra-tumoral administration of type-I IFN could mimic the effects of irradiation on tumor regression¹⁶⁰. Furthermore, the STING-dependent inflammatory response in tumor cells is linked to the abscopal effects on distinct lesions and sensitivity to anti-CTLA4 treatment⁸³. Similarly, inhibition of colony-stimulating factor-1 receptor (CSF-1R) resulted in enhanced IFN signaling in breast cancer and led to an increased sensitivity to chemotherapy¹⁶¹.

Also, the anti-neoplastic effects of the anti-mitotic drug paclitaxel have been related to inflammatory micronucleus formation¹⁶². For a long time, the cytotoxic effects of the microtubule drug paclitaxel were related to its ability to arrest cells in mitosis. However, paclitaxel treatment was also shown to induce aberrant mitotic exit and extensive micronucleation^{163,164}. Importantly, the paclitaxel-induced micronucleus formation went along with DNA damage induction, but not apoptosis induction per se. Conversely, the ability of cancer cells to induce IFN signaling in response to DNA damage was shown to confer treatment resistance. Specifically, in a TREX1 deficient background, breast cancer cells became resistant to radiotherapy⁵⁷. This was attributed to the role of TREX1 in the clearance of irradiation-induced cytoplasmic DNA, which is in part caused by the formation of ssDNA fragments⁵⁷. In line with this notion, irradiation was shown to be more effective in repeated low doses compared to high doses to prevent induction of TREX1 and to effectively trigger IFN production¹⁵⁴. The expression of certain nucleases in tumor cells might therefore serve as a marker to guide irradiation dose and fractioning.

PARP inhibitors have been shown to effectively target tumors with BRCA1/2 defects and are described to target HR-defective tumors based on synthetic lethality¹⁶⁵. Currently, several PARP inhibitors are approved for the treatment of *BRCA1/2*-mutant high-grade serous ovarian cancer, breast cancer, and pancreatic cancer. Recently, the effective killing of HR-deficient tumor cells upon PARP inhibitor treatment was shown to involve defects in mitosis, leading to micronucleation and mitotic catastrophe³⁴. In line with these observations,

PARP inhibitor treatment was shown to trigger an anti-tumor immune response via tumor-derived cGAMP which activated STING signaling in immune cells in a BRCA1-deficient tumor model¹⁶⁶. Furthermore, treatment with PARP inhibitors upregulated PD-L1 expression on tumor cells, and a combination with anti-PD-1 enhanced the survival of BRCA1-tumor bearing mice^{166,167}. Importantly, treatment with PARP inhibitor also triggered the accumulation of cytoplasmic DNA and thus cGAS/STING activation independent of *BRCA1/2* mutation status¹⁶⁸. Finally, the effectiveness of PARP inhibitor treatment, especially in HR-deficient tumors, seemed to be dependent on tumor infiltration of CD8⁺ T cells¹⁶⁹. These data further support the rationale of combining PARP inhibitors with immune checkpoint therapies.

In good agreement with inflammatory signaling being a determinant of therapy response, expression of a set of IFN-induced genes in cancer cell lines was shown to correlate with chemotherapy or radiotherapy resistance and could be used to separate high- from low-risk patients¹⁷⁰. Specifically, a panel of seven of these IFN-induced genes could identify resistance to chemo- and radiotherapy in breast cancer patients. Silencing of these IFN-induced genes could subsequently reverse the resistance of triple-negative breast cancer cells to chemo- and radiotherapy, again underscoring that IFN is not a bystander effect but is causally involved in treatment outcome¹⁷¹. Similarly, activation of IFN/STAT1 signaling was shown to predict chemotherapy response in ER-negative breast cancer¹⁷². These studies indicate further that IFN signaling plays an important role in therapy sensitivity, immune cell activity, and underscores the potential value to target this response in tumor cells.

Therapeutic activation of STING signaling

The importance of STING-induced IFN signaling in tumor responses to genotoxic agents might be of use to therapeutically activate STING intratumorally and thereby enhancing innate immune responses. The flavonoid DMXAA was shown to function as a mouse-specific STING ligand and has anti-tumor effects in solid tumors^{173,174}. Intra-tumoral injection of DMXAA or human STING-specific cyclic dinucleotide derivatives induced regression of established tumors as well as metastatic lesions¹⁷⁵. Specifically, intra-tumoral injection of STING agonists in multiple cancer mouse models improved anti-tumor CD8⁺ T cell responses, which were further enhanced by immune checkpoint inhibition^{176,177}. Surprisingly, type I IFN production in one of these studies was shown to come from tumor-associated endothelial cells rather than tumor cells or dendritic cells¹⁷⁶. In this context, the administration of liposomal nanoparticle-delivered cGAMP was shown to be more effective than soluble cGAMP, circumventing the need for intra-tumoral injections¹⁷⁸. Nanoparticle delivery of cGAMP was effective in different tumor models resistant to PD-L1 checkpoint blockade, whereas the observed tumor regression was lost in STING- or IFNAR-deficient mice¹⁷⁸. In good agreement with the described roles of irradiation on STING-induced IFN responses, cGAMP treatment in combination with irradiation further increased anti-tumor CD8⁺ T cell responses, in a STING-dependent fashion¹¹⁶.

Targeting innate immune checkpoints

The described effects of cGAS/STING pathway activation on innate immunity suggest a prominent role for immune checkpoint inhibition in genomically unstable tumors. cGAS and STING protein levels were shown to correlate with PD-L1 levels in ovarian cancer cell lines and PD-L1 levels were further enhanced by cGAMP treatment¹⁷⁹. Furthermore, combined treatment of cGAMP with anti-PD-L1 increased the anti-tumor effects of *in vivo* injected melanoma cell lines, which was attributed to enhanced STING-dependent tumor antigen cross-presentation in dendritic cells¹⁸⁰. PD-L1 expression was also increased upon induction of DNA DSBs, through activation of the ATM, ATR, and Chk1 kinases, and was further increased upon loss of DNA repair proteins, including BRCA2 or Ku70/80¹⁴¹. Thus, combination treatment of agents that induce DSBs while inhibiting cell cycle checkpoint inhibitors (e.g. ATM, ATR or

Chk1), might therefore prevent an increase of PD-L1 expression and thus decrease response to immune checkpoint inhibitors¹⁸¹.

Conclusions and outlook

Vertebrates have evolved an elegant system by which detection of foreign DNA in the cytosol triggers an innate immune response. This same mechanism is also triggered by cytoplasmic self DNA, a frequently occurring feature of tumor cells due to their genomic instability or induced by genotoxic treatments. The response to cytoplasmic DNA in tumor cells has gained enormous attention over the past few years because cGAS/STING signaling was shown to be activated upon cytoplasmic DNA, which established a direct link between genomic instability and inflammatory signaling. The subsequent type-I IFN response plays important roles in tumor growth, immune evasion, and determines treatment outcome.

The increasing knowledge of the impact of cGAS/STING signaling on anti-tumor immunity has led to increasing endeavors to target this pathway therapeutically. STING agonists have been developed, including synthetic cGAMP, and are used to boost infiltration and activation of immune cells into the tumor microenvironment. However, cGAMP administration alone might not be sufficient, as STING activation by cGAMP on its own resembles immune cells with low cross-priming activity¹¹⁹. Combining cGAMP treatment with genotoxic therapies, such as irradiation, could enhance these responses through the recruitment of multiple immune cells and the engagement of several DNA damage response pathways.

However, caution should be taken regarding cGAMP treatment in tumors that are not chromosomal unstable, as has been shown that cGAMP increases invasion and migration of cells with low chromosomal instability, probably due to the tumor-promoting effects of non-canonical NF- κ B activation^{127,182}. Also, treatment schedule and dosing may be of impact on the effectiveness of cGAMP treatment. Repeated treatments and high dosages were found to be unfavorable for long-term tumor-specific T cell responses¹⁷⁷. Important in this context is the notion that the induction of STING-mediated inflammatory signaling has both pro-tumorigenic and anti-tumorigenic effects. Currently, it is unclear how tumor cells have adapted to deal with STING activation and shape the downstream effects into effects that promote growth and evasion of immune clearance. Multiple non-exclusive mechanisms may be responsible, including increased autophagy and non-canonical effects of oncogene activation.

Acknowledgments and funding

F.T. and M.A.T.M.v.V. are supported by the Dutch Cancer Society/Alpe D'huzes (Grant EMCR2014-7048). M.A.T.M.v.V. is supported by the European Research Council (ERC CoS Grant 682421).

References

1. Hanahan, D. & Weinberg, R. A. Hallmarks of Cancer: The Next Generation. *Cell* 144, 646–674 (2011).
2. Antoniou, A. et al. Average Risks of Breast and Ovarian Cancer Associated with BRCA1 or BRCA2 Mutations Detected in Case Series Unselected for Family History: A Combined Analysis of 22 Studies. *Am. J. Hum. Genet.* 72, 1117–1130 (2003).
3. Li, G.-M. Mechanisms and functions of DNA mismatch repair. *Cell Res.* 18, 85–98 (2008).
4. Hampel, H. et al. Screening for the Lynch Syndrome (Hereditary Nonpolyposis Colorectal Cancer). *N. Engl. J. Med.* 352, 1851–1860 (2005).
5. Koopman, M. et al. Deficient mismatch repair system in patients with sporadic advanced colorectal cancer. *Br. J. Cancer* 100, 266–273 (2009).
6. Latham, A. et al. Microsatellite Instability Is Associated With the Presence of Lynch Syndrome Pan-Cancer. *J. Clin. Oncol.* 37, 286–295 (2019).

7. Curtin, N. J. DNA repair dysregulation from cancer driver to therapeutic target. *Nat. Rev. Cancer* 12, (2012).
8. Maciejowski, J. & de Lange, T. Telomeres in cancer: tumour suppression and genome instability. *Nat. Rev. Mol. Cell Biol.* 18, 175–186 (2017).
9. von Morgen, P. & Maciejowski, J. The ins and outs of telomere crisis in cancer. *Genome Med.* 10, 89 (2018).
10. Maciejowski, J., Li, Y., Bosco, N., Campbell, P. J. & de Lange, T. Chromothripsis and Kataegis Induced by Telomere Crisis. *Cell* 163, 1641–1654 (2015).
11. Kotsantis, P., Petermann, E. & Boulton, S. J. Mechanisms of Oncogene-Induced Replication Stress: Jigsaw Falling into Place. *Cancer Discov.* 8, 537–555 (2018).
12. Schoonen, P. M., Guerrero Llobet, S. & van Vugt, M. A. T. M. Replication stress: Driver and therapeutic target in genomically instable cancers. *Adv. Protein Chem. Struct. Biol.* 115, 157–201 (2019).
13. Kim, J. K. & Diehl, J. A. Nuclear cyclin D1: An oncogenic driver in human cancer. *J. Cell. Physiol.* 220, 292–296 (2009).
14. Malumbres, M. & Barbacid, M. RAS oncogenes: the first 30 years. *Nat. Rev. Cancer* 3, 459–465 (2003).
15. Macheret, M. & Halazonetis, T. D. Intragenic origins due to short G1 phases underlie oncogene-induced DNA replication stress. *Nature* 555, 112–116 (2018).
16. Poli, J. et al. dNTP pools determine fork progression and origin usage under replication stress. *EMBO J.* 31, 883–94 (2012).
17. Bester, A. C. et al. Nucleotide deficiency promotes genomic instability in early stages of cancer development. *Cell* 145, 435–46 (2011).
18. Neelsen, K. J., Zanini, I. M. Y., Herrador, R. & Lopes, M. Oncogenes induce genotoxic stress by mitotic processing of unusual replication intermediates. *J. Cell Biol.* 200, 699–708 (2013).
19. Jones, R. M. et al. Increased replication initiation and conflicts with transcription underlie Cyclin E-induced replication stress. *Oncogene* 32, 3744–3753 (2013).
20. Hirao, A. et al. DNA damage-induced activation of p53 by the checkpoint kinase Chk2. *Science* 287, 1824–7 (2000).
21. Kastan, M. B., Onyekwere, O., Sidransky, D., Vogelstein, B. & Craig, R. W. Participation of p53 protein in the cellular response to DNA damage. *Cancer Res.* 51, 6304–11 (1991).
22. Negrini, S., Gorgoulis, V. G. & Halazonetis, T. D. Genomic instability — an evolving hallmark of cancer. *Nat. Rev. Mol. Cell Biol.* 11, 220–228 (2010).
23. Halazonetis, T. D., Gorgoulis, V. G. & Bartek, J. An Oncogene-Induced DNA Damage Model for Cancer Development. *Science* (80-.). 319, 1352–1355 (2008).
24. Gorgoulis, V. G. et al. Activation of the DNA damage checkpoint and genomic instability in human precancerous lesions. *Nature* 434, 907–913 (2005).
25. Kandoth, C. et al. Mutational landscape and significance across 12 major cancer types. *Nature* 502, 333–339 (2013).
26. Synnott, N. C. et al. Mutant p53: a novel target for the treatment of patients with triple-negative breast cancer? *Int. J. Cancer* 140, 234–246 (2017).
27. Cole, A. J. et al. Assessing mutant p53 in primary high-grade serous ovarian cancer using immunohistochemistry and massively parallel sequencing. *Sci. Rep.* 6, 26191 (2016).
28. Koboldt, D. C. et al. Comprehensive molecular portraits of human breast tumours. *Nature* 490, 61–70 (2012).
29. De Witt Hamer, P. C., Mir, S. E., Noske, D., Van Noorden, C. J. F. & Würdinger, T. WEE1 kinase targeting combined with DNA-damaging cancer therapy catalyzes mitotic catastrophe. *Clin. Cancer Res.* 17, 4200–7 (2011).
30. Bartek, J. & Lukas, J. Chk1 and Chk2 kinases in checkpoint control and cancer. *Cancer Cell* 3, 421–429 (2003).
31. Naim, V., Wilhelm, T., Debatisse, M. & Rosselli, F. ERCC1 and MUS81-EME1 promote sister chromatid separation by processing late replication intermediates at common fragile sites during mitosis. *Nat. Cell Biol.* 15, 1008–15 (2013).

32. Minocherhomji, S. et al. Replication stress activates DNA repair synthesis in mitosis. *Nature* 528, 286–290 (2015).
33. Ying, S. et al. MUS81 promotes common fragile site expression. *Nat. Cell Biol.* 15, 1001–7 (2013).
34. Schoonen, P. M. et al. Progression through mitosis promotes PARP inhibitor-induced cytotoxicity in homologous recombination-deficient cancer cells. *Nat. Commun.* 8, 15981 (2017).
35. Gisselsson, D. et al. Chromosomal breakage-fusion-bridge events cause genetic intratumor heterogeneity. *Proc. Natl. Acad. Sci.* 97, 5357–5362 (2000).
36. Janssen, A., van der Burg, M., Suzhai, K., Kops, G. J. P. L. & Medema, R. H. Chromosome segregation errors as a cause of DNA damage and structural chromosome aberrations. *Science* 333, 1895–8 (2011).
37. Crasta, K. et al. DNA breaks and chromosome pulverization from errors in mitosis. *Nature* 482, 53–8 (2012).
38. Sheltzer, J. M. et al. Aneuploidy drives genomic instability in yeast. *Science* 333, 1026–30 (2011).
39. Liu, S. et al. Nuclear envelope assembly defects link mitotic errors to chromothripsis. *Nature* 561, 551–555 (2018).
40. Terradas, M., Martín, M. & Genescà, A. Impaired nuclear functions in micronuclei results in genome instability and chromothripsis. *Arch. Toxicol.* 90, 2657–2667 (2016).
41. Soto, M., García-Santisteban, I., Krenning, L., Medema, R. H. & Raaijmakers, J. A. Chromosomes trapped in micronuclei are liable to segregation errors. *J. Cell Sci.* 131, jcs214742 (2018).
42. Bakhoun, S. F. & Cantley, L. C. The Multifaceted Role of Chromosomal Instability in Cancer and Its Microenvironment. *Cell* 174, 1347–1360 (2018).
43. Zhang, C.-Z. et al. Chromothripsis from DNA damage in micronuclei. *Nature* 522, 179–184 (2015).
44. Hatch, E. M., Fischer, A. H., Deerinck, T. J. & Hetzer, M. W. Catastrophic nuclear envelope collapse in cancer cell micronuclei. *Cell* 154, 47–60 (2013).
45. Kalsbeek, D. & Golsteyn, R. M. G2/M-Phase Checkpoint Adaptation and Micronuclei Formation as Mechanisms That Contribute to Genomic Instability in Human Cells. *Int. J. Mol. Sci.* 18, (2017).
46. Heijink, A. M. et al. BRCA2 deficiency instigates cGAS-mediated inflammatory signaling and confers sensitivity to tumor necrosis factor- α -mediated cytotoxicity. *Nat. Commun.* 10, 100 (2019).
47. Parkes, E. E. et al. Activation of STING-Dependent Innate Immune Signaling By S-Phase-Specific DNA Damage in Breast Cancer. *J. Natl. Cancer Inst.* 109, djw199 (2017).
48. Laulier, C., Cheng, A. & Stark, J. M. The relative efficiency of homology-directed repair has distinct effects on proper anaphase chromosome separation. *Nucleic Acids Res.* 39, 5935–44 (2011).
49. Williams, J. S. & Kunkel, T. A. Ribonucleotides in DNA: Origins, repair and consequences. *DNA Repair (Amst.)* 19, 27–37 (2014).
50. Bartsch, K. et al. Absence of RNase H2 triggers generation of immunogenic micronuclei removed by autophagy. *Hum. Mol. Genet.* 26, 3960–3972 (2017).
51. Cornelio, D. A., Sedam, H. N. C., Ferrarezi, J. A., Sampaio, N. M. V. & Argueso, J. L. Both R-loop removal and ribonucleotide excision repair activities of RNase H2 contribute substantially to chromosome stability. *DNA Repair (Amst.)* 52, 110–114 (2017).
52. Fenech, M. The cytokinesis-block micronucleus technique: a detailed description of the method and its application to genotoxicity studies in human populations. *Mutat. Res.* 285, 35–44 (1993).
53. Härtlova, A. et al. DNA Damage Primes the Type I Interferon System via the Cytosolic DNA Sensor STING to Promote Anti-Microbial Innate Immunity. *Immunity* 42, 332–343 (2015).
54. Chabanon, R. M., Soria, J.-C., Lord, C. J. & Postel-Vinay, S. Beyond DNA repair: the novel immunological potential of PARP inhibitors. *Mol. Cell. Oncol.* 6, 1585170 (2019).
55. Flynn, R. L. & Zou, L. ATR: a master conductor of cellular responses to DNA replication stress. *Trends Biochem. Sci.* 36, 133–40 (2011).
56. Hashimoto, Y., Ray Chaudhuri, A., Lopes, M. & Costanzo, V. Rad51 protects nascent DNA from Mre11-dependent degradation and promotes continuous DNA synthesis. *Nat. Struct. Mol. Biol.* 17, 1305–1311 (2010).
57. Erdal, E., Haider, S., Rehwinkel, J., Harris, A. L. & McHugh, P. J. A prosurvival DNA damage-induced cytoplasmic interferon response is mediated by end resection factors and is limited by Trex1. *Genes Dev.* 31, 353–369 (2017).

58. Wolf, C. et al. RPA and Rad51 constitute a cell intrinsic mechanism to protect the cytosol from self DNA. *Nat. Commun.* 7, 11752 (2016).
59. Coquel, F. et al. SAMHD1 acts at stalled replication forks to prevent interferon induction. *Nature* 557, 57–61 (2018).
60. Beloglazova, N. et al. Nuclease activity of the human SAMHD1 protein implicated in the Aicardi-Goutieres syndrome and HIV-1 restriction. *J. Biol. Chem.* 288, 8101–10 (2013).
61. Daddacha, W. et al. SAMHD1 Promotes DNA End Resection to Facilitate DNA Repair by Homologous Recombination. *Cell Rep.* 20, 1921–1935 (2017).
62. Luecke, S. et al. cGAS is activated by DNA in a length-dependent manner. *EMBO Rep.* 18, 1707–1715 (2017).
63. Kranzusch, P. J., Lee, A. S.-Y., Berger, J. M. & Doudna, J. A. Structure of human cGAS reveals a conserved family of second-messenger enzymes in innate immunity. *Cell Rep.* 3, 1362–8 (2013).
64. Wu, J. et al. Cyclic GMP-AMP Is an Endogenous Second Messenger in Innate Immune Signaling by Cytosolic DNA. *Science* (80-.). 339, 826–830 (2013).
65. Sun, L., Wu, J., Du, F., Chen, X. & Chen, Z. J. Cyclic GMP-AMP Synthase Is a Cytosolic DNA Sensor That Activates the Type I Interferon Pathway. *Science* (80-.). 339, 786–791 (2013).
66. Ishikawa, H. & Barber, G. N. STING is an endoplasmic reticulum adaptor that facilitates innate immune signalling. *Nature* 455, 674–8 (2008).
67. Abe, T. & Barber, G. N. Cytosolic-DNA-mediated, STING-dependent proinflammatory gene induction necessitates canonical NF- κ B activation through TBK1. *J. Virol.* 88, 5328–41 (2014).
68. Ishikawa, H., Ma, Z. & Barber, G. N. STING regulates intracellular DNA-mediated, type I interferon-dependent innate immunity. *Nature* 461, 788–92 (2009).
69. Stetson, D. B. & Medzhitov, R. Recognition of cytosolic DNA activates an IRF3-dependent innate immune response. *Immunity* 24, 93–103 (2006).
70. Ma, F. et al. Positive feedback regulation of type I IFN production by the IFN-inducible DNA sensor cGAS. *J. Immunol.* 194, 1545–54 (2015).
71. Ning, X. et al. Apoptotic Caspases Suppress Type I Interferon Production via the Cleavage of cGAS, MAVS, and IRF3. *Mol. Cell* 74, 19–31.e7 (2019).
72. Unterholzner, L. et al. IFI16 is an innate immune sensor for intracellular DNA. *Nat. Immunol.* 11, 997–1004 (2010).
73. Ponomareva, L. et al. AIM2, an IFN-Inducible Cytosolic DNA Sensor, in the Development of Benign Prostate Hyperplasia and Prostate Cancer. *Mol. Cancer Res.* 11, 1193–1202 (2013).
74. Schroder, K., Muruve, D. A. & Tschopp, J. Innate Immunity: Cytoplasmic DNA Sensing by the AIM2 Inflammasome. *Curr. Biol.* 19, R262–R265 (2009).
75. Fernandes-Alnemri, T., Yu, J.-W., Datta, P., Wu, J. & Alnemri, E. S. AIM2 activates the inflammasome and cell death in response to cytoplasmic DNA. *Nature* 458, 509–513 (2009).
76. Hornung, V. et al. AIM2 recognizes cytosolic dsDNA and forms a caspase-1-activating inflammasome with ASC. *Nature* 458, 514–8 (2009).
77. Burdette, D. L. & Vance, R. E. STING and the innate immune response to nucleic acids in the cytosol. *Nat. Immunol.* 14, 19–26 (2013).
78. Zhao, Y., Ye, X., Dunker, W., Song, Y. & Karijolich, J. RIG-I like receptor sensing of host RNAs facilitates the cell-intrinsic immune response to KSHV infection. *Nat. Commun.* 9, 4841 (2018).
79. Chan, Y. K. & Gack, M. U. Viral evasion of intracellular DNA and RNA sensing. *Nat. Rev. Microbiol.* 14, 360–373 (2016).
80. Franz, K. M., Neidermyer, W. J., Tan, Y.-J., Whelan, S. P. J. & Kagan, J. C. STING-dependent translation inhibition restricts RNA virus replication. *Proc. Natl. Acad. Sci. U. S. A.* 115, E2058–E2067 (2018).
81. Rodier, F. et al. Persistent DNA damage signalling triggers senescence-associated inflammatory cytokine secretion. *Nat. Cell Biol.* 11, 973–9 (2009).
82. Di Maggio, F. et al. Portrait of inflammatory response to ionizing radiation treatment. *J. Inflamm.* 12, 14 (2015).
83. Harding, S. M. et al. Mitotic progression following DNA damage enables pattern recognition within micronuclei. *Nature* 548, 466–470 (2017).

84. Glück, S. et al. Innate immune sensing of cytosolic chromatin fragments through cGAS promotes senescence. *Nat. Cell Biol.* 19, 1061–1070 (2017).
85. Li, T. & Chen, Z. J. The cGAS-cGAMP-STING pathway connects DNA damage to inflammation, senescence, and cancer. *J. Exp. Med.* 215, 1287–1299 (2018).
86. Mankan, A. K. et al. Cytosolic RNA:DNA hybrids activate the cGAS-STING axis. *EMBO J.* 33, 2937–46 (2014).
87. Crow, Y. J. & Manel, N. Aicardi–Goutières syndrome and the type I interferonopathies. *Nat. Rev. Immunol.* 15, 429–440 (2015).
88. Crow, Y. J. et al. Mutations in genes encoding ribonuclease H2 subunits cause Aicardi–Goutières syndrome and mimic congenital viral brain infection. *Nat. Genet.* 38, 910–6 (2006).
89. Mackenzie, K. J. et al. Ribonuclease H2 mutations induce a cGAS/STING-dependent innate immune response. *EMBO J.* 35, 831–844 (2016).
90. Maelfait, J., Bridgeman, A., Benlahrech, A., Cursi, C. & Rehwinkel, J. Restriction by SAMHD1 Limits cGAS/STING-Dependent Innate and Adaptive Immune Responses to HIV-1. *Cell Rep.* 16, 1492–1501 (2016).
91. Yang, Y.-G., Lindahl, T. & Barnes, D. E. Trex1 Exonuclease Degrades ssDNA to Prevent Chronic Checkpoint Activation and Autoimmune Disease. *Cell* 131, 873–886 (2007).
92. Rice, G. I., Rodero, M. P. & Crow, Y. J. Human Disease Phenotypes Associated With Mutations in TREX1. *J. Clin. Immunol.* 35, 235–243 (2015).
93. Ablasser, A. et al. TREX1 deficiency triggers cell-autonomous immunity in a cGAS-dependent manner. *J. Immunol.* 192, 5993–7 (2014).
94. Yan, N., Regalado-Magdos, A. D., Stiggelbout, B., Lee-Kirsch, M. A. & Lieberman, J. The cytosolic exonuclease TREX1 inhibits the innate immune response to human immunodeficiency virus type 1. *Nat. Immunol.* 11, 1005–1013 (2010).
95. Gao, D. et al. Cyclic GMP-AMP synthase is an innate immune sensor of HIV and other retroviruses. *Science* 341, 903–6 (2013).
96. Stetson, D. B., Ko, J. S., Heidmann, T. & Medzhitov, R. Trex1 prevents cell-intrinsic initiation of autoimmunity. *Cell* 134, 587–98 (2008).
97. Chien, Y. et al. Control of the senescence-associated secretory phenotype by NF- κ B promotes senescence and enhances chemosensitivity. *Genes Dev.* 25, 2125–36 (2011).
98. Kang, T.-W. et al. Senescence surveillance of pre-malignant hepatocytes limits liver cancer development. *Nature* 479, 547–551 (2011).
99. Sagiv, A. & Krizhanovsky, V. Immunosurveillance of senescent cells: the bright side of the senescence program. *Biogerontology* 14, 617–628 (2013).
100. Yang, H., Wang, H., Ren, J., Chen, Q. & Chen, Z. J. cGAS is essential for cellular senescence. *Proc. Natl. Acad. Sci. U. S. A.* 114, E4612–E4620 (2017).
101. Dou, Z. et al. Cytoplasmic chromatin triggers inflammation in senescence and cancer. *Nature* 550, 402–406 (2017).
102. Comb, W. C., Cogswell, P., Sitcheran, R. & Baldwin, A. S. IKK-dependent, NF- κ B-independent control of autophagic gene expression. *Oncogene* 30, 1727–32 (2011).
103. Nassour, J. et al. Autophagic cell death restricts chromosomal instability during replicative crisis. *Nature* 53, (2019).
104. Gui, X. et al. Autophagy induction via STING trafficking is a primordial function of the cGAS pathway. *Nature* 1 (2019) doi:10.1038/s41586-019-1006-9.
105. Diamond, M. S. et al. Type I interferon is selectively required by dendritic cells for immune rejection of tumors. *J. Exp. Med.* 208, 1989–2003 (2011).
106. Fuertes, M. B. et al. Host type I IFN signals are required for antitumor CD8⁺ T cell responses through CD8 α ⁺ dendritic cells. *J. Exp. Med.* 208, 2005–16 (2011).
107. Muthuswamy, R. et al. NF- κ B hyperactivation in tumor tissues allows tumor-selective reprogramming of the chemokine microenvironment to enhance the recruitment of cytolytic T effector cells. *Cancer Res.* 72, 3735–43 (2012).
108. Woo, S.-R. et al. STING-dependent cytosolic DNA sensing mediates innate immune recognition of

- immunogenic tumors. *Immunity* 41, 830–42 (2014).
109. Ho, S. S. W. et al. The DNA Structure-Specific Endonuclease MUS81 Mediates DNA Sensor STING-Dependent Host Rejection of Prostate Cancer Cells. *Immunity* 44, 1177–89 (2016).
 110. Zhang, C. et al. STING signaling remodels the tumor microenvironment by antagonizing myeloid-derived suppressor cell expansion. *Cell Death Differ.* (2019) doi:10.1038/s41418-019-0302-0.
 111. Lam, A. R. et al. RAE1 Ligands for the NKG2D Receptor Are Regulated by STING-Dependent DNA Sensor Pathways in Lymphoma. *Cancer Res.* 74, 2193–2203 (2014).
 112. Gasser, S., Orsulic, S., Brown, E. J. & Raulet, D. H. The DNA damage pathway regulates innate immune system ligands of the NKG2D receptor. *Nature* 436, 1186–1190 (2005).
 113. Lawrence, T. & Natoli, G. Transcriptional regulation of macrophage polarization: enabling diversity with identity. *Nat. Rev. Immunol.* 11, 750–761 (2011).
 114. Wang, N., Liang, H. & Zen, K. Molecular mechanisms that influence the macrophage m1-m2 polarization balance. *Front. Immunol.* 5, 614 (2014).
 115. Aras, S. & Zaidi, M. R. TAMEless traitors: macrophages in cancer progression and metastasis. *Br. J. Cancer* 117, 1583–1591 (2017).
 116. Deng, L. et al. STING-Dependent Cytosolic DNA Sensing Promotes Radiation-Induced Type I Interferon-Dependent Antitumor Immunity in Immunogenic Tumors. *Immunity* 41, 843–852 (2014).
 117. Ablasser, A. et al. Cell intrinsic immunity spreads to bystander cells via the intercellular transfer of cGAMP. *Nature* 503, 530–4 (2013).
 118. Marcus, A. et al. Tumor-Derived cGAMP Triggers a STING-Mediated Interferon Response in Non-tumor Cells to Activate the NK Cell Response. *Immunity* 49, 754-763.e4 (2018).
 119. Sundararaman, S. K. & Barbie, D. A. Tumor cGAMP Awakens the Natural Killers. *Immunity* 49, 585–587 (2018).
 120. Chen, Q. et al. Carcinoma–astrocyte gap junctions promote brain metastasis by cGAMP transfer. *Nature* 533, 493–498 (2016).
 121. Liang, H. et al. Host STING-dependent MDSC mobilization drives extrinsic radiation resistance. *Nat. Commun.* 8, 1736 (2017).
 122. Lemos, H. et al. STING Promotes the Growth of Tumors Characterized by Low Antigenicity via IDO Activation. *Cancer Res.* 76, 2076–81 (2016).
 123. Coussens, L. M. & Werb, Z. Inflammation and cancer. *Nature* 420, 860–7 (2002).
 124. Benci, J. L. et al. Tumor Interferon Signaling Regulates a Multigenic Resistance Program to Immune Checkpoint Blockade. *Cell* 167, 1540-1554.e12 (2016).
 125. Manguso, R. T. et al. In vivo CRISPR screening identifies Ptpn2 as a cancer immunotherapy target. *Nature* 547, 413–418 (2017).
 126. Patel, S. J. et al. Identification of essential genes for cancer immunotherapy. *Nature* 548, 537–542 (2017).
 127. Bakhom, S. F. et al. Chromosomal instability drives metastasis through a cytosolic DNA response. *Nature* 553, 467–472 (2018).
 128. Krtolica, A., Parrinello, S., Lockett, S., Desprez, P. Y. & Campisi, J. Senescent fibroblasts promote epithelial cell growth and tumorigenesis: a link between cancer and aging. *Proc. Natl. Acad. Sci. U. S. A.* 98, 12072–7 (2001).
 129. Liu, D. & Hornsby, P. J. Senescent Human Fibroblasts Increase the Early Growth of Xenograft Tumors via Matrix Metalloproteinase Secretion. *Cancer Res.* 67, 3117–3126 (2007).
 130. Orimo, A. et al. Stromal Fibroblasts Present in Invasive Human Breast Carcinomas Promote Tumor Growth and Angiogenesis through Elevated SDF-1/CXCL12 Secretion. *Cell* 121, 335–348 (2005).
 131. Begley, L., Monteleon, C., Shah, R. B., Macdonald, J. W. & Macoska, J. A. CXCL12 overexpression and secretion by aging fibroblasts enhance human prostate epithelial proliferation in vitro. *Aging Cell* 4, 291–8 (2005).
 132. Milanovic, M. et al. Senescence-associated reprogramming promotes cancer stemness. *Nature* 553, 96–100 (2018).
 133. Demaria, M. et al. Cellular Senescence Promotes Adverse Effects of Chemotherapy and Cancer Relapse. *Cancer Discov.* 7, 165–176 (2017).

134. Liu, H. et al. Nuclear cGAS suppresses DNA repair and promotes tumorigenesis. *Nature* (2018) doi:10.1038/s41586-018-0629-6.
135. Jiang, H. et al. The innate immune DNA sensor cGAS is a negative regulator of DNA repair hence promotes genome instability and cell death. *bioRxiv* 465401 (2018) doi:10.1101/465401.
136. Gisselsson, D. et al. Abnormal nuclear shape in solid tumors reflects mitotic instability. *Am. J. Pathol.* 158, 199–206 (2001).
137. Ng, K. W., Marshall, E. A., Bell, J. C. & Lam, W. L. cGAS–STING and Cancer: Dichotomous Roles in Tumor Immunity and Development. *Trends Immunol.* 39, 44–54 (2018).
138. Xia, T., Konno, H., Ahn, J. & Barber, G. N. Deregulation of STING Signaling in Colorectal Carcinoma Constrains DNA Damage Responses and Correlates With Tumorigenesis. *Cell Rep.* 14, 282–97 (2016).
139. Xia, T., Konno, H. & Barber, G. N. Recurrent Loss of STING Signaling in Melanoma Correlates with Susceptibility to Viral Oncolysis. *Cancer Res.* 76, 6747–6759 (2016).
140. Konno, H. et al. Suppression of STING signaling through epigenetic silencing and missense mutation impedes DNA damage mediated cytokine production. *Oncogene* 37, 2037–2051 (2018).
141. Sato, H. et al. DNA double-strand break repair pathway regulates PD-L1 expression in cancer cells. *Nat. Commun.* 8, 1751 (2017).
142. Jain, M. et al. Sustained loss of a neoplastic phenotype by brief inactivation of MYC. *Science* 297, 102–4 (2002).
143. Zeng, M. et al. Targeting MYC dependency in ovarian cancer through inhibition of CDK7 and CDK12/13. *Elife* 7, 1–20 (2018).
144. Horiuchi, D. et al. MYC pathway activation in triple-negative breast cancer is synthetic lethal with CDK inhibition. *J. Exp. Med.* 209, 679–96 (2012).
145. Kortlever, R. M. et al. Myc Cooperates with Ras by Programming Inflammation and Immune Suppression. *Cell* 171, 1301–1315.e14 (2017).
146. Rakhra, K. et al. CD4(+) T cells contribute to the remodeling of the microenvironment required for sustained tumor regression upon oncogene inactivation. *Cancer Cell* 18, 485–98 (2010).
147. Casey, S. C. et al. MYC regulates the antitumor immune response through CD47 and PD-L1. *Science* 352, 227–31 (2016).
148. Hänggi, K. & Ruffell, B. Oncogenic KRAS Drives Immune Suppression in Colorectal Cancer. *Cancer Cell* 35, 535–537 (2019).
149. Lau, A., Gray, E. E., Brunette, R. L. & Stetson, D. B. DNA tumor virus oncogenes antagonize the cGAS-STING DNA-sensing pathway. *Science* (80-.). 350, 568–571 (2015).
150. Davoli, T., Uno, H., Wooten, E. C. & Elledge, S. J. Tumor aneuploidy correlates with markers of immune evasion and with reduced response to immunotherapy. *Science* (80-.). 355, (2017).
151. Budczies, J. et al. Integrated analysis of the immunological and genetic status in and across cancer types: impact of mutational signatures beyond tumor mutational burden. *Oncoimmunology* 7, e1526613 (2018).
152. Karantza-Wadsworth, V. et al. Autophagy mitigates metabolic stress and genome damage in mammary tumorigenesis. *Genes Dev.* 21, 1621–35 (2007).
153. Mathew, R. et al. Autophagy suppresses tumor progression by limiting chromosomal instability. *Genes Dev.* 21, 1367–81 (2007).
154. Vanpouille-Box, C. et al. DNA exonuclease Trex1 regulates radiotherapy-induced tumour immunogenicity. *Nat. Commun.* 8, 15618 (2017).
155. Lewis, C. W. & Golsteyn, R. M. Cancer cells that survive checkpoint adaptation contain micronuclei that harbor damaged DNA. *Cell Cycle* 15, 3131–3145 (2016).
156. Hermine, T., Jones, N. J. & Parry, J. M. Comparative induction of micronuclei in repair-deficient and -proficient Chinese hamster cell lines following clastogen or aneugen exposures. *Mutat. Res.* 392, 151–63 (1997).
157. Kubara, P. M. et al. Human cells enter mitosis with damaged DNA after treatment with pharmacological concentrations of genotoxic agents. *Biochem. J.* 446, 373–81 (2012).
158. Khodarev, N. N. et al. STAT1 is overexpressed in tumors selected for radioresistance and confers

- protection from radiation in transduced sensitive cells. *Proc. Natl. Acad. Sci. U. S. A.* 101, 1714–9 (2004).
159. Sistigu, A. et al. Cancer cell-autonomous contribution of type I interferon signaling to the efficacy of chemotherapy. *Nat. Med.* 20, 1301–9 (2014).
 160. Burnette, B. C. et al. The efficacy of radiotherapy relies upon induction of type I interferon-dependent innate and adaptive immunity. *Cancer Res.* 71, 2488–96 (2011).
 161. Salvagno, C. et al. Therapeutic targeting of macrophages enhances chemotherapy efficacy by unleashing type I interferon response. *Nat. Cell Biol.* 21, 511–521 (2019).
 162. Mitchison, T. J., Pineda, J., Shi, J. & Florian, S. Is inflammatory micronucleation the key to a successful anti-mitotic cancer drug? *Open Biol.* 7, 170182 (2017).
 163. ordan, M. A. et al. Mitotic block induced in HeLa cells by low concentrations of paclitaxel (Taxol) results in abnormal mitotic exit and apoptotic cell death. *Cancer Res.* 56, 816–25 (1996).
 164. Shi, J., Orth, J. D. & Mitchison, T. Cell Type Variation in Responses to Antimitotic Drugs that Target Microtubules and Kinesin-5. *Cancer Res.* 68, 3269–3276 (2008).
 165. Lord, C. J. & Ashworth, A. PARP inhibitors: Synthetic lethality in the clinic. *Science* (80-.). 355, 1152–1158 (2017).
 166. Ding, L. et al. PARP Inhibition Elicits STING-Dependent Antitumor Immunity in Brca1-Deficient Ovarian Cancer. *Cell Rep.* 25, 2972-2980.e5 (2018).
 167. Jiao, S. et al. PARP Inhibitor Upregulates PD-L1 Expression and Enhances Cancer-Associated Immunosuppression. *Clin. Cancer Res.* 23, 3711–3720 (2017).
 168. Shen, J. et al. PARPi Triggers the STING-Dependent Immune Response and Enhances the Therapeutic Efficacy of Immune Checkpoint Blockade Independent of BRCAness. *Cancer Res.* 79, 311–319 (2019).
 169. Pantelidou, C. et al. PARP inhibitor efficacy depends on CD8+ T cell recruitment via intratumoral STING pathway activation in BRCA-deficient models of triple-negative breast cancer. (2019) doi:10.1158/2159-8290.CD-18-1218.
 170. Weichselbaum, R. R. et al. An interferon-related gene signature for DNA damage resistance is a predictive marker for chemotherapy and radiation for breast cancer. *Proc. Natl. Acad. Sci.* 105, 18490–18495 (2008).
 171. Boelens, M. C. et al. Exosome Transfer from Stromal to Breast Cancer Cells Regulates Therapy Resistance Pathways. *Cell* 159, 499–513 (2014).
 172. Legrier, M.-E. et al. Activation of IFN/STAT1 signalling predicts response to chemotherapy in oestrogen receptor-negative breast cancer. *Br. J. Cancer* 114, 177–87 (2016).
 173. Conlon, J. et al. Mouse, but not Human STING, Binds and Signals in Response to the Vascular Disrupting Agent 5,6-Dimethylxanthenone-4-Acetic Acid. *J. Immunol.* 190, 5216–5225 (2013).
 174. Kim, S. et al. Anticancer Flavonoids Are Mouse-Selective STING Agonists. *ACS Chem. Biol.* 8, 1396–1401 (2013).
 175. Corrales, L. et al. Direct Activation of STING in the Tumor Microenvironment Leads to Potent and Systemic Tumor Regression and Immunity. *Cell Rep.* 11, 1018–1030 (2015).
 176. Demaria, O. et al. STING activation of tumor endothelial cells initiates spontaneous and therapeutic antitumor immunity. *Proc. Natl. Acad. Sci.* 112, 15408–15413 (2015).
 177. Sivick, K. E. et al. Magnitude of Therapeutic STING Activation Determines CD8+ T Cell-Mediated Antitumor Immunity. *Cell Rep.* 25, 3074-3085.e5 (2018).
 178. Cheng, N. et al. A nanoparticle-incorporated STING activator enhances antitumor immunity in PD-L1–insensitive models of triple-negative breast cancer. *JCI Insight* 3, (2018).
 179. Grabosch, S. et al. Cisplatin-induced immune modulation in ovarian cancer mouse models with distinct inflammation profiles. *Oncogene* 1 (2018) doi:10.1038/s41388-018-0581-9.
 180. Wang, H. et al. cGAS is essential for the antitumor effect of immune checkpoint blockade. *Proc. Natl. Acad. Sci. U. S. A.* 114, 1637–1642 (2017).
 181. Mouw, K. W. & Konstantinopoulos, P. A. From checkpoint to checkpoint: DNA damage ATR/Chk1 checkpoint signalling elicits PD-L1 immune checkpoint activation. *Br. J. Cancer* 118, 933–935 (2018).
 182. Wang, J., Yi, S., Zhou, J., Zhang, Y. & Guo, F. The NF-κB subunit RelB regulates the migration and invasion abilities and the radio-sensitivity of prostate cancer cells. *Int. J. Oncol.* 49, 381–92 (2016).

Progression through mitosis promotes PARP inhibitor-induced cytotoxicity in homologous recombination-deficient cancer cells

Pepijn M. Schoonen¹, Francien Talens^{1,*}, Colin Stok^{1,*}, Ewa Gogola², Anne Margriet Heijink¹, Peter Bouwman², Floris Foijer³, Madalena Tarsounas⁴, Sohvi Blatter⁵, Jos Jonkers², Sven Rottenberg⁵ & Marcel A.T.M. van Vugt¹

¹ Department of Medical Oncology, University Medical Center Groningen, University of Groningen, Groningen, The Netherlands.

² Division of Molecular Pathology and Cancer Genomics Netherlands, The Netherlands Cancer Institute, Amsterdam, The Netherlands.

³ European Research Institute for the Biology of Ageing, University of Groningen University Medical Center Groningen, Groningen, The Netherlands.

⁴ The CRUK/MRC Oxford Institute, Old Road Campus Research Building, Oxford, United Kingdom.

⁵ Institute of Animal Pathology, Vetsuisse Faculty, University of Bern, Bern, Switzerland.

* These authors contributed equally

Nature communications (2017) 17;8:15981

Abstract

Mutations in homologous recombination (HR) genes *BRCA1* and *BRCA2* predispose to tumorigenesis. HR-deficient cancers are hypersensitive to Poly (ADP ribose)-polymerase (PARP) inhibitors but can acquire resistance and relapse. Mechanistic understanding of how PARP inhibition induces cytotoxicity in HR-deficient cancer cells is incomplete. Here we find PARP inhibition to compromise replication fork stability in HR-deficient cancer cells, leading to mitotic DNA damage and consequent chromatin bridges and lagging chromosomes in anaphase, frequently leading to cytokinesis failure, multinucleation, and cell death. PARP-inhibitor-induced multinucleated cells fail clonogenic outgrowth, and high percentages of multinucleated cells are found in vivo in remnants of PARP inhibitor-treated *Brca2*^{-/-}; *p53*^{-/-} and *Brca1*^{-/-}; *p53*^{-/-} mammary mouse tumours, suggesting that mitotic progression promotes PARP-inhibitor-induced cell death. Indeed, enforced mitotic bypass through *EMI1* depletion abrogates PARP-inhibitor-induced cytotoxicity. These findings provide insight into the cytotoxic effects of PARP inhibition and point at combination therapies to potentiate PARP inhibitor treatment of HR-deficient tumours.

BRCA1 and *BRCA2* function in the repair of DNA double-strand breaks (DSBs) through homologous recombination (HR), and ensure the protection of stalled replication forks¹. Defective HR is thought to underlie the progressive accumulation of genomic aberrations, leading to malignant transformation. Indeed, mutations in *BRCA1* and *BRCA2* predispose to tumorigenesis, most frequently involving breast and ovarian cancer²⁻⁴. Due to their DNA repair defect, *BRCA1/2* mutant cancer cells are more sensitive to platinum-based chemotherapeutics, as observed in preclinical models and clinical studies⁵⁻⁷. In addition, *BRCA1/2* mutant cancers were found to be selectively sensitive to inhibition of the poly-(ADP)ribose polymerase *PARP1*⁷⁻⁹. Unfortunately, however, *BRCA1/2* mutant cancers can acquire resistance and relapse¹⁰.

Mechanistically, *PARP1* promotes the repair of non-toxic single-strand DNA breaks¹¹, which are converted into potentially toxic DSBs during S-phase^{8,9}. These DSBs depend on HR for repair and hence were suggested to cause cell death in HR-defective cancer cells. However, the number of single-strand DNA breaks was not found to be increased after *PARP1* depletion or *PARP* inhibition¹¹⁻¹³, and the synthetic lethal interaction between *PARP* inhibition and HR deficiency may therefore involve other mechanisms^{14,15}. Indeed, *PARP1* and *BRCA1/2* were shown to orchestrate the protection and restart of stalled replication forks¹⁶⁻²⁰. Analogously, *PARP1* activity increases during replication²¹, and sensitivity to *PARP* inhibition in *BRCA2* mutant cancer cells can be rescued by mutations that prevent replication fork degradation²². Notably, aberrant replication intermediates may persist in G2-phase, and can even be propagated into mitosis²³⁻²⁷, and cause mitotic aberrancies²⁸⁻³⁰. Whether DNA lesions induced by *PARP* inhibition in HR-deficient cells persist into mitosis, and if they affect cell division remains unclear.

Here, we study the mechanisms by which *PARP*-inhibitor-induced DNA lesions affect mitotic progression. We describe that *PARP* inhibition compromises replication fork stability and leads to DNA lesions that are transmitted into mitosis. During mitosis, these DNA lesions cause chromatin bridges and lead to cytokinesis failure, multinucleation, and cell death. Importantly, our data show that progression through mitosis promotes *PARP*-inhibitor-induced cell death, since forced mitotic bypass abrogates *PARP*-inhibitor-induced cytotoxicity.

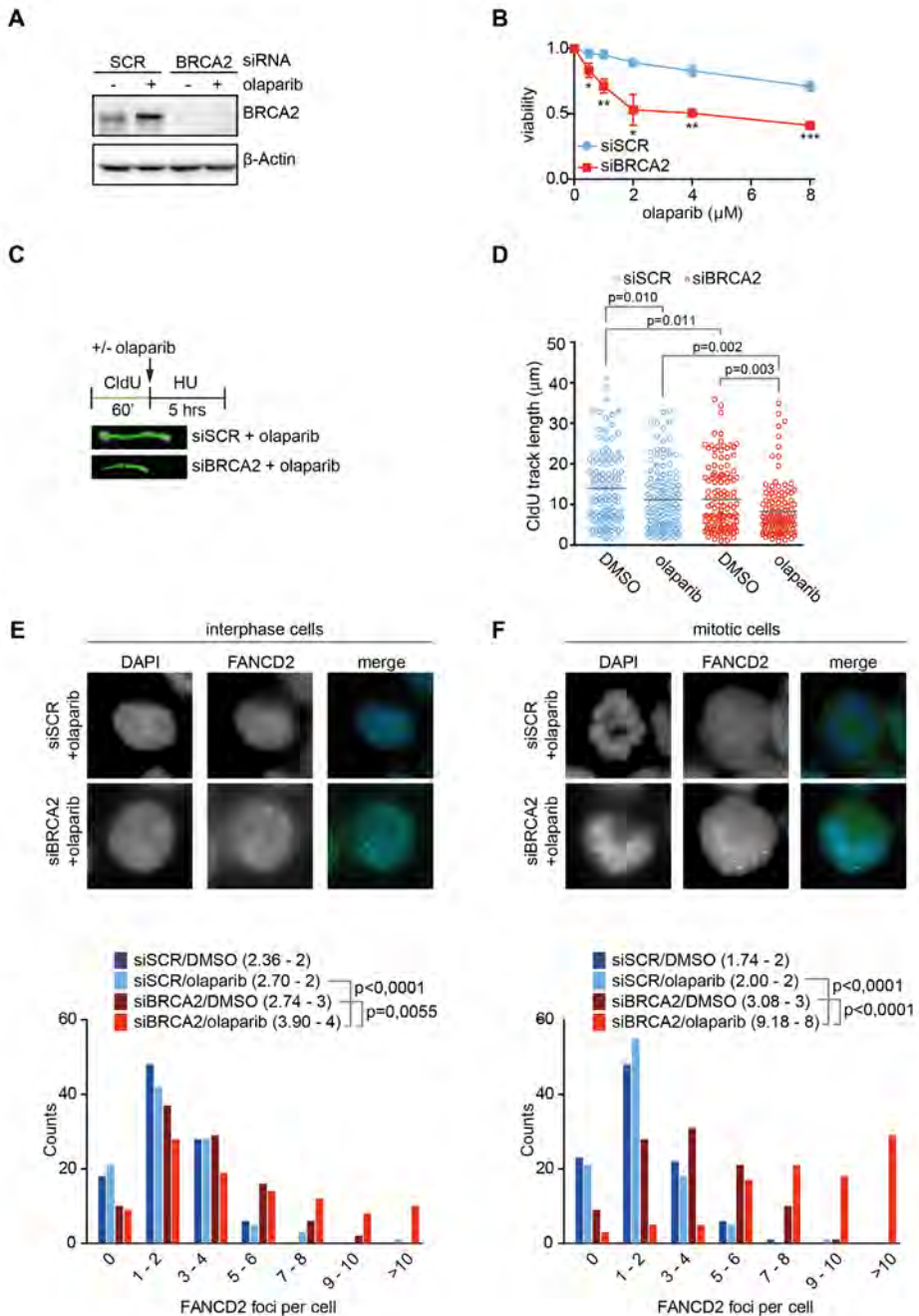


Figure 1. PARP-inhibitor-induced lesions are transmitted into mitosis. A) Immunoblotting of BRCA2 and β -Actin at 48 h after transfection of indicated siRNAs in HeLa cells. Lines next to blots indicate positions of molecular weight markers. **B)** HeLa cells were transfected with indicated siRNAs for 24 h and subsequently replated and treated with indicated olaparib concentrations for 72 h. Viability

was assessed by MTT conversion. Shown graphs are representative of three independent experiments, with three technical replicates each. *P* values were calculated using two-tailed Student's *t*-test. 'NS' indicates not significant. * indicates *P*0.05, ** indicates *P*0.01, *** indicates *P*0.001. **C**) HeLa cells were transfected with indicated siRNAs and labelled with CldU as indicated. Cells were then treated with HU (5mM) and DMSO or olaparib (0.5 mM) for 5 h. The DNA was spread into single fibres and CldU track length was determined (125 fibres per condition). **D**) Quantification of fibre lengths described in c. *P* values were calculated using two-tailed Mann–Whitney test. **E,F**) HeLa cells were transfected with siRNA targeting BRCA2 and treated with DMSO or olaparib (0.5 mM) for 24 h. Cells were stained for FANCD2 (green) and counterstained with DAPI (blue) and the number of FANCD2 foci per nuclei were quantified for interphase cells (E) and mitotic cells (F). Per condition n/100 nuclei were analysed. Indicated numbers between brackets represent (average—median) from three independent experiments. *P* values were calculated using two-tailed Mann–Whitney test. Throughout the figure 'NS' indicates not significant. All error bars indicate s.d. of three independent experiments.

Results

PARP-inhibitor-induced lesions are transmitted into mitosis

To explore the consequences of PARP inhibition on mitotic progression in HR-defective cancer cells, we depleted BRCA2 in HeLa cells (**Fig. 1A**). As expected, treatment with the PARP inhibitor olaparib resulted in the selective killing of BRCA2-depleted cells (**Fig. 1B**). In line with roles for BRCA2 and PARP in facilitating replication fork stability²², we observed compromised replication fork protection using single DNA fiber analysis upon BRCA2 depletion, which was aggravated upon PARP inhibition (**Fig. 1C,D**). These findings show that PARP inhibition in BRCA2-deficient cancer cells incrementally interferes with replication fork stability. In line with previous studies showing the involvement of Mre11 and PTIP in the degradation of stalled replication fork in BRCA2-deficient cells, Mre11 inhibition using mirin or PTIP depletion alleviated the fork protection defects (**Supplementary Fig. 1A,B**)^{20,22}.

Defective replication fork stability upon PARP inhibition was further underscored by the increase in FANCD2 foci in interphase cells upon BRCA2 depletion. A significant further increase was observed when BRCA2-depleted cells were treated with a PARP inhibitor (**Fig. 1E**). Surprisingly, the increase in FANCD2 foci was only accompanied by minor increases in the numbers of γ -H2AX foci in interphase, suggesting that replication lesions do not per se result in DNA breaks (**Supplementary Fig. 1C**).

The observed replication lesions were not resolved before mitotic entry, as increased numbers of FANCD2 foci were observed in BRCA2-depleted mitotic cells (**Fig. 1F**). Again, the numbers of FANCD2 foci increased further upon PARP inhibitor treatment (**Fig. 1F**). Of note, in PARP inhibitor-treated, BRCA2-depleted mitotic cells, numbers of γ -H2AX foci were increased similarly to FANCD2 foci (**Supplementary Fig. 1D**). Combined, these data show that PARP inhibition in BRCA2-defective cells leads to replication intermediates that are transmitted into mitosis.

PARP inhibition causes mitotic chromatin bridges

Since the persistence of unresolved replication intermediates into mitosis may interfere with proper chromosome segregation, we tested whether PARP inhibition-induced mitotic aberrancies. Whereas PARP inhibition did not affect the percentages of anaphase or telophase cells containing chromatin bridges in control cells, depletion of BRCA2 in HeLa cells led to an increased percentage of cells showing chromatin bridge formation, which remained unresolved up until telophase (14 and 17% in BRCA2-depleted cells versus 2% in control-depleted cells) (**Fig. 2A,B**), in line with previous observations³¹. Strikingly, the number of BRCA2-depleted cells containing anaphase chromatin bridges markedly increased upon olaparib treatment (59 and 65% in BRCA2-depleted, olaparib-treated cells versus 20%

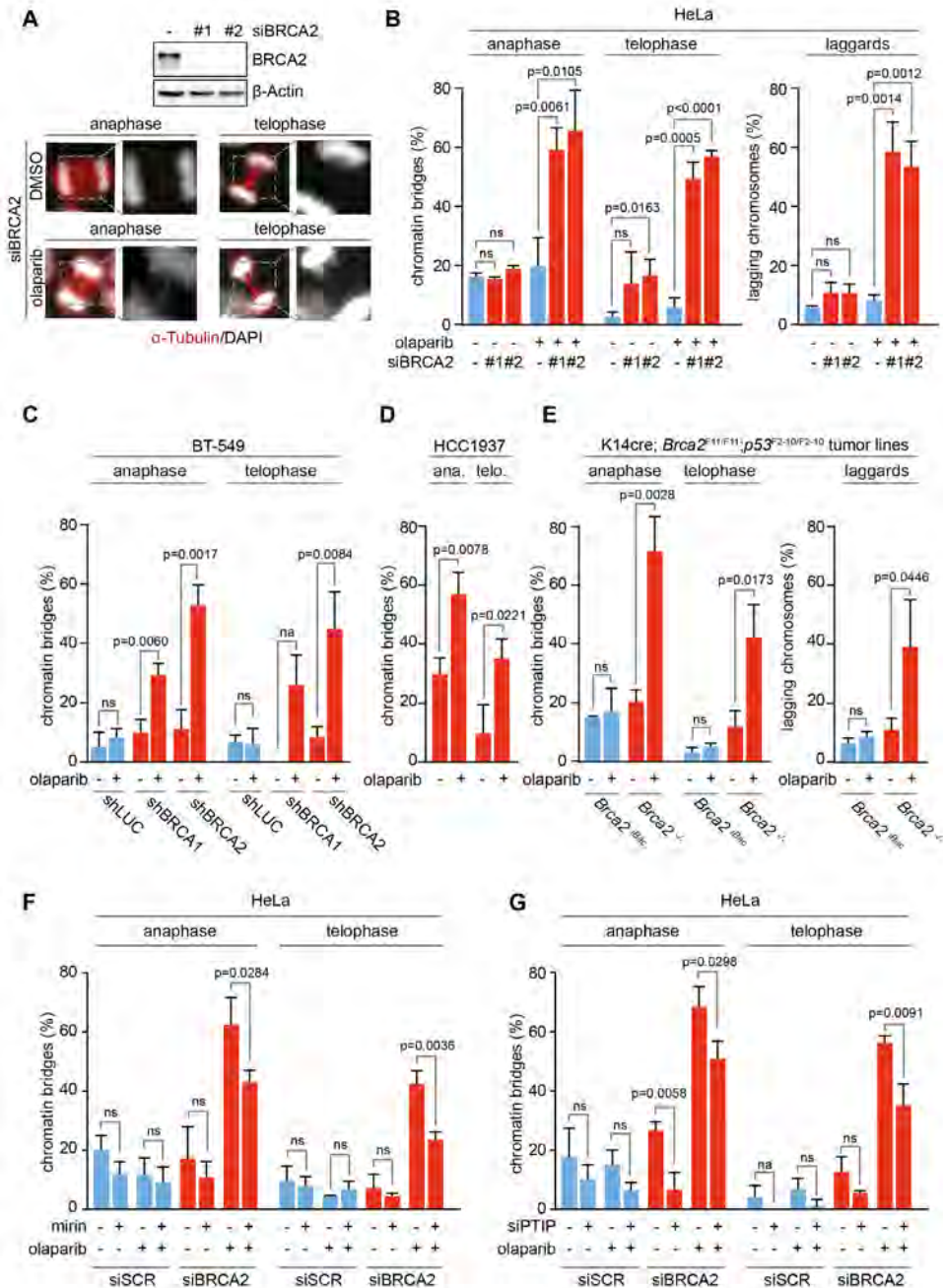


Figure 2. PARP inhibition causes mitotic chromatin bridges. Throughout the figure blue bars represent BRCA1/2 proficient cells, red bars represent BRCA1/2 deficient cells, and P values were calculated using two-tailed Student's t-test. **A)** HeLa cells were transfected with indicated siRNAs and immunoblotted for BRCA2 and β -Actin levels after 48 h. Lines next to blots indicate positions of molecular weight markers. In parallel, cells were treated with DMSO or olaparib (0.5 mM) for 24 h and stained for α -Tubulin (red)

and counterstained with DAPI (white). Representative immunofluorescence images are presented. Scale bars represent 5 μ m. **B)** HeLa cells were treated as for a. The percentages of cells containing chromatin bridges (n420 events per condition) and lagging chromosomes (n440 events per condition) were quantified. **C)** BT-549 cells harbouring indicated shRNA vectors were pretreated with doxycycline for 48 h and treated with olaparib (0.5 mM) or DMSO for 24 h. Percentages of cells containing chromatin bridges in anaphase and telophase (n420 events per condition) were quantified. **D)** HCC1937 cells were treated with olaparib (0.5 mM) or DMSO for 24 h. Percentages of anaphase (ana.) or telophase (telo.) cells containing chromatin bridges (n420 events per condition) were quantified. **E)** KB2P1.21 (*Brca2*) and KB2P1.21R1 (*Brca2iBac*) cells were treated with olaparib (0.5 mM) or DMSO for 24 h. Percentages of anaphase or telophase cells containing chromatin bridges (left panel, n420 events per condition) and cells containing lagging chromosomes (right panel, n440 events per condition) were quantified. **F,G)** HeLa cells were transfected with indicated siRNAs and after 24 h were treated with olaparib (0.5 mM) or DMSO and/or mirin (50 mM) for 24 h. The percentages of anaphase or telophase cells containing chromatin bridges (n420 events per condition) were quantified. Throughout the figure 'NS' indicates not significant and 'NA' indicates not analysable. All error bars indicate s.d. of three independent experiments.

in control-depleted cells treated with olaparib) (**Fig. 2A,B**). Interestingly, whereas most of the olaparib-induced chromatin bridges were resolved before telophase in control cells, chromatin bridges persisted throughout mitosis in BRCA2-depleted cells (49 and 57% in BRCA2-depleted cells versus 6% in control-depleted cells) (**Fig. 2B**). Furthermore, PARP inhibition also markedly increased the numbers of lagging chromosomes in BRCA2-depleted cells (58 and 53% in BRCA2-depleted cells versus 8% in control-depleted cells) (**Fig. 2B**, right panel).

These observations were not specific for BRCA2, as depletion of BRCA1 (**Supplementary Fig. 2A,B**) or RAD51 (**Supplementary Fig. 2C,D**) also showed a clear induction of PARP-inhibitor-induced chromatin bridges persisting throughout mitosis. Notably, BRCA1 or RAD51 depletion in HeLa cells also increased the number of lagging chromosomes upon PARP inhibition, although to a lesser extent in BRCA1-depleted cells when compared to RAD51 or BRCA2-depleted cells (**Fig. 2B**, right panel and **Supplementary Fig. 2B,D**, right panels). Similar results were obtained upon depletion of BRCA1 or BRCA2 in BT-549 breast cancer cells treated with olaparib. Specifically, PARP inhibitor sensitivity greatly increased upon doxycycline-induced shRNAs depletion of BRCA1 or BRCA2 (**Supplementary Fig. 2E,F**). Importantly, the numbers of unresolved chromosome bridges (**Fig. 2C**), and lagging chromosomes (**Supplementary Fig. 2G**) increased significantly in BRCA1/2-depleted BT-549 cells upon olaparib treatment.

We next investigated whether permanent genetic inactivation of BRCA1 shows a similar increase in the number of mitotic chromatin bridges when compared to acute siRNA-mediated BRCA2/BRCA1 inactivation. Indeed, the human HCC1937 breast cancer cell line, harbouring a *BRCA1* deletion as well as a hypomorphic BRCA1 allele with a 5382insC frameshift mutation, showed increased chromatin bridges in anaphase and telophase upon olaparib treatment (**Fig. 2D**), as well as lagging chromosomes (**Supplementary Fig. 2H**). To validate these results using isogenic models, we next used a tumour cell line derived from a *K14cre;Brca2^{del/del};p53^{del/del}* mouse mammary tumour (denoted as *Brca2^{-/-}*)³². As a control, we used an isogenic cell line in which BRCA2 was reconstituted using an infectious bacterial artificial chromosome (iBAC), harbouring the mouse *Brca2* gene (denoted as *Brca2^{iBAC}*)³³. *Brca2^{iBAC}* expression functionally restored BRCA2 function as judged by irradiation-induced foci formation of RAD51 (**Supplementary Fig. 3A**), and rescue from PARP inhibitor sensitivity (**Supplementary Fig. 3B**).

In accordance with our observations after transient BRCA2 depletion, PARP inhibition in *Brca2^{-/-}* cells resulted in an increased percentage of cells harbouring chromatin bridges in anaphase (71% in *Brca2^{-/-}* cells versus 17% in *Brca2^{iBAC}* cells), which to a large degree remained unresolved until telophase (42% in *Brca2^{-/-}* cells versus 5% in *Brca2^{iBAC}* cells) (**Fig. 2E**, left panel).

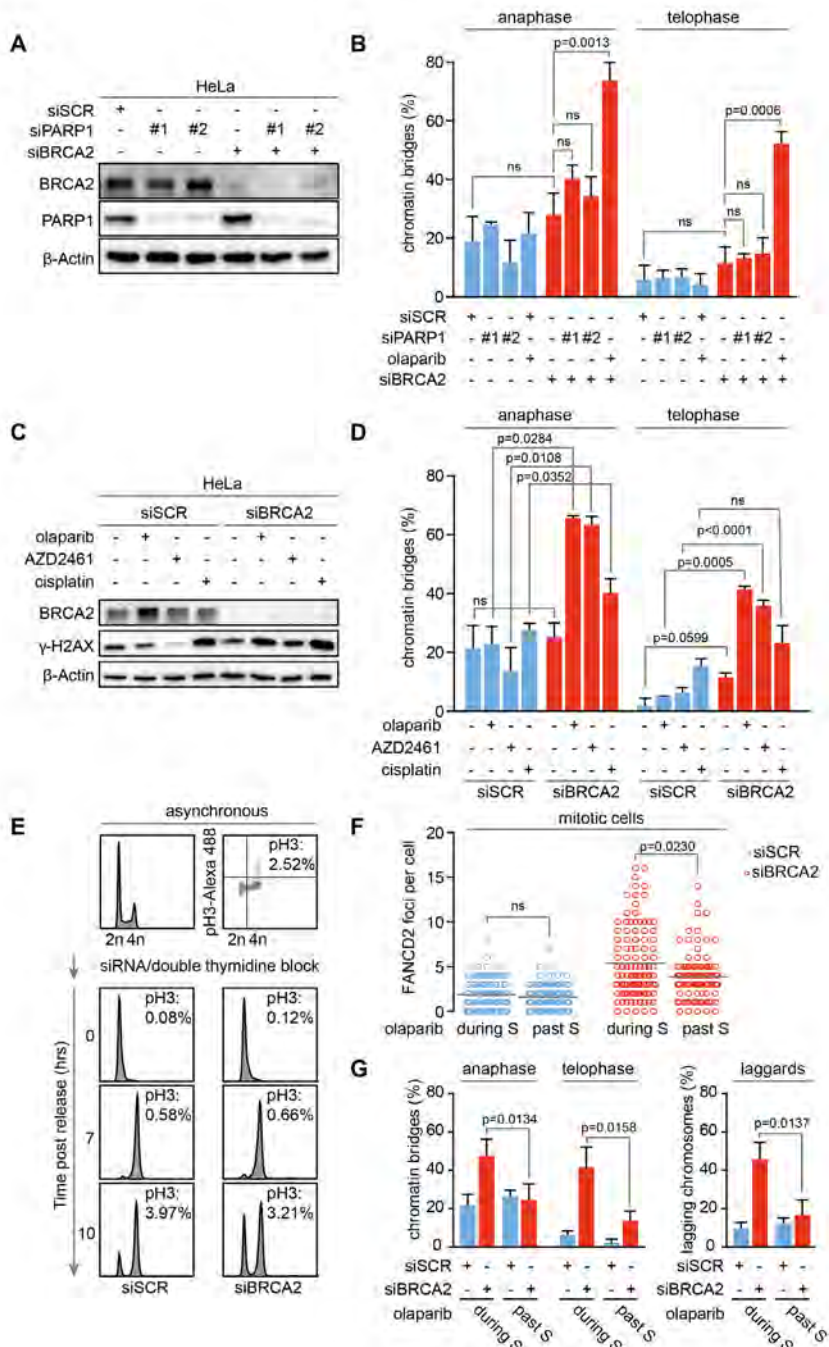


Figure 3. PARP trapping during S-phase is required for mitotic chromatin bridge formation. Throughout the figure blue bars represent BRCA1/2 proficient cells, red bars represent BRCA1/2 deficient cells. **A)** HeLa cells were transfected with indicated siRNAs, and immunoblotting for BRCA2, PARP1 and b-Actin

was done at 48 h after transfection. Lines next to blots indicate positions of molecular weight markers. **B)** HeLa cells were transfected with indicated siRNAs and after 24 h were treated with olaparib (0.5 mM) or DMSO for 24 h. Percentages of cells containing chromatin bridges (n420 events per condition) were quantified. *P* values were calculated using two-tailed Student's *t*-test. **C)** HeLa cells were transfected with indicated siRNAs, and after 24 h were treated with olaparib (0.5 mM), AZD2461 (1 mM), cisplatin (1 mM) or DMSO for another 24 h. Immunoblotting was performed for BRCA2, γ -H2AX and b-Actin **D)** HeLa cells were treated as for B. Percentages of cells containing chromatin bridges (n420 events per condition) were quantified. *P* values were calculated using two-tailed Student's *t*-test. **E-G)** HeLa cells were transfected with indicated siRNAs and after 24 h were synchronized in the G1/S-phase border by a double-thymidine block. Cells were either treated with 0.5 mM olaparib for 3 h directly after release from the thymidine block ('during S' treatment) or 7 h after release ('past S' treatment). Representative flow cytometry images are presented (E). Cells were then fixed and assessed for mitotic FANCD2 foci (F), chromatin bridges and lagging chromosomes (G). *P* values for FANCD2 foci were calculated using the two-tailed Mann–Whitney test. The number of cells containing chromatin bridges (n420 events per condition) and lagging chromosomes (n440 events per condition) were quantified. *P* values were calculated using two-tailed Student's *t*-test. Throughout the figure 'NS' indicates not significant. All error bars indicate s.d. of three independent experiments.

Again, also the percentage of cells with lagging chromosomes was increased (39% versus 8% in *Brca2*^{-/-} and *Brca2*^{2^{BAC}} cells, respectively) (**Fig. 2E**, right panel). These observations again likely reflected generic consequences of defective HR, as very similar defects were observed in a tumour cell line derived from *K14cre;Brca1*^{F5-13/F5-13};*p53*^{F2-10/F2-10} mice (**Supplementary Fig. 3C**). These observations were further validated in DLD-1 human colorectal adenocarcinoma cells, in which *BRCA2* was inactivated using CRISPR-Cas9. In complete accordance to what was observed in mouse *Brca2*-null cells, *BRCA2*^{-/-} DLD-1 cells were sensitive to PARP inhibition (**Supplementary Fig. 3D**), and PARP inhibition greatly enhanced the formation of chromatin bridges as well as lagging chromosomes in *BRCA2*^{-/-}, but not in *BRCA2*^{+/+} DLD-1 cells (**Supplementary Fig. 3E**). Combined, these findings indicate that PARP inhibition induces mitotic defects when HR is inactivated acutely or permanently, in a species-independent fashion.

Since the formation of mitotic chromatin bridges and lagging chromosomes in HR-deficient cancer cells are a likely consequence of disturbed replication fork integrity, we tested the involvement of Mre11 and PTIP. Mre11 inhibition or PTIP depletion, which alleviated the PARP-inhibitor-induced replication fork instability (**Supplementary Fig. 1A,B**), also reduced the amounts of mitotic chromatin bridges (**Fig. 2F,G**). These findings further corroborate that aberrant control of replication fork stability underlies PARP-inhibitor-induced chromosome bridge formation in mitosis. Notably, the number of lagging chromosomes was not reduced upon Mre11 or PTIP inactivation, suggesting different biological origins of these lesions (**Supplementary Fig. 3F,G**).

PARP trapping is required for chromatin bridge formation

Cytotoxicity of PARP inhibitors was previously associated with the ability of PARP inhibitor to trap PARP onto DNA, rather than its effects on PARP catalytic activity¹⁵. To test whether PARP trapping is required for the observed mitotic defects, we depleted PARP1 using siRNA (**Fig. 3A**). In contrast to treatment with olaparib, a PARP inhibitor which has trapping activity, depletion of PARP1 did not significantly induce mitotic chromatin bridges, nor lagging chromosomes in BRCA2-depleted cells (**Fig. 3B** and **Supplementary Fig. 4A**). Also, very similar levels of mitotic chromatin bridges and lagging chromosomes were observed in response to the structurally unrelated PARP inhibitor AZD2461 (**Fig. 3C,D** and **Supplementary Fig. 4B**). Of note, the observed increase in chromosome bridges in PARP inhibitor-treated cells was much more pronounced when compared to cisplatin treatment, at a dose that efficiently caused DNA breaks as judged by γ -H2AX (**Fig. 3C,D**).

Since PARP is involved in multiple cellular processes, we next tested whether the

PARP-inhibitor-induced mitotic defects required treatment during S-phase. To this end, cells were synchronized at the G1/S-phase of the cell cycle using a double-thymidine block (**Fig. 3E**). Cells treated during S-phase displayed significantly increased numbers of mitotic cells with FANCD2 foci (**Fig. 3F**), chromosome bridges as well as lagging chromosomes (**Fig. 3G**). In line with expectations, BRCA2-depleted cells with chromosome bridges also contained higher numbers of mitotic FANCD2 foci, when compared to cells without chromosome bridges (**Supplementary Fig. 4C**). Importantly, when cells were treated with olaparib past S-phase (at 7h after release from thymidine block), the number of FANCD2 foci in mitotic cells (**Fig. 3F**), chromosome bridges as well as lagging chromosomes (**Fig. 3G**) was significantly reduced. Taken together, these data show that PARP trapping during S-phase is required for the induction of mitotic chromosome bridges.

Chromatin bridges cause multinucleation and cell death

Unresolved chromatin bridges can cause genomic aberrations, multinucleation, and cell death. To investigate the consequences of PARP-inhibitor-induced chromatin bridges for HR-deficient cells, live-cell imaging was used in combination with the stable expression of fluorescently tagged Histone-H2B to visualize chromosome dynamics (**Fig. 4A**). Although some chromatin bridge events were observed in DMSO-treated control cells, the majority of mitoses proceeded either without any visible chromatin bridges (cells with chromatin bridge: 24%) or with chromatin bridges that were resolved during mitosis (6%) (**Fig. 4B**). Very comparable results were found for control-depleted cells treated with a PARP inhibitor (chromatin bridge: 32%; resolved bridge: 14%), or BRCA2-depleted cells treated with DMSO (chromatin bridge: 26%; resolved bridge: 12%) (**Fig. 4B**). In stark contrast, the number of aberrant mitoses was strongly increased in BRCA2-depleted cells treated with a PARP inhibitor (chromatin bridge: 64%; resolved bridge: 13%) (**Fig. 4B and Supplementary Fig. 5A**). Furthermore, in a large fraction of BRCA2-depleted cells, unresolved mitotic chromatin bridges resulted in failed cytokinesis leading to multinucleation (29% of total mitoses) or were followed by cell death, (22% of total mitoses), indicating that mitotic failure following PARP inhibitor treatment is often detrimental for BRCA2-deficient cells (**Fig. 4B and Supplementary Fig. 5A**).

Similar phenotypes were observed in *Brca2*-null mouse mammary tumour cells, expressing GFP-tagged Histone-H2B and mCherry-tagged α -Tubulin (**Fig. 4C**). Again, PARP inhibitor treatment of *Brca2*-null mouse cells greatly enhanced the number of cells with chromatin bridges (82% versus 22% in *Brca2*^{-/-} and *Brca2*^{iBAC}, respectively, **Fig. 4C**). Furthermore, most of the chromatin bridges in *Brca2*^{-/-} cells were not resolved during mitosis and lead to cytokinesis failure, accompanied with multinucleation (32% versus 5% in *Brca2*^{-/-} and *Brca2*^{iBAC}, respectively), or cell death (16% versus 1% in *Brca2*^{-/-} and *Brca2*^{iBAC}, respectively) (**Fig. 4C**). These effects were not caused by expression of GFP-HistoneH2B or mCherry- α -Tubulin, as similar amounts of cells with >4n DNA content were observed using flow cytometry in BRCA2-depleted HeLa cells or *Brca1/2*-null cells lacking these reporters (**Fig. 4D-F, Supplementary Fig. 5B-D**). In conclusion, PARP inhibition in cells with inactivated BRCA2 leads to chromatin bridges, which frequently remain unresolved and are associated with multinucleation and cell death.

As PARP inhibitor treatment resulted in a large fraction of multinucleated cells upon cytokinesis failure, we wondered to what extent these cells contribute to clonogenic survival. We therefore sorted BRCA2-depleted cells based on DNA content and separately plated cells with 2n, 4n, and >4n DNA content (**Fig. 5A and Supplementary Fig. 6A-C**). As expected, DMSO-treated, BRCA2-depleted HeLa cells with either 2n or 4n DNA content resulted in efficient clonogenic outgrowth (**Fig. 5B**). Similarly, 2n or 4n *Brca2*^{-/-} cells showed comparable numbers of colonies (**Fig. 5C**). Notably, DMSO-treated cells with >4n DNA content showed a ~50% decrease in clonogenic potential, indicating that multinucleation reduces viability, but does not per se preclude long-term survival of tumour cells, in line

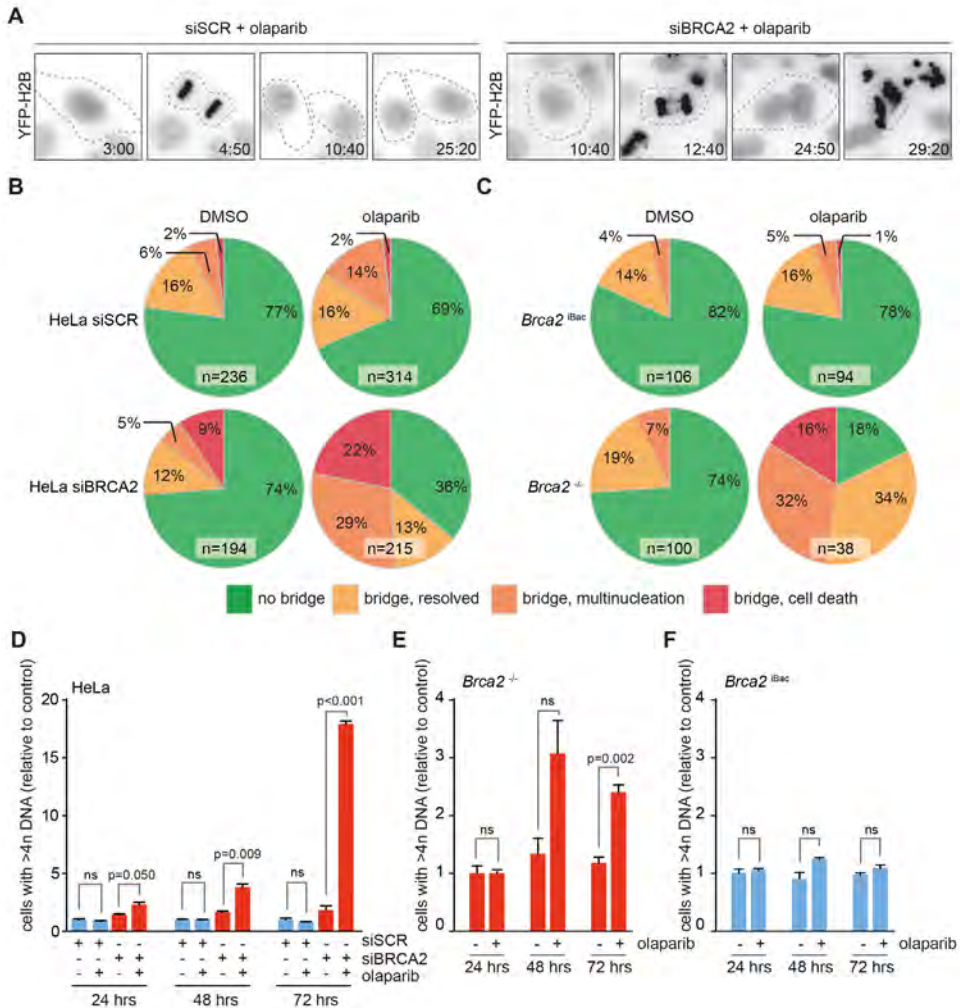


Figure 4. Chromatin bridges cause multinucleation and cell death. **A)** HeLa cells stably expressing YFP-H2B were transfected with indicated siRNAs for 24 h and subsequently treated with olaparib (0.5 mM) for 24 h. Subsequently, cells were analysed by live-cell microscopy for 36 h. Representative YFP-H2B images are shown. Dotted lines indicate cell boundaries as based on the phase-contrast images. **B)** HeLa cells stably expressing YFP-H2B were treated as for a. All anaphase cells were scored for the presence of anaphase cells and cell fate was analysed. **C)** KB2P1.21 (*Brca2*^{-/-}) and KB2P1.21R1 (*Brca2*^{IBac}) cells were treated with olaparib (0.5 mM) for 24 h after which they were analysed for at least 48 h by live-cell microscopy. All anaphase cells were scored for chromatin bridges and cell fate was analysed. **D)** HeLa cells were transfected with control (blue) or BRCA2 siRNAs (red) for 24 h and then treated with olaparib (0.5 mM) for 24, 48 or 72 h. Then, cells were fixed and DNA content was analysed by flow cytometry. Indicated percentages show 44n DNA content. P values were calculated using two-tailed Student's t-test. **E,F)** KB2P1.21 (*Brca2*^{-/-}, red bars, E) and KB2P1.21R1 (*Brca2*^{IBac}, blue bars, F) cells were treated with olaparib (0.5 mM for 24, 48 or 72 h, after which cells were fixed and DNA content was analysed. Percentages of cells with 44n DNA content are indicated. Averages and s.d. from three technical replicates are indicated. P values were calculated using two-tailed Student's t-test. Throughout the figure 'NS' indicates not significant.

with previous reports^{34,35}. Indeed, multinucleated cells did not display an intrinsic inability to replicate, as judged by BrdU incorporation (**Supplementary Fig. 6D,E**). Importantly, upon PARP inhibition, clonogenic survival was markedly decreased in both BRCA2-depleted HeLa cells as well as *Brca2*^{-/-} cells, with 4n DNA-containing cells consistently showing a more pronounced decrease in clonogenic outgrowth (**Fig. 5B,C**). Notably, cells with >4n DNA content showed a near-complete loss of colony formation, showing that PARP-induced multinucleation precludes long-term viability in cells lacking functional BRCA2.

To test whether these observations could be extrapolated *in vivo*, we analysed *Brca2*^{-/-};*p53*^{-/-} mammary tumours, generated in *K14cre;Brca2*^{f/f};*p53*^{f/f} mice, orthotopically transplanted into syngeneic wild-type (wt) mice and treated with vehicle or olaparib for 28 days (**Fig. 5D**). Notably, remnants of olaparib-treated *Brca2*^{-/-};*p53*^{-/-} tumours showed significantly increased numbers of multinucleated cells (**Fig. 5D,E**). To test if this phenotype is generic for HR-deficient tumours, we also analysed *Brca1*^{-/-};*p53*^{-/-} mammary tumours, derived from *K14cre;Brca1*^{f/f};*p53*^{f/f} mice (**Fig. 5F**). Again, tumour remnants of olaparib-treated *Brca1*^{-/-};*p53*^{-/-} tumours showed significantly increased numbers of multinucleated cells (**Fig. 5F,G**). Taken together, these data confirm PARP-inhibitor-induced multinucleation in BRCA1- or BRCA2-deficient tumour cells, and suggest that failed mitosis may contribute to the cytotoxicity of PARP inhibition in these cancer cells.

Mitotic progression promotes PARP-inhibitor cytotoxicity

We next investigated to what extent the progression through mitosis contributes to the cytotoxic effects of PARP inhibitor treatment in these tumour cells. To address this, we aimed to prevent progression through mitosis, while still allowing for DNA replication. To this end, we inactivated the early mitotic inhibitor-1 (EMI1). During interphase, EMI1 keeps the APC/C E3 ligase inactive and thereby allows for the accumulation of numerous mitotic regulators, including B-type cyclins³⁶. Inactivation of EMI1 leads to premature APC/C activation in G2-phase, interferes with cyclin B accumulation, and consequently precludes mitotic entry. As a result, EMI1-depleted cells bypass mitosis and enter cycles of endoreplication³⁷. Indeed, following EMI1 depletion, HeLa cells were unable to enter mitosis, yet continued DNA replication as judged by a large population of endoreplicating cells (>4n DNA content) by flow cytometry (**Fig. 6A,B**). Subsequently, HeLa cells were depleted for BRCA2 either alone or in combination with EMI1, and induction of apoptosis was analysed by annexin-V staining (**Fig. 6C**). Whereas olaparib treatment resulted in clear induction of apoptosis in BRCA2-depleted cells, co-depletion of EMI1 rescued the induction of apoptosis (**Fig. 6C,D**). Next, we assessed whether these effects translated into altered short-term cell survival. Interestingly, the olaparib sensitivity of BRCA2-depleted cells was largely nullified by concomitant EMI1 depletion (**Fig. 6E**). These observations were confirmed in *BRCA2*^{-/-} DLD-1 cells, in which PARP inhibitor sensitivity was rescued when mitosis was bypassed due to EMI1 depletion (**Fig. 6F,G**). Importantly, EMI1 depletion did not alleviate induction of DNA lesions in response to PARP inhibition in BRCA2-depleted cells, as judged by foci analysis of FANCD2 (**Supplementary Fig. 7A**) and γ -H2AX (**Supplementary Fig. 7B**). Also, loss of PARP inhibitor sensitivity could not be attributed to decreased proliferation rates, since EdU incorporation was not impaired after BRCA2 and EMI1 co-depletion, when compared to depletion of BRCA2 alone (**Supplementary Fig. 7C**). Taken together, our data show that forced bypass of mitosis results in decreased PARP inhibition-induced cytotoxicity, and indicate that progression through mitosis promotes cell death in BRCA2-deficient cancer cells treated with PARP inhibitor.

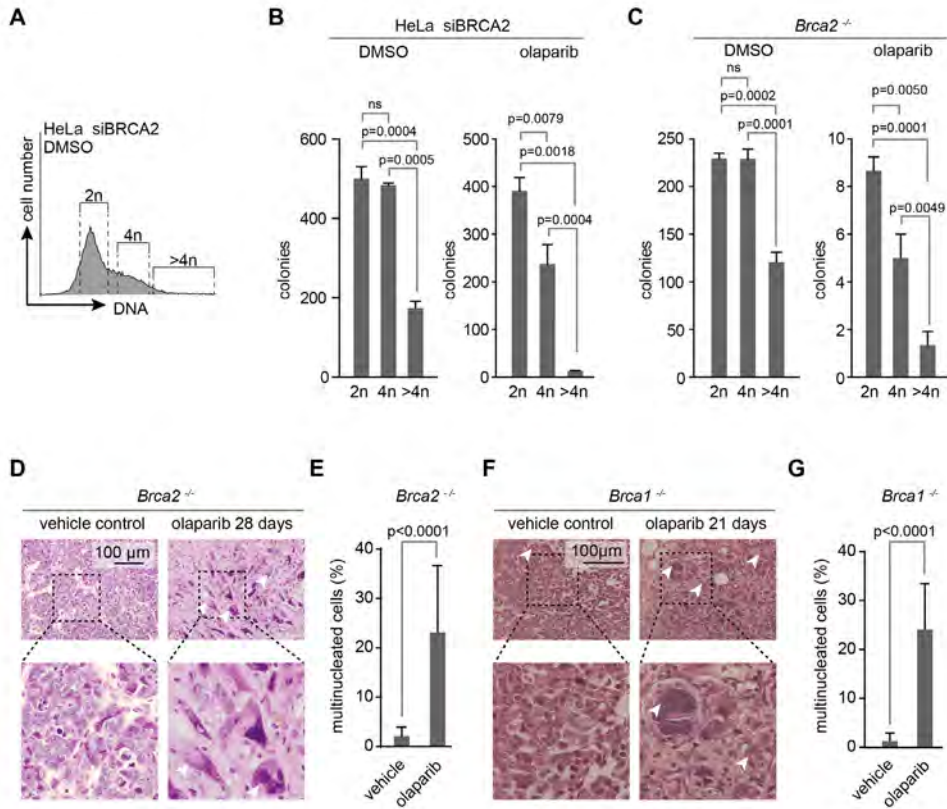


Figure 5. Multinucleated BRCA2-deficient cells arising from failed chromatin bridge resolution after PARP inhibitor treatment are not viable. **A,B)** HeLa cells were transfected with siRNA targeting BRCA2 for 24 h and were then treated with olaparib (0.5 μM) or DMSO for 72 h. Cells were then incubated with Hoechst for 45 min at 37°C, after which cells containing 2n, 4n or >4n were sorted as shown in a. Subsequently, cells were sorted at a density of 5,000 cells per well in six-wells plates. After 7 days, colony formation was quantified. The graph shows averages and s.d.'s from three replicates. P values were calculated using two-tailed Student's t-test. **C)** KB2P1.21 (*Brca2*^{-/-}) cells were treated, sorted and stained as described for a and b. After 7 days, colony formation was quantified. The graph shows means with error bars indicating s.d. of three replicates. P values are calculated using two-tailed Student's t-test. **D)** H&E staining of a *Brca2*^{-/-};p53^{-/-} mammary tumour derived from a tumour-bearing mouse, treated with vehicle or olaparib (50 mg/kg¹) for 21 days i.p. daily. Arrowheads indicate multinucleated cells. Scale bars represent 100 μm . **E)** Quantification of the percentage of multinucleated cells in tumours described in D. **F)** H&E staining of a *Brca1*^{-/-};p53^{-/-} tumour derived from a tumour-bearing mouse, treated with vehicle or olaparib (50 mg/kg¹) for 21 days i.p. daily. Multinucleated cells and apoptotic cells are indicated. Scale bars represent 100 μm . **G)** Quantification of the percentage of multinucleated cells in tumours described in f. P values were calculated using two-tailed Student's t-test. Throughout the figure 'NS' indicates not significant.

Discussion

Our findings on PARP-inhibitor-induced cytotoxicity in HR-deficient cancer cells extend on recent findings that mitotic processing of DNA lesions is linked to genome stability^{24,25,38-40}. Further, our data challenge the dogma that accumulation of DNA DSBs due to a combined

loss of base excision repair and HR is the main contributor to synthetic lethality. While DSBs do occur, other aberrant replication intermediates also arise during replication in HR-deficient cells treated with PARP inhibitors²³⁻²⁷. Furthermore, our data show that these lesions do not immediately lead to cell death, but can be transferred into mitosis, resulting in chromatin bridging and subsequent cytotoxicity. Inactivation of HR components BRCA1/2 or RAD51³¹, or Fanconi Anemia components³⁰, has been previously linked to mitotic defects. Loss of either BRCA1/2 or RAD51 was found to increase the percentage of cells with ultra-fine anaphase bridges as well as bulky chromatin bridges during anaphase³¹, in agreement with our data. Previously, PARP inhibition was shown to promote mitotic aberrancies and multinucleation⁴¹. Similar to our data, these reports showed that PARP inhibition alone does not appear to induce severe effects on mitosis in wt cells. Rather, our data indicate that severe mitotic defects only arise when PARP inhibitors are combined with an HR defect.

Chromatin bridges were previously described to frequently arise as a consequence of unresolved replication lesions²⁶. Since PARP inhibition in HR-deficient cells also leads to replication fork instability, it is conceivable that unresolved replication intermediates underlie the formation of chromatin bridges in HR-deficient cells upon PARP inhibition. Although the exact nature of these lesions remains obscure, the observed FANCD2-positive foci in mitosis suggest that under-replicated regions may persist after replication fork stalling. Indeed, secondary mutations that rescue replication fork stability in BRCA2-deficient cancer cells, rendering them resistant to PARP inhibition²².

Late-stage replication intermediates that persist up until mitosis are normally cleared by DNA resolvases^{40,42}. Specifically, the structure-specific endonuclease complex MUS81-EME1 operates in conjunction with SLX4 and GEN1 to resolve DNA joint molecules, and these enzymes are known to be highly active during mitosis and are required for proper chromosome segregation^{39,43}. One could therefore speculate that the amount of DNA lesions induced by PARP inhibition in HR-defective cells exceeds the resolvase capacity during mitosis, and leads to the accumulation of toxic DNA lesions.

Interestingly, forced mitotic bypass through EMI1 depletion could largely rescue the viability of HR-deficient cells upon PARP inhibition. This implies that progression through mitosis facilitates PARP-induced cytotoxicity, at least in short-term assays. Since *EMI1* is an essential gene *in vivo*⁴⁴ and is also required for long-term growth *in vitro*⁴⁵⁻⁴⁷, we do not consider EMI1 downregulation as a clinically relevant means to achieve long-term PARP inhibitor resistance. Rather, EMI1 served as a tool to bypass mitosis without impairing replication. In line with this notion, RNA sequencing analysis of *Brca2* mutant cancers that were either sensitive or resistant to PARP inhibition did not provide evidence that EMI1 loss is involved in PARP inhibitor resistance (**Supplementary Fig. 7D**).

In addition, our results suggest that PARP-inhibitor-induced cytotoxicity requires cycles of both replication and mitosis and that tumour cells that remain in G1- or G2-phase longer are more resistant to PARP-inhibitor-induced cytotoxicity. Conversely, drugs that promote mitotic entry, such as WEE1 or DDR kinase inhibitors, may potentiate PARP inhibitor treatment. Preliminary evidence indeed shows additive effects of combined inhibition of PARP and WEE1 in BRCA2-deficient cells, which warrants further investigation (**Supplementary Fig. 8**).

Alternatively, targeting the mitotic spindle using tubulin poisons could be an interesting approach to potentiate PARP inhibitor treatment in HR-deficient cells. Further characterization of the nature of the DNA lesions that underlie mitotic chromatin bridges and the pathways that respond to these structures is required to elucidate how PARP inhibitor therapy functions at the molecular and cellular level. These insights could then aid in designing rational combination therapies to potentiate PARP inhibitor treatment.

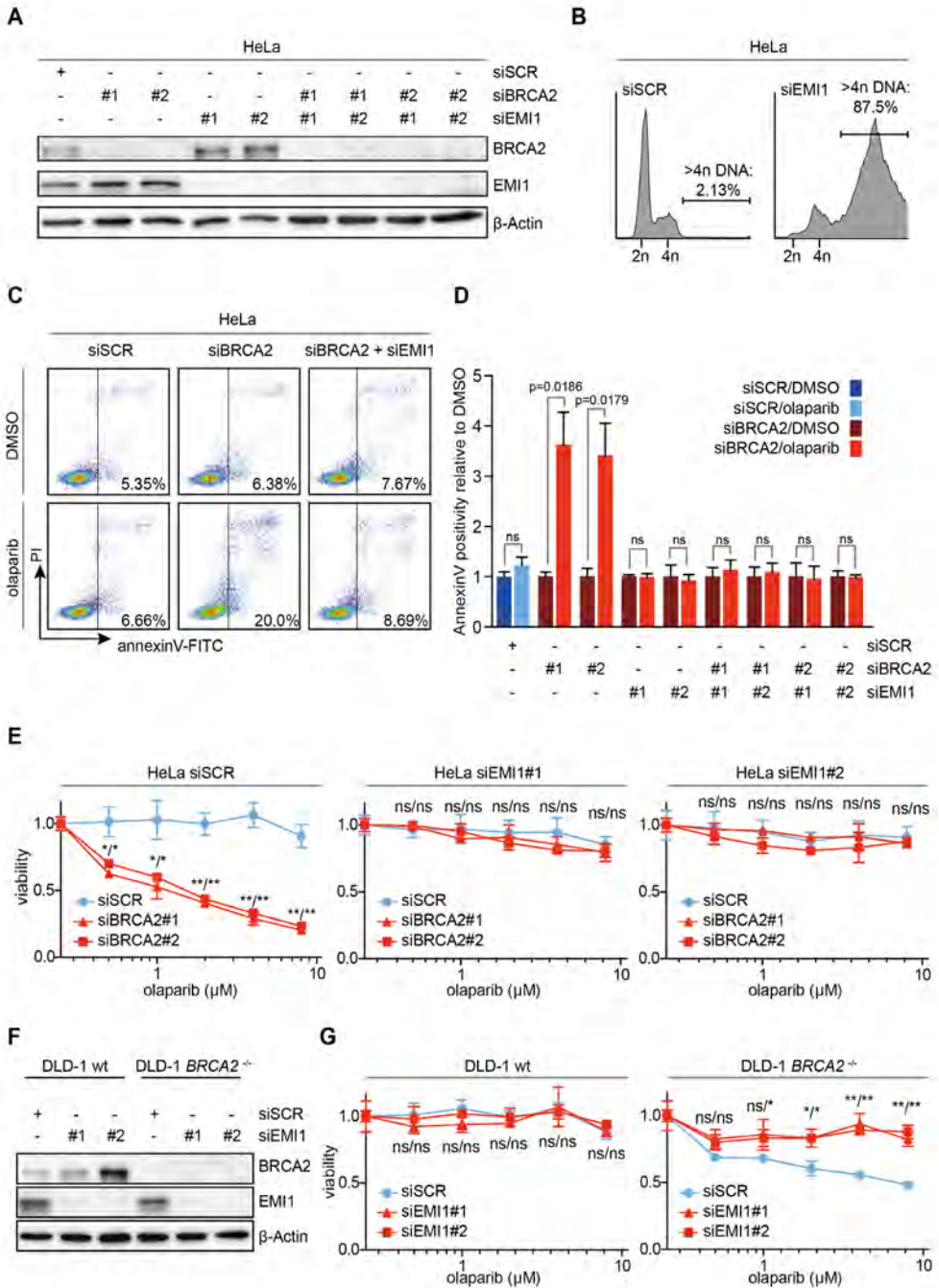


Figure 6. Mitotic progression promotes PARP-inhibitor cytotoxicity. A) HeLa cells were transfected with indicated siRNAs, and immunoblotting for BRCA2, EMI1 and β -Actin was performed at 48 h after transfection. Lines next to blots indicate positions of molecular weight markers. **B)** HeLa cells were

Methods

Cell culture and cell cycle synchronization

HeLa human cervical cancer cells, HEK293T human embryonic kidney cells and human BT-549 and HCC1937 breast cancer cell lines were obtained from ATCC (#CCL2, #CRL3216, #HTB122 and #CRL2336 respectively). DLD-1 human colorectal adenocarcinoma cells were from Horizon (Cambridge, UK). HeLa and DLD-1 cells were cultured in Dulbecco's Modified Eagle's Medium (DMEM). BT-549 and HCC1937 cells were cultured in RPMI medium. Media were supplemented with 10% fetal calf serum (FCS) and cells were cultured at 37°C in a humidified incubator supplied with 5% CO₂. The KB2P1.21 cell line (denoted in the manuscript text as *Brca2*^{-/-}) was established from a mammary tumour from *K14cre;Brca2*^{F11/F11};*p53*^{F2-10/F2-10} mice and the KB1P-B11 cell line (denoted in manuscript text as *Brca1*^{-/-}) was established from a mammary tumour from *K14cre;Brca1*^{F5-13/F5-13};*p53*^{F2-10/F2-10} mice^{7,48}. The KP3.33 cell line (denoted in the manuscript text as *p53*^{-/-}) was established from a mammary tumour from *K14cre;p53*^{F2-10/F2-10} mice³². The KB2P1.21R1 cell line (denoted as *Brca2*^{IBAC}) was generated through stable introduction of an iBAC containing the entire mouse *Brca2* gene into the KB2P1.21 cell line³². All mouse cell lines were cultured in DMEM/F-12 medium, supplemented with 10% FCS, 50 units per ml penicillin, 50 µgml⁻¹ streptomycin, 5 µgml⁻¹ insulin (Sigma), 5 ngml⁻¹ epidermal growth factor (Life Technologies) and 5 ngml⁻¹ cholera toxin (Gentaur), at 37°C under hypoxic conditions (1% O₂, 5% CO₂). Cell cycle synchronization was achieved using a double-thymidine block. Specifically, cells were treated with thymidine (2mM) for 17h, washed twice with PBS and were incubated in warm medium for 9h. Subsequently, cells were again incubated in thymidine for 17h, washed with PBS and released in pre-warmed medium and collected at indicated time points. For treatment of cells during S-phase, cells were treated immediately following release from thymidine. For treatment after S-phase, cells were treated at 7h after release from thymidine.

Virus infection

VSV-G pseudotyped retroviral particles were produced as described previously⁴⁹. In short, HEK293T cells were transfected with 10 µg of indicated pRetroX or pLKO vector, combined with 2.5 µg pMD/p and 7.5 µg pMDg plasmids, expressing the gag/pol and envelop proteins,

*transfected with indicated siRNAs for 48 h, and subsequently fixed. DNA content was analysed by flow cytometry. The percentage of cells containing >4n DNA is indicated. C) HeLa cells were transfected with BRCA2 siRNAs or control siRNA (SCR), either alone or in combination with EMI1 siRNAs. After 24 h, cells were replated and treated with olaparib (0.5 µM) for 72 h, after which cells were stained with annexin-V-FITC and propidium iodide, and were analysed by flow cytometry. D) HeLa cells were treated and analysed as for c. Averages and s.d. of three independent experiments are shown. P values were calculated using two-tailed Student's t-test. E) HeLa cells were transfected with two independent BRCA2 siRNAs or control siRNA (SCR), either alone or in combination with siRNAs targeting EMI1. After 24 h, cells were replated and allowed to attach for 3 h. Subsequently, cells were treated with indicated concentrations of olaparib for 72 h, and viability was assessed by MTT conversion. Graphs are representative of three independent experiments, and error bars indicate s.d. of three technical replicates. P values were calculated using two-tailed Student's t-test. F,G) DLD-1 BRCA2^{-/-} cells were transfected with two independent siRNAs targeting EMI1 or control siRNA (SCR). After 24 h, cells were replated and incubated for 3 h. Subsequently, cell lysates were immunoblotted for BRCA2, EMI and 6-Actin (F). In parallel, cells were treated with indicated concentrations of olaparib for 72 h, and viability was assessed by MTT conversion (G). Graphs are representative of three independent experiments, and error bars indicate s.d. of three technical replicates. P values were calculated using two-tailed Student's t-test. Throughout the figure 'NS' indicates not significant, * indicates P<0.05 and ** indicates P<0.01.*

respectively. The supernatant containing retrovirus was harvested at 48–72h following transfection, was filtered through a 0.45- μ M syringe filter and was subsequently used to infect target cells. Establishment of HeLa cells stably expressing YFP-H2B cells was described previously²⁷. In short, HeLa cells were retrovirally infected with pBabe-H2B-YFP, and selected with blasticidine (5 μ gram ml⁻¹, Sigma). To establish KB2P1.21 and KB2P1.21R1 cell lines expressing H2B-EGFP and α -tubulin-mCherry, cells were first transduced with pRetro-rTTa virus and selected with Geneticin (400 μ gml⁻¹). Subsequently, cells were infected with a pRetrox-Tight-Pur virus harbouring H2B-EGFP-T2A- α -tubulin-mCherry and selected in puromycin (1 μ gml⁻¹). H2B-EGFP and α -tubulin-mCherry expression was induced by incubation with doxycycline (0.5 μ gml⁻¹, Sigma).

MTT assays

HeLa, DLD-1, BT-549, HCC1937, KB2P1.21 and KB2P1.21R1 tumour cell lines were plated in 96-wells plates. BT-549 cells were pre-treated with 1 μ gml⁻¹ doxycycline for 48h. HeLa were plated at 2,000 cells per well, DLD-1 cells at 5,000 cells per well, BT-549 and HCC1937 cells at 1,000 cells per well, and KB2P1.21 and KB2P1.21R1 were plated at 1,200 cells per well. Cells were allowed to attach for 3 or 24h and were treated with indicated concentrations of olaparib, MK-1775, or MK4827 (all from Axon Medchem, Groningen, the Netherlands) for 3 or 4 days. Methyl-thiazol tetrazolium (MTT) was added to cells at a concentration of 5mgml⁻¹ for 4h, after which culture medium was removed and formazan crystals were dissolved in DMSO. Absorbance values were determined using a Bio-Rad benchmark III Biorad microtiter spectrophotometer at a wavelength of 520nm. Proliferation was determined as the relative decrease in signal compared to DMSO-treated cells. Unless mentioned otherwise, statistical significance was tested using Student's *t*-test.

RNA interference

Cells were transfected with 40nM siRNAs (Ambion Stealth RNAi, ThermoFisher) targeting *BRCA2* (sequence 1: #HSS186121 and sequence 2: sequence #HSS101095), *BRCA1* (sequence 1: #HSS101089 and sequence 2: #HSS186096), *RAD51* (sequence HSS1299001), *PARP1* (sequence 1: #HSS100243 and sequence 2: #HSS100244), *PAXIP1* (encoding PTIP) (sequence #HSS117971), *EMI1* (sequence 1: #HSS119992 and sequence 2: #HSS119993) or a scrambled (SCR) control sequence (sequence #12935300) with oligofectamine (Invitrogen) by using manufacturer's guidelines. Alternatively, cells were transduced with Tet-pLKO-puro vectors, for doxycycline-inducible expression of shRNAs (Addgene plasmid #219125, a kind gift from Dmitri Wiederschain⁵⁰). The shRNA sequences are: Luciferase ('LUC'): 5'-AGAGCTGTTTCTGAGGAGCC-3', *BRCA1*: 5'-CCCTAAGTTTACTTCTCTAAA-3' and *BRCA2*: 5'-AACACAATTACGAACCAAACCTT-3'. shRNAs were induced using 1 μ gml⁻¹ doxycycline (Sigma) for 48h.

Western blotting

Cells were lysed using mammalian protein extraction reagent (Thermo Scientific), supplemented with protease inhibitor and phosphatase inhibitor cocktail (Thermo Scientific). Protein content was determined with a Bradford assay after which 20 μ g of protein sample was separated by sodium dodecyl sulfate (SDS)/PAGE, transferred to polyvinylidene fluoride (immobilon) membranes and blocked in 5% skimmed milk (Sigma) in Tris-buffered saline (TBS) containing 0.05% Tween20 (Sigma). Immunodetection was performed with antibodies directed against *BRCA2* (Calbiochem, #OP95), *BRCA1* (Cell Signaling, #9010), *RAD51* (GeneTex, #gtx70230), *EMI1* (Invitrogen, #37-6600), γ -H2AX (Cell Signaling, #9718), *PTIP* (Abcam, ab70434) all diluted 1:1,000 and *Beta-Actin* (MP Biomedicals, #69100) diluted 1:10,000.

Horseshoe peroxidase-conjugated secondary antibodies (DAKO) were diluted 1:2,500 and used for visualization using chemiluminescence (Lumi-Light, Roche Diagnostics) on a Bio-Rad bioluminescence device, equipped with Quantity One/ChemiDoc XRS software (Bio-Rad). Uncropped versions of all western blots can be found in Supplementary Fig. 9.

Flow cytometry

For apoptosis analysis by annexin V staining, total cell populations were collected by trypsinization and stained with annexin-V-FITC (1:20) and propidium iodide as per manufacturer's instructions (Immune Quality Products). Cells were then analysed on a LSR-II (Becton Dickinson) cytometer using FACSDiva software (Becton Dickinson). For cell cycle analysis, BrdU and phospho-HistoneH3 analysis, cells were fixed in ice-cold 70% ethanol or methanol for at least 6h and were then immunostained with an Alexa-488-conjugated antibody targeting BrdU (MoBU1, #B35130, 1:200), or anti-phospho-histone-H3 (Ser10, Cell Signaling, #9701, 1:300) in combination with Alexa-488-conjugated secondary antibodies (1:300). DNA staining was performed using propidium iodide in the presence of RNase. At least 10,000 events per sample were analysed on a FACScalibur (Becton Dickinson). Data was analysed using FlowJo software.

Immunofluorescence microscopy

HeLa, KB2P1.21 and KB2P21R1 cells were seeded on glass coverslips in six-well plates. When indicated, HeLa cells were transfected with siRNAs for 48h or were treated with olaparib (0.5 μ M) for 24h as indicated. If indicated, KB2P1.21 and KB2P21R1 cells were irradiated (5Gy) using a CIS International/IBL 637 caesium¹³⁷ source (dose rate: 0.010124Gys⁻¹). Cells were fixed using 4% formaldehyde or paraformaldehyde in PBS, and subsequently permeabilized for 5min in PBS with 0.1% Triton X-100. After extensive washing, cells were stained with antibodies targeting α -Tubulin (Cell Signaling, #2125, 1:100), RAD51 (GeneTex, #gtx70230, 1:400), FANCD2 (SantaCruz Biotechnology, #sc20022, 1:200) or γ -H2AX (Cell Signaling, #9718, 1:200), in combination with Alexa-488 or Alexa-647-conjugated secondary antibodies (1:300), and were counterstained with DAPI. Early anaphases in which chromosome packs were separated less than 10nm were excluded for analysis. Anaphase and telophase cells were distinguished based on α -Tubulin staining. Images were acquired on a Leica DM6000B microscope using a \times 63 immersion objective (PL S-APO, numerical aperture: 1.30) with LAS-AF software (Leica).

Live-cell microscopy

KB2P2.21 and KB2P2.21R1 transduced with H2B-EGFP-IRES- α -tubulin-mCherry and HeLa cells transduced with H2B-EGFP were seeded in eight-chambered cover glass plates (Lab-Tek-II, Nunc) at 10,000 cells per well. Cells were then treated with 0.5 μ M olaparib at 24h before imaging, and were followed for at least 36h on a DeltaVision Elite microscope, equipped with a CoolSNAP HQ2 camera and a \times 40 immersion objective (U-APO 340, numerical aperture: 1.35). Images were obtained each 10min, with 12 images being acquired in the Z-axis, at 0.5 μ m interval. Image analysis was done using SoftWorX software (Applied Precision/GE Healthcare). The fate of all cells that entered mitosis and proceeded at least until anaphase were included for analysis.

DNA fibre analysis

To assess replication fork protection. HeLa cells were pulse-labelled with CldU (25 μ M) for 60min. Next, cells were washed with medium and incubated with hydroxyurea (HU, 5mM)

for 5 h. Cells were harvested using trypsin and lysed on microscopy slides in lysis buffer (0.5% SDS, 200 mM Tris (pH 7.4), 50 mM EDTA). DNA fibres were spread by tilting the slide and were subsequently air dried and fixed in methanol/acetic acid (3:1) for 10 min. For immunolabelling, spreads were treated with 2.5 M HCl for 1.5 h. CldU was detected by staining with rat anti-BrdU (1:1,000, AbD Serotec) for 1 h and was further incubated with AlexaFluor 488-conjugated anti-rat IgG (1:500) for 1.5 h. Images were acquired on a Leica DM-6000RXA fluorescence microscope, equipped with Leica Application Suite software. The lengths of CldU and IdU tracks were measured blindly using ImageJ software. Statistical analysis was performed using two-sided Mann–Whitney tests with 95% confidence intervals.

Generation of mammary tumours

Brca1^{-/-};p53^{-/-} and *Brca2^{-/-};p53^{-/-}* mammary tumours were generated in *K14cre;Brca1^{F/F};p53^{F/F}* and *K14cre;Brca2^{F/F};p53^{F/F}* mice, respectively, genotyped, and orthotopically transplanted into syngeneic wt mice as described⁷. Starting 2 weeks after tumour grafting, in female FVB/N mice (6–8 weeks old), the onset of tumour growth was checked at least three times per week. Mammary tumour size was determined by caliper measurements. When mammary tumours reached a size of ~200 mm³, treatment was initiated. Olaparib was used by diluting 50 mg per ml stocks in DMSO with 10% 2-hydroxyl-propyl- β -cyclodextrine/PBS such that the final volume administered by intraperitoneally (i.p.) injection was 10 μ g⁻¹ of body weight. Olaparib (50 mg kg⁻¹) was given i.p. daily for 21 or 28 consecutive days. Controls were dosed with vehicle only. Animals were killed with CO₂ at the end of treatment when the minimal residual disease stage was reached. At this point, olaparib-treated tumour explants had an approximate size of 1 mm³, whereas control-treated tumour explants had a volume of ~1 cm³. Tumour samples were fixed in 4% formaline and processed for hematoxylin/eosin staining. S.d. represent 10 different fields, containing at least 100 cells. All experimental procedures on animals were approved by the Animal Ethics Committee of the Netherlands Cancer Institute.

RNA sequencing and analysis

Fresh-frozen tumour tissues of AZD2461-sensitive ($n=23$) and AZD2461-resistant ($n=36$) *Brca2^{-/-};p53^{-/-}* tumours (described in ²²), were placed in 1 ml of TRIreagent (Bioline) and subjected to mechanical disruption with Tissue Lyser LT (Qiagen, oscillation: 50 s⁻¹, time: 10 min). Homogenized lysates were further processed for RNA isolation following TRIreagent manufacturer's protocol. Quality and quantity of the total RNA was assessed by the 2100 Bioanalyzer using a Nano chip (Agilent, Santa Clara, CA). Total RNA samples having RIN > 8 were subjected to library generation. Strand-specific libraries were generated using the TruSeq Stranded mRNA sample preparation kit (Illumina Inc., San Diego, RS-122-2101/2), according to the manufacturer's instructions (Illumina, Part #15031047 Rev. E). Briefly, polyadenylated RNA from intact total RNA was purified using oligo-dT beads. Following purification, the RNA was fragmented, random primed and reverse transcribed using SuperScript II Reverse Transcriptase (Invitrogen, part #18064-014) with the addition of Actinomycin D. Second strand synthesis was performed using Polymerase I and RNaseH with replacement of dTTP for dUTP. The generated cDNA fragments were 3'-end adenylated and ligated to Illumina Paired-end sequencing adapters and subsequently amplified by 12 cycles of polymerase chain reaction. The libraries were analysed on a 2100 Bioanalyzer using a 7500 chip (Agilent, Santa Clara, CA), diluted and pooled equimolar into a 10 nM sequencing stock solution. Illumina TruSeq mRNA libraries were sequenced with 50 base single reads on a HiSeq2000 using V3 chemistry (Illumina Inc., San Diego). The resulting reads were trimmed using Cutadapt (version 1.12)⁸ to remove any remaining adapter sequences, filtering reads

shorter than 20bp after trimming to ensure efficient mapping. The trimmed reads were aligned to the GRCm38 reference genome using STAR (version 2.5.2b)⁹. QC statistics from Fastqc (version 0.11.5) and the above-mentioned tools were collected and summarized using Multiqc (version 0.8)⁵¹. Gene expression counts were generated by featureCounts (version 1.5.0-post3)⁵², using gene definitions from Ensembl GRCm38 version 76. Normalized expression values were obtained by correcting for differences in sequencing depth between samples using DESeq median-of-ratios approach⁵³, and subsequent log-transformation the normalized counts.

Data availability

The data that support the findings of this study are available from the corresponding author upon reasonable request. RNA sequence data has been deposited at the European Nucleotide Archive (ENA) under accession number PRJEB20535.

Acknowledgments and funding

We are grateful to van Vugt lab members for constructive comments. We thank H.R. de Boer for technical assistance and critical review of the manuscript, G. Berger for technical assistance and A. Bhattacharya for help with statistics. Financial support came from the Dutch Cancer Society (RUG 2011–5093 to M.A.T.M.v.V. and NKI 2011–5220 to J.J. and S.R.), the Netherlands Organization for Scientific Research (NWO-VIDI 916–76062 to M.A.T.M.v.V.), the European Research Council (ERC-CoG-682421 to M.A.T.M.v.V. and ERC-CoG-681572 to S.R.), the Swiss National Science Foundation (310030_156869 to S.R.) and Swiss Cancer Research (MD-PhD fellowship MD-PhD-3446-01-2014 to S.B.).

Author contributions

P.M.S. and M.A.T.M.v.V. conceived the project and analysed data. P.M.S., F.T. and C.S. performed *in vitro* experiments. F.F. assisted with live-cell microscopy and establishing reporter cell lines. E.G. and S.R. performed *in vivo* experiments and analysed RNAseq data. P.M.S., F.T., C.S., E.G., S.B., S.R. and M.A.T.M.v.V. analysed data. A.M.H., P.B., J.J. and M.T. established or provided reagents. P.M.S. and M.A.T.M.v.V. wrote the manuscript. All authors assisted in editing the manuscript and approved it before submission.

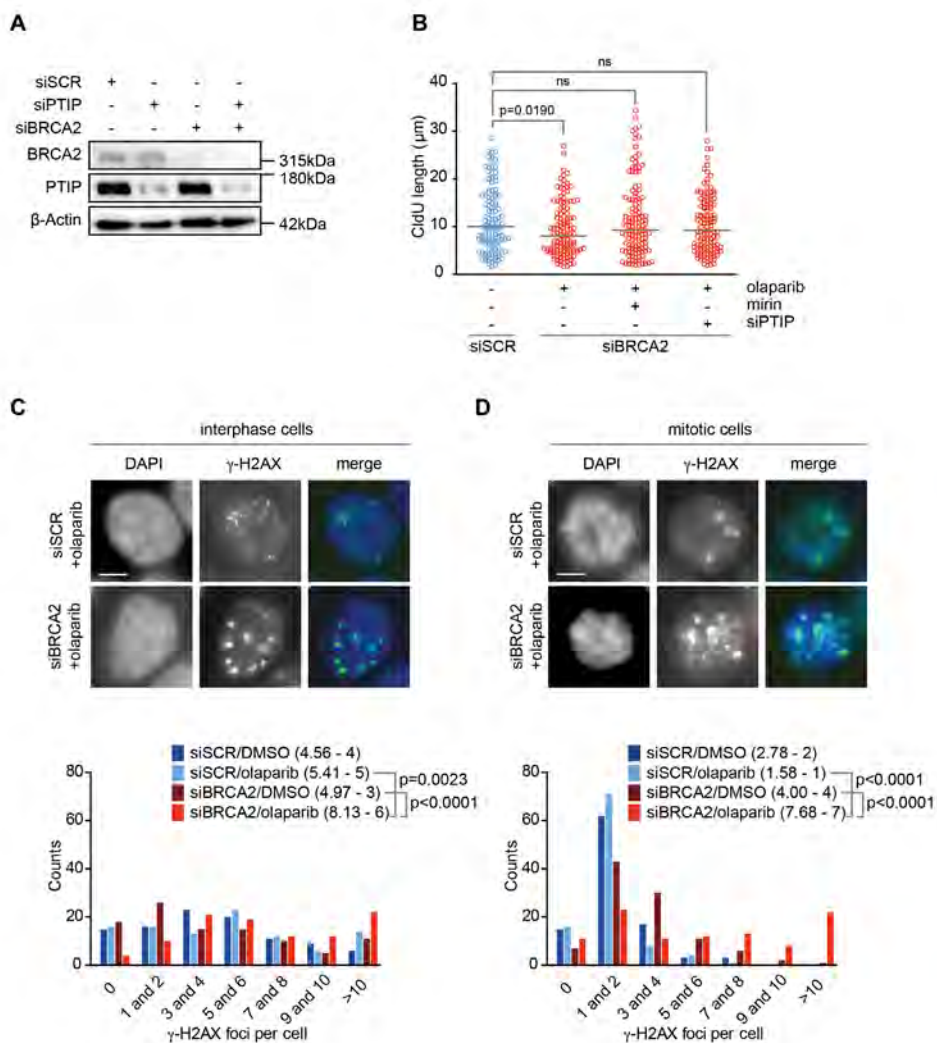
References

1. Michl, J., Zimmer, J. & Tarsounas, M. Interplay between Fanconi anemia and homologous recombination pathways in genome integrity. *EMBO J.* 35, 909–923 (2016).
2. Wooster, R. et al. Localization of a breast cancer susceptibility gene, BRCA2, to chromosome 13q12-13. *Science* 265, 2088–2090 (1994).
3. Futreal, P. A. et al. BRCA1 mutations in primary breast and ovarian carcinomas. *Science* 266, 120–122 (1994).
4. Miki, Y. et al. A strong candidate for the breast and ovarian cancer susceptibility gene BRCA1. *Science* 266, 66–71 (1994).
5. Byrski, T. et al. Pathologic complete response rates in young women with BRCA1-positive breast cancers after neoadjuvant chemotherapy. *J. Clin. Oncol.* 28, 375–379 (2010).
6. Silver, D. P. et al. Efficacy of neoadjuvant Cisplatin in triple-negative breast cancer. *J. Clin. Oncol.* 28, 1145–1153 (2010).
7. Rottenberg, S. et al. High sensitivity of BRCA1-deficient mammary tumors to the PARP inhibitor AZD2281 alone and in combination with platinum drugs. *Proc. Natl Acad. Sci. USA* 105, 17079–17084 (2008).
8. Bryant, H. E. et al. Specific killing of BRCA2-deficient tumours with inhibitors of poly(ADP-ribose) polymerase. *Nature* 434, 913–917 (2005).

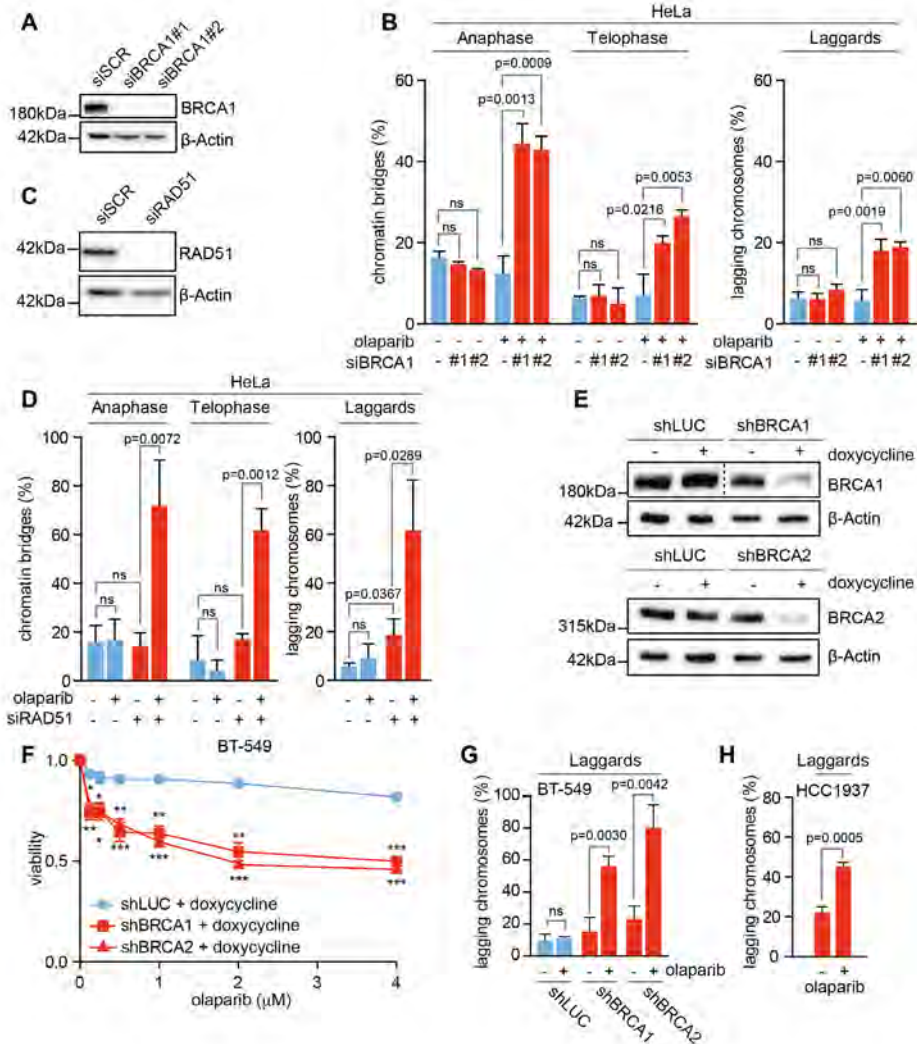
9. Farmer, H. et al. Targeting the DNA repair defect in BRCA mutant cells as a therapeutic strategy. *Nature* 434, 917–921 (2005).
10. Lord, C. J. & Ashworth, A. Mechanisms of resistance to therapies targeting BRCA-mutant cancers. *Nat. Med.* 19, 1381–1388 (2013).
11. Fisher, A. E. O., Hohegger, H., Takeda, S. & Caldecott, K. W. Poly(ADPribose) polymerase 1 accelerates single-strand break repair in concert with poly(ADP-ribose) glycohydrolase. *Mol. Cell Biol.* 27, 5597–5605 (2007).
12. Ström, C. E. et al. Poly(ADP-ribose) polymerase(PARP) is not involved in base excision repair but PARP inhibition traps a single-strand intermediate. *Nucleic Acids Res.* 39, 3166–3175 (2011).
13. Gottipati, P. et al. Poly(ADP-ribose) polymerase is hyperactivated in homologous recombination-defective cells. *Cancer Res.* 70, 5389–5398 (2010).
14. Helleday, T. The underlying mechanism for the PARP and BRCA synthetic lethality: clearing up the misunderstandings. *Mol. Oncol.* 5, 387–393 (2011).
15. Murai, J. et al. Trapping of PARP1 and PARP2 by clinical PARP inhibitors. *Cancer Res.* 72, 5588–5599 (2012).
16. Bryant, H. E. et al. PARP is activated at stalled forks to mediate Mre11-dependent replication restart and recombination. *EMBO J.* 28, 2601–2615 (2009).
17. Ying, S., Hamdy, F. C. & Helleday, T. Mre11-dependent degradation of stalled DNA replication forks is prevented by BRCA2 and PARP1. *Cancer Res.* 72, 2814–2821 (2012).
18. Yang, Y.-G., Cortes, U., Patnaik, S., Jasin, M. & Wang, Z.-Q. Ablation of PARP-1 does not interfere with the repair of DNA double-strand breaks, but compromises the reactivation of stalled replication forks. *Oncogene* 23, 3872–3882 (2004).
19. Schlacher, K., Wu, H. & Jasin, M. A distinct replication fork protection pathway connects Fanconi anemia tumor suppressors to RAD51-BRCA1/2. *Cancer Cell* 22, 106–116 (2012).
20. Schlacher, K. et al. Double-strand break repair-independent role for BRCA2 in blocking stalled replication fork degradation by MRE11. *Cell* 145, 529–542 (2011).
21. Lehmann, A. R., Kirk-Bell, S., Shall, S. & Whish, W. J. The relationship between cell growth, macromolecular synthesis and poly ADP-ribose polymerase in lymphoid cells. *Exp. Cell Res.* 83, 63–72 (1974).
22. Ray Chaudhuri, A. et al. Replication fork stability confers chemoresistance in BRCA-deficient cells. *Nature* 535, 382–387 (2016).
23. Chan, K.-L., Palmal-Pallag, T., Ying, S. & Hickson, I. D. Replication stress induces sister-chromatid bridging at fragile site loci in mitosis. *Nat. Cell Biol.* 11, 753–760 (2009).
24. Naim, V., Wilhelm, T., Debatisse, M. & Rosselli, F. ERCC1 and MUS81-EME1 promote sister chromatid separation by processing late replication intermediates at common fragile sites during mitosis. *Nat. Cell Biol.* 15, 1008–1015 (2013).
25. Ying, S. et al. MUS81 promotes common fragile site expression. *Nat. Cell Biol.* 15, 1001–1007 (2013).
26. Mankouri, H. W., Huttner, D. & Hickson, I. D. How unfinished business from S-phase affects mitosis and beyond. *EMBO J.* 32, 2661–2671 (2013).
27. Hengeveld, R. C. C. et al. Rif1 is required for resolution of ultrafine DNA bridges in anaphase to ensure genomic stability. *Dev. Cell* 34, 466–474 (2015).
28. Zhang, Y. et al. ZNF365 promotes stability of fragile sites and telomeres. *Cancer Discov.* 3, 798–811 (2013).
29. Ichijima, Y. et al. DNA lesions induced by replication stress trigger mitotic aberration and tetraploidy development. *PLoS ONE* 5, e8821 (2010).
30. Vinciguerra, P., Godinho, S. A., Parmar, K., Pellman, D. & D’Andrea, A. D. Cytokinesis failure occurs in Fanconi anemia pathway-deficient murine and human bone marrow hematopoietic cells. *J. Clin. Invest.* 120, 3834–3842 (2010).
31. Laulier, C., Cheng, A. & Stark, J. M. The relative efficiency of homologydirected repair has distinct effects on proper anaphase chromosome separation. *Nucleic Acids Res.* 39, 5935–5944 (2011).
32. Evers, B. et al. Selective inhibition of BRCA2-deficient mammary tumor cell growth by AZD2281 and cisplatin. *Clin. Cancer Res.* 14, 3916–3925 (2008).
33. Evers, B. et al. A high-throughput pharmaceutical screen identifies compounds with specific toxicity against BRCA2-deficient tumors. *Clin. Cancer Res.* 16, 99–108 (2010).

34. Fujiwara, T. et al. Cytokinesis failure generating tetraploids promotes tumorigenesis in p53-null cells. *Nature* 437, 1043–1047 (2005).
35. Shi, Q. & King, R. W. Chromosome nondisjunction yields tetraploid rather than aneuploid cells in human cell lines. *Nature* 437, 1038–1042 (2005).
36. Reimann, J. D. et al. Emi1 is a mitotic regulator that interacts with Cdc20 and inhibits the anaphase promoting complex. *Cell* 105, 645–655 (2001).
37. Machida, Y. J. & Dutta, A. The APC/C inhibitor, Emi1, is essential for prevention of rereplication. *Genes Dev.* 21, 184–194 (2007).
38. Wyatt, H. D. M., Laister, R. C., Martin, S. R., Arrowsmith, C. H. & West, S. C. The SMX DNA repair tri-nuclease. *Mol. Cell* 65, 848–860.e11 (2017).
39. Sarbajna, S., Davies, D. & West, S. C. Roles of SLX1-SLX4, MUS81-EME1, and GEN1 in avoiding genome instability and mitotic catastrophe. *Genes Dev.* 28, 1124–1136 (2014).
40. Minocherhomji, S. et al. Replication stress activates DNA repair synthesis in mitosis. *Nature* 528, 286–290 (2015).
41. Dale Rein, I., Solberg Landsverk, K., Micci, F., Patzke, S. & Stokke, T. Replication-induced DNA damage after PARP inhibition causes G2 delay, and cell line-dependent apoptosis, necrosis and multinucleation. *Cell Cycle* 14, 3248–3260 (2015).
42. Wild, P. & Matos, J. Cell cycle control of DNA joint molecule resolution. *Curr. Opin. Cell Biol.* 40, 74–80 (2016).
43. Garcí'a-Luis, J. & Machi'n, F. Mus81-Mms4 and Yen1 resolve a novel anaphase bridge formed by noncanonical Holliday junctions. *Nat. Commun.* 5, 5652 (2014).
44. Lee, H. et al. Mouse emi1 has an essential function in mitotic progression during early embryogenesis. *Mol. Cell. Biol.* 26, 5373–5381 (2006).
45. Blomen, V. A. et al. Gene essentiality and synthetic lethality in haploid human cells. *Science* 350, 1092–1096 (2015).
46. Hart, T. et al. High-resolution CRISPR screens reveal fitness genes and genotype-specific cancer liabilities. *Cell* 163, 1515–1526 (2015).
47. Wang, T. et al. Identification and characterization of essential genes in the human genome. *Science* 350, 1096–1101 (2015).
48. Liu, X. et al. Somatic loss of BRCA1 and p53 in mice induces mammary tumors with features of human BRCA1-mutated basal-like breast cancer. *Proc. Natl Acad. Sci. USA* 104, 12111–12116 (2007).
49. van Vugt, M. A. T. M. et al. A mitotic phosphorylation feedback network connects Cdk1, Plk1, 53BP1, and Chk2 to inactivate the G(2)/M DNA damage checkpoint. *PLoS Biol.* 8, e1000287 (2010).
50. Wiederschain, D. et al. Single-vector inducible lentiviral RNAi system for oncology target validation. *Cell Cycle* 8, 498–504 (2009).
51. Ewels, P., Magnusson, M., Lundin, S. & Kä'ller, M. MultiQC: summarize analysis results for multiple tools and samples in a single report. *Bioinformatics* 32, 3047–3048 (2016).
52. Liao, Y., Smyth, G. K. & Shi, W. featureCounts: an efficient general purpose program for assigning sequence reads to genomic features. *Bioinformatics* 30, 923–930 (2014).
53. Anders, S. & Huber, W. Differential expression analysis for sequence count data. *Genome Biol.* 11, R106 (2010).

Supplementary Figures

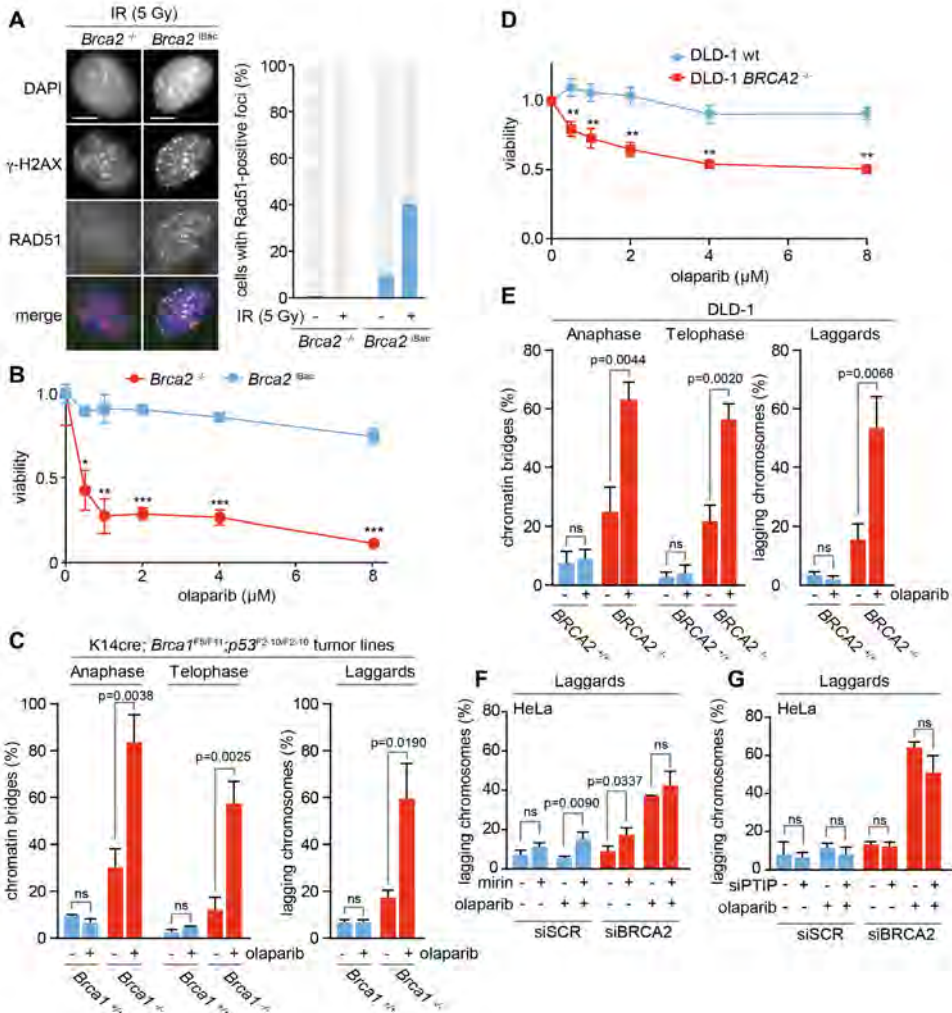


Supplementary Figure 1: PARP inhibition leads to MRE11/PTIP-dependent replication fork degradation in BRCA2 depleted cells, and ensuing mitotic DNA lesions. A) Immunoblotting for BRCA2, PTIP and β -actin at 48 hours after transfection with indicated siRNAs in HeLa cells. **B)** HeLa cells were transfected with indicated siRNAs and labeled with CldU. Cells were then treated with HU (5 mM) and DMSO, olaparib (0.5 μ M) and/or mirin (50 μ M) as indicated for 5 hours. DNA was spread into single fibers and CldU track length was determined of 125 fibers per condition. *P* values were calculated using two-tailed Mann-Whitney test. **C, D)** HeLa cells were transfected with BRCA2 siRNA and treated with DMSO or olaparib (0.5 μ M) for 24 hours. Cells were stained for γ -H2AX (green) and counterstained with DAPI (blue) and the number of γ -H2AX foci per nucleus were quantified for interphase cells (panel C) and mitotic cells (panel D). Scale bars indicate 5 μ m. Per condition, 100 nuclei were analyzed. Indicated numbers between brackets represented averages and medians respectively. *P* values were calculated using a two-tailed Mann-Whitney test. Throughout the figure 'ns' indicates not significant.

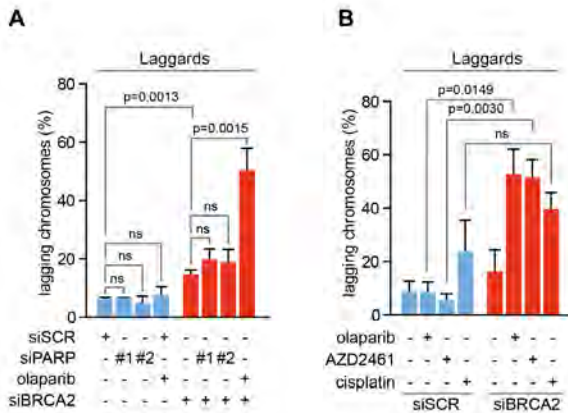


Supplementary Figure 2: PARP inhibition leads to chromatin bridges and lagging chromosomes in anaphase in HR-defective cancer cells. **A)** Immunoblotting of BRCA1 and β -Actin at 48 hours after siRNA transfection in HeLa cells. **B)** HeLa cells were transfected with indicated siRNAs and after 24 hours were treated with olaparib (0.5 μ M) or DMSO for 24 hours. Percentages of cells containing chromatin bridges ($n > 20$ events per condition per experiment) and lagging chromosomes ($n > 40$ events per condition per experiment) were quantified. **C)** Immunoblotting of RAD51 and β -Actin, at 48 hours after siRNA transfection in HeLa cells. **D)** HeLa cells were transfected with indicated siRNAs and treated as for panel B. Percentages of cells containing chromatin bridges ($n > 20$ events per condition) and lagging chromosomes ($n > 40$ events per condition) were quantified. **E)** Immunoblotting of BRCA1, BRCA2 and β -Actin at 4 days after doxycycline treatment of BT-549 cells, stably transduced with indicated doxycycline-inducible shRNAs. Dashed line indicates site where blot was cut. **F)** BT-549 cells with indicated shRNAs were treated with doxycycline for 48 hours. Cells were subsequently treated with indicated olaparib concentrations for 4 days, after which MTT conversion was assessed. Averages and standard deviations of 4 independent experiments are shown. **G)** BT-549 cells were pre-treated

with doxycycline for 48 hours, and subsequently treated with olaparib (0.5 μM) or DMSO for 24 hours. Percentages of cells containing lagging chromosomes ($n>40$ events per condition) were quantified. **H)** HCC1937 cells were treated with olaparib (0.5 μM) or DMSO for 24 hours. Percentages of cells containing lagging chromosomes (>40 events per condition) were quantified. Throughout the figure, *P* values were calculated using two-tailed Student's *t*-test. 'ns' indicates not significant, 'na' indicates not analyzable, * indicates $p<0.05$, ** indicates $p<0.01$, *** indicates $p<0.001$. All error bars indicate standard deviations of 3 independent experiments.



Supplementary Figure 3: PARP inhibition leads to chromatin bridges and lagging chromosomes in HR-defective cancer cells, and lagging chromosomes are not rescued by MRE11/PTIP inactivation. A) KB2P1.21 (*Brca2*^{-/-}) and KB2P1.21R1 (*Brca2*^{IBac}) cells were irradiated (5 Gy), fixed after 6 hours and stained with γ -H2AX (red) and RAD51 (green) and counterstained with DAPI (blue). Quantification of RAD51 foci is shown in the right panel. Nuclei with >5 RAD51 foci were considered positive and $n>50$ nuclei per condition were analyzed. Scale bars indicate 5 μm . **B)** KB2P1.21 (*Brca2*^{-/-}) and KB2P1.21R1 (*Brca2*^{IBac}) cells were treated with indicated olaparib concentrations for 72 hours, after which viability was assessed

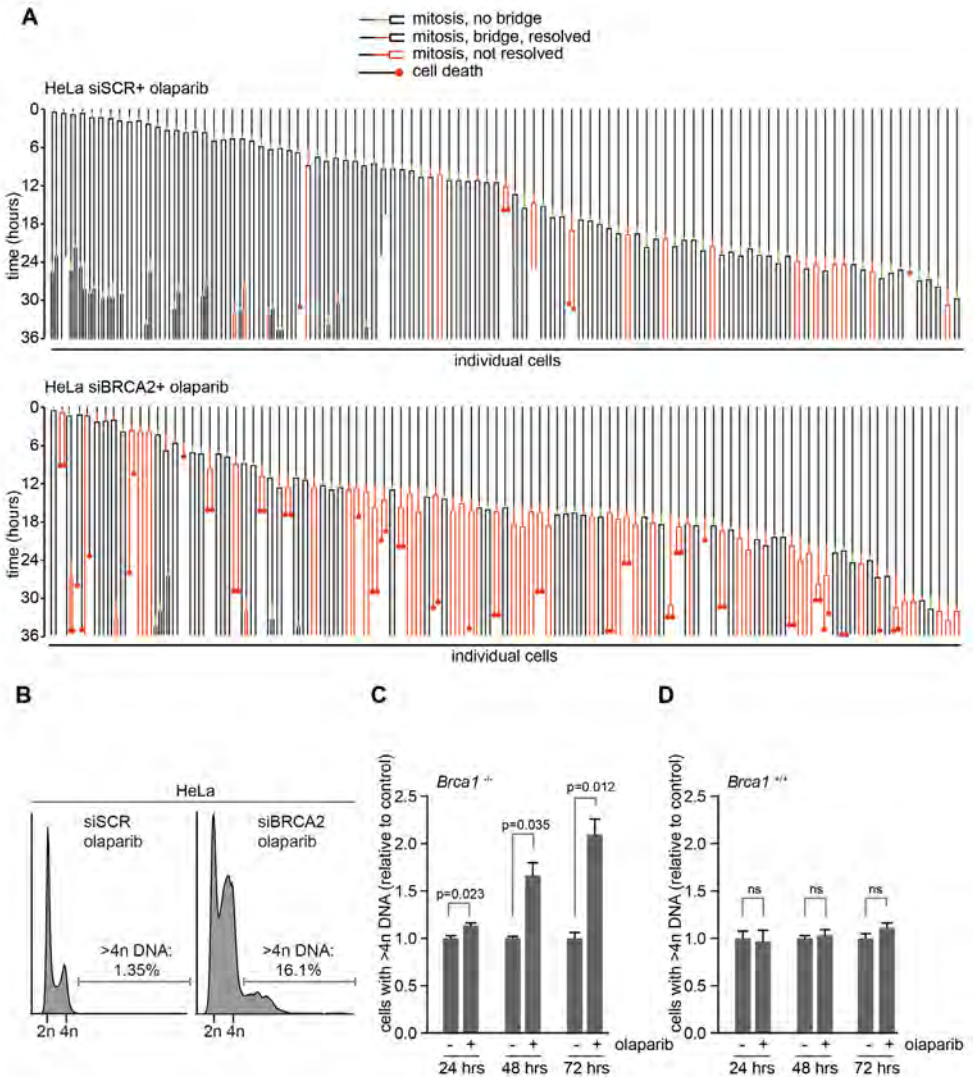


Supplementary Figure 4: PARP inhibition, but not PARP depletion, leads to lagging chromosomes in mitosis, and BRCA2-depleted cells with chromatin bridges have higher levels of mitotic DNA lesions.

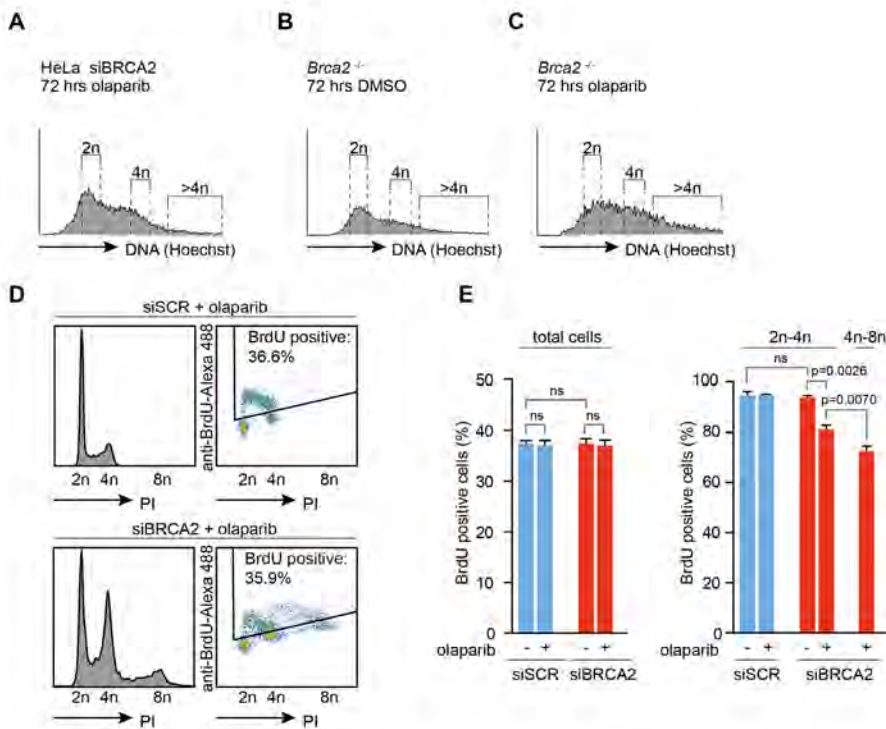
A, B) HeLa cells were transfected with indicated siRNAs and after 24 hours were treated with olaparib (0.5 μ M), AZD2461 (1 μ M), cisplatin (1 μ M) or DMSO for 24 hours. Percentages of cells containing lagging chromosomes ($n > 40$ events per condition) were quantified. P values were calculated using two-tailed Student's t test. **C)** HeLa cells were treated as for Figure 3E. BRCA2-depleted, olaparib-treated cells were harvested at 10 hours after release from thymidine, and anaphase cells were stained for FANCD2. Graph shows pooled data of cells treated with

PARP inhibitor in S-phase and cells treated G2-phase. Foci were counted in 100 individual anaphase cells. For each cell, the presence of DAPI-positive chromatin bridges was determined. A Mann-Whitney test was performed to compare the number of foci in anaphase cells with and without chromatin bridges. Throughout the figure 'ns' indicates not significant. Horizontal bars indicate means, and all error bars indicate standard deviations of 3 independent experiments.

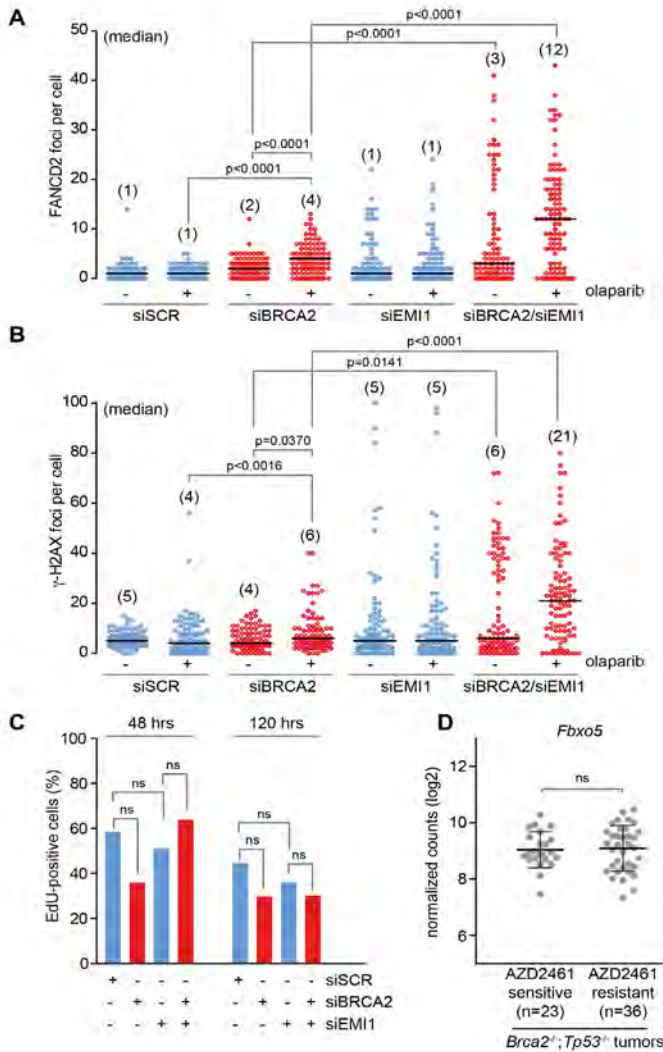
by MTT conversion. Shown graphs represent averages from three replicates. **C)** KB1P-B11 (*Brca1*^{-/-}) and KP3.33 (*Brca1*^{+/+}) cells were treated with olaparib (0.5 μ M) or DMSO for 24 hours. Percentages of cells containing chromatin bridges ($n > 20$ events per condition) and lagging chromosomes ($n > 40$ events per condition) were quantified. **D)** DLD-1 *BRCA2*^{+/+} and *BRCA2*^{-/-} cells were treated with indicated olaparib concentrations for 72 hours, after which viability was assessed by MTT conversion. Shown graphs represent averages from three replicates. **E)** DLD-1 *BRCA2*^{+/+} and *BRCA2*^{-/-} cells were treated with olaparib (0.5 μ M) or DMSO for 24 hours. Percentages of cells containing chromatin bridges ($n > 20$ events per condition) and lagging chromosomes ($n > 40$ events per condition) were quantified. **F, G)** HeLa cells were transfected with indicated siRNAs and after 24 hours were treated with olaparib (0.5 μ M) or DMSO and/or mirin (50 μ M) for 24 hours. Percentages of cells containing lagging chromosomes ($n > 40$ events per condition) were quantified. Throughout the figure, P values were calculated using two-tailed Student's t-test. 'ns' indicates not significant, * indicates $p < 0.05$, ** indicates $p < 0.01$, *** indicates $p < 0.001$. All error bars indicate standard deviations of 3 independent experiments.



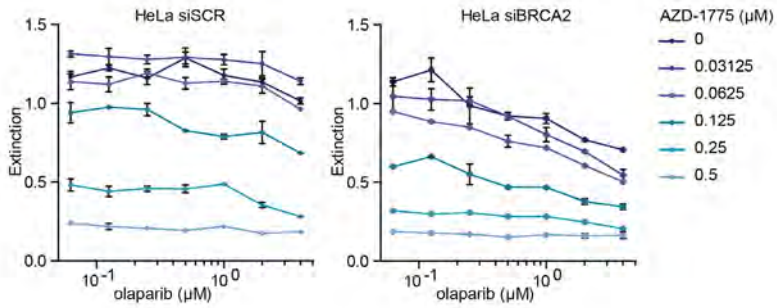
Supplementary Figure 5: Live cell imaging and flow cytometry analysis of mitotic failure and polyploidization of HR-defective cells upon PARP inhibition. **A)** HeLa cells were transfected and treated as for Figure 4A. Cellular behavior of individual cells is plotted for control-transfected and siBRCA2-transfected HeLa cells treated with olaparib. **B)** HeLa cells were transfected with indicated siRNAs for 24 hours and then treated with olaparib (0.5 μ M) for 72 hours. Then, cells were fixed and DNA content was analyzed by flow cytometry. Indicated percentages show >4n DNA content. **C, D)** KB1P-B11 cells (*Brca1*^{-/-}, panel C) and KP3.33 cells (*Brca1*^{+/+}, panel D) were treated with olaparib (0.5 μ M) for 24, 48 or 72 hours after which cells were fixed and DNA content was analyzed. Percentages of cells with >4n DNA content are indicated. Error bars indicate standard deviations from three technical replicates. Throughout the figure 'ns' indicates not significant. P values were calculated using two-tailed Student's t test.



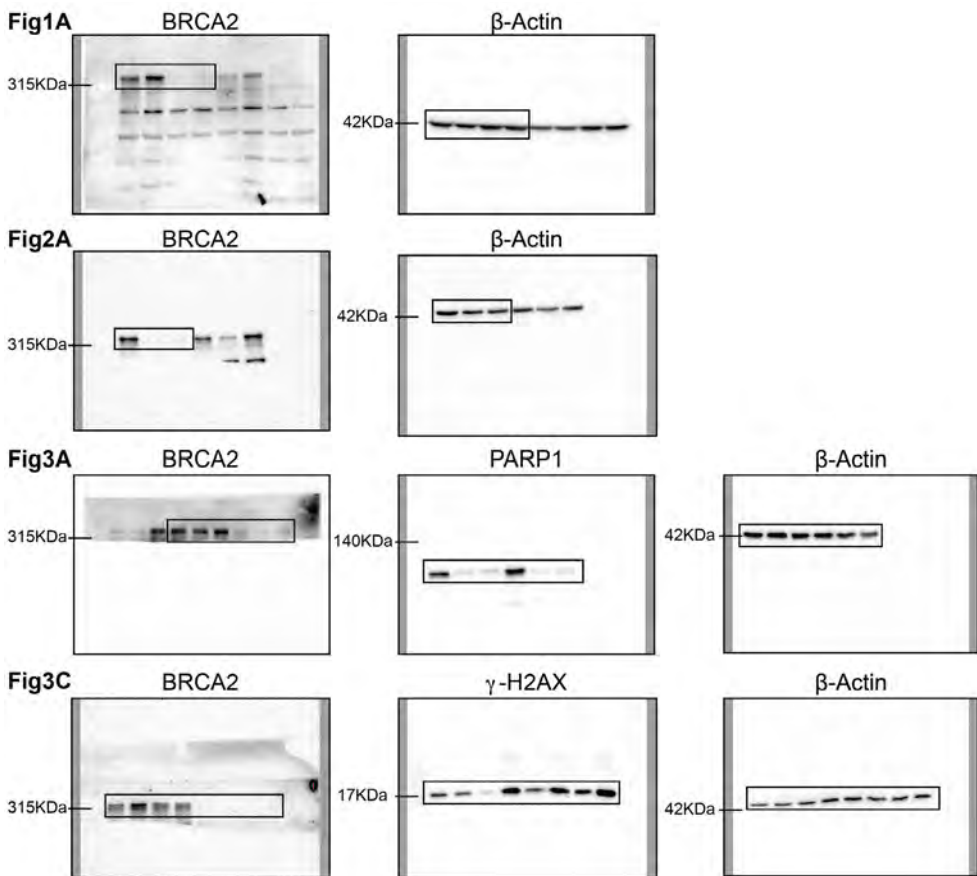
Supplementary Figure 6: PARP inhibition decreases, but does not block proliferation in BRCA2-defective cancer cells. **A)** HeLa cells were transfected with siRNA targeting BRCA2 for 24 hours and were then treated with olaparib (0.5 μ M) for 72 hours. Cells were then incubated with Hoechst for 45 min at 37°C, after which cells containing 2n, 4n or >4n were sorted as indicated. **B, C)** KB2P1.21 (*Brca2*^{-/-}, panel B) and KB2P1.21R1 (*Brca2iBac*, panel C) were treated, sorted and stained as described for panel A. **D)** HeLa cells were transfected with indicated siRNAs and after 24 hours cells were treated with olaparib (1 μ M) or DMSO for 72 hours. One hour prior to harvesting, cells were incubated with BrdU (10 μ M). DNA content and BrdU-positivity was analyzed by flow cytometry. **E)** Left panel: Quantification of BrdU-positive cells from panel D. Error bars indicate standard deviations of 3 independent experiments. Right panel: BrdU-positivity was determined for cells with DNA content between 2n and 4n, and for cells with DNA content between 4n and 8n. Error bars indicate standard deviations from three technical replicates. Throughout the figure 'ns' indicates not significant. P values were calculated using the Student's t-test.

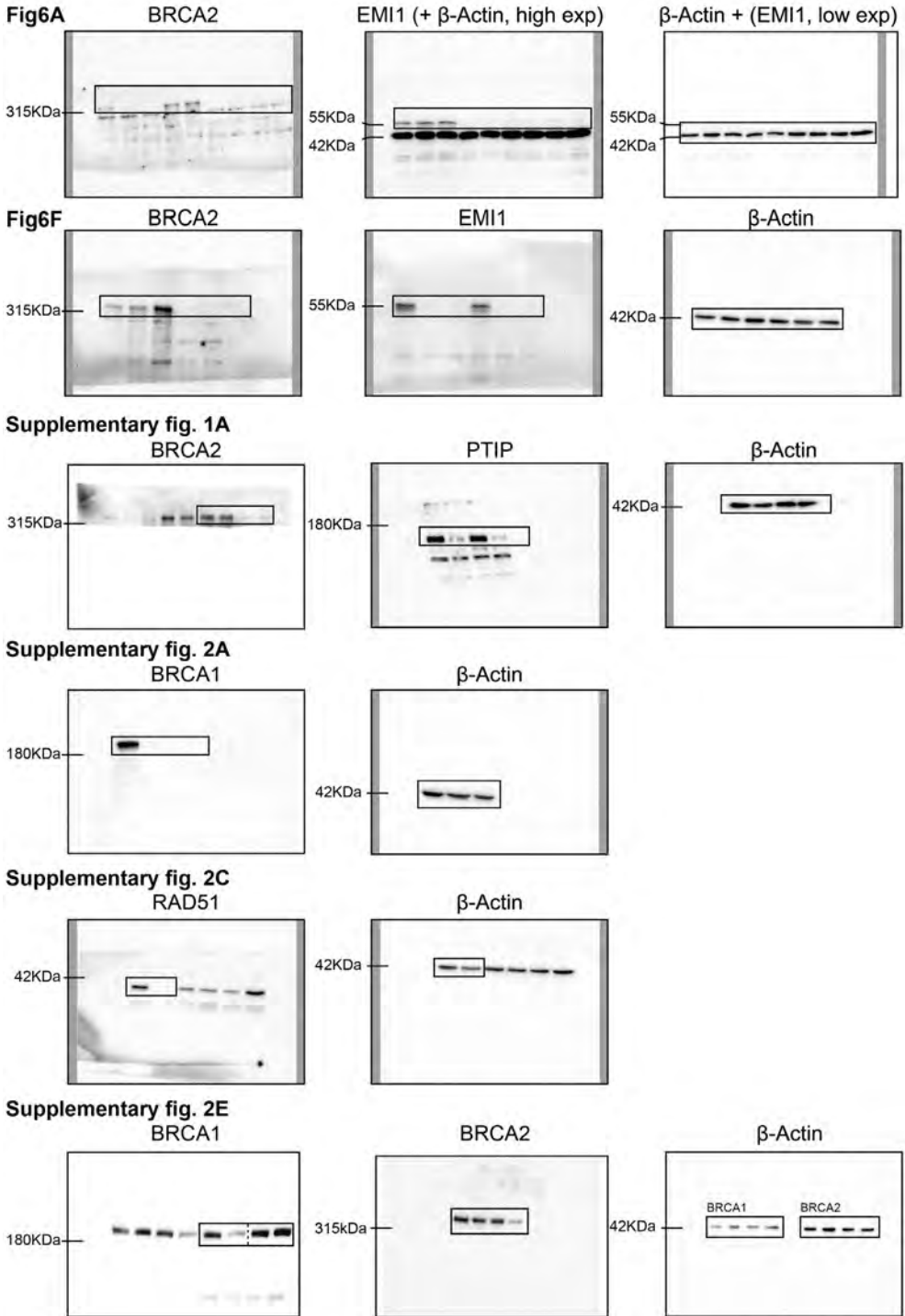


Supplementary Figure 7: EMI1 depletion does not rescue accumulation of DNA lesions nor cell proliferation in BRCA2-depleted cells, and is not differentially expressed in PARP inhibitor sensitive versus resistant tumors. Throughout the figure, control depleted cells are indicated with blue bars/dots, whereas BRCA2-depleted cells are indicated with red bars/dots. **A, B**) HeLa cells were transfected with indicated siRNAs for 24 hours and were then treated with DMSO or olaparib (0.5 μ M) for 24 hours. Cells were stained for FANCD2 or and counterstained with DAPI, and the number of FANCD2 foci per nucleus (Panel A) or γ -H2AX foci per nucleus (panel B) were quantified in interphase cells. Per condition $n=100$ nuclei were analyzed. P values were calculated using two-tailed Mann-Whitney test. **C**) HeLa cells were transfected with indicated siRNAs. After 48 hours, cells were incubated with EdU (10 μ M) for 15 minutes and were subsequently fixed in 4% formaldehyde. EdU was conjugated to azide-Alexa488 and analyzed by fluorescence microscopy. At least 50 cells were analyzed per condition were analyzed. P values were calculated using two-tailed Student's t -test. **D**) AZD2461 sensitive ($n=23$) or resistant ($n=36$) *Brca2*^{-/-}; *p53*^{-/-} tumors were analyzed by RNA sequencing. Normalized counts for *Fbxo5* (encoding EMI1) are indicated. P value was calculated using two-tailed Student's t -test. Throughout the figure 'ns' indicates not significant.



Supplementary Figure 8: Combined treatment of BRCA2-depleted HeLa cells with AZD-1775 and olaparib. HeLa cells were transfected with BRCA2 siRNA or control siRNA (SCR) for 24 hours and subsequently treated with indicated concentrations of olaparib and WEE1 inhibitor (AZD-1775) for 72 hours. MTT conversion was measured as a proxy for cell viability. Error bars indicate standard deviations of two independent experiments.





Supplementary Figure 9: Uncropped western blots

BRCA2 deficiency instigates cGAS-mediated inflammatory signaling and confers sensitivity to tumor necrosis factor-alpha-mediated cytotoxicity

Francien Talens^{1,*}, Anne Margriet Heijink^{1,*}, Lucas T. Jae²,
Stephanie E. van Gijn¹, Rudolf S.N. Fehrmann¹, Thijn R.
Brummelkamp³ & Marcel A.T.M. van Vugt¹

¹Department of Medical Oncology, University Medical Center Groningen, University of Groningen, Groningen, The Netherlands.

²Gene Center and Department of Biochemistry, Ludwig-Maximilians-Universität München, Munich, Germany.

³Oncode Institute, Division of Biochemistry, Netherlands Cancer Institute, Amsterdam, The Netherlands.

* These authors contributed equally

Nature communications (2019) 9;10(1):100

Abstract

Loss of BRCA2 affects genome stability and is deleterious for cellular survival. Using a genome-wide genetic screen in near-haploid KBM-7 cells, we show that tumor necrosis factor- α (TNF α) signaling is a determinant of cell survival upon BRCA2 inactivation. Specifically, inactivation of the TNF receptor (TNFR1) or its downstream effector SAM68 rescues cell death induced by BRCA2 inactivation. BRCA2 inactivation leads to proinflammatory cytokine production, including TNF α , and increases sensitivity to TNF α . Enhanced TNF α sensitivity is not restricted to BRCA2 inactivation, as BRCA1 or FANCD2 inactivation, or hydroxyurea treatment also sensitizes cells to TNF α . Mechanistically, BRCA2 inactivation leads to cGAS-positive micronuclei and results in a cell-intrinsic interferon response, as assessed by quantitative mass-spectrometry and gene expression profiling, and requires ASK1 and JNK signaling. Combined, our data reveal that micronuclei induced by loss of BRCA2 instigate a cGAS/STING-mediated interferon response, which encompasses rewired TNF α signaling and enhances TNF α sensitivity.

4

Cells are equipped with evolutionary conserved pathways to deal with DNA lesions¹. These signaling pathways are collectively called the ‘DNA damage response’ (DDR), and constitute a complex signaling network, displaying multiple levels of cross-talk and feedback control. Multiple parallel kinase-driven DDR signaling axes ensure rapid responses to DNA lesions, whereas a complementary transcriptional DDR axis warrant maintained signaling. Ultimately, activation of the DDR results in an arrest of ongoing proliferation, which provides time to repair DNA damage. In case of sustained or excessive levels of DNA damage, the DDR can instigate a permanent cell cycle exit (senescence) or initiate programmed cell death (apoptosis)².

DNA damage can arise from extracellular sources, including ultraviolet light exposure or anti-cancer treatment, and also originates from intracellular sources, such as oxygen radicals. An alternative source of DNA damage is defective DNA repair. Multiple syndromes are caused by germline mutations in DNA repair genes, which lead to accumulation of DNA damage, and ensuing adverse phenotypes such as accelerated aging, neurodegeneration and predisposition to cancer.

For instance, homozygous hypomorphic mutations of the DNA repair genes *BRCA1* and *BRCA2* are associated with the development of Fanconi anemia^{3,4}, whereas heterozygous *BRCA1* or *BRCA2* mutations predispose affected individuals to early-onset breast and ovarian cancer⁵⁻⁷. Both *BRCA1* and *BRCA2* are key players in DNA damage repair through homologous recombination (HR)⁸. *BRCA1* functions upstream in HR, where it controls the initiation of DNA-end resection at sites of double-stranded breaks (DSBs), in conjunction with CtIP and the MRN complex^{1,2,8}. Once *BRCA1* has been recruited to sites of DNA breaks, it associates with PALB2, which ultimately recruits *BRCA2*. In turn, *BRCA2* controls the loading of the RAD51 recombinase onto resected DNA ends⁹.

Inactivation of *BRCA1*, *BRCA2*, or other HR components severely compromises homology-driven repair of DSBs^{8,10,11}. Since HR is vital to repair double-stranded breaks that spontaneously arise during DNA replication, functional HR is required to maintain genomic integrity^{9,12-14}. In line with this notion, homozygous loss of *Brca1* or *Brca2* leads to the accumulation of DNA breaks and results in activation of p53, which promotes cell cycle arrest and activation of apoptosis and senescence programs¹⁵⁻¹⁸. As a result, *BRCA1* or *BRCA2* loss is not tolerated during human or mouse development and leads to embryonic lethality^{9,12-14}. Importantly, *Brca1* and *Brca2* are not only essential in the context of development but also deletion of these genes severely impacts proliferation *in vitro*, indicating that *BRCA1* and *BRCA2* are intrinsically essential to cellular viability^{12,14,15}.

In clear contrast, loss of *BRCA1* or *BRCA2* is tolerated in breast and ovarian cancers affected by *BRCA1* or *BRCA2* mutations. It remains incompletely understood how these tumor cells remain viable, despite their continuous accumulation of DNA

lesions¹⁹. The observation that *BRCA1* or *BRCA2* mutant cancers almost invariably have inactivated *TP53* points at p53 signaling forming a barrier to cellular proliferation in the absence of *BRCA1* or *BRCA2*. Indeed, concomitant deletion of *Tp53* in mice delays early embryonic lethality in *Brca1*^{-/-} or *Brca2*^{-/-} embryos^{20,21}, and is required to promote tumor formation²². However, *Tp53* inactivation only partially rescued embryonic lethality and cellular viability of *Brca1* or *Brca2* mutant cells, indicating that additional mechanisms are likely to play a role in the survival of these cells.

Despite the extensive knowledge of DDR signaling and insight into DNA repair mechanisms, it currently remains incompletely clear how cells with DNA repair defects are eliminated and, conversely, how such cells can escape clearance. Several gene mutations have previously been described to rescue survival of *BRCA1*-deficient cells, but for *BRCA2*-deficient cancer cells, this remains less clear^{23–27}. Here, we used a haploid genomic screen to identify gene mutations that modify cell viability in *BRCA2*-inactivated cells. We find that loss of the tumor necrosis factor- α (TNF α) receptor, or its downstream signaling component SAM68, rescues cytotoxicity induced by *BRCA2* inactivation in KBM-7 cells. Enhanced TNF α appears to be part of a cell-intrinsic and cGAS/STING-dependent interferon response, triggered by the formation of micronuclei. Combined, our results describe a mechanism by which autocrine TNF α signaling, induced by cGAS/STING signaling upon loss of the *BRCA2* tumor-suppressor gene, limits tumor cell viability.

Results

Screening mutations that rescue *BRCA2*-mediated cell death

To identify gene mutations that rescue cytotoxicity induced by loss of *BRCA2*, monoclonal KBM-7 cell lines were engineered to express doxycycline-inducible *BRCA2* short hairpin RNAs (shRNAs; **Fig. 1A**, **Supplementary Fig. 1A**). To test whether doxycycline treatment resulted in functional inactivation of *BRCA2*, we tested two previously described functions of *BRCA2*: facilitating recruitment of RAD51 to sites of DNA breaks¹⁰ and protection of stalled replication forks²⁸. After 48h of doxycycline treatment, ionizing radiation (IR)-induced recruitment of RAD51 to foci was lost (**Fig. 1B**, **Supplementary Fig. 1B**). Analogously, the ability to protect stalled replication forks, as assessed by DNA fiber analysis, was weakened significantly (**Fig. 1C**). Specifically, control cells maintained nascent DNA at replication forks upon hydroxyurea (HU)-induced replication fork stalling. In contrast, *BRCA2*-depleted cells showed defective protection of stalled forks, as indicated by decreased CldU fiber length after HU treatment (**Fig. 1C**). Finally, analysis of cell numbers showed that proliferation ceased from 4 days after doxycycline treatment onwards in sh*BRCA2* cells, and a near-complete loss of cell viability was seen in less than 2 weeks of *BRCA2* depletion (**Fig. 1D**). Importantly, these effects were observed with two independent *BRCA2* shRNAs. Notably, KBM-7 cells harbor a loss-of-function *TP53* mutation, and our results therefore show that p53 inactivation per se does not preclude the cytotoxic effects of *BRCA2* loss^{9,20}.

The virtually complete cell death after *BRCA2* depletion in the near-haploid KBM-7 cells allowed us to use insertional mutagenesis to screen for gene mutations that confer a survival advantage upon *BRCA2* depletion (**Fig. 1E**). To this end, we mutagenized KBM-7-sh*BRCA2* #2 cells using a retroviral 'gene-trap' vector to obtain a collection of $\sim 100 \times 10^6$ mutants^{29,30}. Massive parallel sequencing was performed on genomic DNA isolated from cells that were allowed to grow for 19 days in the presence of doxycycline. To filter out mutations that affect doxycycline-mediated expression of shRNAs, we performed a cross-comparison with a screen for gene mutations that reversed cell death induced by shRNA-mediated loss of the essential mitotic spindle component Eg5³¹. As expected, multiple dominant integration

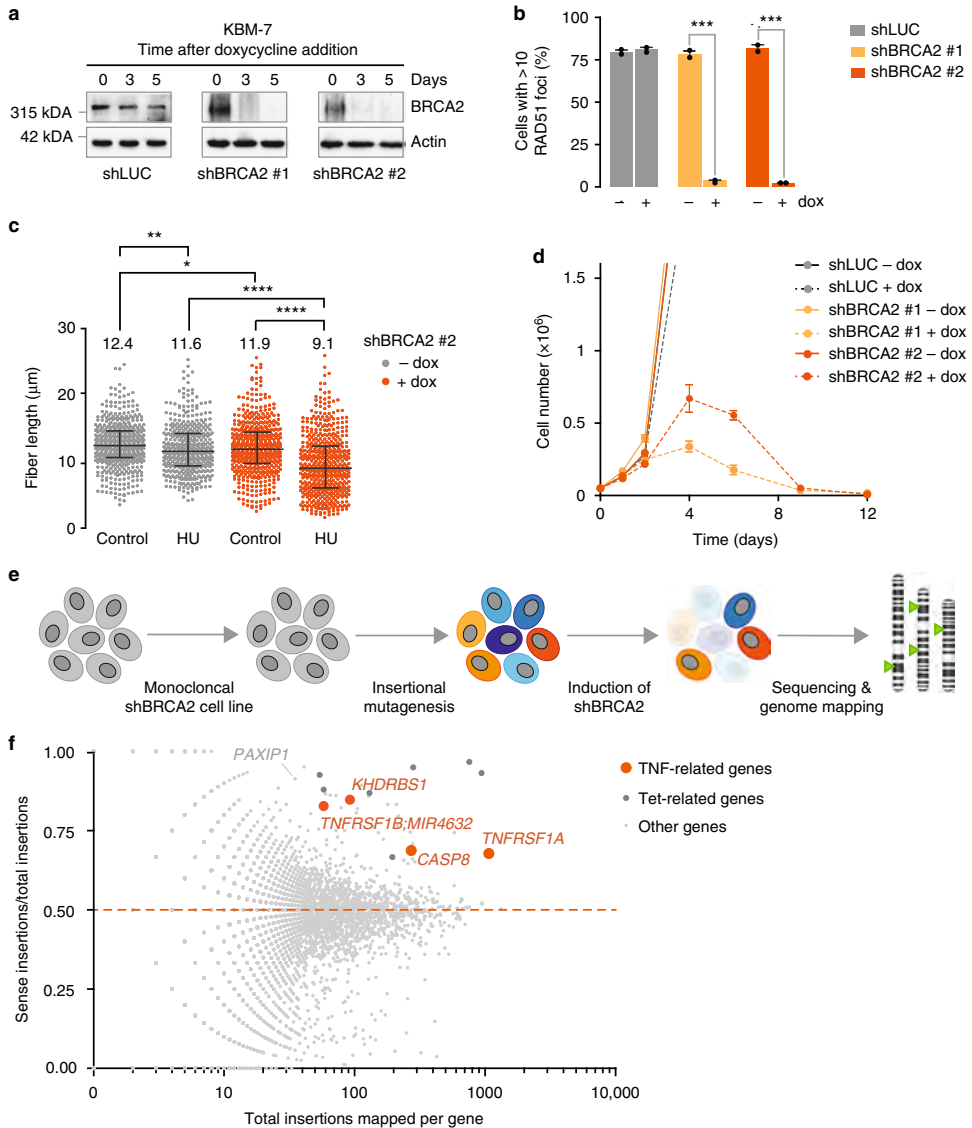


Figure 1. Genetic determinants of cellular survival in BRCA2-depleted KBM-7 cells. A) KBM-7 cells were stably transduced with indicated doxycycline-inducible shRNA vectors. Cells were treated with doxycycline for 3 or 5 days and lysates were immunoblotted for BRCA2 and Actin. **B)** Quantification of the percentage of cells with ≥ 10 RAD51 foci after 5Gy irradiation. KBM-7 cells harboring indicated shRNAs were treated with doxycycline for 96h prior to irradiation. Approximately 100 cells were scored per condition per replicate. Error bars indicate s.d. of two independent experiments. P values were calculated using two-tailed Student's t-test. **C)** KBM-7 cells expressing shBRCA2 #2 were processed for DNA fiber analysis after treatment with doxycycline for 96h. Cells were then incubated with CldU (25 μ M) for 40min to label replication tracks and subsequently treated with HU (2mM) for 4h. CldU track lengths are plotted for ± 500 fibers per condition. Median values are indicated and error bars

hotspots identified in the shBRCA2 screen marked doxycycline-related genes which will nullify shRNA-mediated BRCA2 depletion, including *SUPT3H*, *POU2F1*, and *NONO* (**Supplementary Table 1 and Fig. 1F**). Specifically, in BRCA2-depleted cells, we observed an enrichment of insertion sites in the *PAXIP1* gene, encoding PTIP, which was recently identified to control replication fork degradation in BRCA2-inactivated cells²⁷. Among the most significantly enriched gene mutations, we identified multiple components of the TNF α receptor complex, including *TNFRSF1A* (encoding TNFR1) and *KHDRBS1* (encoding SAM68) (**Fig. 1F**).

TNF α signaling determines viability in BRCA2-depleted cells

To assess whether *BRCA2* mutations in cancers are associated with decreased expression of identified genes, we analyzed the serous ovarian cancers (SOC) within The Cancer Genome Atlas (TCGA) dataset³². We specifically analyzed SOC, since *BRCA2* germline mutations are most frequently found within this subgroup of ovarian cancers. Interestingly, the TNF α pathway component *KHDRBS1* on average showed lower median messenger RNA (mRNA) levels in *BRCA2*-mutated vs. *BRCA2* wildtype (wt) tumors (**Supplementary Fig. 1C**). *KHDRBS1* showed a larger difference in expression level when compared to *PAXIP1*, although differences for both genes were not statistically significant, likely due to the low number of *BRCA2* mutant cancers. According to literature, the *KHDRBS1* gene product SAM68 is recruited to TNFR1 upon activation with TNF α , where it functions as a scaffold for nuclear factor (NF)- κ B activation (**Fig. 2A**, 'complex 1')³³. In a delayed response upon TNF α administration, TNFR1 is internalized and SAM68 and RIPK1 disassociate from the TNF α receptor. Together with FADD (Fas-associated protein with death domain) and caspase-8 (**Fig. 2A**, 'complex 2'), SAM68 and RIPK1 initiate activation of intrinsic caspases and thereby promote cell death³³.

To validate whether TNFR1 or SAM68 inactivation confers a survival advantage upon BRCA2 depletion, KBM-7-shBRCA2 cells were infected with plasmids harboring shRNAs targeting TNFR1 or SAM68 while also encoding an internal ribosome entry site (IRES)-driven mCherry cassette (**Supplementary Fig. 2A**). In line with our screening data, BRCA2-depleted KBM-7 cells that were also depleted for TNFR1 or SAM68 showed a survival advantage over cells only depleted for BRCA2, as judged from the gradual increase in mCherry-positive cells (**Fig. 2B,C**). Notably, TNFR1- or SAM68-depleted KBM-7 cells did not confer a survival advantage through compromising the shRNA-induced knockdown of BRCA2 (**Supplementary Fig. 2B**). In contrast, BRCA2 depletion was nullified by small interfering RNA (siRNA)-mediated knockdown of *SUPT3H*, in line with our expectations (**Supplementary Fig. 2C**).

Depletion of TNFR1 or SAM68 did not reduce the total level of DNA damage induced by BRCA2 loss, as γ H2AX levels were similar (**Supplementary Fig. 2D**). Moreover, loss of TNFR1 or SAM68 did not confer a generic survival advantage, as TNFR1 or SAM68 depletion did not rescue cytotoxicity induced by Eg5 depletion (**Supplementary Fig. 2E**). It should be noted that TNF α receptor signaling controlled cell death upon BRCA2 loss was not observed in all cell line models. When *Brca2*^{F/F}:*Tp53*^{F/F} mouse embryonic fibroblasts (MEFs) were infected with

indicate s.d. *P* values were calculated using two-tailed Student's *t*-test. **D**) Indicated KBM-7 cells were plated in the presence or absence of doxycycline. At indicated time points, cell numbers were assessed. Error bars indicate s.d. of three independent experiments. **E**) Workflow of genetic screen in near-haploid KBM-7 cells. **F**) Insertions sites identified in gene-trap mutagenized KBM-7 cells which survived doxycycline-induced BRCA2 inactivation (shBRCA2 #2). Dots represent individual genes. The frequency of insertions mapped to a specific gene is plotted on the x-axis. The ratio of gene-traps inserted in the sense orientation over total insertions are plotted on the y-axis. Genes that are neutral in conferring a survival advantage in BRCA2-depleted cells have a sense/total insertion ratio of 0.5 (indicated by the red dashed line). Insertion site ratios >0.5 represent genes that when mutated confer survival benefit to BRCA2-depleted cells. Throughout the figure, **P*<0.05, ***P*<0.01, ****P*<0.001 and *****P*<0.0001

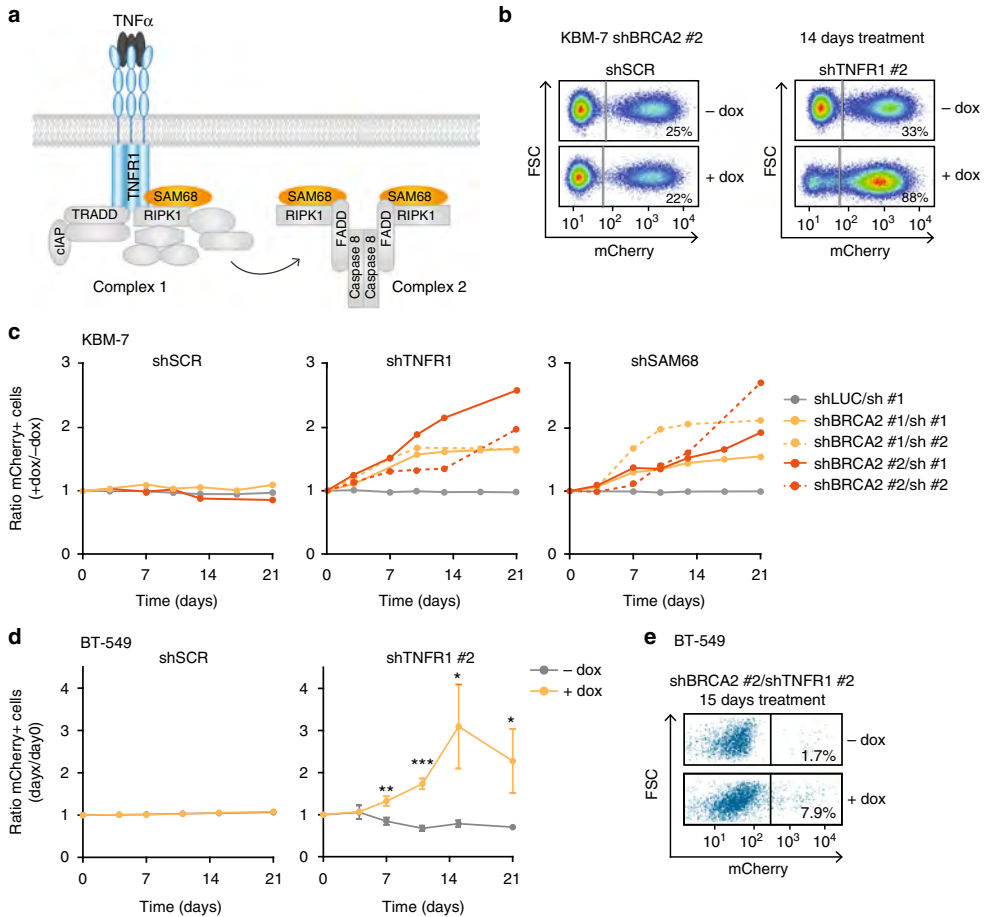


Figure 2. Loss of TNFR1 and SAM68 rescues cellular viability in BRCA2-depleted cancer cells. A) Schematic overview of TNFR1 complex formation upon TNF α binding, leading to cell survival (complex I) or delayed caspase activation and cell death (complex II). **B)** Flow cytometry analysis of KBM-7-shBRCA2 #2 cells, additionally carrying indicated shRNA vectors with IRES-driven mCherry cassettes. Cells were treated with doxycycline for 14 days and percentages of mCherry-positive cells were measured. **C)** Indicated KBM-7-shBRCA2 cells carrying mCherry shRNA cassettes targeting TNFR1, SAM68 or a control sequence ('SCR') were treated with or without doxycycline to induce BRCA2 shRNA expression. Percentages of mCherry-positive cells were measured every 3 or 4 days for 3 weeks after start of doxycycline treatment. Ratios of mCherry-positive cells in doxycycline treated cultures vs. untreated cultures are indicated. Per condition, at least 30,000 events were measured. **D)** BT-549 cells, stably transduced with pLKO.tet.shBRCA2 #2, were infected with IRES mCherry shRNA vectors as for B. Cells were treated with or without doxycycline, and percentages of mCherry-positive cells were measured. Ratios of mCherry-positive cells at indicated time points vs. mCherry-positive percentages at day 0 are indicated. Error bars indicate s.d. of three independent experiments. P values were calculated using two-tailed Student's t-test. * $P < 0.05$, ** $P < 0.01$ and *** $P < 0.001$. **E)** Representative flow cytometry plots of BT-549-shBRCA2 #2 cells from d are shown, carrying mCherry shRNA cassette for TNFR1 #2. Cells were treated for 15 days with or without doxycycline and gated based on mCherry positivity. Numbers indicate the percentages of mCherry-positive cells

Cre recombinase to induce loss of BRCA2 and p53, this resulted in efficient gene inactivation and interfered with cellular viability (**Supplementary Fig. 3A**). Of note, shRNA-mediated inactivation of TNFR1 or SAM68 did not significantly rescue cellular survival (**Supplementary Fig. 3B,C**). In line with these cells not being responsive to TNF α receptor signaling, inactivation of *Brca2* did not confer sensitivity to recombinant TNF α (**Supplementary Fig. 3D**).

Next, two triple-negative breast cancer (TNBC) cell lines, BT-549 and MDA-MB-231, were depleted for BRCA2 (**Supplementary Fig. 4A**). In line with our results in KBM-7 cells, BRCA2 depletion interfered with long-term survival (**Supplementary Fig. 4B**). Assessing the effects of TNFR1 inactivation on the survival of BRCA2-depleted MDA-MB-231 was not feasible, because TNFR1 appeared essential for viability in this cell line, regardless of BRCA2 status (**Supplementary Fig. 4C-E**). In contrast, a stable population of TNFR1-depleted BT-549 cells was established (**Supplementary Fig. 4F,G**), and showed that TNFR1 inactivation results in a survival benefit in BRCA2-depleted BT-549 cells (**Fig. 2D,E**). However, SAM68 depletion interfered with the survival of BT-549 cells independent of BRCA2 status, as hardly any cells survived constitutive SAM68 depletion (**Supplementary Fig. 4G,H**). Combined, our data show that loss of TNFR1 or SAM68 confers a survival advantage in BRCA2-depleted cells, in situations where TNFR1 or SAM68 are not essential for viability, suggesting a mechanistic link between TNF α signaling and BRCA2 function in a context-dependent fashion.

Cytokine production and TNF α signaling upon BRCA2 loss

To further investigate the relation between BRCA2 inactivation and TNF α signaling, we first tested whether limiting the available TNF α pool would alter the reduced cellular viability induced by BRCA2 depletion. Indeed, upon addition of the TNF α -neutralizing antibody infliximab to culture media, cellular viability of BRCA2-depleted KBM-7 cells increased (**Fig. 3A**). Importantly, and in line with these findings, BRCA2 depletion in KBM-7 cells resulted in increased levels of TNF α secretion, as measured using enzyme-linked immunosorbent assay (ELISA; **Fig. 3B**). Of note, TNF α production appeared to be part of a broader panel of upregulated pro-inflammatory cytokines in response to BRCA2 depletion, including interleukin (IL)-6 and IL-8 (**Fig. 3B**). In contrast, the anti-inflammatory cytokine IL-10 was not elevated after BRCA2 depletion (**Fig. 3B**).

Although the levels of TNF α reproducibly increased upon BRCA2 loss, the overall level of TNF α was limited, and we wondered whether this increase accounted for activation of the TNF α signaling cascade. To test this, we measured the levels of c-Jun N-terminal kinase (JNK) phosphorylation (p-JNK), p38 phosphorylation (p-p38), DNA double-strand break accumulation (γ H2AX), and PARP (poly (ADP-ribose) polymerase) cleavage (cPARP) by immunoblotting (**Fig. 3C**) and flow cytometry (**Fig. 3D**). Clearly, BRCA2 depletion for 2, 4 or 7 days resulted in increased levels of p-p38 and p-JNK (**Fig. 3C,D**). Following these observations, the levels of γ H2AX and cleaved PARP were also elevated over time upon BRCA2 loss (**Fig. 3C-E**). Thus, BRCA2 loss instigates a TNF α signaling cascade, leading to cell death in KBM-7 cells, which can be circumvented by sequestering the levels of circulating TNF α .

BRCA2 inactivation leads to increased TNF α sensitivity

Since the overall levels of secreted TNF α after BRCA2 depletion were limited, we wondered whether increased cellular sensitivity to TNF α could also play a role. To test whether BRCA2 inactivation increases sensitivity to TNF α , BRCA2-depleted KBM-7 cells were treated with recombinant TNF α . Indeed, BRCA2-depleted but not control-depleted KBM-7 cells showed significantly increased sensitivity to recombinant TNF α (**Fig. 4A**). Notably, the co-depletion of BRCA2 with SAM68 or TNFR1 rescued the observed sensitivity to TNF α (**Fig. 4B, Supplementary Fig. 5A**). These responses were not specific to KBM-7 cells, as increased TNF α sensitivity was also observed in a dose-dependent manner upon BRCA2

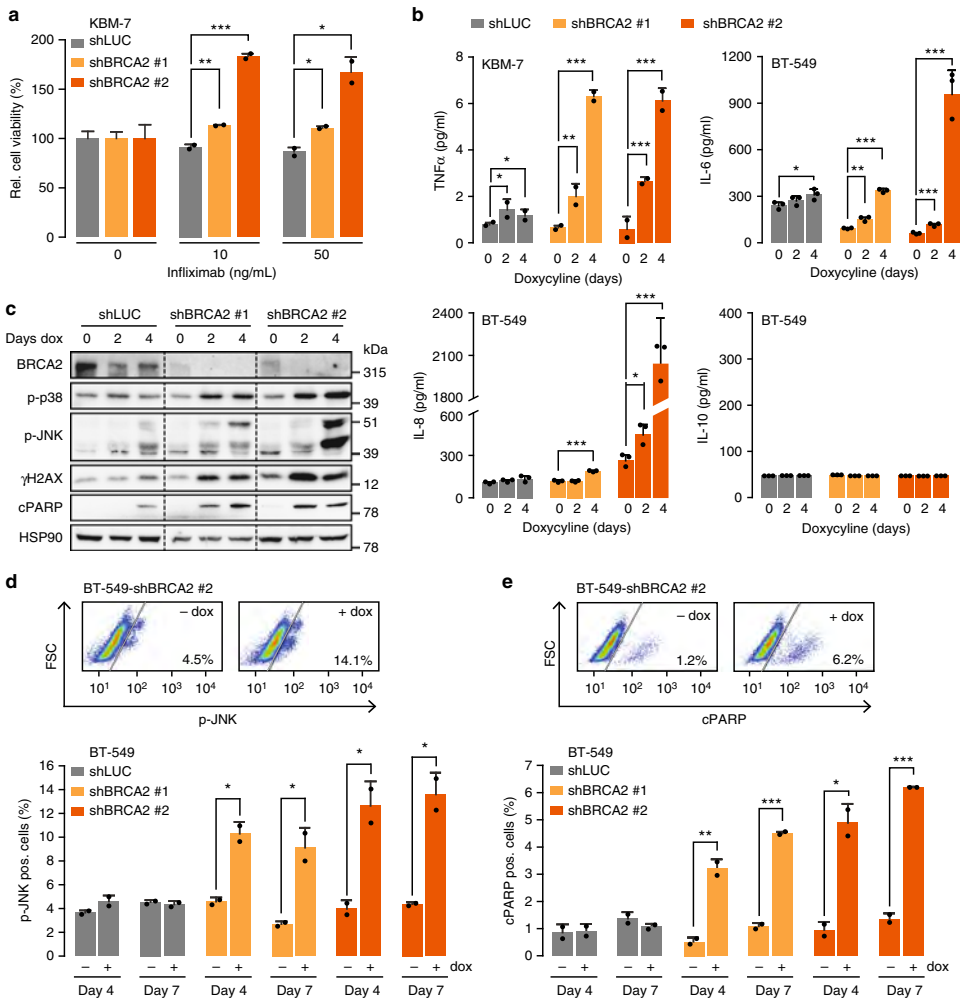


Figure 3. BRCA2 depletion results in increased TNF α signaling. **A)** KBM-7 cells harboring indicated shRNAs were treated with doxycycline for 48h and subsequently plated and treated with indicated concentrations of infliximab for 5 days. Error bars indicate s.d. of two independent experiments. **B)** Levels of TNF α , IL-6, IL-8 and IL-10 secretion upon BRCA2 depletion. After 0, 2 or 4 days of doxycycline treatment, medium was harvested. TNF α was measured using ELISA. IL-6, IL-8 and IL-10 were measured using bead-arrays. Error bars indicate s.d. of two or three independent experiments. **C)** Immunoblotting of BT-549 cells harboring indicated shRNAs after 0, 2 or 4 days of doxycycline treatment. Levels of p-p38, p-JNK, γ H2AX, cleaved PARP ('cPARP') and HSP90 were analyzed. Both JNK isoforms (p46 and p54) are indicated. Dotted lines are used to indicate different shRNAs. **D)** BT-549 cells harboring indicated shRNAs were treated with doxycycline for the indicated time periods, and analyzed by flow cytometry for p-JNK expression. Gating was performed as shown in the top panel. Numbers indicate the percentages of living cells stained positive for p-JNK. Error bars indicate s.d. of two independent experiments. **E)** BT-549 cells were treated as described in D. Cells were analyzed by flow cytometry for cleaved PARP. Gating was performed as shown in the top panel. Numbers indicate the percentages of living cells stained positive for cleaved PARP. Error bars indicate s.d. of two independent experiments. Throughout the figure, P values were calculated using two-tailed Student's t-test. *P<0.05, **P<0.01, ***P<0.001

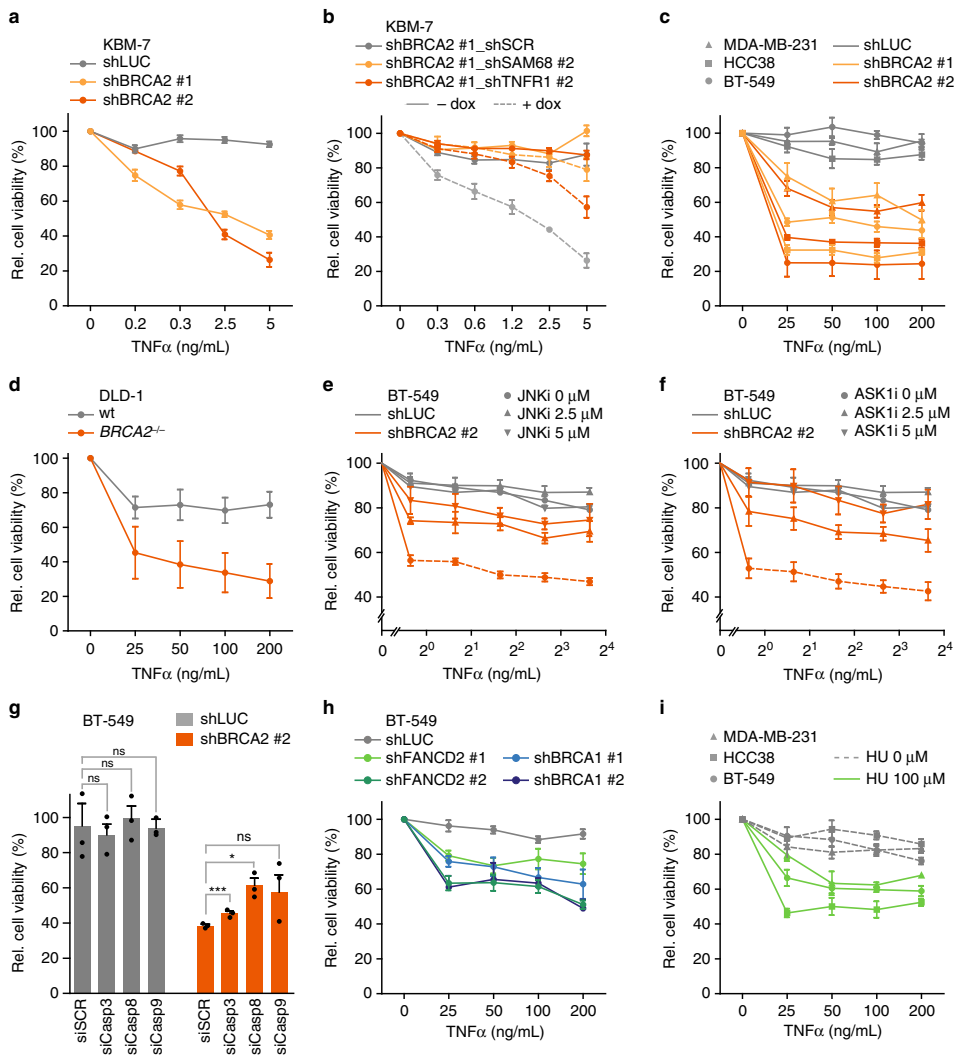


Figure 4. BRCA2 inactivation causes sensitivity to TNF α in cancer cells. **A) KBM-7 harboring shRNAs targeting BRCA2 were treated with doxycycline for 48h and subsequently plated and treated with indicated TNF α concentrations for 5 days. **B)** KBM-7-shBRCA2 #1 cells with shRNAs targeting SAM68, TNFR1 or SCR were treated with or without doxycycline and treated with indicated TNF α concentrations for 5 days. **C)** Breast cancer cell lines MDA-MB-231, HCC38 and BT-549 harboring shLUC, shBRCA2 #1 or shBRCA2 #2 were pre-treated for 48h with doxycycline and subsequently treated with indicated TNF α concentrations for 5 days. **D)** DLD-1 wt or BRCA2^{-/-} cells were plated and treated for 5 days with indicated TNF α concentrations. **E,F)** BT-549 cells harboring shLUC or shBRCA2 #2 were treated with doxycycline for 48h and subsequently treated with indicated concentrations of TNF α , in the presence or absence of JNK inhibitor (E) or ASK1 inhibitor (F) for 5 days. **G)** BT-549 cell lines harboring indicated shRNAs were transfected with indicated siRNAs for 24h, and were subsequently treated with doxycycline for 48h. Cells were re-plated and treated with indicated TNF α concentrations for 5 days. Error bars represent s.e.m. of three independent experiments, with three technical replicates each. P values were calculated using two-tailed Student's t-test. *P<0.05, ***P<0.001. **H)** BT-549 cells harboring shRNAs targeting BRCA1 or FANCD2 were treated with doxycycline for 48h, and subsequently plated and treated**

with indicated TNF α concentrations for 5 days. **J**) MDA-MB-231, HCC38 or BT-549 cells were plated and treated with or without 100 μ M HU and indicated TNF α concentrations for 5 days. Throughout the figure, cell viability was assessed by MTT conversion, and error bars indicate s.e.m. of at least three independent experiments with three technical replicates each. Measurements were normalized to untreated cells. *P* values were calculated using two-tailed Student's *t*-test.

depletion in a panel of TNBC cell lines (**Fig. 4C, Supplementary Fig. 4A, 5B**) and in the colorectal cancer cell line DLD-1, in which the *BRCA2* gene was inactivated using CRISPR/Cas9 (clustered regularly interspaced short palindromic repeats/CRISPR-associated 9) (**Fig. 4D, Supplementary Fig. 5C**). Importantly, the increased sensitivity to TNF α in *BRCA2*-depleted cells could not be attributed to changes in TNFR1 expression levels upon *BRCA2* inactivation (**Supplementary Fig. 5D,E**). Taken together, these results show that *BRCA2* inactivation not only induces TNF α signaling but also results in increased TNF α sensitivity.

In physiological conditions, TNF α -induced NF- κ B pro-survival signaling dominates apoptosis signaling³⁴. However, the sustained activity of JNK (MAPK8), which together with the ASK1 kinase (MAP3K5) acts downstream of the TNF receptor, can 'overrule' NF- κ B pro-survival signaling and drive apoptosis³⁵. Our observation that *BRCA2* depletion leads to increased JNK activity (**Fig. 3C,D**) would be in line with such a mechanism. To test if the sustained activity of ASK1 or JNK kinases is required to mediate TNF α -induced cell death in *BRCA2*-depleted cells, we chemically inhibited JNK (**Fig. 4E, Supplementary Fig. 5F**) or ASK1 (**Fig. 4F, Supplementary Fig. 5F**), in combination with TNF α treatment. Control-depleted BT-549 and HCC38 cells were not sensitive to TNF α , and their viability was not affected by JNK or ASK1 inhibition (**Fig. 4E,F, Supplementary Fig. 5F**). In contrast, *BRCA2*-depleted cells again showed decreased viability upon TNF α administration. Notably, these effects were dose-dependently reversed by JNK or ASK1 inhibition (**Fig. 4E,F, Supplementary Fig. 5F**). To test if the observed increase in TNF α sensitivity upon *BRCA2* depletion was driven by apoptosis-mediated cell death, we depleted caspase-3, -8, or -9 using siRNAs (**Supplementary Fig. 5G**). Especially depletion of caspase-8 and -9 resulted in reduced sensitivity to TNF α in *BRCA2*-depleted cells, while the viability of control-depleted cells was not significantly affected (**Fig. 4G, Supplementary Fig. 5H**). Blocking caspase activity using the broad-spectrum caspase inhibitor zVAD-FMK confirmed the requirement of caspase activity, as TNF α -induced cell death in *BRCA2*-depleted BT-549 and HCC38 cells was significantly rescued by zVAD-FMK treatment (**Supplementary Fig. 5I**). Combined, these data point at JNK and ASK1 kinases and caspase-8 and -9 to drive TNF α -induced cell death upon *BRCA2* inactivation.

To check whether increased TNF α sensitivity was selectively induced by *BRCA2* inactivation, BT-549 and HCC38 cells were depleted for the DNA repair proteins *BRCA1* or *FANCD2* (**Supplementary Fig. 6A,B**). Depletion of *BRCA1* or *FANCD2* decreased long-term survival, comparable to *BRCA2* depletion (**Supplementary Fig. 6C**). Importantly, depletion of *BRCA1* or *FANCD2* also resulted in sensitivity to recombinant TNF α , both in BT-549 and HCC38 cells (**Fig. 4H and Supplementary Fig. 6D**). Of note, induction of replication stress with a non-toxic dose of hydroxyurea (HU) (**Supplementary Fig. 6E,F**) also sensitized TNBC cell lines to recombinant TNF α (**Fig. 4I, Supplementary Fig. 6G**). Thus, TNF α sensitivity is not specific to *BRCA2* inactivation but is also induced by inactivation of *BRCA1* or *FANCD2*, or chemical induction of replication stress.

BRCA2 inactivation leads to an interferon response

To investigate how *BRCA2* inactivation underlies differential activation of the TNF α pathway, we assessed global changes in protein abundance using SILAC-MS (Stable Isotope Labeling by Amino acids in Cell culture—mass spectrometry) (**Fig. 5A**). Labeled ('heavy') or unlabeled ('light') protein extracts from *BRCA2*-depleted or control-depleted BT-549 or HCC38 cells were

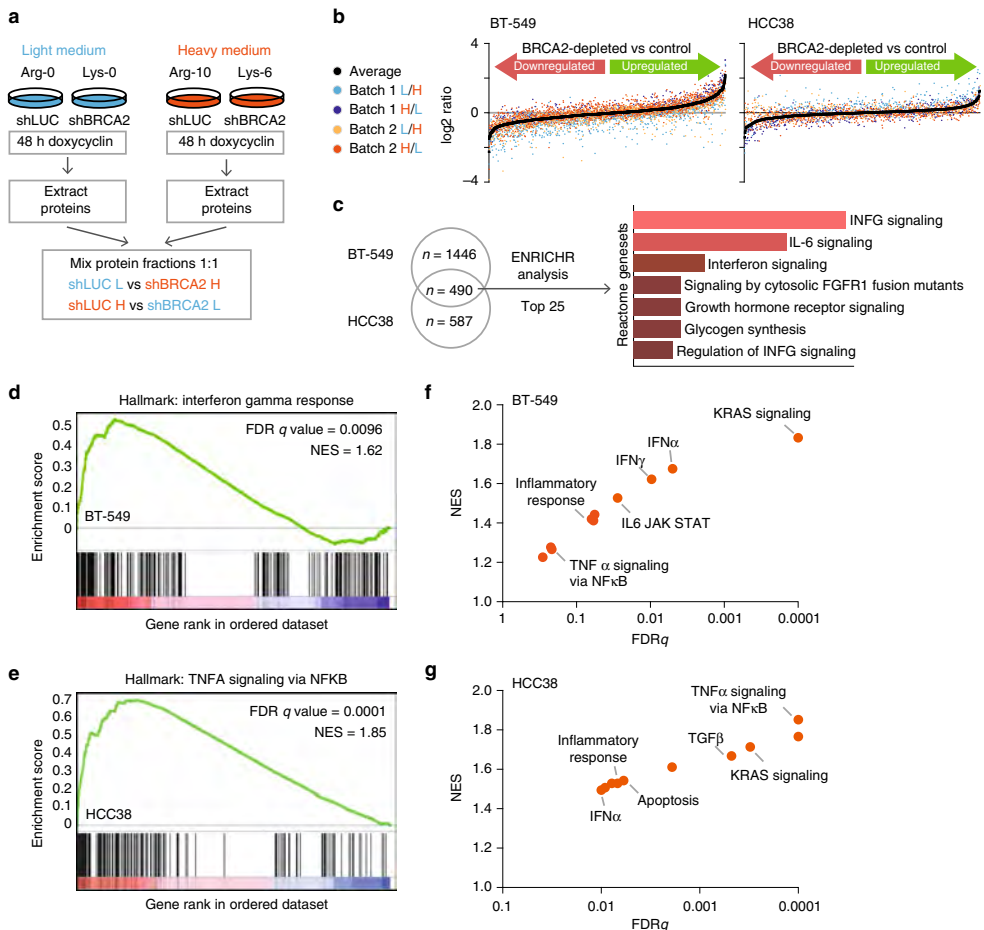


Figure 5. Proteomic and transcriptomic analysis reveals upregulation of pro-inflammatory genes upon BRCA2 depletion. **A)** Workflow of SILAC-MS analysis of BT-549 and HCC38 cell lines with indicated shRNAs. **B)** Log₂ ratios (heavy vs light) of proteins that were measured in at least three out of four independent MS analyses in BT-549 (left panel) or HCC38 (right panel) cells. Black dots represent the mean of log₂ ratios from three or four experiments. **C)** ENRICHR was used to analyze pathway enrichment in top 25 upregulated proteins in response to BRCA2 depletion in BT-549 cells and HCC38 cells. The top 10 enriched Reactome datasets are displayed. **D,E)** RNA sequencing was performed on BT-549 and HCC38 cells harboring shLUC or shBRCA2 #2, treated for 72 h with or without doxycycline. Gene set enrichment analysis (GSEA) using ‘Hallmark’ gene sets showed enrichment of Interferon Gamma response (D) and TNFA signaling via NF- κ B (E) in BRCA2-depleted cells. **F,G)** Top 10 enriched Hallmark gene sets in BRCA2-depleted BT-549 (F) and HCC38 (G) cells compared to control cell lines. The top 10 list of enriched pathways can be found in Supplementary Fig. 7.

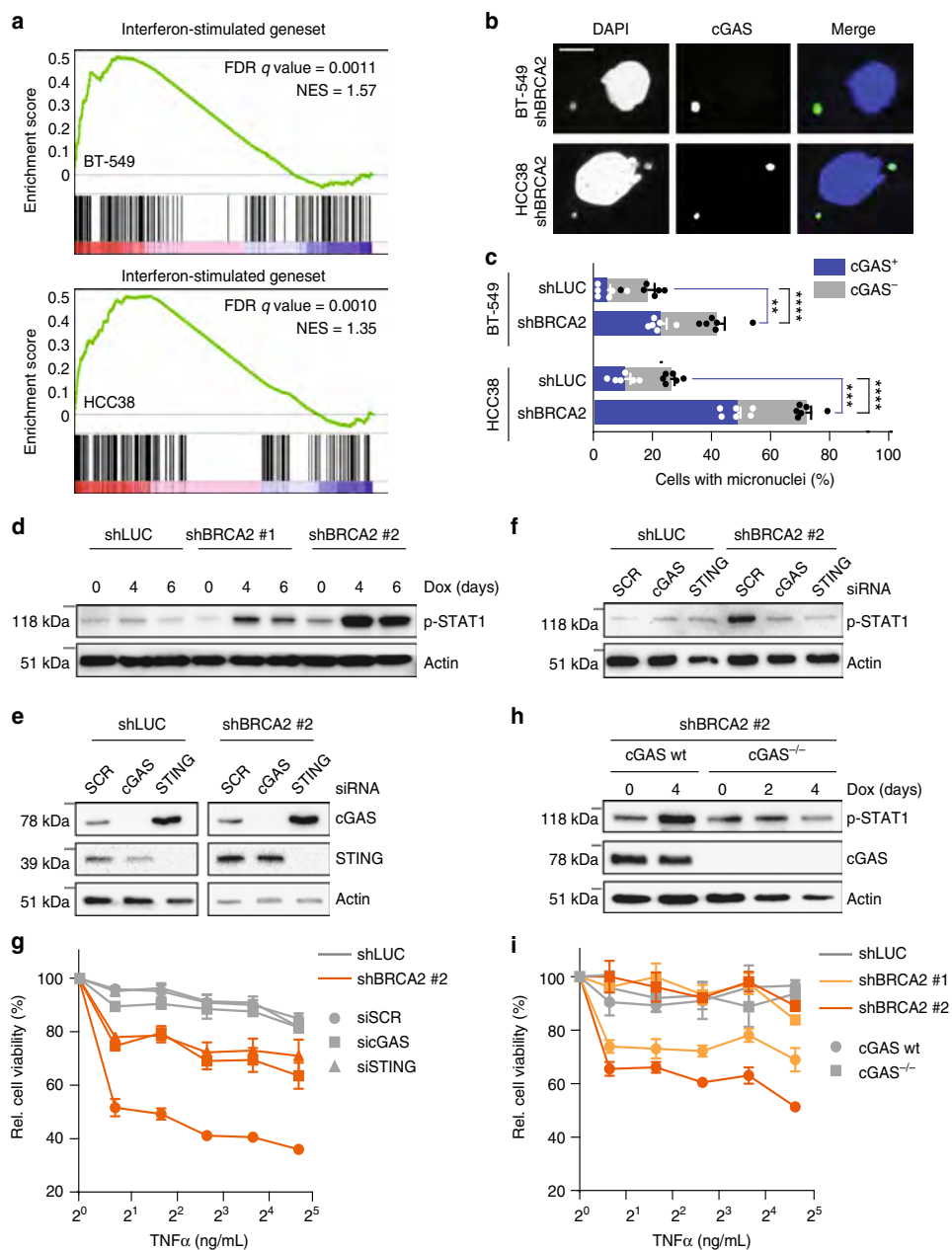
mixed and analyzed by mass spectrometry (MS). To control for potential effects of metabolic labeling, label-swap controls were included (Fig. 5A). Common differentially expressed proteins measured in at least three out of four independent MS runs were plotted (Fig. 5B). Interestingly, depletion of BRCA2 resulted in a common set of upregulated proteins (Fig. 5C). When the top 25 upregulated proteins were analyzed using gene set enrichment, a clear enrichment for interferon- α and interferon- γ pathways was found (Fig. 5C). Because mass

spec proteomics only captures a subset of the proteome, we validated these observations using gene expression profiling. To this end, gene set enrichment analysis was performed on RNA-sequencing (RNAseq) data derived from control-depleted or BRCA2-depleted BT-549 or HCC38 cells (**Fig. 5D-G**). The most significantly enriched gene sets in both cell lines included interferon- γ and interferon- α responses, as well as activation of TNF α -responsive pathways (**Fig. 5D-G, and Supplementary Fig. 7A,B**).

cGAS/STING-dependent TNF α sensitivity upon BRCA2 loss

Previous studies from us and others have demonstrated that defective DNA repair can lead to aberrant mitoses and micronuclei^{36,37}. Recently, cells harboring micronuclei were shown to express a distinct gene expression profile, characterized by cGAS/STING (cyclic GMP-AMP synthase/stimulator of interferon genes)-dependent interferon signaling³⁸. RNAseq analysis of BRCA2-depleted BT-549 and HCC38 cells showed significant enrichment for this 'interferon-stimulated geneset' (**Fig. 6A**)³⁸. In line with this notion, we observed elevated levels of micronuclei and cGAS-positive micronuclei upon BRCA2 depletion in BT-549 and HCC38 cells (**Fig. 6B,C**), which was accompanied by elevated levels of phosphorylated signal transducer and activator of transcription 1 (STAT1), a key mediator of interferon-induced transcription (**Fig. 6D, Supplementary Fig. 7C**). Importantly, siRNA-mediated depletion of cGAS or STING resulted in reduced levels of STAT1 phosphorylation in BRCA2-depleted BT-549 and HCC38 cells (**Fig. 6E,F and Supplementary Fig. 7D,E**). Furthermore, depletion of cGAS or STING rescued the sensitivity of TNF α upon BRCA2 inactivation in BT-549 and HCC38 cells (**Fig. 6G and Supplementary Fig. 7F**). These results were confirmed in BT-549 cells in which cGAS was mutated using CRISPR/Cas9. Specifically, mutation of cGAS rescued long-term viability in BRCA2-depleted cells (**Supplementary Fig. 7G,H**). Also, TNF α sensitivity and STAT1 phosphorylation upon BRCA2 depletion were rescued in cGAS^{-/-} cells compared to cGAS wt cells (**Fig. 6H,I and Supplementary Fig. 7I,J**). Combined, these data show that BRCA2 inactivation instigates a cGAS/STING-dependent pro-inflammatory response which enhances TNF α sensitivity (**Fig. 7**).

Figure 6. Micronuclei formation and cGAS/STING-dependent STAT1 activation upon BRCA2 depletion. **A)** GSEA shows significant enrichment of interferonstimulated genes in BRCA2-depleted BT-549 (left panel) or HCC38 (right panel) cells. **B)** BT-549 and HCC38 cell lines harboring shLUC or shBRCA2 #2 were treated with doxycycline for 4 days, and stained with anti-cGAS and DAPI. Scale bar represents 15 μ m. **C)** EQuantification of cGAS-positive micronuclei as described in (B). ≥ 300 Cells were counted per condition. Error bars indicate s.e.m. of six independent experiments. P values were calculated using twotailed Student's t-test. **P < 0.01, ***P < 0.001, ****P < 0.0001. **D)** BT-549 cells harboring shLUC or shBRCA2 #2 were treated with doxycycline for indicated time periods. Phosphorylation status of STAT1 was analyzed by immunoblotting. **E)** BT-549 cells harboring shLUC or shBRCA2 #2 were transfected with indicated siRNAs. Levels of cGAS and STING were analyzed by immunoblotting at 5 days post transfection. **F)** BT-549 cells harboring shLUC or shBRCA2 cells were transfected with indicated siRNAs for 24 h, and subsequently treated with doxycycline for 48 h. Phosphorylation status of STAT1 was analyzed by immunoblotting. **G)** BT-549 cells harboring shLUC or shBRCA2 cells were transfected with indicated



siRNAs for 24 h. Cells were re-plated and treated with doxycycline for 48 h, followed by treatment with indicated TNF α concentrations for 5 days. **H)** cGAS^{-/-} or wt BT-549 cells with indicated shRNAs were pre-treated for 48 h with doxycycline and subsequently treated with indicated TNF α concentrations for 5 days. **I)** cGAS^{-/-} or wt BT-549 cells with shBRCA2 #2 were treated with doxycycline for indicated time periods. Phosphorylation status of STAT1 and expression of cGAS were analyzed by immunoblotting. For G, H, cell viability was assessed by MTT conversion. Error bars indicate s.e.m. of at least three independent experiments with three technical replicates each.

Discussion

DNA repair defects facilitate genome instability and the ensuing accumulation of cancer-promoting mutations³⁹. Indeed, inherited or somatic mutations in DNA repair genes are frequently observed in cancer¹. Yet, defective DNA repair compromises cellular viability, and it remains incompletely clear how (tumor) cells respond to a loss of DNA repair pathways. In this study, we describe a prominent transcriptional interferon response upon BRCA2 inactivation, which can be ascribed to genome instability and ensuing cytoplasmic DNA. This response leads to wide-spread cellular re-wiring, including enhanced sensitivity to TNF α . This latter feature was the basis on which TNFRSF1A (encoding TNFR1) and KHDRBS1 (encoding SAM68) were identified to rescue cell death in BRCA2-depleted KBM-7 cells. Specifically, HR-deficiency instigates the production of pro-inflammatory cytokines, including TNF α , which activates TNF α receptor-mediated cell death. Interference with the cytosolic DNA sensor cGAS/STING, the TNF α -receptor, or its downstream signaling components rescued TNF α -induced cell death in BRCA2-depleted cells.

TNF α signaling has previously been described to context-dependently promote cellular survival or promote apoptosis³⁴. We find that TNF α signaling in the context of accumulated DNA damage exerts pro-apoptotic effects, either in the context of defective DNA repair or through HU-induced replication stress. These conditions have in common that they induce micronuclei, which were recently shown to be a source of cytoplasmic DNA^{38,40}. cGAS/STING activation was previously described to instigate a cell-intrinsic interferon response, resulting in STAT signaling⁴¹. Indeed, BRCA2 depletion induced cGAS-positive micronuclei, along with increased levels of phosphorylated STAT1 (Fig. 6). The observed cellular re-wiring resulted in enhanced TNF α sensitivity, which depended on ASK1 and JNK kinases as well as caspase-8 and -9. Our observation that multiple caspases are involved in TNF α -mediated cell death in BRCA2-defective cells is in line with caspase-8 being engaged in TNF α -mediated apoptosis⁴², caspase-9 being involved in intrinsic, DNA damage-induced apoptosis⁴³, and caspase-3 being a common downstream factor in programmed cell death.

Our findings are also in good agreement with previous reports of increased transcription of TNF α upon irradiation⁴⁴, enhanced sensitivity of FANC-C mutant cells to TNF α ⁴⁵, irradiation-induced re-wiring of TNF α signaling which limited cellular survival⁴⁶ and STING activation in response to S-phase DNA damage⁴⁷. Furthermore, treatment with recombinant TNF α was shown to sensitize cancer cells for genotoxic agents⁴⁸.

Multiple other mutations have previously been described to rescue cell death upon loss of homologous recombination genes. Most of these mutations (including TP53BP1, MAD2L2, HELB, RIF1 and Shieldin complex members) could rescue cell death and PARP1 inhibitor sensitivity induced by inactivation of BRCA1 but not BRCA2, which is likely due to BRCA2 functioning downstream of DNA-end resection^{23,25,26,49,50}. Recently, inactivation of PAXIP1 (encoding PTIP) was shown to rescue cell death induced by BRCA2 mutation²⁷. PAXIP1 was identified in our screen, albeit less significantly enriched when compared to TNFR1 and SAM68.

Constitutive NF- κ B activation is described to often occur in different types of cancers and is associated with aggressive tumor growth and therapy resistance⁵¹. Recently, and in line with our observations, cancer-associated genomic instability was shown to drive NF- κ B activation through a cytosolic DNA response⁵². Such NF- κ B activity might be accompanied by autocrine TNF α secretion, as has been demonstrated for head-and-neck cancers⁵³. NF- κ B activation was previously described in response to DSB formation, where it provides an initial cellular stress response to DNA damage^{54,55}. Paradoxically, sustained levels of DNA damage (in our models caused by BRCA2 deficiency) lead to prolonged JNK activation, which is normally suppressed by NF- κ B^{56,57}. Consequently, sustained JNK signaling can promote pro-apoptotic

signaling upon TNF α -induced TNFR1 activation^{58,59}.

TNF α , in analogy to NF- κ B signaling, has also been described to play a role in cancer. Recombinant TNF α was shown to induce cancer cell senescence when combined with interferon- γ treatment and was demonstrated to induce tumor cell death in metastatic melanoma via isolated limb perfusion^{60,61}. Our observations of TNF α sensitivity of BRCA2-defective cancer cells suggest that BRCA2 mutant tumors may be selectively sensitive to TNF α . Unfortunately, the development of TNF α -based treatment modalities was not successful due to toxicity⁶². Conversely, our data suggest that modulation of TNF α or cGAS/STING signaling may allow survival of BRCA-deficient tumor cells, and warrants care in using TNF α antagonists in BRCA mutation carriers.

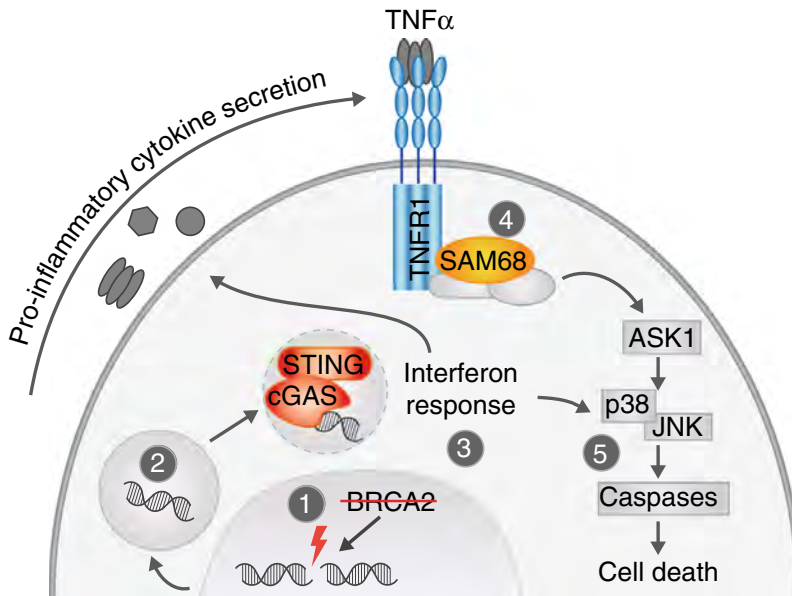


Figure 7. Schematic model of inflammatory signaling upon BRCA2 inactivation. BRCA2 inactivation (1) leads to micronuclei formation (2) and cGAS/STING-dependent activation of an interferon response (3). This leads to pro-inflammatory cytokines production, and sensitivity to TNF α , in a TNFR1/SAM68 (4) and ASK1/JNK-dependent fashion (5).

Methods

Cell culture

KBM-7, BT-549, HCC38, MDA-MB-231 and HEK293T cells were obtained from ATCC. DLD-1 human colorectal adenocarcinoma cells were from Horizon (Cambridge, UK). MEFs harboring the *Brca2*^{sko} allele were a kind gift of Jos Jonkers and Peter Bouwman (Netherlands Cancer Institute, Amsterdam, The Netherlands). Human near-haploid KBM-7 cells were cultured in Iscove's modified Dulbecco's medium. MDA-MB-231 breast cancer cells, 293T human embryonic kidney cells, DLD-1 cells and mouse embryonic fibroblasts were cultured in Dulbecco's modified Eagle's medium. BT-549 and HCC38 were cultured in Roswell Park Memorial Institute (RPMI) medium. Growth media for each line were supplemented with 10% fetal calf serum and penicillin/streptomycin (100 units per mL). All human cell lines were

cultured at 37 °C in a humidified incubator supplied with 5% CO₂. MEFs were cultured in a low-oxygen (1% O₂) incubator. For stable isotope labeling, BT-549 or HCC38 cells harboring shLUC and shBRCA2 #2 were cultured for at least four cell passages (~14 days) in RPMI medium with unmodified arginine (Arg) and Lysine (Lys) (Light 'L') or with stable isotope-labeled Arg¹⁰ and Lys⁶ (Heavy 'H') (Silantes).

Viral transduction

To generate KBM-7 and breast cancer cell lines with doxycycline-inducible shRNAs, cells were infected with Tet-pLKO-puro, harboring shRNAs directed against luciferase ('shLUC', 5'-AAGAGCTGTTTCTGAGGAGCC-3'), KIF11 (5'-CACGTACCCTTCATCAAATTT-3'), BRCA2 (#1 5'-GAAGAATGCAGGTTTAATA-3' and #2 5'-ACAACAATTACGAACCAAACCTT-3'), BRCA1 (#1 5'-CCCACCTAATTGACTGAATT-3' and #2 5'-GAGTATGCAAACAGCTATAAT-3') and FANCD2 (#1 5'-AAGGGAGAAGTCATCGAAGTA-3' and #2 5'-GGAGATTGATGGTCTACTAGA-3'). Tet-pLKO-puro was a gift from Dmitri Wiederschain (Addgene plasmid #21915)⁶³.

To validate hits from the genetic screens, KBM-7, MEFs and breast cancer cells were transduced with pLKO.1 vectors, which in addition to the shRNA cassette either carried an IRES mCherry cassette (pLKO.1-mCherry, a kind gift from Jan Jacob Schuringa (UMCG, The Netherlands)) or a puromycin resistance cassette (pLKO.1-puro, a gift from David Root, Addgene plasmid #10878)⁶⁴. Both pLKO.1 plasmids were used as described previously³⁰. shRNAs against TNFRSF1A and KHDRBS1 were cloned into pLKO.1 vectors using the AgeI and EcoRI restriction sites. The shRNA targeting sequences that were used are: TNFRSF1A (#1, 5'-GGAGCTGTTGGTGGGAATATA-3' and #2, 5'-TCCTGTAGTAACTGTAAGAAA-3'), KHDRBS1 (#1, 5'-ACCCACAACAGACAAGTAATT-3' and #2, 5'-GATGAGGAGAATTACTTGGAT-3') and SCR (5'-CAACAAGATGAAGAGCACCAA-3'). For MEF cells, shRNA sequences used were for TNFRSF1A (5'-GGCTCTGCTGATGGGGATACA-3'), KHDRBS1 (5'-GACGAGGAGAATTATTTGGAT-3') and SCR (5'-CAACAAGATGAAGAGCACCAA-3'). Lentiviral particles were produced as described previously³⁰. In brief, HEK293T packaging cells were transfected with 4 μg pLKO.1 DNA in combination with the packaging plasmids lenti-VSV-G and lenti-ΔYPR using a standard calcium phosphate protocol. Virus-containing supernatant was harvested at 48 and 72 h after transfection and filtered through a 0.45 μm syringe filter with the addition of 4 μg per mL polybrene. Supernatants were used to infect target cells in three consecutive 12 h periods.

MEFs were transduced with pRetroSuper retrovirus as described previously²³. Briefly, HEK293T cells were grown to 70% confluency and transfected with 10 μg retroviral vector encoding 'Hit-and-run' Cre recombinase together with Gag-Pol packaging and VSV-G⁶⁵. Supernatants were harvested at 48 and 72 h after transfection and filtered through a 0.45 μm syringe filter. MEFs were plated and infected for 24 h with retroviral supernatant with an additional second and third round of infection after 24 and 32 h. At 24 h after the last infection, cells were washed and cultured in fresh medium with puromycin (2 μg per mL) for 48 h. Switching of the conditional sko allele upon Cre retrovirus, resulting in a 110 base-pair fragment, was shown by PCR amplification of genomic DNA with the following primers: 5'-GTG GGC TTG TAC TCG GTC AT-3' (forward) and 5'-GTA ACC TCT GCC GTT CAG GA-3' (reverse).

Generation of cGAS knockout cells by the CRISPR/Cas9 system

CRISPR guide RNAs were generated against cGAS (#1 caccgGGCATTCCGTGCGGAAGCCT; #2 caccgTGAACGGATTCTTCTTTTCG) and cloned into the Cas9 plasmid using the AgeI and EcoRI restriction sites. The pSpCas9(BB)-2A-Puro V2.0 (PX459) was a gift from Feng Zhang (Addgene plasmid #62988)⁶⁶. BT-549 cells were transfected with both guide RNA plasmids

simultaneously (2 µg) using FuGene (Promega) according to the manufacturer's instructions. After transfection, cells were selected with puromycin (1 µg per mL) for 2–3 days. Single cell cGAS^{-/-} clones were confirmed by immunoblotting. Subsequently, cGAS^{-/-} or parental cells were infected with Tet-pLKO-puro shRNAs targeting BRCA2 or Luciferase as described before.

Gene-trap mutagenesis and mapping of insertion sites

KBM-7 cells were infected with pLKO.1-tet-puro-BRCA2 #2 and puromycin-resistant clones were sorted into monoclonal cell lines. The resulting monoclonal KBM-7-shBRCA2 #2 cell line was mutagenized using retroviral infection as described previously⁶⁷. In short, approximately 64×10E6 KBM-7 cells were retrovirally infected with the gene-trap vector pGT, containing a strong splice acceptor. After three consecutive rounds of infection, an ~75% infection rate was achieved based on green fluorescent protein positivity. All mutagenized cells were pooled and 20×10E6 cells were treated with 1 µg per mL doxycycline. At 5 days after doxycycline addition, cells were plated at 20,000 cells per well in 40 96-well plates to allow competitive selection for 14 days. Subsequently, cell pellets were frozen and DNA was isolated. Viral insertions were amplified using LAN PCR, identified by massive parallel sequencing and mapped to the human genome as described previously⁶⁸. DNA sequencing data are available at the NCBI short read archive (PRJNA299537).

Western blotting

Knockdown efficiencies and biochemical responses were analyzed by western blotting. Cells were lysed in Mammalian Protein Extraction Reagent (MPER, Thermo Scientific), supplemented with protease inhibitor and phosphatase inhibitor cocktail (Thermo Scientific). Separated proteins were transferred to polyvinylidene fluoride membranes and blocked in 5% milk in Tris-buffered saline, with 0.05% Tween-20. Immunodetection was done with antibodies directed against BRCA2 (1:1000, Calbiochem, #OP95), TNFR1 (1:500, Cell Signaling, #3736; 1:1000, Santa Cruz, sc-8436), SAM68 (1:1000, Santa Cruz, sc-333), BRCA1 (1:1000, Cell Signaling, #9010), FANCD2 (1:200, Santa Cruz, sc-20022), phospho-JNK (1:1000, Cell Signaling, #9251), phospho-p38 (1:1000, Cell Signaling, #4511), cleaved PARP (1:1000, Cell Signaling, #5625), γH2AX (1:1000, Cell Signaling, #9718), phospho-STAT1 (1:1000, Cell Signaling, #9167, #8826), HSP90 (1:1000, Santa Cruz, #sc-69703), cGAS (1:1000, Cell Signaling, #15102), STING (1:1000, Cell Signaling, #13647), caspase-3 (1:1000, Cell Signaling, #9662), caspase-8 (1:1000, Enzo, #ALX-804-242), caspase-9 (1:1000, Cell Signaling, #9502) and beta-Actin (1:10,000, MP Biochemicals, #69100). Appropriate horseradish peroxidase-conjugated secondary antibodies (1:2500, DAKO) were used and signals were visualized with enhanced chemiluminescence (Lumilight, Roche diagnostics) on a Bio-Rad Bioluminescence device, equipped with Quantity One/Chemidoc XRS software (Bio-Rad). Uncropped versions of all western blots can be found in Supplementary Fig. 8-13.

Quantitative RT-qPCR

Cell pellets from KBM-7-shBRCA2 #1, KBM-7-shBRCA2 #2 or KBM-7-shLUC treated with doxycycline (1 µg per mL) for 0 or 4 days were harvested. Total RNA was isolated using the RNeasy Mini Kit (Qiagen) and complementary DNA (cDNA) was synthesized using SuperScript III (Invitrogen) according to the manufacturer's instructions. Quantitative reverse transcription-PCR (RT-PCR) for BRCA2 mRNA expression levels was performed in triplicate using the following oligos: 5'-TTGTTTCTCCGGCTGCAC-3' (forward) and 5'-CGTATTTGGTGCCACAACCT-3' (reverse). Glyceraldehyde 3-phosphate dehydrogenase (GAPDH) was used as a reference and experiments were performed on an Applied Biosystems Fast 7500 machine. Alternatively, KBM-7-shBRCA2 #2 cells were pre-treated with doxycycline for 24h prior to transfection

with 40nM SUPTH3 siRNA (Thermo Scientific; ON-TARGETplus SMART pool, #L-019548-00) or 'medium GC duplex' control siRNA (Life Technologies, #12935-300). At 72h after siRNA transfection, cell pellets were harvested and BRCA2 mRNA levels were determined as above.

Immunofluorescence microscopy

KBM-7 cells were left untreated or were irradiated using a Cesium¹³⁷ source (CIS international/IBL 637 irradiator, dose rate: 0.01083Gy per second). After 3h, cells were washed in phosphate-buffered saline (PBS) and then fixed in 2% paraformaldehyde with 0.1% Triton X-100 in PBS for 30min at room temperature. Cells were permeabilized in 0.5% Triton X-100 in PBS for 10min. Subsequently, cells were extensively washed and incubated with PBS containing 0.05% Tween-20 and 4% bovine serum albumin (fraction V) (PBS-Tween-BSA) for 1h to block nonspecific binding. For micronuclei staining, BT-549 and HCC38 cells were grown on coverslips and treated with doxycycline for 4 days. Cells were fixed in 4% paraformaldehyde for 15min at room temperature. Subsequently, cells were permeabilized with 0.1% Triton X-100 in PBS for 1min followed by blocking in 0.05% Tween-20 and 2.5% BSA in PBS for 1h. Cells were incubated overnight at 4°C with primary antibodies targeting RAD51 (GeneTex, GTX70230, 1:400), γ H2AX (Cell Signaling, #9718, 1:100) or cGAS (Cell Signaling, #15102, 1:200) in PBS-Tween-BSA. Cells were extensively washed and incubated for 1h with Alexa-conjugated secondary antibodies (1:400) and counterstained with 4',6-diamidino-2-phenylindole (DAPI). Slides were mounted with ProLong Antifade Mountant (Thermofisher). Images were acquired on a Leica DM-6000RXA fluorescence microscope, equipped with Leica Application Suite software.

DNA fiber assay

To assess replication fork protection during replication stress, KBM-7-shBRCA2 #2 cells were pre-treated with doxycycline (1 μ g per mL) for 96h, and then pulse-labeled with chlorodeoxyuridine (CldU, 50 μ M) for 40min. Subsequently, cells were washed with medium and incubated with HU (2mM) for 4h. Cells were lysed on microscopy slides in lysis buffer (0.5% sodium dodecyl sulfate (SDS), 200mM Tris (pH 7.4), 50mM EDTA). DNA fibers were spread by tilting the slide and were subsequently air-dried and fixed in methanol/acetic acid (3:1) for 10min. Fixed DNA spreads were stored for 24h at 4°C, and prior to immuno-labeling, spreads were treated with 2.5M HCl for 1.5h. CldU was stained with rat anti-BrdU (1:750, AbD Serotec) for 2h and slides were further incubated with AlexaFluor 488-conjugated anti-rat IgG (1:500) for 1.5h. Images were acquired on a Leica DM-6000RXA fluorescence microscope, equipped with Leica Application Suite software. The lengths of CldU and IdU tracks were measured using ImageJ software.

Flow cytometry

To measure changes in the fraction of shRNA-containing mCherry-positive cells, cells were re-plated every 3 or 4 days. At those time points, approximately 25% of the culture was used to measure the percentage of mCherry-positive cells by flow cytometry, whereas the remaining cells were re-plated for further time points. If indicated, cells were treated with doxycycline (1 μ g per mL) or ethanol as a solvent control. At least 10,000 (BT-549) or 30,000 (KBM-7) events were analyzed per sample on an LSR-II (Becton Dickinson). Cells, pre-treated with doxycycline (1 μ g per mL) or HU, were harvested at different time points, washed and fixed in ice-cold 70% ethanol. Cells were permeabilized and blocked with PBS-1% BSA-0.05% Tween-20 or with PBS-2% BSA-0.1% Triton for 1h and stained with rabbit anti-cleaved PARP (1:100, Cell Signaling, #5625), rabbit anti-phospho-SAPK/JNK (Thr183/Tyr185) (1:100, Cell

Signaling, #9251), rabbit anti-TNFR1 (1:100, Abcam, #19140) or rabbit anti- γ H2AX (1:100, Cell Signaling, #9718) overnight at 4°C. Samples were subsequently stained with AlexaFluor 488-conjugated goat anti-rabbit secondary antibody (1:400) for 1h and analyzed on a FACS Calibur (Becton Dickinson). Data were analyzed with FlowJo software.

Clonogenic survival assays

BT-549 cells or MEFs were plated in 6-well plates (1000 cells per well) and treated with doxycycline (1 μ g per mL) or recombinant TNF α as indicated. MEFs were pre-infected with retroviral 'Hit-and-run' Cre recombinase and selected with puromycin (2 μ g per mL). After 14 days, cells were fixed in 4% formaldehyde–PBS and stained with 0.1% crystal violet in H₂O. Clonogenic assays were measured and quantified using an EliSpot reader (Alpha Diagnostics International) with vSpot Spectrum software.

MTT assays

KBM-7, MDA-MB-231, BT-549, HCC38 and MEF cells were plated in 96-wells plates (600–1000 cells per well), and pre-treated with or without doxycycline (1 μ g per mL) for 2 days. MEFs were pre-infected with retroviral 'Hit-and-run' Cre recombinase and selected with puromycin (2 μ g per mL). If indicated, BT-549 and HCC38 cells were transfected with siRNAs for 24–48h prior to plating cells in 96-well plates. Specifically, cells were transfected with siRNA smartpools (final concentration 100nM), targeting cGAS (#015607, Dharmacon), STING (#024333, Dharmacon), caspase-3 (#29237, Santa Cruz), caspase-8 (#29930, Santa Cruz), caspase-9 (#29931, Santa Cruz) or a negative control sequence (#12935300, ThermoFisher) using oligofectamine (Invitrogen), according to the manufacturer's guidelines. Cells were treated with indicated concentrations of the following agents: Infliximab (Merck, Sharp and Dome), HU (Sigma), ASK1 inhibitor NQDI-1 (Axon Medchem, #2179), JNK inhibitor SP600125 (Selleck Chemicals, #S1460), Pan caspase inhibitor (Z-VAD-FMK, Promega) and/or recombinant TNF α (ThermoFisher). After 5 days of treatment, methyl thiazol tetrazolium (MTT) was added to a final concentration of 5mg per mL for 4h. Medium was removed and formazan crystals were dissolved in dimethyl sulfoxide (DMSO). The absorbance was measured at 520nm with a Bio-Rad iMark spectrometer. Cell viability was calculated as the relative value in signal compared to DMSO or untreated cells. Unless mentioned otherwise, statistical significance was tested using two-sided Student's *t*-tests.

Cytokine analysis

To analyze excreted TNF α levels, KBM-7-shBRCA2 or KBM-7-shLUC cells were treated with doxycycline (1 μ g per mL) for 48h. Proteins in supernatant culture media were concentrated using Microcon-30kDa centrifugal filter units with Ultracel-30 membrane (Millipore). Subsequently, TNF α concentrations were determined using a human TNF α ELISA kit (KHC3011, Life Technologies).

IL-6, IL-8 and IL-10 levels were analyzed using the Human Inflammatory Cytokine Kit (BD Bioscience, #551811), according to the manufacturer's protocol. In short, media were collected from BT-549 cells harboring different shRNAs, after treatment with doxycycline for 0, 2 or 4 days. Media samples (50 μ L per sample) were incubated with IL-6, IL-8 and IL-10 capture beads for 3h at room temperature. After two wash steps, samples were measured on an LSR-II (Becton Dickinson). Data were analyzed using FlowJo software, and cytokine concentrations were calculated using cytokine standards (BD Bioscience).

In-gel digestion and liquid chromatography/tandem mass spectrometry

BT-549 cells and HCC38 were cultured in light ('L') or heavy ('H') SILAC media and were treated with doxycycline for 48h. Cells were harvested and lysed in NP-40 buffer (20mM Tris pH 7.4, 150mM NaCl, 0.2% v/v Igepal, 10% glycerol) supplemented with a protease/phosphate inhibitor cocktail (ThermoFisher). Protein concentrations were determined using Bradford assay and 50µg of proteins from shLUC-'L' cells was mixed with shBRCA2 #2-'H' cells and vice versa. Proteins were separated by sodium dodecyl sulfate–polyacrylamide gel electrophoresis (SDS-PAGE). Gel lanes were cut into slices for in-gel digestion. Slices were cut into 1mm pieces and destained with 100mM ammonium bicarbonate (ABC) in 50–70% acetonitrile. Reduction (10mM dithiothreitol in 100mM ABC) and alkylation (55mM iodoacetamide in 100mM ABC) steps were performed to block cysteines. Gel pieces were dehydrated and incubated overnight with 10ng per µL trypsin (Promega), diluted in 100mM ABC at 37°C. Peptides were subsequently extracted with 5% formic acid for 20min.

Online chromatography of the extracted tryptic peptides was performed using an Ultimate 3000 HPLC system (ThermoFisher Scientific), coupled to a Q-Exactive-Plus mass spectrometer with a NanoFlex source (ThermoFisher Scientific), equipped with a stainless-steel emitter. Tryptic digests were loaded onto a 5mm×300µm internal diameter (i.d.) trapping micro column packed with PepMAP100, 5µm particles (Dionex) in 0.1% formic acid at the flow rate of 20µl per min. After loading and washing for 3min, trapped peptides were back-flush eluted onto a 50cm×75µm i.d. nanocolumn, packed with Acclaim C18 PepMAP RSLC, 2µm particles (Dionex). Column temperature was maintained at 40°C. Eluents used were 100:0 H₂O/acetonitrile (volume/volume (V/V)) with 0.1% formic acid (Eluent A) and 0:100 H₂O/acetonitrile (v/v) with 0.1% formic acid (Eluent B). The following mobile phase gradient was delivered at the flow rate of 300nL per min: 3–50% of solvent B in 90min; 50–80% B in 1min; 80% B during 9min, and back to 1% B in 1min and held at 1% A for 19min which results in a total run time of 120min. MS data were acquired using a data-dependent acquisition (DDA) top-12 method dynamically choosing the most abundant not-yet-sequenced precursor ions from the survey scans (300–1650Th) with a dynamic exclusion of 20s. Survey scans were acquired at a resolution of 70,000 at mass-to-charge (m/z) 200 with a maximum inject time of 50ms or AGC 3E6. DDA was performed via higher energy collisional dissociation fragmentation with a target value of 5×10^4 ions determined with predictive automatic gain control in centroid mode. Isolation of precursors was performed with a window of 1.6 m/z . Resolution for HCD spectra was set to 17,500 at m/z 200 with a maximum ion injection time of 50ms. Normalized collision energy was set at 28. The S-lens RF level was set at 60 and the capillary temperature was set at 250°C. Precursor ions with single, unassigned, or six and higher charge states were excluded from fragmentation selection.

MS data analysis

Mass spectrometry raw files were processed in MaxQuant (version 1.5.2.8) containing the integrated Andromeda search engine and searched against the human proteome downloaded from the UniProt database (20,197 entries), using a false discovery rate of 0.01 at the protein and peptide level. Multiplicity was set to 1 with Lys6 and Arg10 selected as labels. Carbamidomethyl was set as a fixed modification and oxidation of methionine as a variable modification. Default parameters were used for all other settings. Proteins were excluded based on the criteria 'marked potential contaminant or reverse protein by MaxQuant' and 'only identified by either light or heavy labeled peptide'. For further analysis, log₂ of protein ratio's (heavy/light) was calculated. Proteins present in at least 3 out of 4 independent analyses were further analyzed. The full datasets as plotted in Fig. 5b were used to select

upregulated proteins upon BRCA2 depletion, compared to control shLUC cells. Proteins that were among the top 25 upregulated proteins in both BT-549 and HCC38 cells were selected. The top 50 upregulated proteins upon BRCA2 depletion in both cell lines can be found in Supplementary Table 2. The average level of upregulation in the BT-549 and HCC38 datasets was used for ENRICH analysis⁶⁹.

Gene expression analysis

For indicated genes, mRNA expression levels from the Ovarian Serous Cystadenocarcinoma TCGA dataset were retrieved from cBioportal. Only tumors with sequencing and CNA data (316 samples) were used, and were subclassified in 'BRCA2 wildtype' (193 samples) and 'germline BRCA2 mutant' (25 samples). Of the 25 germline BRCA2 carriers, 2 cases were excluded because of an additional BRCA1 mutation, resulting in 23 BRCA2 mutant cases. In the 'BRCA2 wildtype' set, only samples were included that did not harbor any alterations (amplification, deletion, mutation, hyper-methylation, mRNA up- or downregulation) in BRCA1 or BRCA2. Two-sided Student's *t*-tests were used to test for statistically significant differences in mRNA expression levels between BRCA2 wt and BRCA2 mutant tumors.

Next-generation RNA sequencing was performed to analyze changes in gene expression upon BRCA2 depletion. To this end, BT-549 or HCC38 cells harboring shBRCA2 #2 or shLUC were treated with doxycycline (1 µg per mL) for 72h. Cells were harvested and frozen at -80°C, and RNA was isolated using the mirVANA kit (Ambion, AM1561). RNA quality was analyzed on microfluidic sipper chips and detected by fluorescence (LabChip GX, Caliper LifeSciences), and samples with RNA Quality Scores (RQS) >5 were included for analysis. The QuantSeq RNAseq 3'mRNA kit (Lexogen) was used to generate cDNA libraries for next-generation sequencing. The cDNA library was purified and PCR amplified with Illumina sequencing adapters were sequenced with 65 base-pair reads on a NextSeq 500 sequencer (Illumina), and generated 7.2 to 19.8 million reads per sample. RNA sequencing quality control was assessed by FastQC and Samtools Flagstat software.

RNA sequencing data analysis

For gene set enrichment analysis (GSEA), genes in each cell line were ranked based on the -log *P* value between doxycycline-treated shBRCA2 #2 cells and three control settings (shLUC cells and untreated shBRCA2 #2 cells). Genes enriched in BRCA2-depleted cells were positive and genes enriched in control cells were negative. The ranked gene lists were loaded into GSEA software and tested against a set of 280 interferon-induced genes⁷⁰. Furthermore, gene sets of the Hallmark collection (MSigDB) were loaded into GSEA and analyzed in both cell lines. RNA sequencing data are accessible at the GEO repository, under accession number GSE116943.

Data availability

RNA sequencing data are accessible at the GEO repository, under accession number GSE116943. The mass spectrometry data have been deposited to the ProteomeXchange Consortium via the PRIDE partner repository with the dataset identifier PXD007253 (BT-549) and HCC38. DNA sequencing data are available at the NCBI short read archive (PRJNA299537). Other data from this study are available from the corresponding author upon request.

Acknowledgements

We thank members of the van Vugt and Brummelkamp labs, Elisabeth de Vries, Maaïke Vreeswijk and John Martens for helpful discussions. This work was financially supported by grants from the Netherlands Organization for Scientific research (NWO-VIDI #91713334 to M.A.T.M.v.V.), the Dutch Cancer Society/Alpe D'huzes (Grant EMCR2014-7048 to M.A.T.M.v.V.), the European Research Council (ERC CoS Grant 682421 to M.A.T.M.v.V.), the Meerema-de Boer Foundation to A.M.H. We thank Jos Jonkers, Peter Bouwman and Christy Hong for reagents, and Anouk Baars, Wellington Mardoqueu Candido and Marieke Everts for technical assistance.

Author contributions

A.M.H., M.A.T.M.v.V. and T.R.B. conceived the project. A.M.H. and L.T.J. performed the genetic screen. A.M.H. and F.T. performed cell biological and biochemical experiments. S.E.v.G. and R.S.N.F. performed RNAseq analysis. A.M.H., F.T., L.T.J., T.R.B. and M.A.T.M.v.V. analyzed data. A.M.H., F.T. and M.A.T.M.v.V. wrote the manuscript. All authors provided feedback on the manuscript before submission.

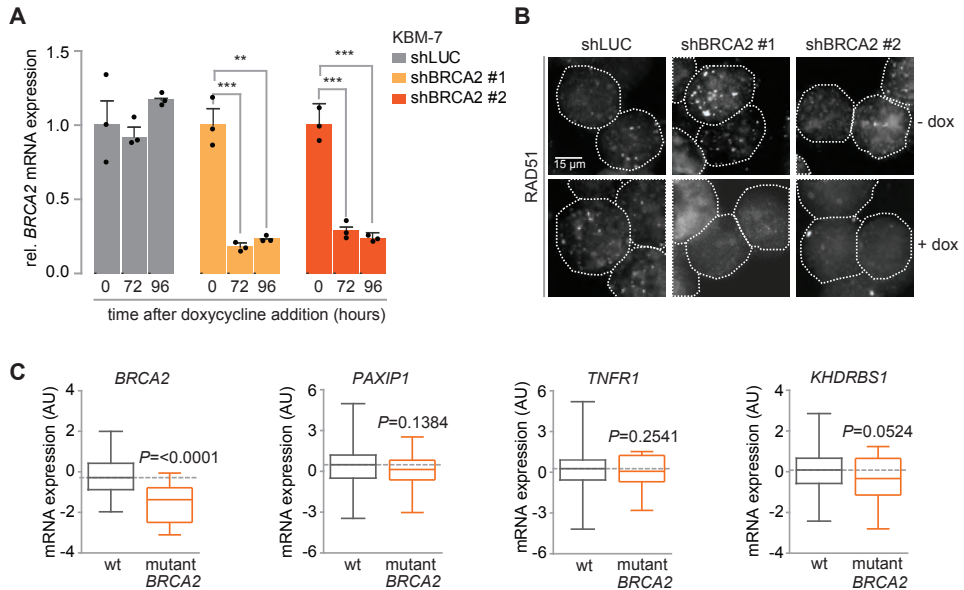
References

1. Jackson, S. P. & Bartek, J. The DNA-damage response in human biology and disease. *Nature* 461, 1071–1078 (2009).
2. Ciccia, A. & Elledge, S. J. The DNA damage response: making it safe to play with knives. *Mol. Cell* 40, 179–204 (2010).
3. Howlett, N. G. et al. Biallelic inactivation of BRCA2 in Fanconi anemia. *Science* 297, 606–609 (2002).
4. Sawyer, S. L. et al. Biallelic mutations in BRCA1 cause a new Fanconi anemia subtype. *Cancer Discov.* 5, 135–142 (2015).
5. Wooster, R. et al. Localization of a breast cancer susceptibility gene, BRCA2, to chromosome 13q12-13. *Science* 265, 2088–2090 (1994).
6. Futreal, P. A. et al. BRCA1 mutations in primary breast and ovarian carcinomas. *Science* 266, 120–122 (1994).
7. Miki, Y. et al. A strong candidate for the breast and ovarian cancer susceptibility gene BRCA1. *Science* 266, 66–71 (1994).
8. Jasin, M. & Rothstein, R. Repair of strand breaks by homologous recombination. *Cold Spring Harb. Perspect. Biol.* 5, a012740 (2013).
9. Sharan, S. K. et al. Embryonic lethality and radiation hypersensitivity mediated by Rad51 in mice lacking Brca2. *Nature* 386, 804–810 (1997).
10. Yuan, S. S. et al. BRCA2 is required for ionizing radiation-induced assembly of Rad51 complex in vivo. *Cancer Res.* 59, 3547–3551 (1999).
11. Moynahan, M. E., Chiu, J. W., Koller, B. H. & Jasin, M. Brca1 controls homology-directed DNA repair. *Mol. Cell* 4, 511–518 (1999).
12. Hakem, R. et al. The tumor suppressor gene Brca1 is required for embryonic cellular proliferation in the mouse. *Cell* 85, 1009–1023 (1996).
13. Suzuki, A. et al. Brca2 is required for embryonic cellular proliferation in the mouse. *Genes Dev.* 11, 1242–1252 (1997).
14. Connor, F. et al. Tumorigenesis and a DNA repair defect in mice with a truncating Brca2 mutation. *Nat. Genet.* 17, 423–430 (1997).
15. Cao, L., Li, W., Kim, S., Brodie, S. G. & Deng, C.-X. Senescence, aging, and malignant transformation mediated by p53 in mice lacking the Brca1 fulllength isoform. *Genes Dev.* 17, 201–213 (2003).
16. Morimatsu, M., Donoho, G. & Hasty, P. Cells deleted for Brca2 COOH terminus exhibit hypersensitivity to gamma-radiation and premature senescence. *Cancer Res.* 58, 3441–3447 (1998).
17. Donoho, G. et al. Deletion of Brca2 exon 27 causes hypersensitivity to DNA crosslinks, chromosomal instability, and reduced life span in mice. *Genes Chromosomes Cancer* 36, 317–331 (2003).
18. Carlos, A. R. et al. ARF triggers senescence in Brca2-deficient cells by altering the spectrum of p53 transcriptional targets. *Nat. Commun.* 4, 2697 (2013).

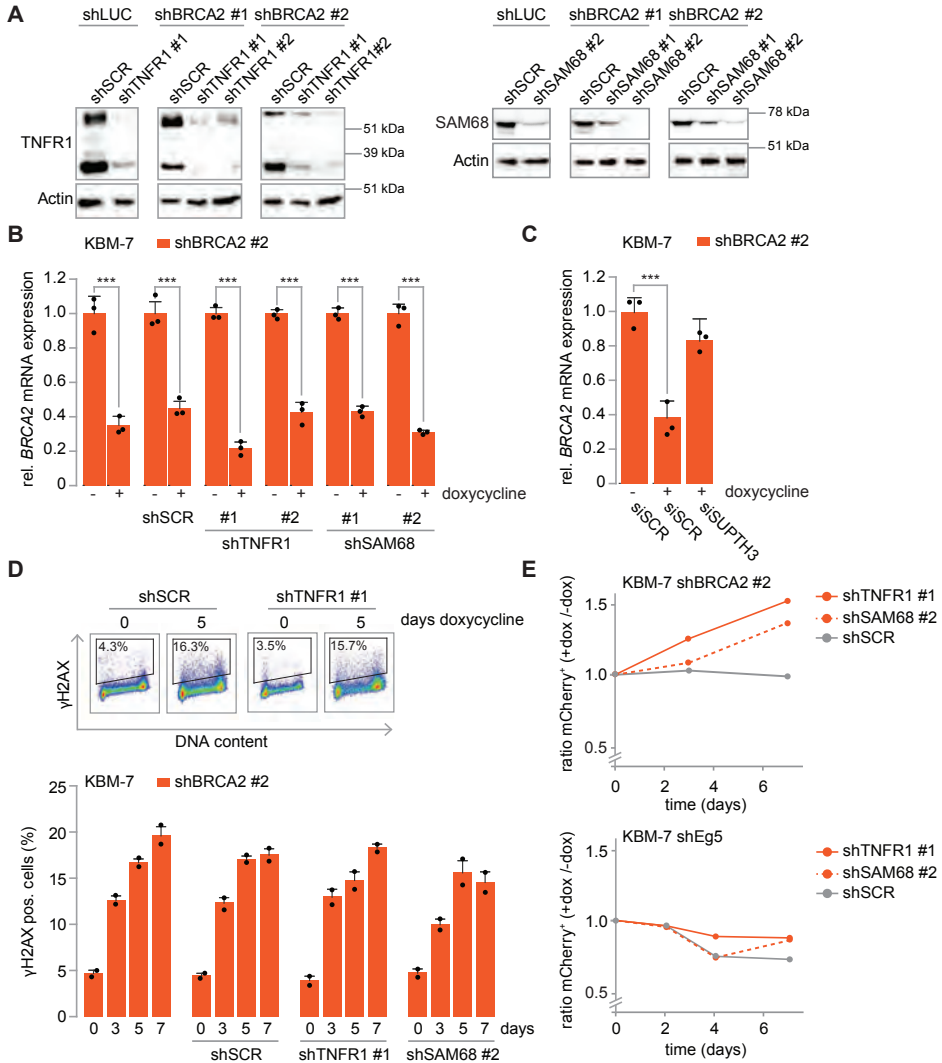
19. Elledge, S. J. & Amon, A. The BRCA1 suppressor hypothesis: an explanation for the tissue-specific tumor development in BRCA1 patients. *Cancer Cell*. 1, 129–132 (2002).
20. Ludwig, T., Chapman, D. L., Papaioannou, V. E. & Efstratiadis, A. Targeted mutations of breast cancer susceptibility gene homologs in mice: lethal phenotypes of *Brca1*, *Brca2*, *Brca1/Brca2*, *Brca1/p53*, and *Brca2/p53* nullizygous embryos. *Genes Dev*. 11, 1226–1241 (1997).
21. Hakem, R., la Pompa de, J. L., Elia, A., Potter, J. & Mak, T. W. Partial rescue of *Brca1* (5-6) early embryonic lethality by *p53* or *p21* null mutation. *Nat. Genet*. 16, 298–302 (1997).
22. Jonkers, J. et al. Synergistic tumor suppressor activity of BRCA2 and *p53* in a conditional mouse model for breast cancer. *Nat. Genet*. 29, 418–425 (2001).
23. Bouwman, P. et al. 53BP1 loss rescues BRCA1 deficiency and is associated with triple-negative and BRCA-mutated breast cancers. *Nat. Struct. Mol. Biol*. 17, 688–695 (2010).
24. Bunting, S. F. et al. 53BP1 inhibits homologous recombination in *Brca1*-deficient cells by blocking resection of DNA breaks. *Cell* 141, 243–254 (2010).
25. Escribano-Díaz, C. et al. A cell cycle-dependent regulatory circuit composed of 53BP1-RIF1 and BRCA1-CtIP controls DNA repair pathway choice. *Mol. Cell* 49, 872–883 (2013).
26. Xu, G. et al. REV7 counteracts DNA double-strand break resection and affects PARP inhibition. *Nature* 521, 541–544 (2015).
27. Ray Chaudhuri, A. et al. Replication fork stability confers chemoresistance in BRCA-deficient cells. *Nature* 535, 382–387 (2016).
28. Schlacher, K. et al. Double-strand break repair-independent role for BRCA2 in blocking stalled replication fork degradation by MRE11. *Cell* 145, 529–542 (2011).
29. Carette, J. E. et al. Global gene disruption in human cells to assign genes to phenotypes by deep sequencing. *Nat. Biotechnol*. 29, 542–546 (2011).
30. Heijink, A. M. et al. A haploid genetic screen identifies the G1/S regulatory machinery as a determinant of Wee1 inhibitor sensitivity. *Proc. Natl Acad. Sci. USA* 2015, 05283 (2015).
31. Mayer, T. U. et al. Small molecule inhibitor of mitotic spindle bipolarity identified in a phenotype-based screen. *Science* 286, 971–974 (1999).
32. Cancer Genome Atlas Research Network. Integrated genomic analyses of ovarian carcinoma. *Nature* 474, 609–615 (2011).
33. Ramakrishnan, P. & Baltimore, D. Sam68 is required for both NF- κ B activation and apoptosis signaling by the TNF receptor. *Mol. Cell* 43, 167–179 (2011).
34. Luo, J.-L., Kamata, H. & Karin, M. IKK/NF- κ B signaling: balancing life and death—a new approach to cancer therapy. *J. Clin. Invest*. 115, 2625–2632 (2005).
35. Tobiume, K. et al. ASK1 is required for sustained activations of JNK/p38 MAP kinases and apoptosis. *EMBO Rep*. 2, 222–228 (2001).
36. Schoonen, P. M. et al. Progression through mitosis promotes PARP inhibitor-induced cytotoxicity in homologous recombination-deficient cancer cells. *Nat. Commun*. 8, 15981 (2017).
37. Fenech, M. et al. Molecular mechanisms of micronucleus, nucleoplasmic bridge and nuclear bud formation in mammalian and human cells. *Mutagenesis* 26, 125–132 (2011).
38. Mackenzie, K. J. et al. cGAS surveillance of micronuclei links genome instability to innate immunity. *Nature* 548, 461–465 (2017).
39. Hanahan, D. & Weinberg, R. A. Hallmarks of cancer: the next generation. *Cell* 144, 646–674 (2011).
40. Harding, S. M. et al. Mitotic progression following DNA damage enables pattern recognition within micronuclei. *Nature* 548, 466–470 (2017).
41. Chen, Q., Sun, L. & Chen, Z. J. Regulation and function of the cGAS-STING pathway of cytosolic DNA sensing. *Nat. Immunol*. 17, 1142–1149 (2016).
42. Varfolomeev, E. E. et al. Targeted disruption of the mouse caspase 8 gene ablates cell death induction by the TNF receptors, Fas/Apo1, and DR3 and is lethal prenatally. *Immunity* 9, 267–276 (1998).
43. Ochs, K. & Kaina, B. Apoptosis induced by DNA damage O6-methylguanine is Bcl-2 and caspase-9/3 regulated and Fas/caspase-8 independent. *Cancer Res*. 60, 5815–5824 (2000).
44. Hallahan, D. E., Spriggs, D. R., Beckett, M. A., Kufe, D. W. & Weichselbaum, R. R. Increased tumor necrosis factor alpha mRNA after cellular exposure to ionizing radiation. *Proc. Natl Acad. Sci. USA* 86, 10104–10107 (1989).
45. Briot, D., Macé-Aimé, G., Subra, F. & Rosselli, F. Aberrant activation of stressresponse pathways leads to TNF-alpha oversecretion in Fanconi anemia. *Blood* 111, 1913–1923 (2008).
46. Biton, S. & Ashkenazi, A. NEMO and RIP1 control cell fate in response to extensive DNA damage via TNF- α feedforward signaling. *Cell* 145, 92–103 (2011).

47. Parkes, E. E. et al. Activation of STING-dependent innate immune signaling by S-phase-specific DNA damage in breast cancer. *J. Natl. Cancer Inst.* 109, djw199 (2017).
48. Sleijfer, S. et al. Combined cytotoxic effects of tumor necrosis factor-alpha with various cytotoxic agents in tumor cell lines that are drug resistant due to mutated p53. *J. Immunother.* 22, 48–53 (1999).
49. Tkáč, J. et al. HELB Is a feedback inhibitor of DNA end resection. *Mol. Cell* 61, 405–418 (2016).
50. Noordermeer, S. M. et al. The shieldin complex mediates 53BP1-dependent DNA repair. *Nature* 560, 117–121 (2018).
51. Chaturvedi, M. M., Sung, B., Yadav, V. R., Kannappan, R. & Aggarwal, B. B. NF- κ B addiction and its role in cancer: ‘one size does not fit all’. *Oncogene* 30, 1615–1630 (2011).
52. Bakhoum, S. F. et al. Chromosomal instability drives metastasis through a cytosolic DNA response. *Nature* 553, 467–472 (2018).
53. Jackson-Bernitsas, D. G. et al. Evidence that TNF-TNFR1-TRADD-TRAF2-RIP-TAK1-IKK pathway mediates constitutive NF-kappaB activation and proliferation in human head and neck squamous cell carcinoma. *Oncogene* 26, 1385–1397 (2007).
54. Volcic, M. et al. NF- κ B regulates DNA double-strand break repair in conjunction with BRCA1-CtIP complexes. *Nucleic Acids Res.* 40, 181–195 (2012).
55. Harte, M. T. et al. NF- κ B is a critical mediator of BRCA1-induced chemoresistance. *Oncogene* 33, 713–723 (2014).
56. De Smaele, E. et al. Induction of gadd45beta by NF-kappaB downregulates pro-apoptotic JNK signalling. *Nature* 414, 308–313 (2001).
57. Tang, G. et al. Inhibition of JNK activation through NF-kappaB target genes. *Nature* 414, 313–317 (2001).
58. Zhang, S. et al. Suppressed NF-kappaB and sustained JNK activation contribute to the sensitization effect of parthenolide to TNF-alpha-induced apoptosis in human cancer cells. *Carcinogenesis* 25, 2191–2199 (2004).
59. Kamata, H. et al. Reactive oxygen species promote TNFalpha-induced death and sustained JNK activation by inhibiting MAP kinase phosphatases. *Cell* 120, 649–661 (2005).
60. Braumüller, H. et al. T-helper-1-cell cytokines drive cancer into senescence. *Nature* 494, 361–365 (2013).
61. Deroose, J. P. et al. Long-term outcome of isolated limb perfusion with tumour necrosis factor- α for patients with melanoma in-transit metastases. *Br.J. Surg.* 98, 1573–1580 (2011).
62. Waters, J. P., Pober, J. S. & Bradley, J. R. Tumour necrosis factor and cancer. *J.Pathol.* 230, 241–248 (2013).
63. Wiederschain, D. et al. Single-vector inducible lentiviral RNAi system for oncology target validation. *Cell Cycle* 8, 498–504 (2009).
64. Moffat, J. et al. A lentiviral RNAi library for human and mouse genes applied to an arrayed viral high-content screen. *Cell* 124, 1283–1298 (2006).
65. Silver, D. P. & Livingston, D. M. Self-excising retroviral vectors encoding the Cre recombinase overcome Cre-mediated cellular toxicity. *Mol. Cell* 8, 233–243 (2001).
66. Ran, F. A. et al. Genome engineering using the CRISPR-Cas9 system. *Nat. Protoc.* 8, 2281–2308 (2013).
67. Carette, J. E. et al. Haploid genetic screens in human cells identify host factors used by pathogens. *Science* 326, 1231–1235 (2009).
68. Blomen, V. A. et al. Gene essentiality and synthetic lethality in haploid human cells. *Science* 350, 1092–1096 (2015).
69. Kuleshov, M. V. et al. Enrichr: a comprehensive gene set enrichment analysis web server 2016 update. *Nucleic Acids Res.* 44, W90–W97 (2016).
70. Saleiro, D. et al. Central role of ULK1 in type I interferon signaling. *Cell Rep.* 11, 605–617 (2015).

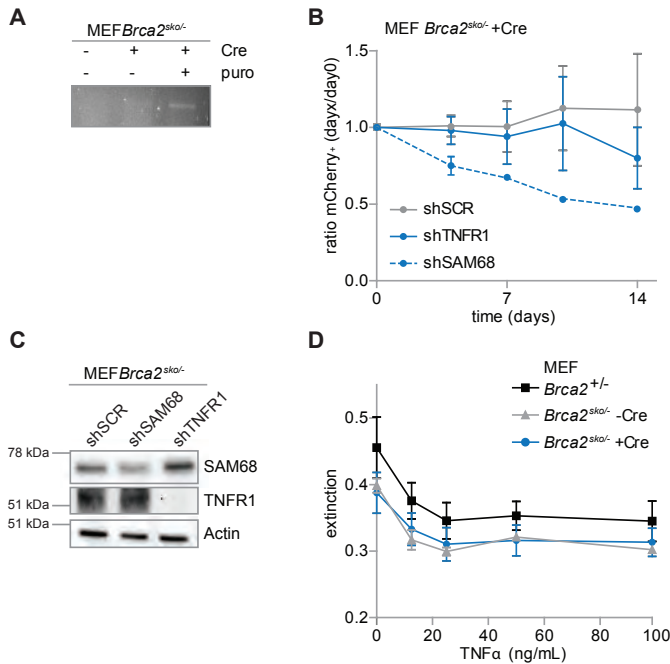
Supplementary Figures



Supplementary Figure 1. BRCA2 deficiency of KBM-7-shBRCA2 cell lines. **A)** KBM-7 cells harboring indicated shRNAs were treated with doxycycline for indicated time periods. BRCA2 mRNA expression was measured using RT-qPCR. Measurements were normalized to expression levels at day 0. Error bars represent s.d. of three independent measurements. *P* values were calculated using two-tailed Student's *t*-test. ** indicates $P < 0.01$, *** indicates $P < 0.001$. **B)** Representative immunofluorescence images of KBM-7 cells harboring indicated hairpins and treated with or without doxycycline for four days. Cells were irradiated (5 Gy) and stained three hours post irradiation with anti-RAD51 and DAPI. **C)** mRNA expression levels of indicated genes were assessed in BRCA2 wt ($n=193$) and germline BRCA2 mutant ($n=23$) serous ovarian cancer cases from the TCGA dataset.

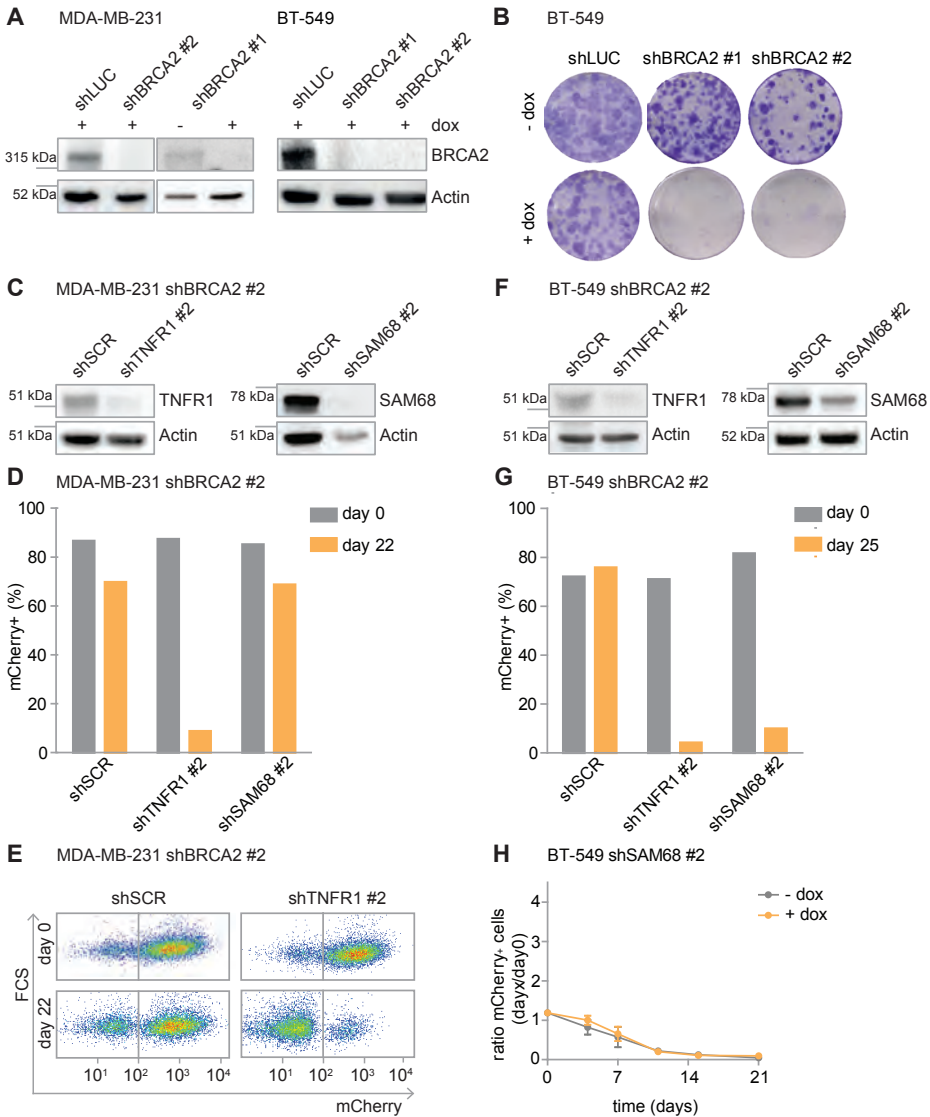


Supplementary Figure 2. Loss of TNFR1 or SAM68 specifically rescues BRCA2 deficiency. **A)** pLKO.tet.shRNA transduced KBM-7 cells, which were additionally infected with indicated shRNA vectors carrying IRES-driven mCherry cassettes. Cells were treated with doxycycline for four days prior to cell lysis, and immunoblotted for TNFR1, SAM68 or Actin. **B)** KBM-7 cells transduced with indicated hairpins were treated with or without doxycycline for four days. BRCA2 mRNA expression was measured using RT-qPCR. Measurements were normalized to expression levels without doxycycline treatment. Error bars represent s.d. of three independent measurements. P values were calculated using two-tailed Student's t-test. *** indicates $P < 0.001$. **C)** KBM-7-shBRCA2 #2 cells were transfected with indicated siRNAs and simultaneously treated with doxycycline for three days. BRCA2 mRNA expression was measured and quantified as for panel (B). **D)** γ H2AX levels were measured by flow cytometry. Indicated KBM-7 cell lines were treated with doxycycline for indicated time periods prior to fixation. Gating was performed as shown in the upper panels. **E)** KBM-7-pLKO.tet.shBRCA2#2 or KBM-7-pLKO.tet.shEg5 cells carrying mCherry shRNA cassettes for TNFR1, SAM68 or SCR were treated with or without doxycycline. Percentages of mCherry-positive cells were measured every two or three days after start of doxycycline treatment. Ratios of mCherry-positive cells in doxycycline treated cultures versus untreated cultures are indicated. Per condition, at least 30,000 events were measured.



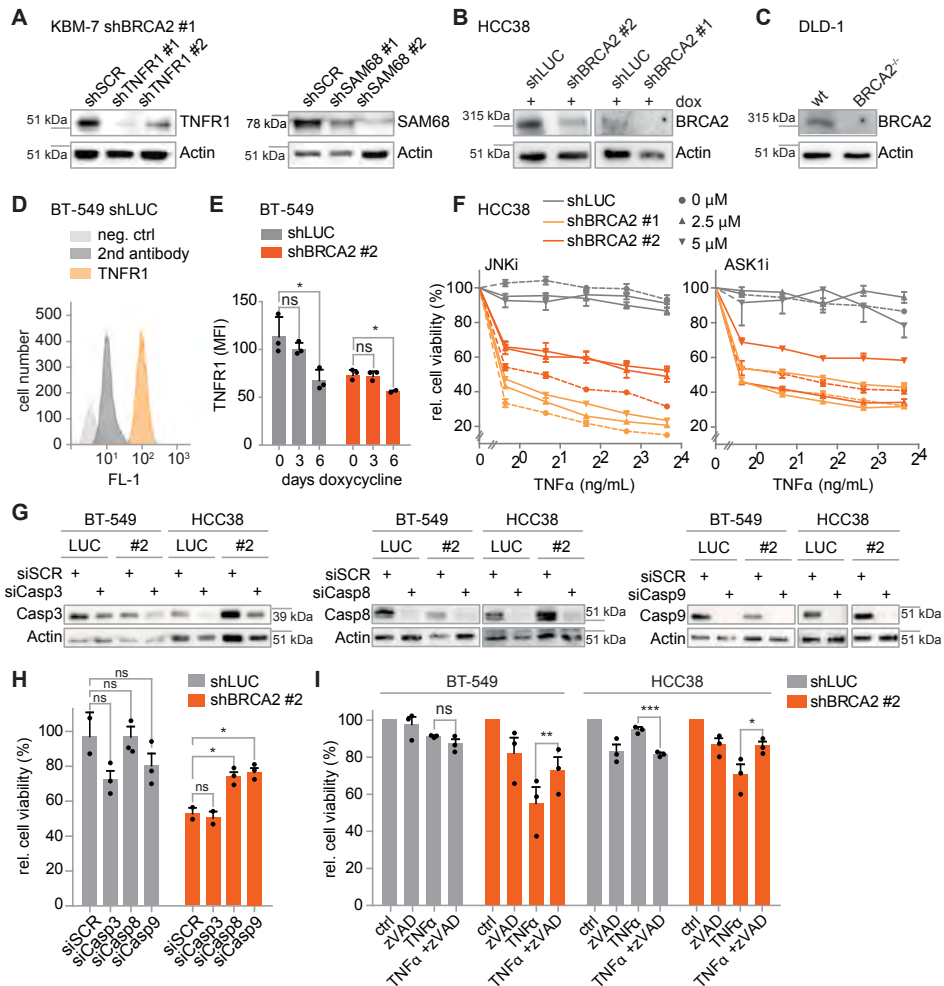
Supplementary Figure 3. TNF α signaling does not interfere with viability of *Brca2*-depleted MEFs.

A) *Brca2*^{sko/-} MEFs were infected with Cre retrovirus and subsequently selected with puromycin for two days (2 μ g per mL). Genomic DNA was isolated and Cre targeting of the *Brca2* allele was detected by genomic PCR (product: 110 base pairs). **B)** *Brca2*^{sko/-} MEFs were infected with mCherry-expressing hairpins against TNFR1, SAM68 or scrambled sequence (SCR). Cells were treated with Cre recombinase and percentages of mCherry-positive cells were measured using flow cytometry. The ratios of mCherry-positive cells at day x compared to percentages of mCherry-positive at day 0 cells were calculated. Error bars represent s.d. of three independent experiments. **C)** Immunoblotting of *Brca2*^{sko/-} MEFs infected with mCherry-expressing hairpins against SAM68 or TNFR1. **D)** Indicated MEF lines were plated and treated with TNF α for five days. Cell viability was assessed by MTT conversion. Error bars represent s.d. of three technical replicates.

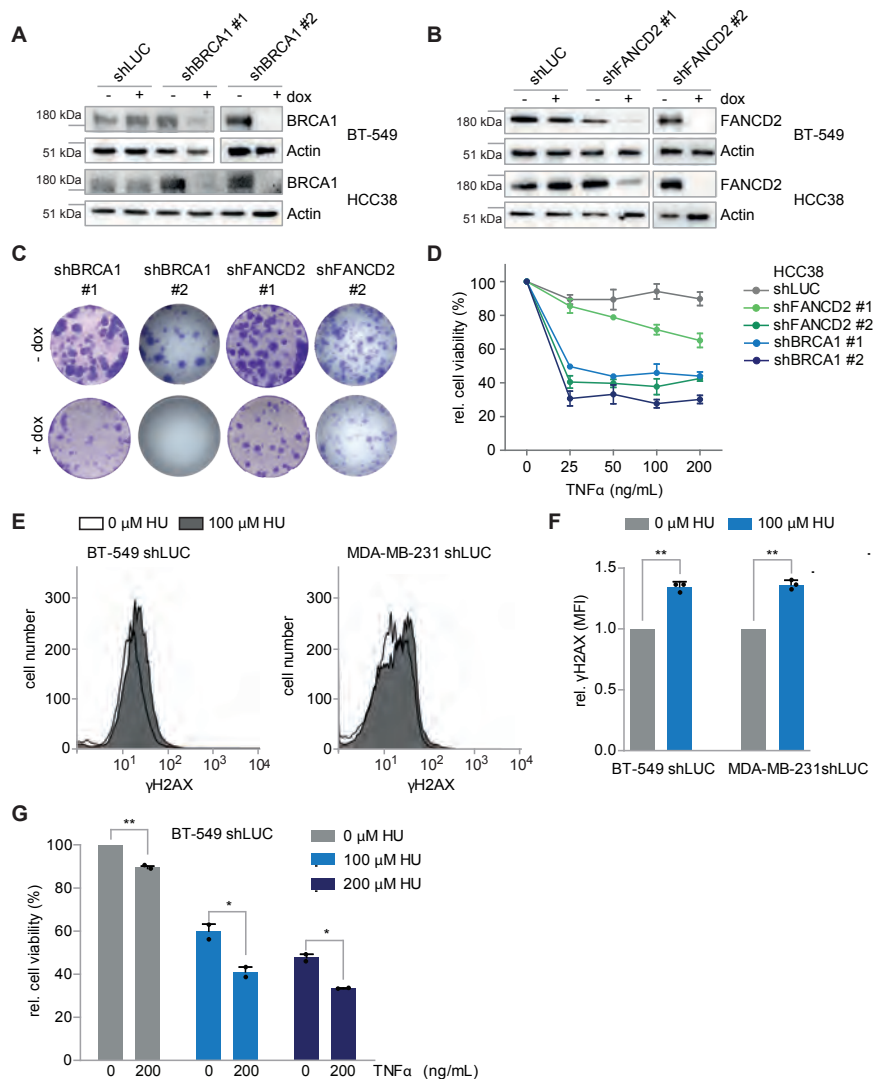


Supplementary Figure 4. Loss of TNFR1 and SAM68 in BT-549 and MDA-MB-231 affects cell viability.

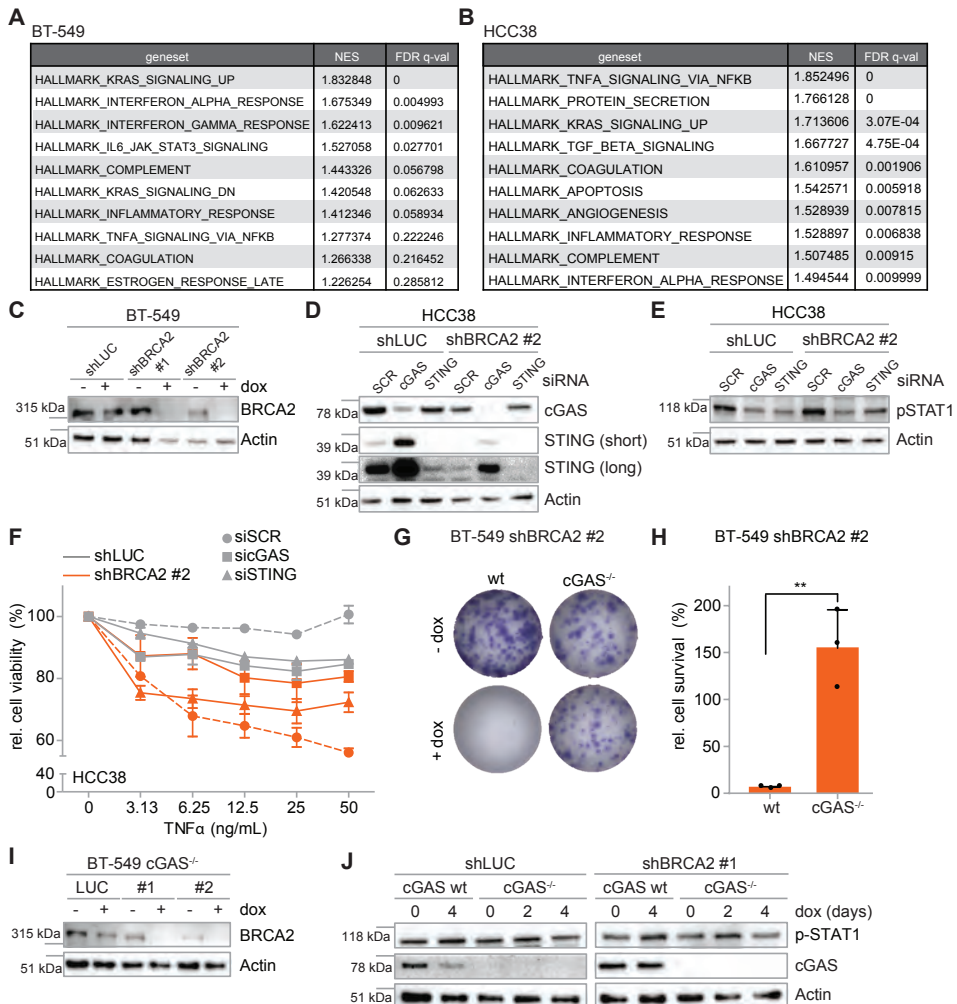
A) MDA-MB-231 and BT-549 cells harboring shLUC, shBRCA2#1 or shBRCA2#2 were treated with or without doxycycline for four days and immunoblotted for BRCA2 and Actin. **B)** BT-549 cells harboring indicated hairpins were plated in 6-well plates and treated with or without doxycycline. Cells were fixed after 14 days and stained with crystal violet. **C)** Immunoblotting of MDA-MB-231-shBRCA2#2 cells infected with shTNFR1#2, shSAM68#2 or shSCR. **D)** Quantification of mCherry-positive MDA-MB-231-shBRCA2#2 cells, after transduction with mCherry-expressing shTNFR1#2, shSAM68#2 or shSCR after 22 days. **E)** Representative flow cytometry plots of MDA-MB-231-shBRCA2#2 with mCherry-expressing shTNFR1#2 or shSCR, treated for 22 days without doxycycline. Cells were gated on mCherry positivity. **F)** Immunoblotting of BT-549-shBRCA2#2 cells infected with shTNFR1#2, shSAM68#2 or shSCR. **G)** Quantification of mCherry-positive BT-549-shBRCA2#2 cells, after transduction with mCherry-expressing shTNFR1#2, shSAM68#2 or shSCR after 25 days. **H)** BT-549-shBRCA2#2 cells harboring mCherry-expressing shSAM68#2 were treated with or without doxycycline for indicated time periods. mCherry positivity was measured by flow cytometry. Percentages were normalized to mCherry percentages at day 0.



Supplementary Figure 5. TNF α sensitivity is ASK1/JNK and caspase dependent and is not due to changes of TNFR1 expression levels. **A)** Immunoblotting of KBM-7 shBRCA2#1 cells with indicated hairpins against SAM68 and TNFR1. **B)** Immunoblotting of HCC38 cells harboring shLUC or shBRCA2#2 treated with doxycycline for four days. **C)** Immunoblotting of DLD-1 wt and BRCA2^{-/-} cells for BRCA2 and Actin. **D)** Representative flow cytometry histogram of BT-549-shLUC cells stained with anti-TNFR1. **E)** BT-549 cells harboring shLUC or shBRCA2 #2 were treated with doxycycline for the indicated time periods. Expression of TNFR1 was measured using flow cytometry as in panel (d). Mean MFI of three independent experiments is indicated. P values were calculated using two-tailed Student's t-test. * indicates P<0.05 **F)** HCC38 cells harboring shLUC, shBRCA2#1 or shBRCA2#2 were treated with doxycycline for 48 hours and subsequently treated with indicated concentrations of TNF α and JNK inhibitor (left panel) or ASK1 inhibitor (right panel) for five days. **G)** Knockdown efficiencies of siRNAs targeting caspase-3, caspase-8 or caspase-9. BT-549 and HCC38 cells carrying shLUC (LUC) or shBRCA2#2 (#2) were transfected with indicated siRNAs and harvested at 5 days after transfection. **H)** HCC38 shLUC and shBRCA2#2 cells were transfected with indicated siRNAs for 24-48 hours, and were subsequently treated with doxycycline for 48 hours. Cells were plated and treated with indicated TNF α concentrations for five days. **I)** BT-549 and HCC38 shLUC or shBRCA2 #2 cells were treated with doxycycline for 48 hours and subsequently treated with zVAD-FMK (25 μ M) and/or TNF α (12.5 ng per mL) for five days. For panels F, H and I, cell viability was assessed by MTT conversion. Error bars indicate s.e.m. of at least three independent experiments, with four technical replicates each. Measurements were normalized to untreated cells. P values were calculated using two-tailed Student's t-test. * indicates P<0.05, ** indicates P<0.01, *** indicates P<0.001.



Supplementary Figure 6. Sensitivity to TNF α is not restricted to BRCA2 inactivation. **A,B)** Immunoblotting of BT-549 and HCC38 cells carrying indicated hairpins targeting BRCA1 (panel A) and FANCD2 (panel B). Cells were treated with or without doxycycline for four days. **C)** Long-term survival assay after BRCA1 and FANCD2 depletion. BT-549 cells harboring indicated hairpins were plated in 6-well plates and treated with or without doxycycline. Cells were fixed after 14 days and stained with crystal violet. **D)** HCC38 cells harboring hairpins against BRCA1 and FANCD2 were treated with doxycycline for 48 hours and subsequently plated and treated with indicated TNF α concentrations for five days. Cell viability was assessed by MTT conversion. Error bars indicate s.e.m. of three independent experiments, with three technical replicates each. **E)** Representative flow cytometry histograms of BT-549-shLUC and MDA-MB-231-shLUC cells treated with or without hydroxyurea (100 μ M) for 24 hours and stained with anti- γ H2AX. **F)** Quantification of mean fluorescence intensity (MFI) of H2AX staining in BT-549-shLUC and MDA-MB-231-shLUC cells as shown in panel (E). H2AX MFI of cells treated with HU was normalized to untreated cells. Error bars show s.d. of three independent experiments. *P* values were calculated using two-tailed Student's *t*-test. * indicates *P*<0.05, ** indicates *P*<0.01, *** indicates *P*<0.001. **G)** BT-549 shLUC cells were plated and treated with or without indicated concentrations of hydroxyurea and TNF α for five days. Cell viability was assessed by MTT conversion. Error bars represent s.d. of two independent experiments. *P* values were calculated using two-tailed Student's *t*-test. * indicates *P*<0.05, ** indicates *P*<0.01, *** indicates *P*<0.001.



Supplementary Figure 7. BRCA2 depletion induces cGAS-STING dependent interferon signaling. **A,B)** Top 20 enriched Hallmark gene sets in BRCA2-depleted BT-549 (A) and HCC38 (B) cells compared to control cell lines. **C)** BT-549 cells with indicated hairpins were treated with or without doxycycline for 6 days. Depletion of BRCA2 was confirmed by immunoblotting. **D)** HCC38 cells with shLUC or shBRCA2#2 were depleted for cGAS or STING. Knockdown efficiency of cGAS and STING was analyzed by immunoblotting five days post transfection. **E)** HCC38 cells with indicated hairpins were depleted for cGAS or STING for 24 hours and subsequently treated with doxycycline for four days. Activation of STAT1 signaling was analyzed by immunoblotting. **F)** Representative flow cytometry plots of MDA-MB-231-shBRCA2 #2 with mCherry-expressing shTNFR1 #2 or shSCR, treated for 22 days without doxycycline. Cells were gated on mCherry positivity. **G)** HCC38 cells with indicated hairpins were depleted for cGAS or STING for 24 hours. Cells were plated and pre-treated with doxycycline for 48 hours and subsequently treated with indicated TNFα concentrations for five days. Cell viability was assessed by MTT conversion. Error bars indicate s.e.m. of three independent experiments with three technical replicates each. **H)** BT-549 cGAS^{-/-} or wt cells harboring shBRCA2#2 were plated in 6-well plates and treated with or without doxycycline. Cells were fixed after 11 days and stained with crystal violet. **I)** Clonogenic cell survival as described in G was quantified. Percentage of cell survival was calculated by normalizing counted colonies to cells without doxycycline treatment. Error bars indicate s.d. of three independent experiments. P values were calculated using two-tailed Student's t-test. ** indicates P<0.01. **J)** BT-549 cGAS^{-/-} cells with indicated BRCA2 shRNAs or shLUC were treated with or without doxycycline for 4 days. Depletion of BRCA2 was confirmed by immunoblotting. **K)** cGAS^{-/-} or wt BT-549 cells with indicated hairpins were treated with doxycycline for indicated time periods. Expression of cGAS and the phosphorylation status of STAT1 were analyzed by immunoblotting.

Supplementary Table 1. Top 50 genes identified in the haploid genetic screens.

shBRCA2#2		shEg5 #1		shBRCA2#2 - shEg5#1	
Gene	FDR-pvalue	Gene	FDR-pvalue	Gene	FDR-pvalue
SUPT3H	3,40E-97	TAF6L	3,27E-255	POU2F1	3,40E-97
POU2F1	4,31E-69	TAF5L	2,81E-162	SUPT3H	4,31E-69
TNFRSF1A	5,99E-47	TADA1	3,08E-147	KDM3B	5,99E-47
USP15	3,99E-26	SUPT3H	3,52E-122	USP15	3,99E-26
KDM3B	7,30E-19	SUPT7L	1,29E-73	TNFRSF1A	7,30E-19
SMARCD2	2,03E-18	POU2F1	4,16E-49	GPATCH8	2,03E-18
TIAL1	3,12E-15	KDM3B	8,63E-21	XPOT	3,12E-15
ARID1A	3,52E-15	ZNF143	9,78E-13	SMARCC1	3,52E-15
GRM8	9,87E-14	RBM19	1,75E-03	RANBP1	9,87E-14
XPOT	6,15E-11	TRIM28	1,75E-03	RBM6	6,15E-11
TAF6L	1,32E-10	GJA1	6,76E-03	SUPT7L	1,32E-10
RUNX1	1,57E-10	LOC126536	6,76E-03	SMARCA4	1,57E-10
GPATCH8	2,23E-09	NRXN3	3,08E-02	TIAL1	2,23E-09
SMARCC1	4,99E-09	CLVS1	3,33E-02	ARID1A	4,99E-09
RANBP1	1,50E-08	PLXNA4	3,44E-02	SMARCD2	1,50E-08
KHDRBS1	2,56E-08	MAGI2	4,48E-02	KHDRBS1	2,56E-08
NONO	3,23E-08	C10orf68	4,55E-02	NGLY1	3,23E-08
CBFA2T3	3,41E-08			TADA1	3,41E-08
SUPT7L	1,21E-06			THRA	1,21E-06
EYS	7,75E-06			DDI2;RSC1A1	7,75E-06
DDI2	1,11E-05			SKI	1,11E-05
RBM6	1,77E-05			PHF6	1,77E-05
PDE4D	5,28E-05			CASP8	5,28E-05
SLC18A1	5,28E-05			LEMD3	5,28E-05
PHIP	6,64E-05			C2orf76	6,64E-05
TADA1	6,64E-05			TAF5L	6,64E-05
THRA	1,29E-04			RAD54L2	1,29E-04
ANGPT1	3,29E-04			NFE2L1	3,29E-04
CTNNA2	3,29E-04			ARID1B	3,29E-04
POLR3GL	4,85E-04			CBFA2T3	4,85E-04
SKAP2	5,16E-04			RBM47	5,16E-04
BRF2	5,25E-04			RQCD1	5,25E-04
NGLY1	7,37E-04			PAXIP1	7,37E-04
SMARCA4	8,70E-04			TNFRSF1B	8,70E-04
RQCD1	8,73E-04			RPRD2	8,73E-04
TAF5L	1,29E-03			CDK6	1,29E-03
ANP32A	1,36E-03			TAF6L	1,36E-03
PNPLA7	1,77E-03			DCK	1,77E-03
SCHIP1	2,28E-03			POLR3GL	2,28E-03
GNAQ	2,73E-03			EIF2C2	2,73E-03
PRKCD	4,65E-03			CRCP	4,65E-03
SAFB	5,37E-03			BEND3	5,37E-03
TNFRSF1B	5,54E-03			PRMT7	5,54E-03
YLPM1	5,54E-03			BRF2	5,54E-03
CDK6	8,11E-03			RUNX1	8,11E-03
CNOT4	8,72E-03			CNOT4	8,72E-03
PHF6	8,72E-03			PRDM1	8,72E-03
GOLGA3	8,88E-03			PHIP	8,88E-03
PAXIP1	1,03E-02			MLL3	1,03E-02
PPM1F	1,11E-02			SNX27	1,11E-02

Supplementary Table 2. Log₂ ratios of identified peptides by mass spectrometry in BRCA2-depleted BT-549 and HCC38 cells

Protein code	Gene	Log ₂ ratio
P05362	ICAM1	2,2107
Q9BZQ8	NIBAN	1,7397
P04179	SODM	1,6698
O00764	PDXK	1,5009
P15144	AMPN	1,4743
P21589	5NTD	1,4511
Q6PIU2	NCEH1	1,4031
P04080	CYTB	1,3958
P29317	EPHA2	1,2887
P51114	FXR1	1,2566
P15311	EZRI	1,2386
P04083	ANXA1	1,1299
P17858	PFKAL	1,1012
P35237	SPB6	1,0980
Q09666	AHNK	1,0616
O60313	OPA1	1,0560
P53004	BIEA	1,0505
Q01650	LAT1	1,0483
P42224	STAT1	1,0299
P36871	PGM1	1,0061
P08195	4F2	1,0044
P55786	PSA	0,9288
P06703	S10A6	0,9075
P02794	FRIH	0,8960
O60664	PLIN3	0,8610
P40261	NNMT	0,8581
P52788	SPSY	0,8308
Q86UP2	KTN1	0,8305
Q9H4M9	EHD1	0,8259
P35241	RADI	0,7846
P00533	EGFR	0,7635
Q16658	FSCN1	0,7396
P40121	CAPG	0,7343
P00558	PGK1	0,7009
Q16555	DPYL2	0,6947
O00629	IMA3	0,6700
P52209	6PGD	0,6640
P11216	PYGB	0,6631
O75874	IDHC	0,6343
P07093	GDN	0,6291
P04040	CATA	0,6251
P35580	MYH10	0,6209
P35080	PROF2	0,5915
P62937	PPIA	0,5860
P16070	CD44	0,5827
Q13177	PAK2	0,5784
P13674	P4HA1	0,5724
O00159	MYO1C	0,5708
P16152	CBR1	0,5518
Q9Y4L1	HYOU1	0,5446

MYC promotes immune-suppression in TNBC via inhibition of IFN signaling

Chiara S Brambillasca^{1,2,*}, Dario Zimmerli^{1,2,*}, Francien Talens^{3,*},
Jinhyuk Bhin^{1,2,4}, Arkajyoti Bhattacharya³, Ana Moises Da
Silva^{1,2}, Stacey Joosten^{2,5}, Max Wellenstein^{2,6}, Kelly Kersten^{2,6},
Maurits Roorda³, Martine van Miltenburg^{1,2}, Roebi de
Bruijn^{1,2}, Stefano Annunziato^{1,2}, Lodewyk Wessels, Karin de
Visser^{2,6}, Wilbert Zwart^{2,5}, Rudolf S.N. Fehrmann³, Marcel
A.T.M. van Vugt^{3,7}, Jos Jonkers^{1,2,7}

¹ Division of Molecular Pathology, Oncode Institute, The Netherlands Cancer Institute, Amsterdam, The Netherlands.

² Oncode Institute, Utrecht, The Netherlands.

³ Department of Medical Oncology, University Medical Center Groningen, University of Groningen, Groningen, The Netherlands.

⁴ Division of Molecular Carcinogenesis, The Netherlands Cancer Institute, Amsterdam, The Netherlands.

⁵ Division of Oncogenomics, Oncode Institute, Netherlands Cancer Institute, 1066 CX, Amsterdam, The Netherlands.

⁶ Division of Tumour Biology & Immunology, The Netherlands Cancer Institute, Amsterdam, The Netherlands.

⁷ Shared corresponding author

* These authors contributed equally

Abstract

Treatment of triple-negative breast cancer (TNBC) patients remains challenging despite recent advances in targeted therapies. Also immune checkpoint inhibitors (ICI) have thus far only shown limited effects in TNBC, presumably due to low or unresponsive lymphocyte infiltration in these tumors. By conducting an extensive genomics and transcriptomics analysis of TNBC patient data, we found a strong correlation between MYC expression and loss of immune signatures. In order to functionally test if MYC suppresses immune responses in TNBC, we used mouse models of TNBC with a mammary gland-specific deletion of *Trp53* alone or in combination with *Brca1* deletion. We observed a dramatic decrease in lymphocyte infiltration upon MYC overexpression in tumors as well as loss of immune signatures, similar to what we saw in patient TNBC samples with high MYC expression. In line with these findings, inactivation of BRCA1 or BRCA2 in human TNBC cell lines lead to inflammatory signaling, which was strongly reduced upon MYC overexpression. Co-culture experiments of tumor cells with lymphocytes revealed reduced attraction and activity of lymphocytes upon MYC overexpression in both human cell lines and mouse organoid models. Chromatin immunoprecipitation (ChIP)-sequencing experiments revealed direct binding of MYC to promoters of multiple interferon/STING signaling genes downregulated upon MYC expression, presenting a mechanism by which MYC suppresses innate immunity and facilitates immune escape. Preclinical intervention studies showed that activation of interferon signaling via STING agonists inhibits tumor progression in a TNBC mouse model. Together, our data reveal a key role for MYC in generating an immune-depleted microenvironment in TNBC by hampering interferon signaling and preventing lymphocyte engagement, thereby explaining the poor immunogenicity observed in MYC overexpressing human TNBCs.

5

Breast cancer is among the leading causes of cancer-associated death in women, with a lifetime risk of ~12.5%¹. Triple-negative breast cancers (TNBCs) lack expression of the ER, PR, and HER2 receptors. Although TNBC only represents 15–20% of breast carcinomas, distant recurrence, and mortality in TNBC are significantly higher when compared to other breast cancer subtypes^{2,3}. As very few targeted therapeutic options are available for patients with TNBC, radiation and neoadjuvant chemotherapy are the current standard-of-care treatments, searching for new effective therapeutic options is necessary^{4–7}.

Increasingly, targeting the immune system is successfully employed as a treatment approach for cancer. Immune checkpoint inhibitors have resulted in survival benefit across tumor types, with high mutational load and tumor-infiltrating lymphocytes (TILs) being associated with response⁸. TNBCs are reported to have high levels of TILs^{9,10}. Moreover, amounts of TILs were shown to be predictive of treatment response to conventional chemotherapeutic treatment^{11–13} and treatment with immune checkpoint inhibitors (ICIs)¹⁴. Unfortunately, the subsequent clinical evaluation of ICIs in patients with TNBC¹⁵ only showed benefit in a minority as a single agent¹⁶. Nevertheless, Atezolimab in combination with paclitaxel has been recently approved in clinics¹⁷.

To delineate responders from non-responders, multiple diagnostic markers have been investigated with limited success, including expression of immunosuppressive proteins, such as PD-L1¹⁸, infiltration by CD8⁺ T cells^{19,20}, and expression of genes involved in inflammatory responses, including IFN- γ target genes²¹. Therefore it remains unclear why many TNBCs with high TILs are unresponsive to ICIs.

The lack of response to immune checkpoint inhibitors is surprising because TNBCs are characterized by multiple features that are associated with a response, including high levels of TILs. Although TNBCs do not typically display a high mutational burden, due to frequently occurring DNA repair defects, TNBCs often have complex genomes with pronounced copy number aberrations and complex rearrangements potentially leading to neo-epitopes^{22,23}

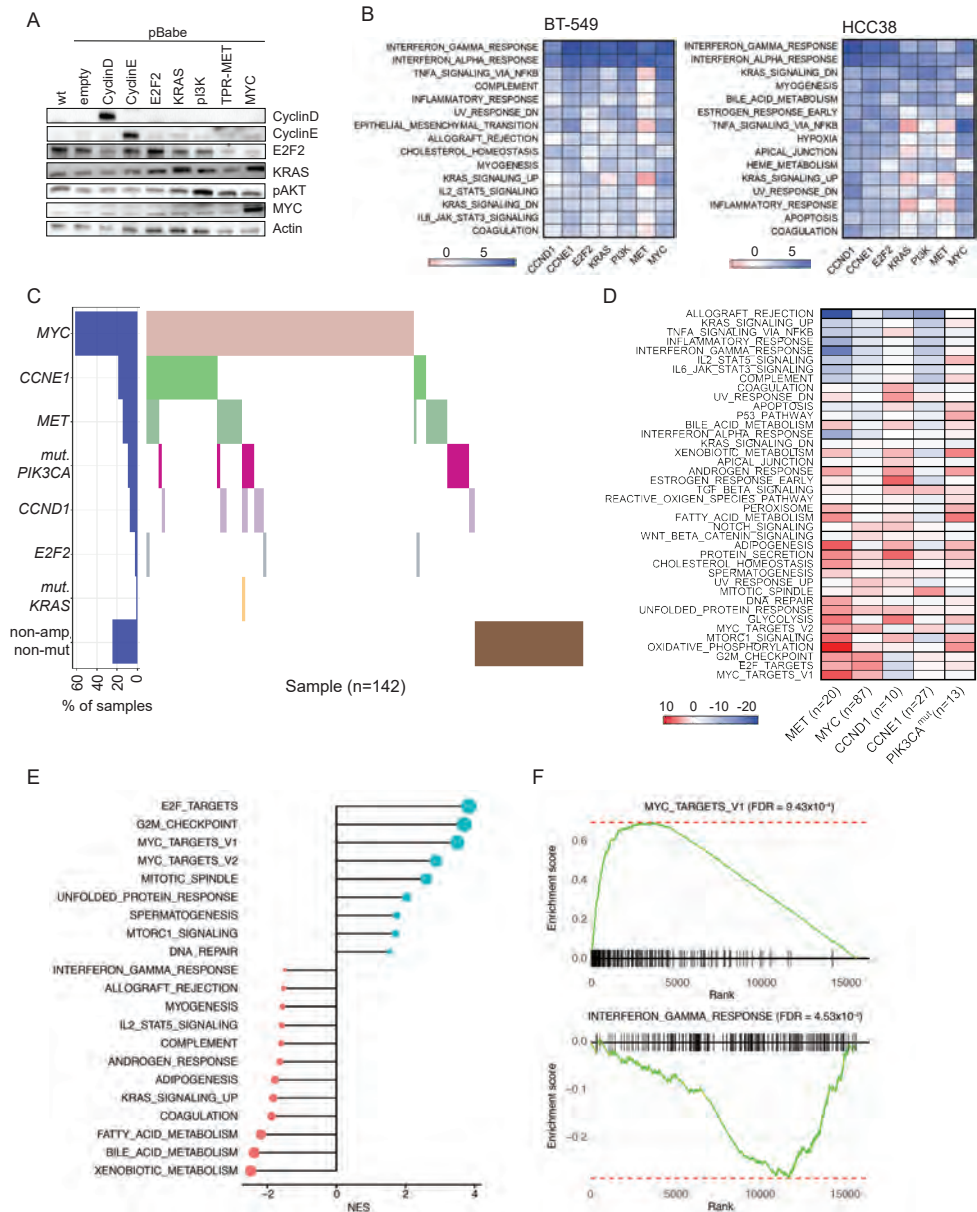


Figure 1. Oncogene expression diminishes inflammatory signaling in breast cancer. **A)** BT-549 cells were overexpressed for several oncogenes with pBABB vectors. Cells were immunoblotted for CyclinD, CyclinE, E2F2, KRAS, pAKT, MYC and Actin. **B)** GSEA analysis of BT-549 and HCC38 cells overexpressed for different oncogenes as shown in A compared to cells expressing pBabe-empty vector. Means from two biological replicates per cell line were used for RNA seq analysis. Z-transformed p values are plotted for the top 15 down-regulated hallmark genesets in BT-549 (left panel) and HCC38 (right panel) cells. **C)** Distribution plot of TNBC samples used for GSEA analysis from TCGA data. In total, 142 samples were included in the analyses. Individual samples are plotted on the x-axis. **D)** GSEA analysis of TNBC samples (n=142). Top 20 up (red) and down (blue) regulated hallmark genesets are plotted in

amplified or mutated vs neutral samples for specific oncogenes. Number of amplified/mutated samples per oncogene is shown. Values plotted are Z-transformed p values. **E**) GSEA for the genes which are positively (cyan) or negatively (pink) correlated with expression of MYC in TONIC trial dataset. The normalized enrichment scores (NES) for the significantly enriched gene sets ($FDR < 0.05$) are presented in the bar plot. MsigDB Hallmark gene sets were used for GSEA analysis. **F**) GSEA plots for two significant gene sets, MYC_TARGETS_V1 (enriched) and INTERFERON_GAMMA_RESPONSE (depleted).

Additionally, inactivation of *BRCA1/2* and the ensuing DNA damage was shown to result in the accumulation of DNA in the cytosol and subsequent activation of the cGAS/STING pathway^{24,25}. The cGAS/STING pathway was originally discovered as an anti-viral pathway responding to non-self DNA in the cytosol (reviewed in²⁶) but was recently described to also respond to 'own' DNA, when outside the nucleus^{27,28}. Interestingly, this innate immune pathway was demonstrated to be required for a robust adaptive anti-tumor immune response²⁹.

TNBCs, and *BRCA1* mutant tumors in particular, have evolved mechanisms to suppress immune responses quite efficiently¹⁴. Multiple recurring gene alterations in tumor-suppressor genes and oncogenes have been described for TNBC. For instance, mutations in the tumor suppressors *TP53* along with *BRCA1*, both crucial for genome integrity, are commonly found in human TNBC³⁰. Also, the transcription factor *MYC*, which resides in the 8q24 locus, is regularly amplified in breast cancer, particularly frequent in TNBC³⁰. *MYC* regulates gene expression globally, promoting growth and many other cellular processes (reviewed in^{31,32}). A transcriptional signature associated with *MYC* amplification is correlated to a gene signature of *BRCA1*-deficient breast cancers^{33,34}. Notably, recent studies have illustrated how oncogenes and tumor suppressors regulate the tumor immune-microenvironment, beyond their roles in tumor cell-intrinsic regulation of tumor progression³⁵⁻⁴⁰.

Interestingly, analysis of human breast cancer gene expression data has provided hints that *MYC* overexpression correlates with low immunogenicity and downregulation of STING signaling⁴¹. Moreover, previous studies showed that *MYC* influenced the host tumor microenvironment and immune effectors in liver and lung cancer^{40,42}, suggesting a role for *MYC* in immune-suppression besides its activity as a mitogen. Importantly, functional proof that *MYC* regulates the immune system in TNBC is still lacking and the possible underlying mechanisms are largely unknown.

Here, we explored whether *MYC* might directly influence anti-cancer immune responses in TNBC, using a mouse model that recapitulates the features of the human disease. We show that *MYC* suppresses STING/IFN signaling in a tumor cell-intrinsic fashion, to shape the tumor microenvironment in TNBC.

Results

Oncogene expression is associated with decreased inflammatory signaling in breast cancer

To study the effects of oncogene overexpression in TNBC models, the TNBC lines BT-549 and HCC38, were engineered to overexpress a panel of established oncogenes, including mutant K-Ras, Cyclin D1, Cyclin E1, mutant PI3K, MET, *MYC*, and E2F2 (**Figure 1A, Figure S1A**). Analysis of mRNA counts from RNA sequencing (RNAseq) data (**Figure S1B**) and immunoblotting (**Figure 1A, Figure S1A**) confirmed the overexpression of introduced oncogenes. To investigate the biological processes that are affected by oncogene expression in TNBC, gene set enrichment analysis (GSEA) of RNAseq data was performed (**Figure 1B**). In both BT-549 and HCC38 cell lines, oncogene overexpression resulted in enrichment of growth pathways (i.e. *MYC* targets, E2F targets, and G2M checkpoint) when compared to control cells. Surprisingly, the majority of oncogenes resulted in reduced expression of gene-sets related to inflammatory signaling (i.e. Interferon (IFN) alpha response, IFN gamma response, and TNF α signaling via NF κ B) (**Figure 1B**).

To confirm these findings, GSEA analysis was performed on mRNA expression data of breast cancer samples from The Cancer Genome Atlas (TCGA) that were stratified for amplification or mutation status of selected oncogenes (**Figure S1C**). Oncogene amplification generally correlated with suppression of gene sets related to inflammatory signaling (**Figure 1D**). Similar inflammatory gene sets were downregulated in oncogene-amplified TNBC samples compared to neutral TNBC samples (**Figure 1C,D**). These data suggest that breast tumors must evade detection by the immune system, which might be achieved by oncogene overexpression.

MYC expression correlates with Down-regulation of IFN-gamma and JAK-STAT pathways in human breast cancer

In TNBCs, the most frequently aberrated oncogene is *MYC*, which was found to be amplified in 62% of all TNBC samples within the TCGA database (**Figure 1C**). *MYC* was also found to be the most commonly amplified gene in BRCA1/2-mutated breast cancers (**Figure S1E**). To assess the impact of *MYC* expression on inflammatory signaling in these breast cancers, we performed GSEA analysis on RNAseq data obtained from tumor samples from the TONIC phase II trial, which evaluates the efficacy of nivolumab after immune induction in TNBC patients¹⁴. As expected, *MYC* expression positively correlated with *MYC* target gene sets and E2F targets (**Figure 1E**). Interestingly, similar to what was observed in our cell line panel and TCGA analysis (**Figure 1B,C**), *MYC* expression negatively correlated with IFN-gamma and JAK-STAT signaling, as well as other inflammatory pathways, including IL2-STAT5 signaling, allograft rejection, and complement activation (**Figure 1E,F**).

MYC-overexpressing mouse TNBCs display an immune-depleted microenvironment

To explore if *MYC* regulates immune responses in mammary tumors *in vivo*, we used four genetically engineered mouse models (GEMMs) of BRCA1-proficient and -deficient TNBC with or without engineered *MYC* overexpression: *WapCre;Trp53^{F/F}* (WP), *WapCre;Trp53^{F/F};Col1a1^{invCAG-Myc-IRES-Luc/+}* (WP-Myc), *WapCre;Brca1^{F/F};Trp53^{F/F}* (WB1P) and *WapCre;Brca1^{F/F};Trp53^{F/F};Col1a1^{invCAG-Myc-IRES-Luc/+}* (WB1P-Myc). GSEA of RNA-sequencing data of mammary tumors from these four GEMMs showed a clear reduction of immune signatures in the WP-Myc and WB1P-Myc tumors with engineered *MYC* overexpression, when compared to WP and WB1P control tumors (**Figure 2A**). Conversely, unsupervised hierarchical clustering of all tumors based on expression of interferon-stimulated genes (ISGs)⁴³ resulted in clustering according to *MYC* status (**Figure S2A**). Immunohistochemical analysis showed a significant reduction in tumor-infiltrating lymphocytes (TILs) in WP-Myc and WB1P-Myc tumors in comparison to WP and WB1P tumors (**Figure 2B,C**).

Since the effect of *MYC* overexpression on CD3⁺ TILs was most profound in the BRCA1-deficient mammary tumors (**Figure 2B**), we decided to focus our efforts on the WB1P model. In line with our transcriptomic and histopathologic analysis, flow cytometry analysis of immune cell populations in WB1P-Myc versus WB1P tumors showed a clear loss of CD3⁺ T cells and decreased numbers of infiltrating CD49b⁺ NK cells and CD11b⁺ myeloid cells in WB1P-Myc tumors (**Figure 2D**). In contrast, we did not observe a difference in CD19⁺ B cell numbers (**Figure 2D**). Of note, draining lymph nodes, spleen, and blood showed similar lymphocyte numbers in WB1P and WB1P-Myc mice, arguing against systemic immune-suppression and pointing towards local dampening of the immune response via paracrine signals from tumor cells (**Figure S2C**). To further corroborate our findings in WB1P and WB1P-Myc mice, we used somatic engineering⁴⁴ to induce mammary tumors in *Brca1^{F/F};Trp53^{F/F}* (B1P) and *Brca1^{F/F};Trp53^{F/F};Col1a1^{invCAG-Myc-IRES-Luc/+}* (B1P-Myc) mice via intraductal injection of a Cre-encoding lentivirus, again resulting in profound TIL depletion in the *MYC*-overexpressing B1P tumors (**Figure 2E**).

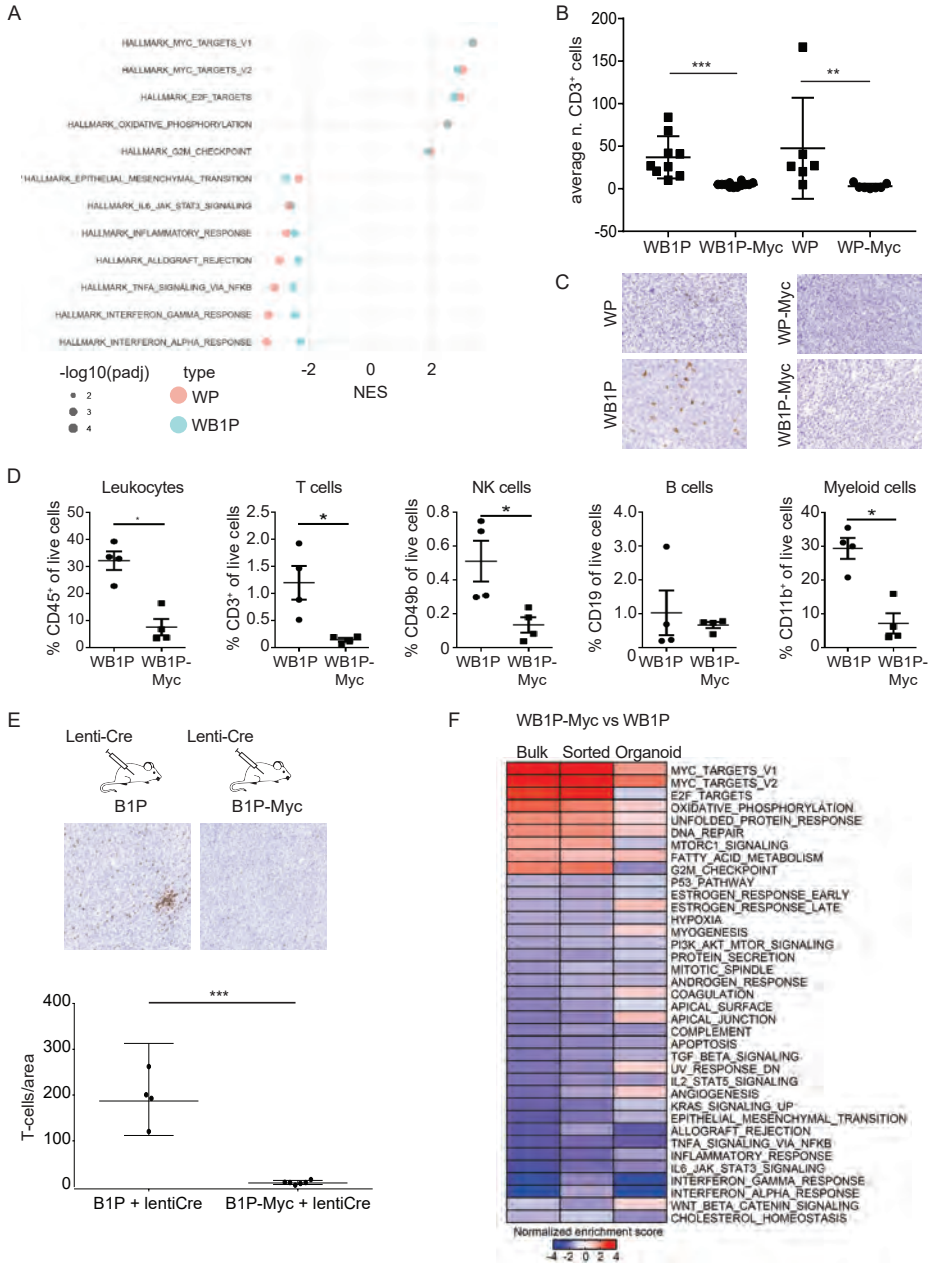


Figure 2. WB1P-MYC mice present an immune-depleted phenotype and reduced inflammatory signatures. **A)** Hallmark gene sets represented by WP vs WP-Myc (pink) and WB1P vs WB1P-Myc (cyan) tumors from GSEA analysis. The normalized enrichment scores (NES) for the significantly enriched gene sets ($FDR < 0.05$) are presented in the bar plot. MsigDB Hallmark gene sets were used for GSEA analysis. **B)** Quantification of CD3⁺ cells in WP, WP-Myc, WB1P and WB1P-Myc tumors (Mann-Whitney test, $p = 0.0047$ and $p = 0.0001$). **C)** Representative immunostainings for CD3⁺ cells in WP, WP-Myc, WB1P and WB1P-Myc tumors. **D)** FACS analysis of Leukocytes (CD45⁺), T cells (CD3⁺), NK cells (CD49b⁺), B cells (CD19⁺) and Myeloid cells (CD11b⁺) in WB1P-Myc tumors in comparison to WB1P tumors. **E)** Upper

To test if the reduced immune cell infiltration was not simply due to faster tumorigenesis in WB1P-Myc mice versus WB1P mice, we generated *WapCre;Brca1^{F/F};Trp53^{F/F};Col1a1^{invCAG-Met-IRES-Luc/+}* (WB1P-Met) mice with tumor-specific overexpression of MET instead of MYC, leading to a very similar decrease in tumor latency as observed in the WB1P-Myc model (**Figure S2D**). In contrast to MYC, MET overexpression did not result in immune suppression, as demonstrated by the comparable numbers of TILs in WB1P-Met versus WB1P tumors (**Figure S2E**). Also clustering based on expression of ISGs resulted in a clear separation between WB1P-Met and WB1P-Myc tumors (**Figure S2F**). To further examine if the immune cell exclusion in WB1P-Myc tumors was not a generic consequence of tumor-promoting mutations, we tested if *Pten* loss would lead to decreased lymphocyte infiltration by performing intraductal injections in WB1P-Cas9 mice³⁰ with lentiviruses encoding a *Pten*-targeting sgRNA alone (Lenti-sgPten) or in combination with MYC (Lenti-sgPten-Myc). TILs were observed in tumors from mice injected with Lenti-sgPten, but not in tumors from mice injected with Lenti-sgPten-Myc, confirming that MYC is selectively responsible for immune cell exclusion (**Figure S2G**).

MYC drives immune cell exclusion in a tumor cell-intrinsic manner

To investigate how MYC is linked to an immune-suppressive phenotype, we performed RNA-sequencing on three different sources of tumor cells. In addition to bulk tumors containing both tumor cells and infiltrating immune cells, we used WB1P and WB1P-Myc tumor organoids containing only tumor cells as well as FACS-sorted ECAD⁺ tumor cells from WB1P and WB1P-Myc tumors. Consistent with our above-mentioned analysis, GSEA showed significant downregulation of immune response pathways and MYC overexpression in the bulk tumor samples (**Figure 2F, Figure S2H**). Although these transcriptomic changes could be due to the decreased presence of immune cells in bulk tumor samples, these immune pathways were also downregulated in sorted tumor cells and organoids, indicating that MYC-associated immune evasion is mediated by a tumor cell-intrinsic mechanism (**Figure 2F**). In support of this notion, the enriched pathways showed strong correlation ($R=0.83$) between WB1P-Myc bulk tumors and sorted tumor cells (**Figure S2H**). Taken together, these results suggest that MYC suppresses IFN signaling in a tumor cell-intrinsic manner.

To assess the immune composition in MYC versus non-MYC tumors in more detail, the immune cell composition was deconvoluted *in-silico* based on RNA-seq data using the ESTIMATE method⁴⁷. Again, a significantly higher immune score in WP and WB1P tumors was observed when compared to WP-Myc and WB1P-Myc tumors (**Figure S3A**). A comparison of our list of differentially expressed genes with published MYC targets⁴⁸ confirmed the functionality of our MYC overexpressing model (**Figure S3B**). Furthermore, single-cell RNA sequencing of WB1P and WB1P-Myc tumors showed that an immune compartment was almost exclusively detected in the WB1P tumors (**Figure S3C**).

To corroborate our *in vivo* findings, we used CIBERSORT analysis on gene expression data from TCGA to estimate the fractions of different immune cell types in human breast cancer samples. Compared to cancers with neutral copy numbers of *MYC*, breast cancers with amplified *MYC* contained lower fractions of monocytes, M2 macrophages, and CD8⁺ T cells, whereas they showed increased fractions of M0/M1 macrophages and regulatory T cells (**Figure S3D**). A similar pattern was observed within the TNBC subset of these cancers

panels: Tumors generated by intraductal lenti-Cre injections in WB1P and WB1P-Myc mice are analyzed via immunohistochemistry for CD3 expression (brown). Quantifications are shown below. P values were calculated using two-tailed Student's t-test, $p < 0.0001$. **F**) Heatmap for the gene sets represented by the comparison of WB1P-Myc versus WB1P tumors, organoids and sorted cancer cells from GSEA analysis. Normalized enrichment scores are plotted for the heatmap.

when *MYC* amplified and *MYC* neutral samples were compared (**Figure S3D**). Taken together, our results show that *MYC* expression drives a dramatic loss in lymphocytic infiltration, as well as other immune cells, including monocytes, macrophages, and NK cells. Furthermore, we demonstrate a cancer cell-intrinsic role for *MYC* in suppressing inflammatory pathways.

MYC overexpression in mammary tumor cells down-regulates interferon stimulated genes

The main downregulated pathways in the *MYC*-overexpressing WB1P tumors were 'Interferon signaling' and 'JAK/STAT signaling' (**Figure 2A,F**), which are both important in inflammatory responses⁴⁶. Recent studies showed that loss of BRCA1 leads to the accumulation of cytosolic DNA, thereby triggering the cGAS/STING pathway^{24,25,49}. To investigate whether the suppression of IFN signaling in WB1P-*Myc* tumors is connected to reduced cGAS/STING pathway activation, we probed our RNA-seq profiles with a previously reported panel of ISGs induced by cGAS/STING signaling²⁷. The expression of these ISGs clearly separated WB1P-*Myc* tumors and organoids, showing significant downregulation of the ISGs in the WB1P tumors/organoids (**Figure 3A**). Specifically, we observed down-regulation of various STING-pathway-related genes, including STAT1, STAT3, CCL20, and IRF9 (**Figure S7B**)^{50,51}. We also observed the downregulation of CD74 and Ciita, two genes regulated directly by STAT1 and important for a functioning adaptive immune (**Figure S4A**)⁵². Downstream activation of cGAS/STING signaling is associated with the secretion of different chemokines and cytokines, including CCL5 and CXCL10^{27,53,54}. Using qRT-PCR on tumor and organoid samples, we confirmed the reduced expression of *Cxcl10* in *Myc*-expressing tumors and organoids (**Figure 3B,C**).

To further confirm the findings, we used immunoblotting for STAT1 and observed reduced levels in organoids derived from WB1P-*Myc* tumors versus those derived from WB1P tumors (**Figure S4B**). Decreased levels of CCL5 were observed in WB1P-*Myc* compared to WB1P organoids in a cytokine-chemokine array (**Figure 3D, Figure S4C**). To confirm the direct role of *MYC* in the downregulation of ISGs, we generated organoids from WB1P tumors containing a tamoxifen-inducible *MycER*⁵² transgene. Flow cytometry analysis of these organoids showed that *MYC* activation decreased phosphorylation of Interferon Regulatory Factor 3 (pIRF3) (**Figure 3E, Figure S4D**), a key transcriptional regulator of IFN and STING responses, as well as phosphorylation of Tank binding kinase (pTBK1) (**Figure S4E**), a central player in the STING signal transduction. These data indicate that *MYC* overexpression can manipulate IFN signaling by reducing the expression of a broad network of genes in our murine tumor model.

To further investigate the role of *MYC* amplification in a BRCA1/2-depleted context, the TNBC cell lines BT-549 and HCC38 were engineered to express doxycycline (dox)-inducible BRCA1 or BRCA2 short hairpin RNAs (shRNAs) either in the presence or absence of constitutive overexpression of *MYC* (**Figure S4F**). As a negative control, CRISPR/Cas9 was used to inactivate *MB21D1* in BT-549 (**Figure S4F**). Of note, dox-mediated activation of the BRCA1 and BRCA2 hairpins resulted in decreased cell proliferation and ultimately cell death (**Figure S4G-I**), which was not rescued by *MYC* overexpression (**Figure S4G-I**). Recently, inactivation of BRCA2 was demonstrated to increase the amount of cGAS-positive micronuclei and trigger cGAS/STING-dependent IFN signaling^{25,27}. In line with these data, BRCA1 and BRCA2 depletion led to increased amounts of cGAS-positive micronuclei when compared to control cells (**Figure 3F,G**). However, *MYC* overexpression did not significantly alter the number of micronuclei in BRCA1 or BRCA2-depleted cells (**Figure 3G**), suggesting that the role of *MYC* in suppressing IFN signaling is downstream of the generation of cytoplasmic DNA.

In line with the formation of micronuclei and ISG gene-set enrichment, both BRCA1 and BRCA2 depletion increased the secretion of CCL5 in BT-549 and HCC38 cells as measured by enzyme-linked immunosorbent assay (ELISA; **Figure 3H**). Interestingly, CCL5 secretion was diminished upon *MYC* overexpression in both cell lines (**Figure 3H**). Decreased secretion of

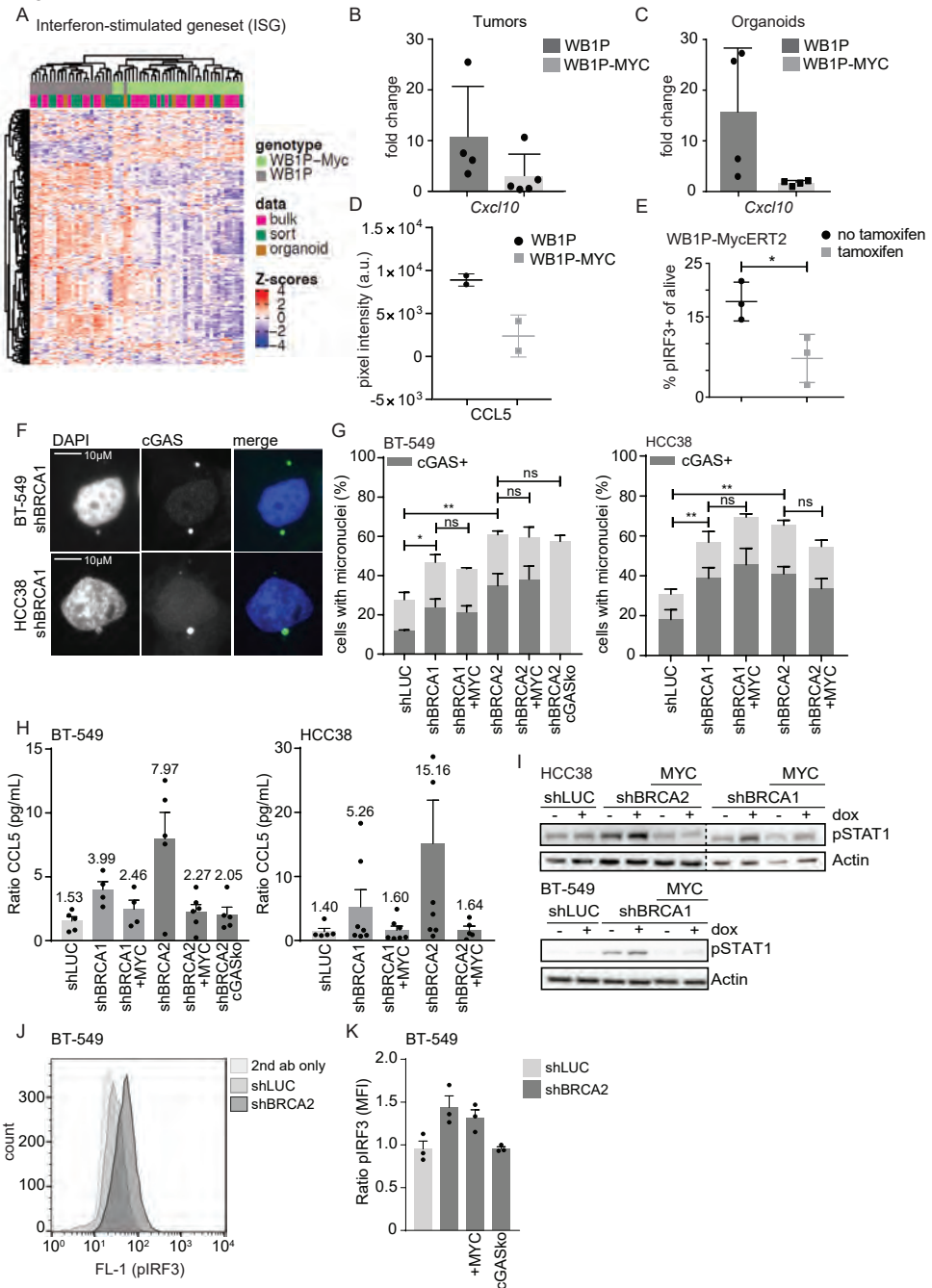


Figure 3. MYC overexpressing mammary epithelial tumor cells down-regulate Interferon Stimulated genes (ISGs). **A)** Heatmap of a comparative analysis of RNAseq on bulk tumors, sorted epithelial tumor cells and organoids for a large comprehensive ‘Interferon Stimulated Gene’ set compiled of the set from^{27,79,80} and the KEGG cytosolic DNA sensing pathway. **B)** qRT-PCR analysis in mouse tumors for

Cxcl10, fold changes normalized to GAPDH are plotted. **C**) qRT-PCR analysis for *Cxcl10* in 3 independent mouse tumor organoid lines each plus a line transfected with *MycERT2* with and without tamoxifen, fold changes normalized to *RPM20* are plotted. **D**) Quantification of cytokine array for *Ccl5* in *WB1P* and *WB1P-Myc* organoids ($n=2$). **E**) Quantification of *pIRF3* by FACS analysis of *WB1P-MycERT2* organoids with and without tamoxifen treatment. ($n=3$, $p= 0.03$) *P* values were calculated using two-tailed Student's *t*-test. **F**) Representative images of *BT-549* and *HCC38* cells harboring *shBRCA2* and treated with *dox* for three days. Cells were stained with anti-*cGAS* and DAPI. **G**) Quantification of *cGAS*-positive micronuclei as described in F. ≥ 100 Cells were counted per condition. Error bars indicate SEM of at least three independent experiments. *P* values were calculated using two-tailed Student's *t*-test. * $P < 0.05$, ** $P < 0.01$. **H**) *BT-549* and *HCC38* cells with indicated hairpins, depleted for *cGAS* or overexpressed for *MYC* were treated with or without *dox* for 6 days. Supernatants were harvested and secretion of *CCL5* was measured with ELISA. Concentrations were normalized to untreated conditions of each cell line. Means are indicated underneath each condition. Error bars indicate SEM of at least 4 independent experiments with two technical replicates each. **I**) *BT-549* and *HCC38* cells with indicated hairpins, depleted for *cGAS* or overexpressed for *MYC* were treated with or without *dox* for 5 days. Phosphorylation status of *STAT1* was analyzed by immunoblotting. **J**) *BT-549* cells with indicated hairpins, were treated with *dox* for 5 days. Phosphorylation levels of *IRF3* were analyzed by flow cytometry. **K**) Phosphorylation levels of *IRF3* were analyzed by flow cytometry as described in J. Median fluorescence intensities (MFI) were normalized to cells treated without *dox*. Error bars indicate SEM of at least 3 independent experiments.

cytokines was confirmed with qRT-PCR analysis using a broader range of STING-dependent chemo- and cytokines. Specifically, *BRCA1/2* depletion increased the levels of *CCL5*, *IFN β* , *IFN γ* , and *CXCL10*, which was suppressed upon *MYC* overexpression (**Figure S5A**). Furthermore, immunoblotting and flow cytometry of *BRCA1*- and *BRCA2*-depleted cells demonstrated increased levels of *pSTAT1* and *pIRF3* (**Figure 3J-K**, **Figure S5B**). Levels of *pSTAT1* were diminished upon *MYC* overexpression, whereas *pIRF3* levels were only marginally affected (**Figure 3J,K**), suggesting context dependency. RNAseq was performed in both *BT-549* and *HCC38* cell lines to further investigate the role of *MYC* on transcriptional re-wiring of *BRCA*-depleted cells. GSEA on significantly downregulated genes in *BRCA2*-depleted cells with *MYC* overexpression compared to *BRCA2*-depleted cells only, resulted in enrichment, and thus downregulation, of gene-sets related to inflammatory signaling (i.e. *IL2* *STAT5* signaling, *TNFA* signaling via *NFKB* and *IFN* gamma response) upon *MYC* overexpression (**Figure S5C,D**).

MYC directly regulates lymphocyte trafficking and activation *in vitro* and *in vivo*

Next, the effect of cytokine secretion induced by *BRCA1/2* depletion on surrounding immune cells was assessed *in vitro*. To this end, we used transwell assays to measure the migration of human isolated *CD8⁺* T cells towards *BT-549* and *HCC38* cells, in which *BRCA1* or *BRCA2* were depleted (**Figure 4A**). Upon *BRCA1/2*-depletion, the numbers of *CD8⁺* T cells that migrated towards the tumor cells increased after 24h and 48h in both *BT-549* and *HCC38* (**Figure 4B**). Interestingly, *MYC* overexpression diminished the amount of migrating *CD8⁺* T cells towards *BRCA1/2*-depleted cells (**Figure 4B**), similar to the negative controls in which *cGAS* was knocked out (**Figure 4B**). Furthermore, we tested if the secreted chemo- and cytokines influenced the activation of T cells. Upon treatment with conditioned medium from the tumor cells, we tracked the proliferation of *CD8⁺* T cells using a fluorescent label, as a readout for their activation (**Figure S5F**). The percentage of activated *CD8⁺* T cells increased in medium harvested from *BRCA1*- or *BRCA2*-depleted cells compared to medium from control cells (**Figure 4C**). Importantly, medium harvested from *MYC*-overexpressing cells, depleted for *BRCA1* or *BRCA2*, decreased the percentage of activated *CD8⁺* T cells (**Figure 4C**). These results suggest that factors secreted by *BRCA1*- or *BRCA2*-depleted breast cancer cells increase the migration and activation of T cells, whereas *MYC* overexpression suppresses the migration and activation of *CD8⁺* T cells in a tumor cell-intrinsic manner.

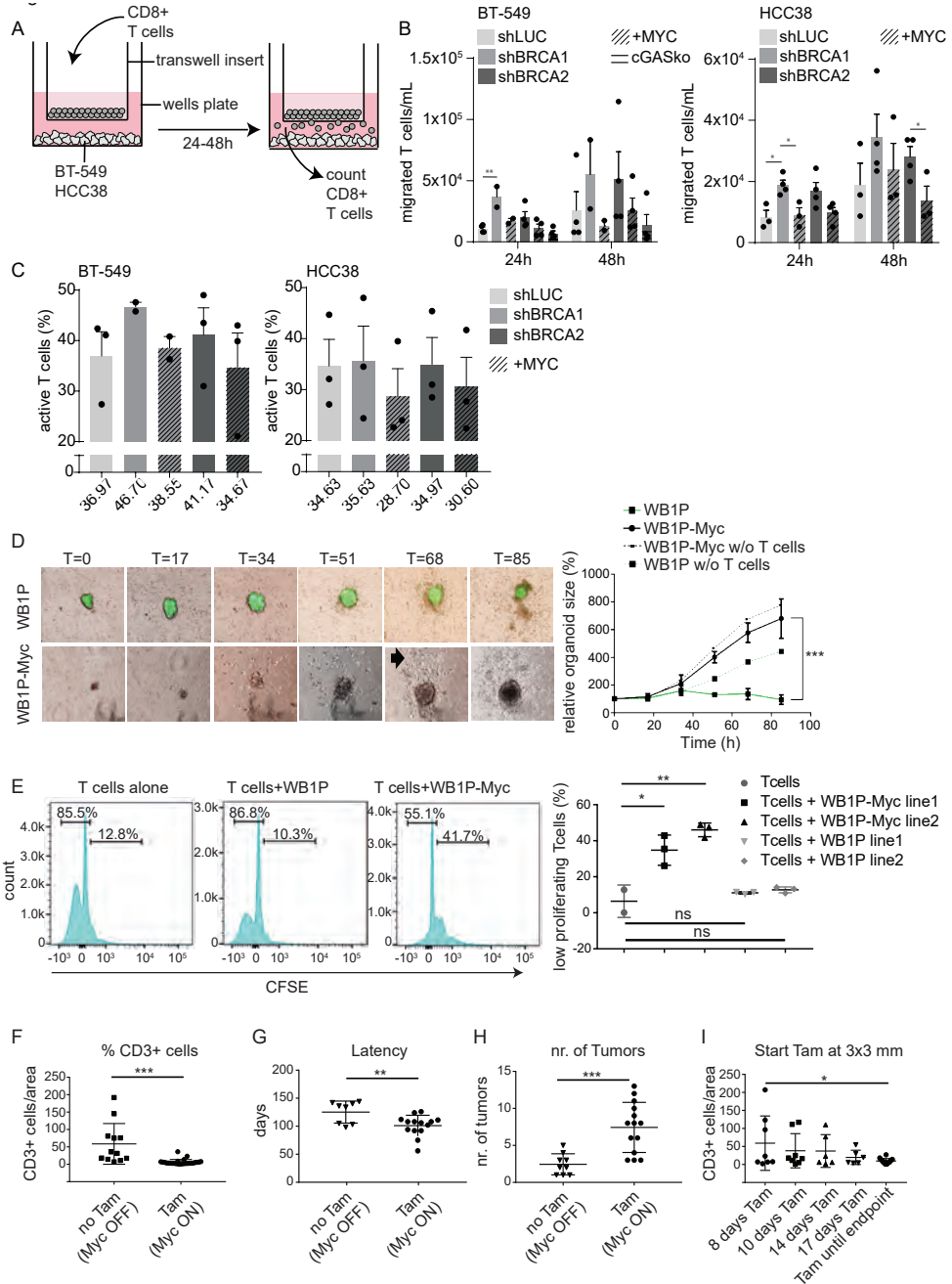


Figure 4. MYC overexpression regulates lymphocyte migration and activation in vitro and in vivo. A) Schematic overview of the transwell assay. BT-549 or HCC38 cells were cultured in wells for 5 days with dox treatment. Isolated human CD8⁺ T cells were added in the transwell insert and cultured for 1 or 2 days. The amount of migrated T cells towards the lower compartment were counted. **B)** Transwell assays were performed as described in A. The amount of migrated T cells towards the tumor cells was counted

after 24 or 48 hours. **C)** The percentage of activated CD8⁺ T cells was measured by flow cytometry 5 days after co-culture with harvested medium from BT-549 or HCC38 cells pre-treated with doxycycline. Gating was performed as shown in S4F. Mean percentages are indicated underneath each condition. Error bars indicate SEM of 2 or 3 independent experiments. **D)** Live imaging of *in vitro* co-culture of WB1P (green) and WB1P-MYC organoids (red) with splenocytes. Time after seeding in hours is indicated on top of the respective panels. Quantification of organoid sizes is quantified in the right panel. **E)** FACS analysis of WB1P and WB1P-MYC tumor derived organoids co-cultured with T-cells and stained for CFSE. Halving in fluorescence intensity marks one cell division. Fluorescence intensity per number of cells is plotted. Quantification for percentage of low proliferating T cells of replicas of 2 different organoid lines each is shown in the right panel. **F)** Counts of CD3⁺ T-cells of tumors in the MycERT GEMM model with and without tamoxifen chow. **G)** Latency analysis in WB1P-MycERT with and without tamoxifen. **H)** Tumor burden in mice with and without tamoxifen administration. **I)** CD3⁺ cell counts in tumors upon starting administration of tamoxifen when tumors are 3 by 3 mm for the time indicated. In panel D-I, *p* values were calculated using unpaired *t*-test. **p*<0.05, ***p*<0.01, ****p*<0.001

To reconcile these results with our murine models, we performed live imaging co-culture experiments with WB1P and WB1P-Myc tumor-derived organoids and syngeneic mouse splenocytes. 7-day time-lapse quantification of organoid size demonstrated clear growth inhibition of WB1P organoids by immune cells, whereas hardly any effects were observed in WB1P-Myc organoids (**Figure 4D**). Also, standard proliferation co-culture assays showed that WB1P-Myc organoids suppressed IL2-induced T-cell proliferation (**Figure 4E**).

To confirm MYC activation as the direct cause of an immune-infiltrate reduction *in vivo*, WB1P tumor-derived organoids were transduced with lentiviral MycERT^{T2} and orthotopically transplanted in the mammary fat pad of syngeneic mice. In vehicle-treated mice, we observed T cells infiltrating the tumors (**Figure S6A**). In contrast, no T cells were detected in the tumors upon tamoxifen administration (**Figure S6A**). These results were confirmed using a reversible *in vivo* activation with MycERT^{T2}Cre delivered to the mammary epithelium via intraductal injection in B1P mice. Sustained MYC expression led to tumor formation in 100% of the cases, with decreased tumor latency as with the B1P-Myc tumors (**Figure S6B**). Interestingly, in the majority of tumors, the reversion of MYC induction led to slower tumor growth and an influx of CD3⁺ cells. Notably, tumors in which MYC induction did not lead to slower tumor growth remained with a low abundance of intra-tumoral T cells (**Figure S6C**).

We next validated these findings using a genetically engineered mouse model (GEMM) containing the Myc^{ERT2} allele and investigated tumor growth and immune infiltration at different time points after MYC induction via tamoxifen chow. Upon feeding tamoxifen at 7 weeks of age until time of sacrifice, we again observed that MYC induction reduced immune cell infiltration and shortened tumor latency compared to WB1P tumors, similar to findings with the WB1P-Myc model (**Figure 4F,G, Figure S6D**). Also, we observed increased tumor numbers, as expected for MYC-driven tumorigenesis (**Figure 4H**). Also, when tamoxifen-induced Myc^{ERT2} translocation was initiated when tumors reached 14mm³, we observed depletion of immune infiltrates. Specifically, a continuous reduction in CD3⁺ T-cells was observed over time after the start of tamoxifen administration until similar low levels as observed in the WB1P-Myc model were reached at the time of humane endpoint (**Figure 4I**). We did not observe significant effects on tumor growth rates of tumors in this instance (**Figure S6D**). These findings confirmed our previous observations, in which MYC expression was directly hindering immune infiltration in *Brca1*-mutant tumors and confirms that the decreased immunogenicity is not a result of different tumor latencies.

MYC controls expression of multiple interferon signaling components in tumors and organoids

To test if MYC directly regulates genes involved in IFN signaling, we performed chromatin immuno-precipitation of MYC, followed by whole-genome sequencing (ChIP-seq) on WB1P and WB1P-Myc organoids as well as tumors. We found 1257 common peaks between the tumor and organoid ChIPs (**Figure 5A**). The majority of peaks were found in promoter regions (**Figure 5B**). Also, using JASPAR to analyze the motif sequences of the ChIP seq peaks, the Myc motif was identified as most prevalent, showing the validity of our ChIP seq experiments (**Figure 57C**). MYC binding was significantly enriched to those genes, that were found to be up-regulated in the RNAseq of WB1P-Myc bulk tumors, sorted tumor cells, and organoids (**Figure 5C**). Next, we intersected the genes bound by MYC in the ChIP-seq with those genes downregulated in the RNA-seq of the different samples (tumors, organoids, and sorted tumor cells) (**Figure 5D, Figure 57A, 57D**). Gene set enrichment analysis revealed IFN signaling, inflammation-related pathways such as TNFA signaling via NFKB, IFN alpha and gamma response as well as IL6 JAK STAT3 signaling (**Figure 5E**) as repressed targets in RNA-seq data and peaks in ChIP-seq data. Using the condition of a MYC ChIP-seq peak in either tumors, organoids, or both yielded 59 IFN signaling pathway-associated genes that were down-regulated in the RNA-seq with tumors, sorted tumor epithelial cells and organoids (**Figure 57B**). The construction of a co-functionality network⁵⁵ from the above mentioned integrated analysis using the total of the 129 downregulated genes, a network of immune- and IFN-related genes was revealed in the MYC target genes, confirming MYC's role in suppressing these pathways (**Figure 5F**). For the upregulated genes, the network did not show any immunity signatures (**Figure 57E**). Combined, our results demonstrate that MYC directly controls anti-tumor immunity via the downregulation of a myriad of inflammatory pathway components.

Discussion

In this study, we aimed to clarify why TNBC, and *BRCA*-mutated breast cancers specifically, despite being viewed as being immunogenic due to the increased amount of neo-antigens induced by the DNA repair defects⁵⁶⁻⁵⁹, rarely respond to immunotherapy¹⁴. Starting from the finding that human TNBCs with high MYC expression are poorly immune-infiltrated, we went on to prove this correlation using mouse models and human tumor cell lines. While our TNBC mouse models usually displayed a substantial amount of immune cell infiltration, this was mostly absent if *Myc* was overexpressed in these models. Mechanistically, we showed that the expression of MYC promotes tumor development and represses anti-tumor immune responses by repressing IFN/STING signaling in a tumor cell-intrinsic manner. We further showed that MYC directly masks cells from immune cell attack and hinders immune cell proliferation. Our findings provide one mode of action how in principle immunogenic TNBCs can evade clearance by the immune system.

Suppression of immune responses against tumor cells was shown to be of great importance for tumor progression. Conversely, therapeutic boosting of the adaptive immune system via inhibition of immune checkpoint components PD1/PD-L1 and CTLA4 has been successfully used to activate T-cell responses to clear tumors. However, boosting T-cell responses requires the presence of T cells in the tumor microenvironment. In line with this notion, these strategies showed promising results in immunogenic and lymphocyte infiltrated tumors such as melanoma while being rather disappointing in less infiltrated tumor types^{8,14}. Surprisingly, response rates of the anti-PD-1 inhibitor pembrolizumab in TNBC was only 20%, despite these tumors being characterized by high levels of genomic instability^{60,61}.

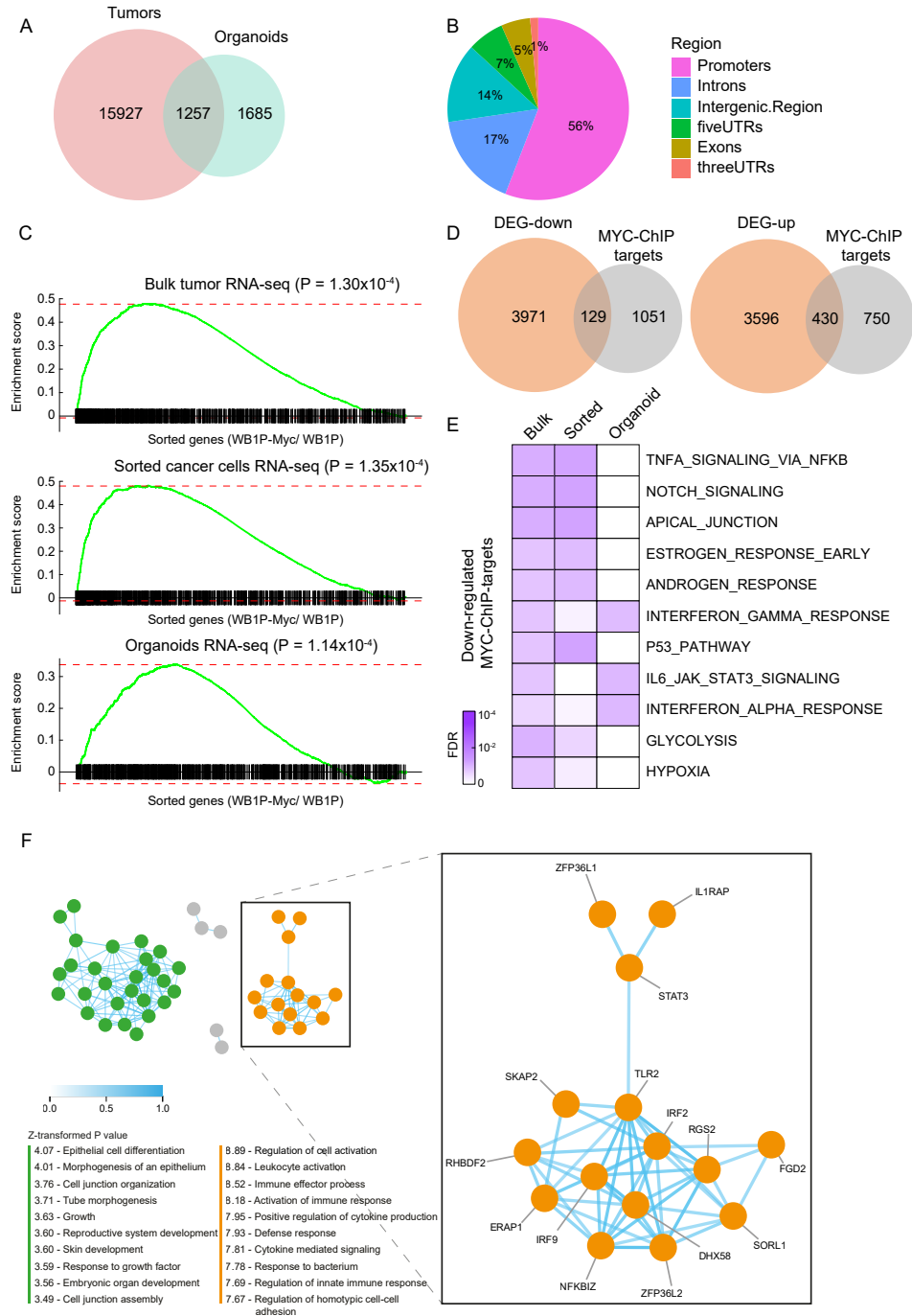


Figure 5. MYC represses the expression of key IFN activating pathways. **A)** Overlap of the MYC-binding loci obtained from the tumor and organoid Chip-seq data. **B)** Genomic distribution of the common MYC-binding loci between tumor and organoid Chip-seq data. **C)** Expression profiles of the MYC targets in comparison of WB1P-Myc versus WB1P in each bulk tumor, sorted cancer cells, and organoids RNA-seq

Our results show that suppression of local immune cells in genomically unstable TNBCs presenting abundant Neo-antigens is – at least partially – driven by MYC. Analysis of oncogene amplification in a cohort of 142 human *BRCA* mutant TNBCs from the TCGA dataset showed MYC amplifications in a majority of cases, far more often than any other oncogene. GSEA of RNA sequencing data from the same cohort showed an association of MYC amplification with a reduction in immune signatures, specifically IFN and inflammatory signaling. Complementary GSEA of a cohort of samples from the TONIC trial confirmed the correlation of high MYC expression with reduced immune signatures¹⁴. This is in line with previous findings, where MYC amplifications were correlated with immune deserts in TNBCs⁴¹ as well as a report in which N-MYC amplification leads to loss of T-cell infiltrates and reduction of IFN signaling in metastatic neuroblastomas⁶².

Inflammatory signaling mediated by the STING pathway and other nucleic acid-sensing molecules was recently shown to drive anti-tumor immunity in DNA repair-deficient tumors^{24,25}. These findings also pointed to activation of the STING pathway as a possible approach to turn immunologically “cold” tumors into “hot” tumors and thereby potentiate immune checkpoint inhibitor treatments^{63,64}.

Using murine TNBC tumor cell-derived organoid cultures; we could confirm that inflammatory pathways were strongly inhibited upon MYC overexpression. Interestingly, loss of *BRCA* in human TNBC cell lines induced micronuclei formation and downstream STING-induced IFN signaling²⁵. While IFN signaling was strongly suppressed by MYC, we did not observe changes in micronuclei formation, suggesting a more downstream mode of action of MYC in suppressing IFN signaling. Cytokine analyses demonstrated that secretion of STING-related chemo- and cytokines were diminished upon MYC overexpression in our *in vivo* and *in vitro* models.

Using the WB1P-MycERT inducible model as well as human breast cancer cell lines, we demonstrated that exclusion of immune cells, specifically T cells, is induced directly by MYC expression *in vitro* as well as *in vivo*, where the T-cell counts dynamically change with MYC status, confirming that these effects are independent of tumor evolution. In line with our data, repression of IFN signaling and invasion of NK and B cells in pancreatic adenocarcinoma was dependent on MYC and *KRAS* expression⁶⁵. Interestingly, a recent study showed that a MycERT allele had a seemingly opposite effect in pancreatic adenocarcinomas⁶⁶. In this model, MYC expression led to a strong attraction of stromal cells to the tumor and regression of tumors upon MYC removal by tamoxifen withdrawal⁶⁶. Of note, stromal infiltrates in pancreatic cancers are associated with bad prognosis, while the opposite is true in mammary tumors⁶⁶. In another report, it was shown that MYC expression mediates the removal of T and B cells, but the attraction of macrophages in lung adenocarcinoma⁶⁷. In our TCGA data analyses using CIBERSORT, we saw that breast cancers with high MYC levels were associated with decreased

data. GSEA was performed to test the significance of the enrichment. MYC targets were defined by the genes nearest to common MYC-binding loci between tumor and organoid Chip-seq. D) Overlap between MYC targets from Chip-seq and differentially expressed genes (DEGs) in the comparison of WB1P-Myc versus WB1P. For the comparison, MYC targets were obtained from the common MYC-binding loci from tumor and organoid Chip-seq data, and DEGs were obtained from the union of the genes showing differential expression between WB1P-Myc versus WB1P in bulk tumor, sorted tumor cells, and organoid RNA-seq data (See Methods). E) Gene sets significantly represented by the down-regulated MYC targets from fisher’s exact test (FDR<0.1). The down-regulated MYC targets were defined by the genes in Figure 5D (129 down-regulated MYC targets) that are differentially expressed between WB1P-Myc and WB1P and have MYC-binding loci from Chip-seq data. F) Left: constructed co-functionality network of genes downregulated by MYC (n=129) retrieved from both MYC-ChIP-seq of WB1P-Myc and and RNA seq data of WB1P and WB1P-Myc tumors and organoids. Right: one of the two resulting clusters in which genes share strong predicted co-functionality (r>0.5) within the co-functionality network which was a cluster enriched for immunity pathways (e.g. leukocyte activation, activation of immune response and positive regulation of cytokine secretion).

fractions of monocytes, macrophages, and CD8⁺ T cells compared to samples with normal MYC levels, while in our mouse models we observed a general exclusion of immune infiltrates. These contrasting findings suggest that the tissue of origin of the tumor is of crucial importance in defining the effect of oncogene expression on tumor development and immune cell infiltration.

Our ChIP-sequencing experiments in tumor organoids as well as murine tumors showed direct binding of MYC to repressed promoters of IFN response genes. The integration of ChIP and RNA-sequencing data showed that MYC binds to and directly represses several downstream components of IFN inducing pathways, thus effectively inhibiting the mounting of an immune response against tumor tissues. Importantly, we found repression of IFN-signaling genes in whole tumor extracts as well as tumor organoids, confirming a tumor cell-intrinsic mechanism of immune suppression.

While the research focused heavily on anti-tumor immune responses launched by the adaptive immune system, previous reports suggested that adaptive anti-tumor responses are triggered by radiation- or chemotherapy-induced IFN signaling^{58,68,69}. An alternative route to trigger IFN signaling could be the inhibition of MYC, but while this still proves challenging, boosting the STING pathway via agonists is efficient^{29,70}. Pilot intervention studies conducted in our mouse models using STING agonists (data not shown), showed the susceptibility of these tumors to the induction of IFN signaling. This gives incentive to the notion of attracting adaptive immune cells to a badly infiltrated tumor via activation of IFN signaling. However, caution is mandated since persistent IFN signaling has also been shown to trigger adaptive resistance to immune checkpoint blockade by STAT-1 related epigenomic changes^{71,72}.

Taken together our findings suggest a role for MYC in counteracting anti-tumor immune responses via direct inhibition of IFN signaling responses and thus hampering immune cell attraction and activation. Low amounts of TILs induced by MYC could explain the ineffectiveness of PD1 treatments in a large part of BRCA-associated TNBCs that are potentially immunogenic due to their genomic instability. Combining STING activating therapies with checkpoint inhibition might be a way of ameliorating relatively poor response rates to such therapies in TNBCs.

Materials and Methods

Mice and *in vivo* procedures

WapCre;Trp53^{F/F} (WP), *WapCre;Brca1^{F/F};Trp53^{F/F} (WB1P)*, *WapCre;Trp53^{F/F};Col1a1^{invCAG-Myc-IRES-Luc/+} (WP-Myc)*, *WapCre;Brca1^{F/F};Trp53^{F/F};Col1a1^{invCAG-Myc-IRES-Luc/+} (WB1P-Myc)*, *WapCre;Brca1^F;Trp53^{F/F};Col1a1^{invCAG-Met-IRES-Luc/+} (WB1P-Met)*, and *WapCre;Brca1^{F/F};Trp53^{F/F};Col1a1^{invCAG-Cas9-IRES-Luc/+} (WB1P-Cas9)* mice were generated as described previously³⁰. In brief, lenti viral particles were injected intraductally into the mammary glands via the nipple of the mouse. After injection, mice were monitored for mammary tumors twice per week and sacrificed upon reaching humane end points or tumor size of 1500mm³. Organoid transplantations into the fat pad of the 4th mammary gland of syngeneic mice were performed as described previously. For activation of Myc ER-T2, tamoxifen 400-citrate pellets were used as staple chow (Envigo, TD55125).

Lentiviral vectors

The following vectors were used as described in³⁰. In brief, for Lenti-Cre-transduction, pBOB-CAG-iCRE-SD (Addgene, plasmid #12336) was used. Lenti-MycP2ACre was cloned as follows: GFP-T2A-puro was removed by AgeI and Sall digest from the SIN.LV.SF-GFP-T2A-puro⁷³ and P2ACre was inserted as AgeI-Sall fragment into the SIN.LV.SF-GFP-T2A-puro backbone. The murine *Myc* cDNA was isolated with BamHI-AgeI overhangs using standard PCR from cDNA

Clone 8861953 (Source BioScience) and inserted into the SIN.LV.SF-P2ACre vector. The Lenti-sgPten, Lenti-sgNT, Lenti-sgPten-Myc and Lenti-sgNT-Myc vectors were generated by inserting the *Myc* cDNA with XbaI-XhoI overhangs into the pGIN lentiviral vector for sgRNA overexpression. The non-targeting sgRNA (TGATTGGGGTCTCGCCCA) and sgRNA targeting mouse *Pten* exon 7 (CCTCAGCCATTGCCTGTGTG) were cloned as described⁷⁴. Sanger sequencing was used for validation of all vectors. Co-transfection of four plasmids was used to produce concentrated VSV-G pseudotyped lentivirus in 293 T-cells⁷⁵. The qPCR lentivirus titration kit from Abm (LV900) was used to determine titers.

Histology and immunohistochemistry

Tissues were formalin-fixed overnight and paraffin-embedded by routine procedures. Haematoxylin and eosin (HE) and immunohistochemical stainings were performed by standard protocols. The following primary rabbit antibodies were used for immunohistochemistry: anti-Myc (Abcam ab32072), anti-CD3 (Thermo Scientific, RM-9107), anti-F4/80 (abD serotec, MCA497) and anti-CD31 (AbCam ab28364) were used. All slides were digitally processed using the Aperio ScanScope (Aperio, Vista, CA, USA) and captured using ImageScope software version 12.0.0 (Aperio).

Human cell lines

Human breast cancer cell lines BT-549 and HCC38 were obtained from ATCC (HTB-122, CRL-2314). Breast cancer cell lines were cultured in Roswell Park Memorial Institute (RPMI) medium supplemented with 10% fetal calf serum and penicillin/streptomycin (100 units per mL). Human cell lines were cultured at 37°C in a humidified incubator with 5% CO₂.

Viral transduction

To generate dox-inducible knockdown cell lines, BT-549 and HCC38 cell lines were infected with Tet-pLKO-puro harboring short hairpin RNAs (shRNAs) as described previously²⁵. Tet-pLKO-puro was a gift from Dmitri Wiederschain (Addgene plasmid #21915). Hairpin targeting sequences that were used are: BRCA1 (5'-GAGTATGCAAACAGCTATAAT-3'), BRCA2 (5'-AACACAATTACGAACCAACT-3'), luciferase ('shLUC', 5'-AAGAGCTGTTTCTGAGGAGCC-3'). To generate overexpressing cell lines, BT-549 and HCC38 cell lines were infected with retrovirus containing pWZL-Blast-myc. pWZL-Blast-myc was a gift from William Hahn (Addgene plasmid #10674). Lentiviral and retroviral particles were produced as described previously²⁵. In brief, HEK293T packaging cells were transfected with 10 µg DNA in combination with the packaging plasmids VSV-G and ΔYPR or Gag-Pol and VSV-G complemented with pAdvantage using a standard calcium phosphate protocol. Virus-containing supernatants were harvested and filtered through a 0.45 µm syringe filter with 4 µg per mL polybrene. Supernatants were used to infect target cells in two or three consecutive 24-hour periods. Infected cells were selected in medium containing puromycin (2 µg per mL) or Blastidin (1 µg per mL) for at least 48 hours. Monoclonal cell lines were grown after single-cell sorting. Knock-down or overexpression was confirmed by immunoblotting.

Generation of cGAS knockout cells by the CRISPR/Cas9 system

Knockout of *cGAS* in human breast cancer cell lines was generated as described previously²⁵. In short, CRISPR guide RNAs were generated against *cGAS* (#1: 5'-caccgGGCATTCCGTGCGGAAGCCT-3'; #2: 5'-caccgTGAACGGATTCTTCTTTCG-3') and cloned into the Cas9 plasmids pSpCas9(BB)-2A-Puro (PX459, Addgene #62988) and pSpCas9(BB)-2A-GFP (PX458, Addgene #48138) using the AgeI and EcoRI restriction sites. BT-549 and HCC38

cells were transfected with both plasmids simultaneously (2 µg) using FuGene (Promega) according to the manufacturer's instructions. After transfection, cells were selected with puromycin (1 µg per mL) for 48 hours or single cell sorted for GFP. Single cell *CGAS*^{-/-} clones were confirmed by immunoblotting. Subsequently, *CGAS*^{-/-} or parental cells were infected with Tet-pLKO-puro shRNAs targeting BRCA1, BRCA2 or Luciferase as described before.

Western blotting

Knockdown efficiencies, overexpression and other protein expressions were analyzed by western blotting. Cultured cells were lysed in Mammalian Protein Extraction Reagent (MPER, Thermo Scientific), supplemented with protease inhibitor and phosphatase inhibitor cocktail (Thermo Scientific). Proteins were separated on SDS-polyacrylamide gels (SDS-PAGE) and transferred onto a polyvinylidene difluoride (PVDF) membrane (Millipore). Membranes were blocked in 5% milk or bovine serum albumin (BSA) in Tris-buffered saline, with 0.05% Tween-20. Immunodetection was done with antibodies directed against BRCA2 (1:1000, Calbiochem, #OP95), BRCA1 (1:1000, Cell Signaling, #9010), cGAS (1:1000, Cell Signaling, #15102), STING (1:1000, Cell Signaling, #13647), cMYC (1:200, Santa Cruz, sc40), pIRF3 (1:1000, Cell Signaling, # 29047), IRF3 (1:1000, Cell Signaling, # 4302), STAT1 (1:1000, Cell Signaling, # 9172), pSTAT1 (1:1000, Cell Signaling, # 8826) and beta-Actin (1:10.000, MP Biochemicals, #69100). Horseradish peroxidase-conjugated secondary antibodies (1:2500, DAKO) were used and visualized with chemiluminescence (Lumi-Light, Roche diagnostics) on a Bio-Rad Bioluminescence device equipped with Quantity One/Chemidoc XRS software (Bio-Rad).

5

Long-term survival and proliferation assays

BT-549 or HCC38 cells with indicated hairpins were plated in 6 wells (500 cells per well) and treated with or without doxycycline (1 µg per mL) for 10-14 days. Cells were fixed in methanol and stained with 0.1% crystal violet in H₂O. Plates were measured and quantified using an EliSpot reader (Alpha Diagnostics International) with vSpot Spectrum software. For proliferation assays, BT-549 and HCC38 cells with indicated hairpins were plated in 48 wells plates (10.000 cells per well) and cultured for up to 10 days with doxycycline (1 µg per mL). At indicated time points, plates were centrifuged (900 RPM) for 10 minutes and cells were fixed with 10% Trichloroacetic acid (TCA) in H₂O overnight at 4 degrees. Plates were washed with tap water and dried by air. Cells were stained with 0.1% Sulforhodamine B (SRB) 1% Acetic acid in H₂O for 30 minutes at room temperature and subsequently washed with 1% Acetic acid-H₂O. Bound SRB dye was dissolved by adding 10 mM Tris-H₂O to wells and OD was measured at 510nM with an iMARK microplate reader (Bio-Rad).

Quantitative RT-qPCR

Cell pellets from BT-549 and HCC38 treated with or without doxycycline (1 µg per mL) for indicated time points were harvested and stored at -20°C. RNA was isolated using the RNeasy Mini Kit (Qiagen) and complementary DNA (cDNA) was synthesized using SuperScript III (Invitrogen) according to the manufacturer's instructions. Quantitative reverse transcription-PCR (RT-PCR) for cytokine mRNA expression levels was performed in triplicate using PowerUp™ SYBR™ Green Master Mix (Thermo Scientific). Glyceraldehyde 3-phosphate dehydrogenase (GAPDH) was used as reference gene and experiments were performed on an Applied Biosystems Fast 7500 machine.

Enzyme-Linked Immuno Sorbent Assay (ELISA)

To analyze cytokines and chemokines secreted by breast cancer cells, BT-549 and HCC38 cells with indicated hairpins were treated with or without doxycycline (1 µg per mL) and plated at similar cell densities. Cell culture media was harvested at indicated time points and stored at -20. Concentrations of CCL5 (R&D Systems, DY278-05) were measured using ELISA according to manufacturer's instructions.

Cytokine and chemokine array

Proteome profiler Mouse XL Cytokine array (R&D system) was performed on whole cell lysate from WB1P and WB1P organoids at indicated time points according to manufacturer's protocol.

Immunofluorescence microscopy

Cells were grown on coverslips and treated with or without doxycycline (1 µg per mL) for indicated time points. For RAD51 foci formation, cells were irradiated with 5Gy using a CIS international/IBL 637 cesium137 source. After 3h of irradiation, cells were washed with PBS and fixed in 2% formaldehyde with 0.1% Triton X-100 in PBS for 30 min at room temperature. Cells were permeabilized in 0.5% Triton X-100 in PBS for 10 min and subsequently blocked with PBS containing 0.05% Tween-20 and 4% BSA for 1 h. For micronuclei staining, cells were fixed in 4% formaldehyde for 15 min at room temperature. Subsequently, cells were permeabilized with 0.1% Triton X-100 in PBS for 1 min followed by blocking in 0.05% Tween-20 and 2.5% BSA in PBS for 1 h. Cells were incubated overnight with primary antibodies against RAD51 (1:400, GeneTex, #gtx70230), Geminin (Cell Signaling, #9718, 1:200) or cGAS (1:200, Cell Signaling, #15102) in PBS-Tween-BSA. Cells were extensively washed and incubated for 1 h with Alexa-conjugated secondary antibodies (1:400) at room temperature in the dark. Slides were mounted with ProLong Diamond Antifade Mountant with DAPI (Thermo Scientific). Images were acquired on a Leica DM-6000RXA fluorescence microscope, equipped with Leica Application Suite software.

ChIP-seq

Duplicate samples were used for Chip-seq data generation. Organoids were cultured in a 15cm dishes. Medium was replaced by PBS containing 1% PFA and plates were left shaking for 10 min at RT. Di(N-succinimidyl) glutarate (DSG) was then added and left shaking for 25 min after which reactions were quenched with 2.5M glycine for 5 min. Organoids were then washed with ice cold PBS+protease inhibitor (Roche). ChIP and sample processing (including carriers) was then performed as described previously (<https://www.life-science-alliance.org/content/2/1/e201800115>). Five µg of cMYC antibody (Y69; Abcam) and 50 µl of magnetic protein A (10008D; Thermo Fisher Scientific) were used per IP. For ChIP-seq of tumor tissue, OCT-embedded tumors were cut in 30µm sections and processed as described⁷⁶. The prepared libraries were sequenced with 65 base single reads on Illumina Hiseq 2500. The sequencing reads were aligned to the mouse genome GRCm38 (mm10) using Burrows-Wheeler Aligner (BWA, v0.7.5a⁷⁷) with a mapping quality >20. Peak calling was performed using both MACS2 v2.1.1.20160309 (q-value threshold 0.01, extension via Phantom Peaks) and DFilter (v1.5), where only peaks were considered that were shared by the two peak callers. For each organoid and tumor dataset, the peaks from duplicate samples were merged based on the peak ranges using ChIPpeakAnno (v3.18.2;⁷⁸) and considered as the MYC binding loci. The gene closest to each marged peak was defined as MYC target based on the GRCm38 (mm10) genome annotation.

Flow cytometry

Tissues were collected in ice-cold PBS. Blood samples were collected in tubes containing heparin (Leo Pharma) and treated with red blood cell lysis buffer (155mM NH₄Cl, 12mM NaHCO₃, 0,1mM EDTA) (RBC). Tumors were mechanically chopped using a Mcllwain Tissue Chopper (Mickle Laboratory Engineering) and digested either for 1 hour at 37°C in a digestion mix of 3 mg/ml collagenase type A (Roche, 11088793001) and 25 µg/ml DNase (Invitrogen, 18068-015) or 30 min at 37°C in 100 µg/ml Liberase (Roche, 5401127001) respectively, in serum-free DMEM (Invitrogen). Reactions were terminated by addition of DMEM containing 8% FCS and cell suspensions were dispersed through a 70 µm cell strainer (BD Falcon, 352350). All single cell suspensions were treated with RBC lysis buffer to remove red blood cells. Single cell suspensions were plated in round bottom 96-wells plates (Thermo Scientific) and incubated for 30 min in the dark at 4°C with different combinations of fluorescently labeled monoclonal antibodies. 7AAD viability staining solution (eBioscience, 00-6993) was added to exclude dead cells. Flow cytometric analysis was performed on a BD LSRII using Diva Software (BD Biosciences). Data analyses were performed using FlowJo Software version 10.0 (Tree Star Inc.). The following antibody panels were used:

Myeloid panel – CD45-eFluor605NC (1:100; clone 30-F11), CD11b-eFluor650NC (1:400; clone M1/70), Ly6G-AlexaFluor700 (1:200; clone 1A8; BD Pharmingen), Ly6C-eFluor450 (1:400; clone HK1.4), F4/80-PE (1:200; clone BM8), CD49d-FITC (1:400; clone R1-2), CD3 PerCP Cy5.5, CD206-FITC (1:200), 7AAD.

Lymphoid panel – CD45-eFluor605NC (1:50; clone 30-F11), CD11b-eFluor650NC (1:400; clone M1/70), CD3-PE-Cy7 (1:200; clone 145-2C11), CD4-APC-eFluor450 (1:200; clone GK1.5), CD8-PerCP-eFluor710 (1:400; clone 53-6.7), CD49b-APC (1:400; clone DX5), CD19-eFluor780 (1:200; clone eBio1D3) 7AAD.

For flow cytometry of human cell lines, BT-549 and HCC38 cells with indicated hairpins were cultured for different time points with dox and harvested by trypsinization and fixed with Fix buffer I (BD bioscience) for 30 min. on ice. Cells were washed with 1% BSA-PBS and permeabilized with Perm Buffer III (BD bioscience) for 30 min. on ice. Samples were washed with 1% BSA-PBS and incubated (150.000 cells per sample) with pIRF3 primary antibody (1:100, Cell signaling, #29047, clone D601M) for 1 hour at 4 °C and subsequently stained with AlexaFluor488-conjugated secondary antibody (1:300) for 1 hour at RT. Samples were measured on the FACS Calibur (Becton Dickinson) and data were analyzed using FlowJo software.

Next-generation RNA sequencing

BT-549 or HCC38 cells were overexpressed for indicated oncogenes with pBABE plasmids for Figure 1. Cells harboring a BRCA2 hairpin with or without MYC overexpression were treated with dox (1 µg per mL) for 6 days for Supplementary Figure 5. Cells were harvested and frozen at -80°C. RNA was isolated using RNeasy Mini Kit (Qiagen) including DNase treatment. RNA was sent to Genomescan (Leiden, the Netherlands) for polyA-enriched mRNA sequencing using Illumina NovaSeq6000. Quality control of RNA samples consisted of fluorescent determination of sample concentration and fragment analysis. Samples were sequenced with 150 base-pair (bp) paired-end reads and generated 20 million reads per sample. RNA sequencing quality control was assessed by FastQC and Samtools Flagstat software. At least 80% of the bases had a Q-score ≥30. At least two or three biological replicates were used per cell line.

For RNA sequencing of mouse tumors, RNA was isolated from tumor pieces with the Qiagen RNA isolation kit. The mRNA library was generated using Illumina TrueSeq Stranded mRNA Library Prep Kit and sequenced with 65 base single-end reads on Illumina Hiseq 2500. The sequencing reads were aligned to the mouse genome GRCm38 (mm10) using TopHat v2.1 and the number of reads mapped to each gene were quantified using

HTSeq. DESeq2 v1.22.2 was used for read count normalization (median ratio method) and differential expression analysis. Genes with adjusted FDR<0.05 (Benjamini-Hochberg procedure) and |fold-changes|>1.5 were defined as differentially expressed genes.

Single cell RNA-sequencing

Drop sequencing according to⁷⁵ was used as described here: <http://mccarrolllab.org/dropseq/>

Transwell T cell migration assay

BT-549 and HCC38 cells with indicated hairpins were plated in 24-well plates (20,000 cells per well) and treated with dox (1 µg per mL) for 4 or 5 days. Human peripheral blood mononuclear cells (PBMCs) were isolated from peripheral blood from healthy volunteers by Ficoll-Paque density centrifugation (Ficoll-Paque PLUS, GE Healthcare Life Sciences) and enriched for CD8⁺ T cells with the MagniSort™ Human CD8⁺ T cell Enrichment Kit (#8804-6812-74, Invitrogen) according to manufacturer's instructions. Enriched CD8⁺ T cells (750,000 cells per transwell) were added on top of the filter membrane of a transwell insert (6.5 mm transwell with 3.0 µm pore, Corning) and incubated for 24 or 48 hours, after which supernatant from the lower chamber was harvested to quantify migrated T cells by microscopy.

T cell proliferation assay

BT-549 and HCC38 cells were plated in 6-well plates (20,000 per well) and treated with dox (1 µg per mL) for 5 days. T cells were harvested and enriched for CD8⁺ T cells as described for the T cell migration assay. Enriched CD8⁺ T cells were stained with CellTrace Violet (#C34557, ThermoFisher) according to manufacturer's instructions and cultured in 96-well plates (100,000 cells per well) with 200 µL conditioned medium harvested from breast cancer cells pre-treated with dox for 5 days. To activate T cells, T cells were co-cultured with Human T-Activator CD3/CD28 dynabeads (#11131D, ThermoFisher) in a bead to T cell ratio of 1:4 or 1:8. For every condition, 2 wells were cultured and combined for analysis. At day of analysis, T cells were pooled, harvested, measured on the FACSVerse (BD Biosciences) and analyzed with FlowJo software.

Organoid splenocytes co-culture

Organoids were derived from WB1P or WB1P-Myc mammary tumors as described⁴⁴. WB1P organoids were transduced with a lenti-GFP and WB1P-Myc with a lenti-mCherry lentivirus. Splenocytes were derived from FVB mouse spleen, by dissociation on a 70µM cell strainer. For the co-culture, 200,00 splenocytes and 10 organoids were plated in a 24-well plate with 50% RPMI medium, 50% ENR medium, supplemented with IL-2 (Preprotech, 300IU/ml). Live cell imaging was performed with a Zeiss AxioObserver Z1 microscope for 7 days. Organoids areas were quantified using Zen software.

TCGA data preprocessing and quality control

Genes having robust average gene expression (Hodges Lehmann estimate) lower than 20, were removed from the analysis. Differences in gene expression due to differences in cancer types were adjusted for every cancer type separately by performing the following steps for each gene: (i) robust average gene expression was obtained using Hodges Lehmann estimator; (ii) robust standard deviation of gene expressions was obtained using Hall's estimator; (iii) gene expression was normalized using the following formula: Adjusted gene expression = (gene expression – robust average)/robust standard deviation.

Differential gene expression analysis

To investigate the differential gene expression in the context of amplification of oncogenes, we retrieved DNA copy number data from The Cancer Genome Atlas (TCGA). For each of the oncogenes, the respective copy number profiles were used to classify samples as either amplified ($\log_2(\text{segment mean copy number}) > 0.3$) or neutral ($0.3 \geq \log_2(\text{segment mean copy number}) \geq -0.3$). Thereafter, Welch t-test was performed to identify genes that were differentially expressed upon amplification of each oncogene. A metric defined by $(-\log_{10}(\text{p-value}) * \text{sign}(t \text{ statistic}))$ for each Welch t-test was obtained to analyze further. The above analysis was done separately on the following sets of samples from TCGA: (i) all breast cancer samples; (ii) TNBC samples; (iii) breast cancer samples with mutation in either *BRCA1* or *BRCA2*; (iv) TNBC samples with mutation in either *BRCA1* or *BRCA2*.

Gene Set Enrichment Analysis (GSEA)

For GSEA of oncogene-expressing and control BT-549 or HCC38 cells, genes were ranked based on the $-\log P$ value between oncogene-expressing cells and control cells (pBABEL-empty). Genes enriched in oncogene-expressing cells were positive and genes enriched in control cells were negative. For GSEA of *BRCA2*-depleted cells with or without *MYC* overexpression, genes were ranked based on the $-\log P$ value between *MYC* overexpressing cells and control cells. Genes enriched in *MYC*-overexpressing cells were positive and genes in control cells were negative. Gene sets of the Hallmark collection (MSigDB) were loaded into GSEA and analyzed in both cell lines. For GSEA of *BRCA2*-depleted cells with or without *MYC* overexpression, only significantly downregulated genes ($p < 0.05$) in *MYC* overexpressing cells were loaded into GSEA software for both cell lines. GSEA was performed utilizing 3 gene set databases (Hallmark, Reactome & Gene Ontology Biological Processes) from the MSigDB.17. Gene sets containing less than 10 genes or more than 500 genes (after filtering out genes that were not present in our data sets) were excluded from further analysis. Enrichment of a gene set was tested according to the two-sample Welch's t-test for unequal variance. Welch's t-test was conducted between the set of metrics obtained from differential gene expression analysis of genes whose corresponding gene identifiers are members of the gene set under investigation and metrics of genes whose corresponding gene identifiers are not members of the gene set under investigation. To be able to compare gene sets of different sizes, Welch's t statistics were transformed to $-\log_{10}(P\text{-value})$.

GSEA of mouse mammary tumors was performed based on the Wald statistic obtained from DESeq2 differential expression analysis using the fgsea Bioconductor package v1.8.0 with 10,000 permutations. MsigDB Hallmark gene sets with minimum size of 15 and maximum size of 3000 were used for enrichment analysis.

Estimating immune cell type abundance

Immune cell type abundance was estimated using CIBERSORT. The abundance of 22 immune cell types were estimated by applying the leukocyte gene signature matrix (LM22) on the mRNA expression profiles from TCGA.

Differential immune cell type abundance analysis

Immune cell type abundance in breast cancer samples from TCGA was estimated using CIBERSORT. The abundance of 22 immune cell types were estimated by applying the leukocyte gene signature matrix (LM22) on the mRNA expression profiles from TCGA. To investigate the differential immune cell type abundance in the context of amplification of *MYC*, we used DNA copy number data from TCGA to classify samples as either *MYC*-amplified ($\log_2(\text{segment mean copy number}) > 0.3$) or neutral ($0.3 \geq \log_2(\text{segment mean copy number})$)

≥ -0.3). Thereafter, Welch t-test was performed to identify immune cell types that showed statistically significantly different abundance in MYC amplified versus neutral samples. A metric defined by $(-\log_{10}(\text{p-value}) * \text{sign}(t \text{ statistic}))$ for each Welch t-test was obtained to explore the result. The above analysis was done separately on the following set of samples from TCGA: (i) all breast cancer samples; (ii) TNBC samples.

Prediction of gene functionalities

A co-functionality network was generated with an integrative tool that predicts gene functions based on a guilt-by-association (GBA) strategy utilizing >106,000 expression profiles as described previously⁵⁵. The analyzer tool is available at <http://www.genetica-network.com>.

References

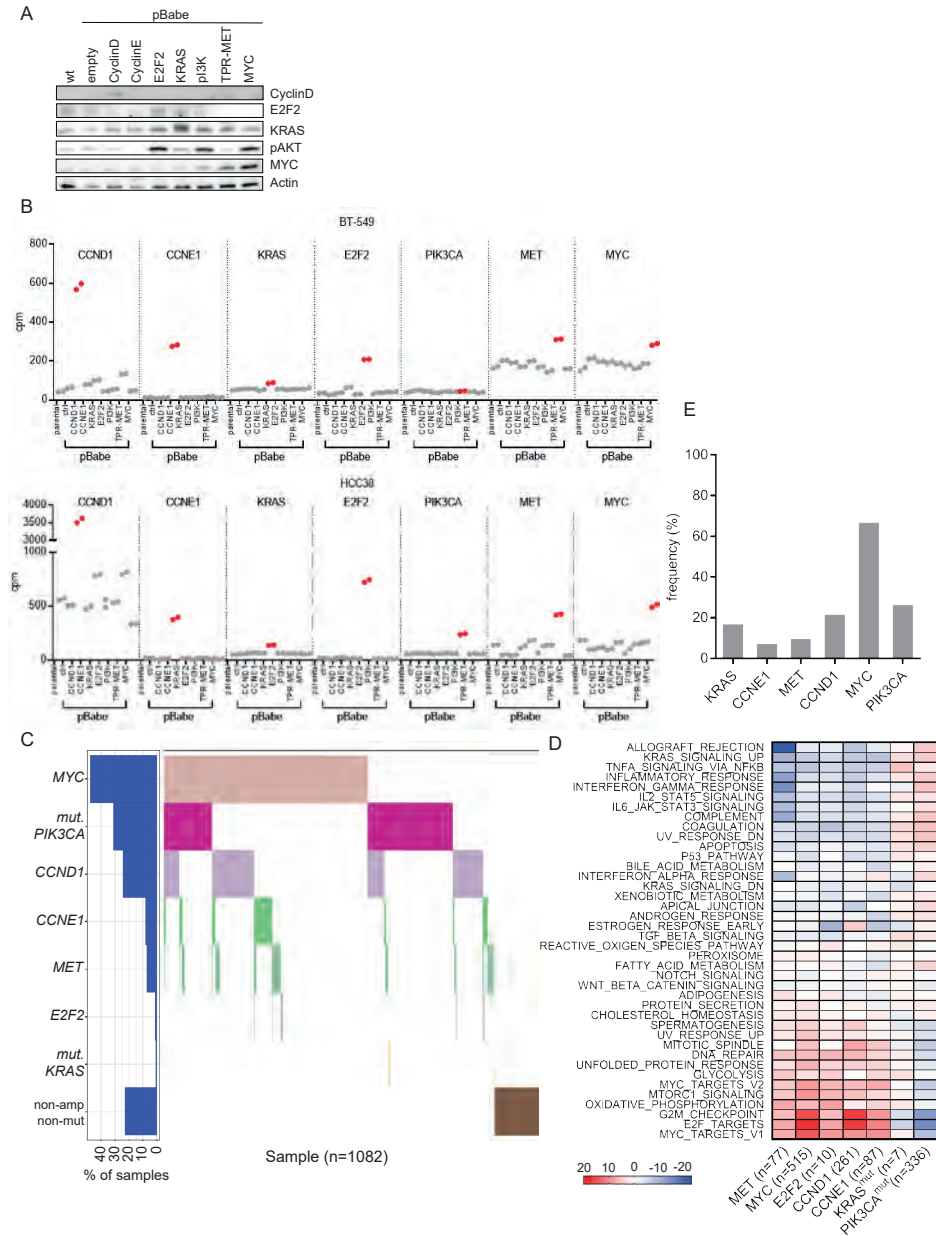
1. Bray, F. *et al.* Global cancer statistics 2018: GLOBOCAN estimates of incidence and mortality worldwide for 36 cancers in 185 countries. *CA. Cancer J. Clin.* 68, 394–424 (2018).
2. Brown, M., Tsoodikov, A., Bauer, K. R., Parise, C. A. & Caggiano, V. The role of human epidermal growth factor receptor 2 in the survival of women with estrogen and progesterone receptor-negative, invasive breast cancer: The California Cancer Registry, 1999–2004. *Cancer* 112, 737–747 (2008).
3. Dent, R. *et al.* Triple-negative breast cancer: Clinical features and patterns of recurrence. *Clin. Cancer Res.* 13, 4429–4434 (2007).
4. Carey, L. A. *et al.* The triple negative paradox: Primary tumor chemosensitivity of breast cancer subtypes. *Clin. Cancer Res.* 13, 2329–2334 (2007).
5. Haffty, B. G. *et al.* Locoregional Relapse and Distant Metastasis in Conservatively Managed Triple Negative Early-Stage Breast Cancer. *J. Clin. Oncol.* 24, 5652–5657 (2006).
6. Wiggans, R. G. *et al.* Phase-II trial of tamoxifen in advanced breast cancer. *Cancer Chemother. Pharmacol.* 3, 45–48 (1979).
7. Lehmann, B. D. *et al.* Refinement of Triple-Negative Breast Cancer Molecular Subtypes: Implications for Neoadjuvant Chemotherapy Selection. *PLoS One* 11, e0157368 (2016).
8. Gong, J., Chehrazhi-Raffle, A., Reddi, S. & Salgia, R. Development of PD-1 and PD-L1 inhibitors as a form of cancer immunotherapy: A comprehensive review of registration trials and future considerations. *Journal for ImmunoTherapy of Cancer* vol. 6 8 (2018).
9. Loi, S. *et al.* Prognostic and predictive value of tumor-infiltrating lymphocytes in a phase III randomized adjuvant breast cancer trial in node-positive breast cancer comparing the addition of docetaxel to doxorubicin with doxorubicin-based chemotherapy: BIG 02-98. *J. Clin. Oncol.* 31, 860–867 (2013).
10. Ibrahim, E. M., Al-Foheidi, M. E., Al-Mansour, M. M. & Kazkaz, G. A. The prognostic value of tumor-infiltrating lymphocytes in triple-negative breast cancer: a meta-analysis. *Breast Cancer Research and Treatment* vol. 148 467–476 (2014).
11. Adams, T. A. *et al.* Composite analysis of immunological and metabolic markers defines novel subtypes of triple negative breast cancer. *Mod. Pathol.* 31, 288–298 (2018).
12. Denkert, C. *et al.* Tumor-infiltrating lymphocytes and response to neoadjuvant chemotherapy with or without carboplatin in human epidermal growth factor receptor 2-positive and triple-negative primary breast cancers. *J. Clin. Oncol.* 33, 983–991 (2015).
13. Bense, R. D. *et al.* Relevance of Tumor-Infiltrating Immune Cell Composition and Functionality for Disease Outcome in Breast Cancer. (2016) doi:10.1093/jnci/djw192.
14. Voorwerk, L. *et al.* Immune induction strategies in metastatic triple-negative breast cancer to enhance the sensitivity to PD-1 blockade: the TONIC trial. *Nature Medicine* vol. 25 920–928 (2019).
15. Kwa, M. J. & Adams, S. Checkpoint inhibitors in triple-negative breast cancer (TNBC): Where to go from here. *Cancer* 124, 2086–2103 (2018).
16. Polk, A., Svane, I. M., Andersson, M. & Nielsen, D. Checkpoint inhibitors in breast cancer – Current

- status. *Cancer Treatment Reviews* vol. 63 122–134 (2018).
17. Schmid, P. *et al.* Atezolizumab and Nab-Paclitaxel in Advanced Triple-Negative Breast Cancer. *N. Engl. J. Med.* 379, 2108–2121 (2018).
 18. Patel, S. P. & Kurzrock, R. PD-L1 expression as a predictive biomarker in cancer immunotherapy. *Molecular Cancer Therapeutics* vol. 14 847–856 (2015).
 19. Tumeah, P. C. *et al.* PD-1 blockade induces responses by inhibiting adaptive immune resistance. *Nature* 515, 568–571 (2014).
 20. Gao, J. *et al.* Loss of IFN- γ Pathway Genes in Tumor Cells as a Mechanism of Resistance to Anti-CTLA-4 Therapy. *Cell* 167, 397–404.e9 (2016).
 21. Zaretsky, J. M. *et al.* Mutations Associated with Acquired Resistance to PD-1 Blockade in Melanoma. *N. Engl. J. Med.* 375, 819–829 (2016).
 22. Severson, T. M. *et al.* BRCA1-like signature in triple negative breast cancer: Molecular and clinical characterization reveals subgroups with therapeutic potential. *Mol. Oncol.* 9, 1528–1538 (2015).
 23. Narang, P., Chen, M., Sharma, A. A., Anderson, K. S. & Wilson, M. A. The neoepitope landscape of breast cancer: Implications for immunotherapy. *BMC Cancer* 19, 200 (2019).
 24. Parkes, E. E. *et al.* Activation of STING-Dependent Innate Immune Signaling By S-Phase-Specific DNA Damage in Breast Cancer. *J. Natl. Cancer Inst.* 109, djw199 (2017).
 25. Heijink, A. M. *et al.* BRCA2 deficiency instigates cGAS-mediated inflammatory signaling and confers sensitivity to tumor necrosis factor-alpha-mediated cytotoxicity. *Nat. Commun.* 10, 100 (2019).
 26. Chen, Q., Sun, L. & Chen, Z. J. Regulation and function of the cGAS-STING pathway of cytosolic DNA sensing. *Nat. Immunol.* 17, 1142–1149 (2016).
 27. MacKenzie, K. J. *et al.* CGAS surveillance of micronuclei links genome instability to innate immunity. *Nature* 548, 461–465 (2017).
 28. Harding, S. M. *et al.* Mitotic progression following DNA damage enables pattern recognition within micronuclei. *Nature* 548, 466–470 (2017).
 29. Weiss, J. M. *et al.* The STING agonist DMXAA triggers a cooperation between T lymphocytes and myeloid cells that leads to tumor regression. *Oncoimmunology* 6, e1346765 (2017).
 30. Annunziato, S. *et al.* Comparative oncogenomics identifies combinations of driver genes and drug targets in BRCA1-mutated breast cancer. *Nat. Commun.* 10, 1–12 (2019).
 31. Meyer, N. & Penn, L. Z. Reflecting on 25 years with MYC. *Nature Reviews Cancer* vol. 8 976–990 (2008).
 32. Kress, T. R., Sabò, A. & Amati, B. MYC: Connecting selective transcriptional control to global RNA production. *Nature Reviews Cancer* vol. 15 593–607 (2015).
 33. Alles, M. C. *et al.* Meta-Analysis and Gene Set Enrichment Relative to ER Status Reveal Elevated Activity of MYC and E2F in the “Basal” Breast Cancer Subgroup. *PLoS One* 4, e4710 (2009).
 34. Chandriani, S. *et al.* A Core MYC Gene Expression Signature Is Prominent in Basal-Like Breast Cancer but Only Partially Overlaps the Core Serum Response. *PLoS One* 4, e6693 (2009).
 35. Shen, Q. *et al.* Notch shapes the innate immunophenotype in breast cancer. *Cancer Discovery* vol. 7 1320–1335 (2017).
 36. Través, P. G., López-Fontal, R., Luque, A. & Hortalano, S. The Tumor Suppressor ARF Regulates Innate Immune Responses in Mice. *J. Immunol.* 187, 6527–6538 (2011).
 37. Buckler, J. L., Liu, X. & Turka, L. A. Regulation of T-cell responses by PTEN. *Immunol. Rev.* 224, 239–248 (2008).
 38. Liao, W. *et al.* KRAS-IRF2 Axis Drives Immune Suppression and Immune Therapy Resistance in Colorectal Cancer. *Cancer Cell* 35, 559–572.e7 (2019).
 39. Balli, D., Rech, A. J., Stanger, B. Z. & Vonderheide, R. H. Immune cytolytic activity stratifies molecular subsets of human pancreatic cancer. *Clin. Cancer Res.* 23, 3129–3138 (2017).
 40. Kortlever, R. M. *et al.* Myc Cooperates with Ras by Programming Inflammation and Immune Suppression. *Cell* 171, 1301–1315.e14 (2017).
 41. Xiao, Y. *et al.* Multi-omics profiling reveals distinct microenvironment characterization and suggests immune escape mechanisms of triple-negative breast cancer. *Clin. Cancer Res.* 25, 5002–5014 (2019).
 42. Casey, S. C. *et al.* MYC regulates the antitumor immune response through CD47 and PD-L1. *Science* (80-.). 352, 227–231 (2016).
 43. Saleiro, D. *et al.* Central Role of ULK1 in Type I Interferon Signaling. *Cell Rep.* 11, 605–617 (2015).

44. Annunziato, S. *et al.* Modeling invasive lobular breast carcinoma by CRISPR/Cas9-mediated somatic genome editing of the mammary gland. *Genes Dev.* 30, 1470–1480 (2016).
45. Duarte, A. A. *et al.* BRCA-deficient mouse mammary tumor organoids to study cancer-drug resistance. *Nat. Methods* 15, 134–140 (2018).
46. Villarino, A. V., Kanno, Y., Ferdinand, J. R. & O’Shea, J. J. Mechanisms of Jak/STAT Signaling in Immunity and Disease. *J. Immunol.* 194, 21–27 (2015).
47. Yoshihara, K. *et al.* Inferring tumour purity and stromal and immune cell admixture from expression data. *Nat. Commun.* 4, 1–11 (2013).
48. Bild, A. H. *et al.* Oncogenic pathway signatures in human cancers as a guide to targeted therapies. *Nature* 439, 353–357 (2006).
49. Ding, L. *et al.* PARP Inhibition Elicits STING-Dependent Antitumor Immunity in Brca1-Deficient Ovarian Cancer. *Cell Rep.* 25, 2972–2980.e5 (2018).
50. Dunphy, G. *et al.* Non-canonical Activation of the DNA Sensing Adaptor STING by ATM and IFI16 Mediates NF- κ B Signaling after Nuclear DNA Damage. *Mol. Cell* 71, 745–760.e5 (2018).
51. Platanitis, E. *et al.* A molecular switch from STAT2-IRF9 to ISGF3 underlies interferon-induced gene transcription. *Nat. Commun.* 10, 1–17 (2019).
52. Muhlethaler-Mottet, A., Berardino, W. Di, Otten, L. A. & Mach, B. Activation of the MHC class II transactivator CIITA by interferon- γ requires cooperative interaction between Stat1 and USF-1. *Immunity* 8, 157–166 (1998).
53. Motani, K., Ito, S. & Nagata, S. DNA-Mediated Cyclic GMP–AMP Synthase–Dependent and –Independent Regulation of Innate Immune Responses. *J. Immunol.* 194, 4914–4923 (2015).
54. Ahn, J. *et al.* Inflammation-driven carcinogenesis is mediated through STING. *Nat. Commun.* 5, 1–9 (2014).
55. Bhattacharya, A. *et al.* Transcriptional effects of copy number alterations in a large set of human cancers. *Nat. Commun.* 11, (2020).
56. Turner, N., Tutt, A. & Ashworth, A. Hallmarks of ‘BRCAness’ in sporadic cancers. *Nature Reviews Cancer* vol. 4 814–819 (2004).
57. Solinas, C. *et al.* BRCA gene mutations do not shape the extent and organization of tumor infiltrating lymphocytes in triple negative breast cancer. *Cancer Lett.* 450, 88–97 (2019).
58. Woo, S.-R., Corrales, L. & Gajewski, T. F. Innate Immune Recognition of Cancer. *Annu. Rev. Immunol.* 33, 445–474 (2015).
59. Kraya, A. A. *et al.* Genomic signatures predict the immunogenicity of BRCA-deficient breast cancer. *Clin. Cancer Res.* 25, 4363–4374 (2019).
60. Nanda, R. *et al.* Pembrolizumab in patients with advanced triple-negative breast cancer: Phase Ib keynote-012 study. *J. Clin. Oncol.* 34, 2460–2467 (2016).
61. Adams, S. *et al.* Pembrolizumab monotherapy for previously untreated, PD-L1-positive, metastatic triple-negative breast cancer: Cohort B of the phase II KEYNOTE-086 study. *Ann. Oncol.* 30, 405–411 (2019).
62. Layer, J. P. *et al.* Amplification of N-Myc is associated with a T-cell-poor microenvironment in metastatic neuroblastoma restraining interferon pathway activity and chemokine expression. *Oncoimmunology* 6, (2017).
63. Li, T. *et al.* Antitumor Activity of cGAMP via Stimulation of cGAS-cGAMP-STING-IRF3 Mediated Innate Immune Response. *Sci. Rep.* 6, 1–14 (2016).
64. Iurescia, S., Fioretti, D. & Rinaldi, M. Targeting cytosolic nucleic acid-sensing pathways for cancer immunotherapies. *Frontiers in Immunology* vol. 9 711 (2018).
65. Muthalagu, N. *et al.* Repression of the Type I Interferon pathway underlies MYC & KRAS-dependent evasion of NK & B cells in Pancreatic Ductal Adenocarcinoma. *Cancer Discov.* CD-19-0620 (2020) doi:10.1158/2159-8290.cd-19-0620.
66. Sodikin, N. M. *et al.* MYC Instructs and Maintains Pancreatic Adenocarcinoma Phenotype. *Cancer Discov.* 10, 588–607 (2020).
67. Kortlever, R. M. *et al.* Myc Cooperates with Ras by Programming Inflammation and Immune Suppression. *Cell* 171, 1301–1315.e14 (2017).
68. Deng, L. *et al.* STING-dependent cytosolic DNA sensing promotes radiation-induced type I interferon-dependent antitumor immunity in immunogenic tumors. *Immunity* 41, 843–852 (2014).
69. Demaria, O. *et al.* STING activation of tumor endothelial cells initiates spontaneous and therapeutic

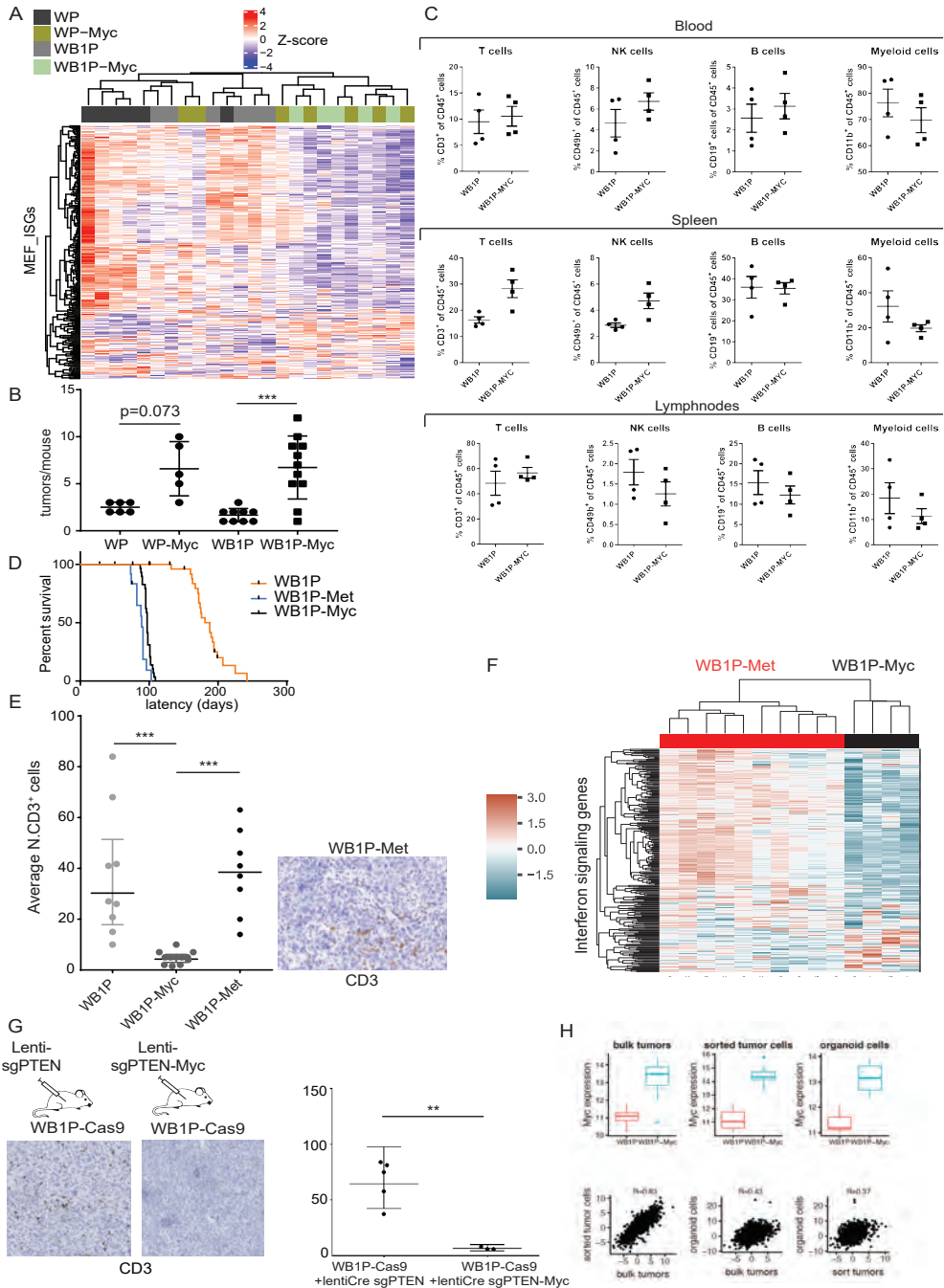
- antitumor immunity. *Proc. Natl. Acad. Sci. U. S. A.* 112, 15408–15413 (2015).
70. Ramanjulu, J. M. *et al.* Design of amidobenzimidazole STING receptor agonists with systemic activity. *Nature* 564, 439–443 (2018).
 71. Benci, J. L. *et al.* Tumor Interferon Signaling Regulates a Multigenic Resistance Program to Immune Checkpoint Blockade. *Cell* 167, 1540–1554.e12 (2016).
 72. Jacquelot, N. *et al.* Sustained Type I interferon signaling as a mechanism of resistance to PD-1 blockade. *Cell Res.* 29, 846–861 (2019).
 73. Kas, S. M. *et al.* Insertional mutagenesis identifies drivers of a novel oncogenic pathway in invasive lobular breast carcinoma. *Nat. Genet.* 49, 1219–1230 (2017).
 74. Sanjana, N. E., Shalem, O. & Zhang, F. Improved vectors and genome-wide libraries for CRISPR screening. *Nature Methods* vol. 11 783–784 (2014).
 75. Follenzi, A., Ailles, L. E., Bakovic, S., Geuna, M. & Naldini, L. Gene transfer by lentiviral vectors is limited by nuclear translocation and rescued by HIV-1 pol sequences. *Nat. Genet.* 25, 217–222 (2000).
 76. Singh, A. A. *et al.* Optimized ChIP-seq method facilitates transcription factor profiling in human tumors. *Life Sci. Alliance* 2, (2019).
 77. Li, H. & Durbin, R. Fast and accurate short read alignment with Burrows-Wheeler transform. 25, 1754–1760 (2009).
 78. Zhu, L. J. *et al.* ChIPpeakAnno: A Bioconductor package to annotate ChIP-seq and ChIP-chip data. *BMC Bioinformatics* 11, 237 (2010).
 79. Ishikawa, H., Ma, Z. & Barber, G. N. STING regulates intracellular DNA-mediated, type I interferon-dependent innate immunity. *Nature* 461, 788–792 (2009).
 80. Grandvaux, N. *et al.* Transcriptional Profiling of Interferon Regulatory Factor 3 Target Genes: Direct Involvement in the Regulation of Interferon-Stimulated Genes. *J. Virol.* 76, 5532–5539 (2002).

Supplementary Figures



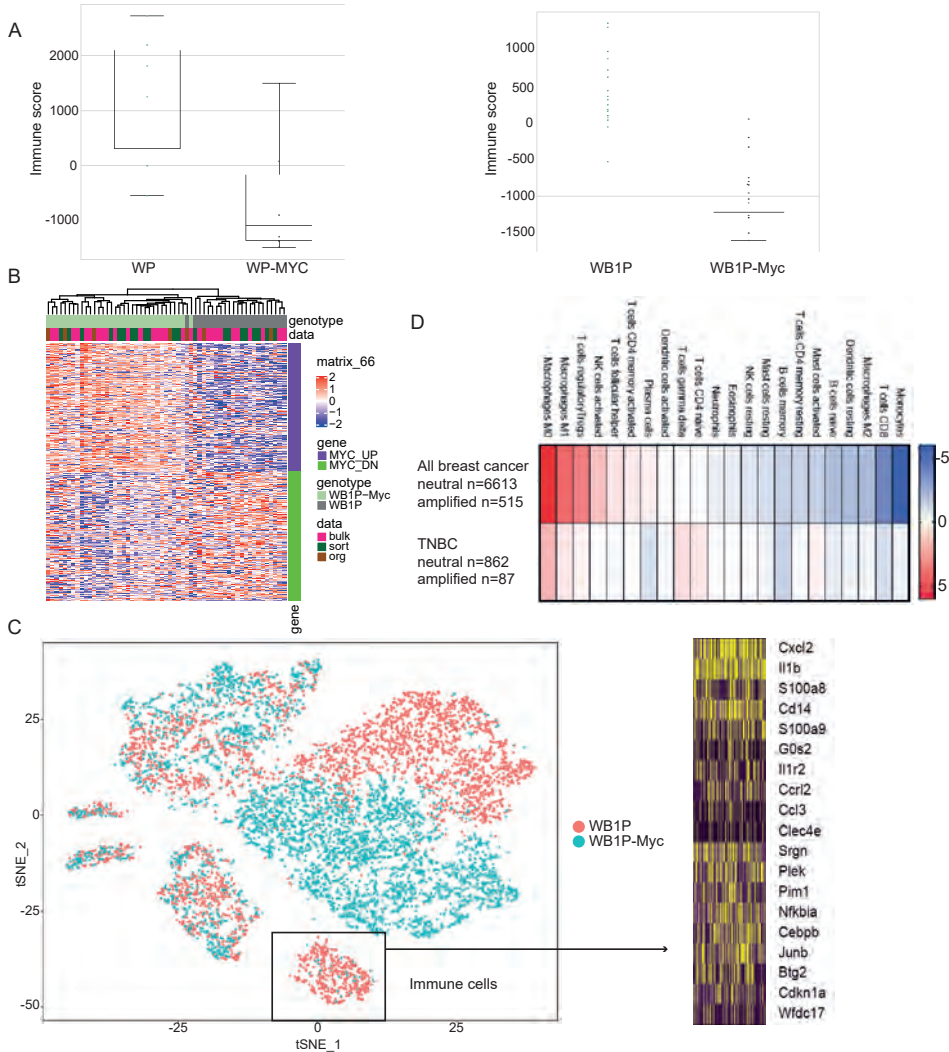
5

Supplementary Figure 1. Oncogene amplification in breast cancer. A) BT-549 cells were overexpressed for oncogenes with pBABE vectors. Cells were immunoblotted for CyclinD, CyclinE, E2F2, KRAS, pAKT, MYC and Actin. **B)** Normalized counts per million of oncogenes in RNA sequencing data of BT-549 and HCC38 cells with pBABE-vectors overexpressing different oncogenes. Red dots represent counts of the oncogene listed above in cells expressing the corresponding pBABE vector. Both biological replicates are plotted per cell line. **C)** Distribution plot of all breast cancer samples used for GSEA analysis from TCGA data. In total, 1028 breast cancer samples were included in the analyses. Individual samples are plotted on the x-axis. **D)** GSEA analysis of breast cancer samples (n=1082). Top 20 up (red) and down (blue) regulated hallmark genesets are plotted in amplified vs neutral samples for specific oncogenes. Number of amplified samples per oncogene is shown. Values plotted are Z-transformed p values.

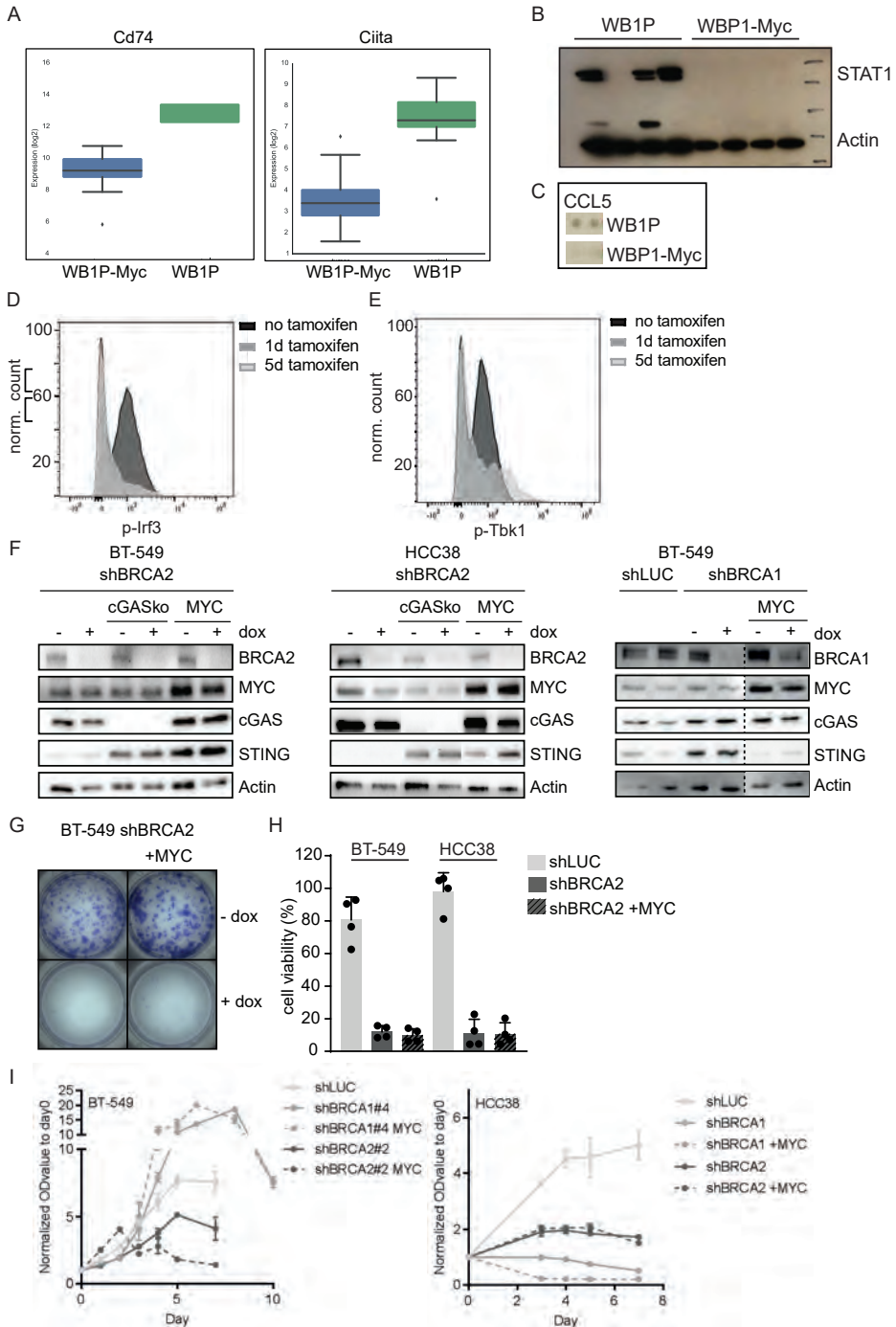


Supplementary Figure 2. MYC activation alters tumor immunity in WB1P mice. A) Heatmap of RNA seq comparing WB1P-Myc, WB1P, WP-Myc and WP tumors. Genes involved in interferon signaling are plotted. **B)** Tumor burden in WP mice ($n=6$) vs WP-Myc ($n=5$), and WB1P ($n=9$) vs WB1P-Myc mice ($n=11$). P values were calculated using unpaired t-test. **C)** Flow cytometric analysis of CD3+, CD49b+, CD19+, CD11b+ in blood, spleen and lymph nodes of WB1P and WB1P-MYC mice. **D)** Latency analysis of WB1P, WB1P-Met, and WB1P-Myc tumors. **E)** Representative histogram of CD3 immunostaining in WB1P-Met tumor. CD3+ cell counts are quantified for WB1P vs WB1P-Myc

vs WB1P-Met tumors. *P* values were calculated using unpaired *t*-test. **F)** Heatmap of RNA-seq of WB1P-Myc vs WB1P-Met tumors. An interferon signature of 336 genes was used. **G)** Representative images of CD3 staining for tumors induced by intraductal injections of guides against *Pten* with and without *Myc* overexpression. Counts of CD3⁺ cells in defined areas are plotted (right). **H)** Upper panels: *Myc* expression in bulk tumors, sorted tumor cells and organoids cells. Lower panels: linear regression analysis between bulk tumors, sorted tumor cells and organoids cells.

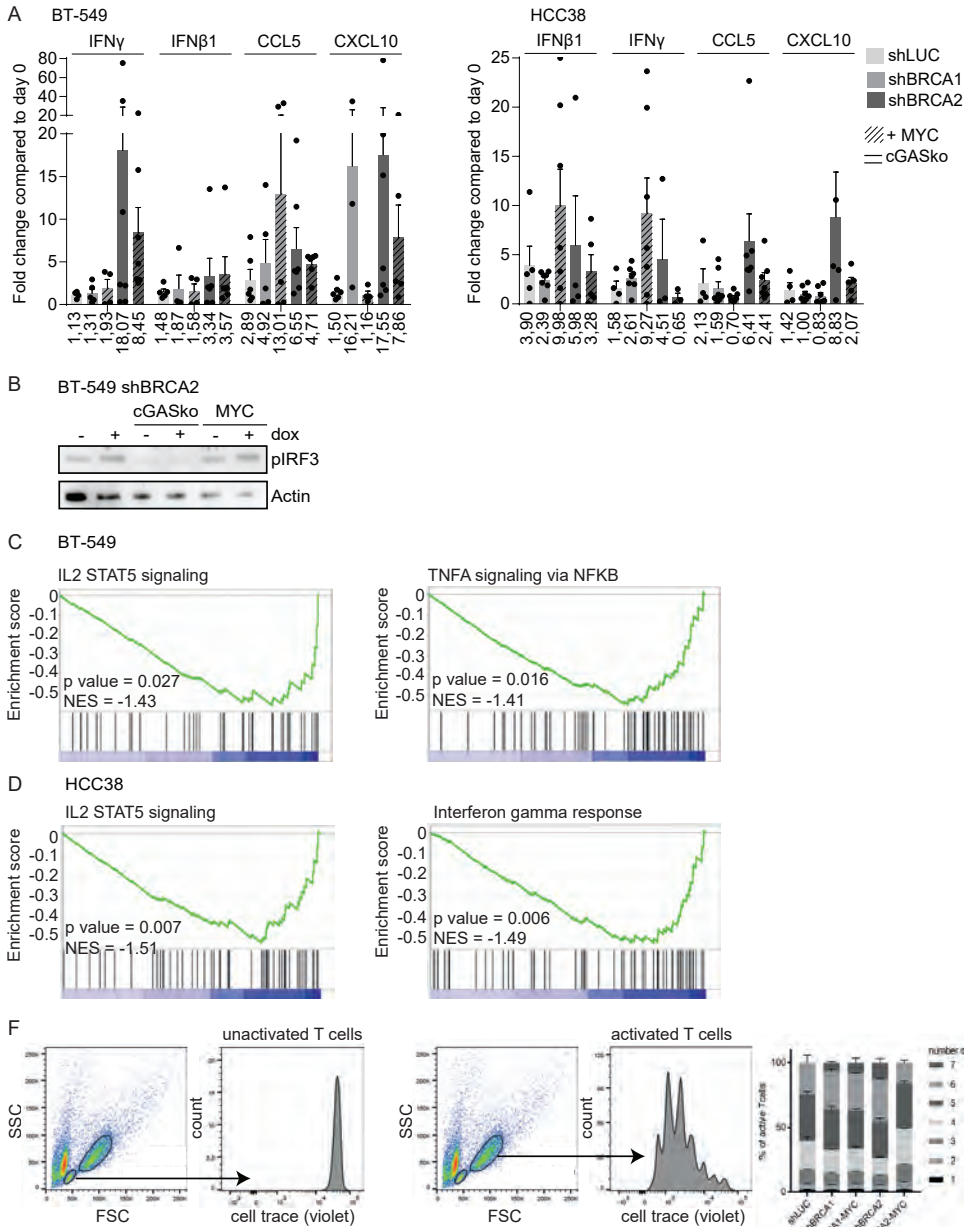


Supplementary Figure 3. MYC activation alters tumor immunity in WB1P mice. A) ESTIMATE deconvolution and immune-score obtained from WP and WP-Myc as well as WB1P and WB1P-Myc RNAseq, showing significantly higher immune-score in WP and WB1P tumors. **B)** Heatmap showing the expression of differentially expressed genes in our experiment using mouse samples in comparison to a published geneset of up- respectively downregulated genes upon *Myc* overexpression. **C)** t-SNE analysis from drop sequencing of one WB1P and one WB1P-Myc tumor (left) and heatmap (right) of the immune cell populations, showing higher number of immune cells in the WB1P tumor. **D)** Distribution of immune cell-type fractions in all breast cancer samples and TNBC only from TCGA were estimated with CIBERSORT analysis. Samples with amplified *Myc* (0.3 cut-off) were compared to samples with neutral *Myc* levels. Fractions of each immune cell type were compared with a Welch's *t*-test. $-\log_{10}(pvalue) \cdot \text{sign}(t \text{ statistic})$ for each immune cell type are plotted. Color indicates a lower (blue) or higher (red) immune cell-type fraction in breast cancer samples with amplified *Myc* compared to neutral *Myc* samples.



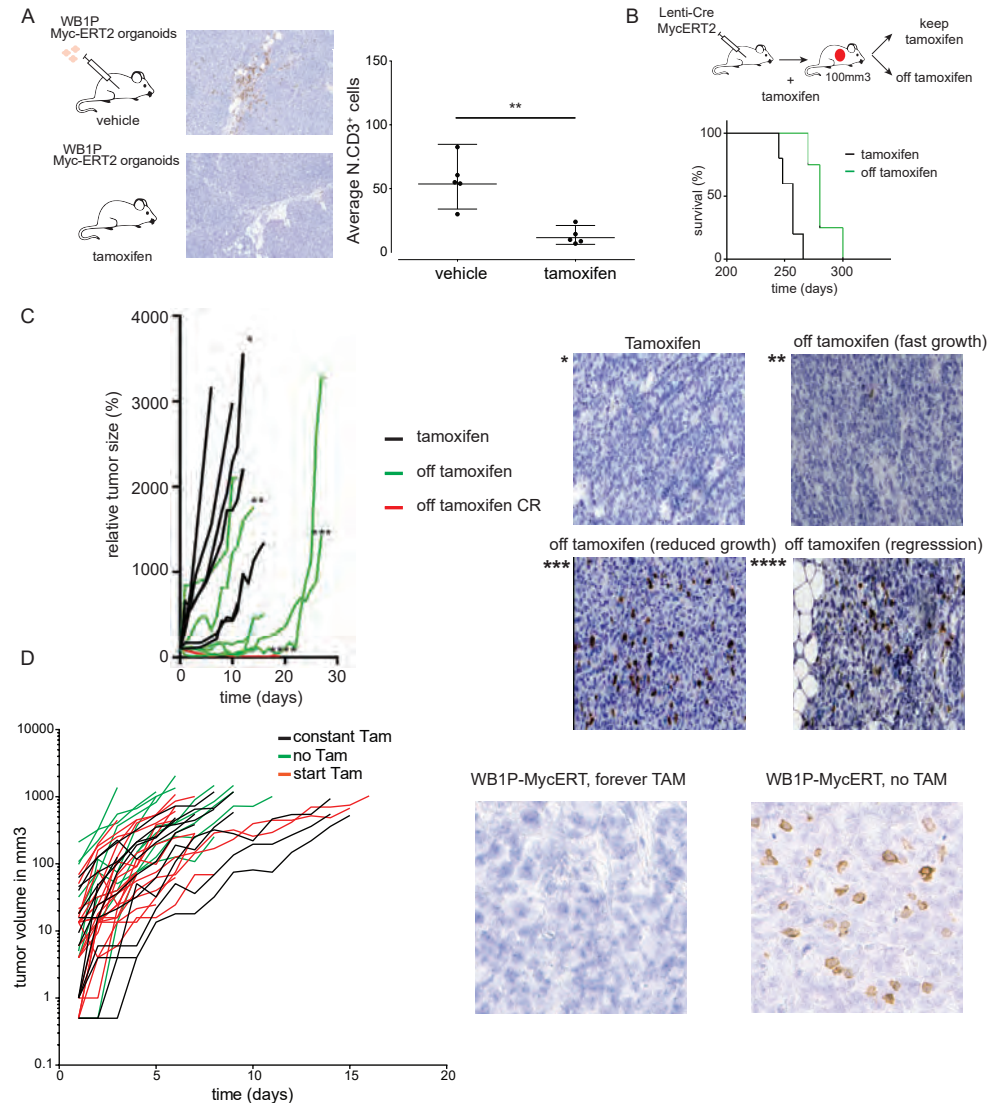
Supplementary Figure 4. Interferon signaling in murine organoids, tumors and human cell line models upon MYC overexpression. A) Boxplots showing downregulation of Cd74 and Ciita in WB1P and WB1P-Myc tumors. **B)** Cytokine array for CCL5 in WB1P and WB1P-Myc organoids. **C)** Representative image of flow cytometry analysis of p-IRF3 expression in WB1P-MycERT2 organoids with 1 day tamoxifen (dark grey), 5 days tamoxifen (light grey) and without (black). **D)** Flow cytometry analysis of

p-IRF3 in WB1P-MycERT2 organoids without Tamoxifen (black), after 1 day with Tamoxifen (dark grey) and after 5 days of Tamoxifen treatment (light grey). **E)** Flow cytometry analysis of *p-TBK1* in WB1P-MycERT2 organoids without Tamoxifen (black), after 1 day with Tamoxifen (dark grey) and after 5 days of Tamoxifen treatment (light grey). **F)** BT-549 and HCC38 cells with indicated hairpins were depleted for BRCA1 or BRCA2, knocked out for *cGAS* or overexpressed for MYC. Cells were treated with or without dox for three days prior to cell lysis, and immunoblotted for BRCA1, BRCA2, MYC, *cGAS*, *STING* and Actin. **G)** Representative image of long-term survival assay in BT-549. BT-549 cells harboring *shBRCA2* with or without WZL-MYC were plated in 6-well plates and treated with or without dox. Cells were fixed after 10-14 days and stained with crystal violet. **H)** Quantification of long-term survival assay as described in A. BT-549 and HCC38 cells were plated in 6 wells with indicated hairpins with or without MYC overexpression and treated with dox. Cells were fixed and stained after 10-14 days. Percentage of cell survival was calculated by normalizing measurements to wells without doxycycline treatment. **I)** Cell proliferation of BT-549 and HCC38 cells was analyzed with SRB assays. Equal numbers of cells were plated in 48 wells plates and treated with doxycycline for several days. At indicated time points, cells were fixed and stained with SRB dye. OD values of dissolved SRB dye were normalized to OD value at day 0 of the same cell line.



Supplementary Figure 5. Interferon signaling in human TNBC human cell lines upon MYC overexpression. A) BT-549 and HCC38 cells with indicated hairpins, depleted for cGAS or overexpressed for MYC were treated with or without dox (1 μ g per mL) for 6 days. RNA of cells was isolated and qRT-PCR was performed to analyze expression of IFN- γ , IFN- β 1, CCL5 and CXCL10. GAPDH was used as reference gene. Fold changes were calculated with untreated conditions of each cell line. Mean fold changes are indicated underneath each condition. Error bars indicate SEM of at least three independent experiments with three technical replicates each. **B)** BT-549 cells with indicated shBRCA2 hairpin, depleted for cGAS or overexpressed for MYC were treated with or without dox for 5 days. Phosphorylation status of IRF3 was analyzed by immunoblotting. **C)** BT-549 shBRCA2 cells with or without MYC overexpression were treated for 5 days with dox and RNAseq was performed. GSEA analysis with hallmark genesets was

performed on significantly downregulated genes in MYC overexpressed cells compared to BRCA2-depleted cells only. Means from three biological replicates per cell line were used for RNA seq analysis. Enrichment scores of two examples are shown. **D)** HCC38 shBRCA2 cells were treated and analyzed as described in C. GSEA analysis with hallmark genesets was performed on significantly downregulated genes in MYC overexpressed cells compared to BRCA2-depleted cells only. Means from three biological replicates per cell line were used for RNA seq analysis. Enrichment scores of two examples are shown. **E)** Representative images of gating strategies from (un)activated T cells co-cultured with supernatant harvested from BT-549 or HCC38 cells. The activation of T cells was confirmed by their proliferation resulting in dilution of the violet celltrace marker per cell division as shown in the most right panel.

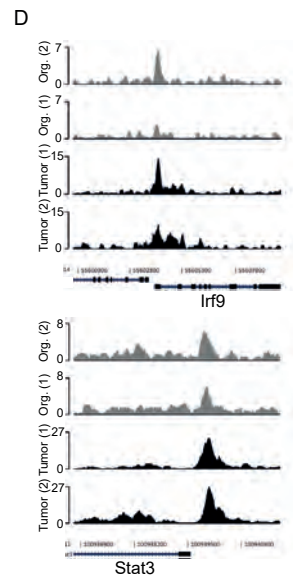
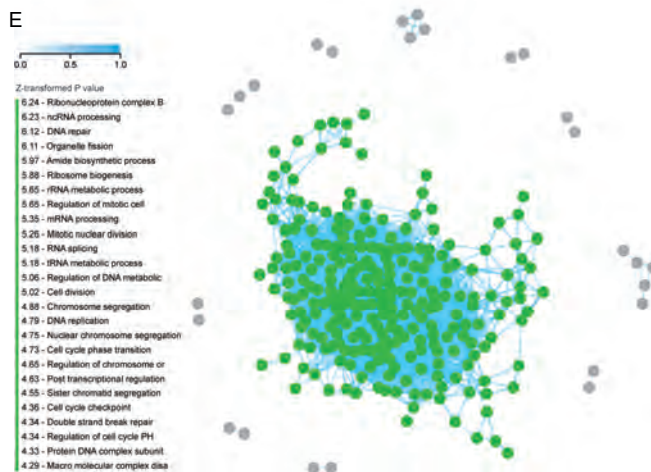
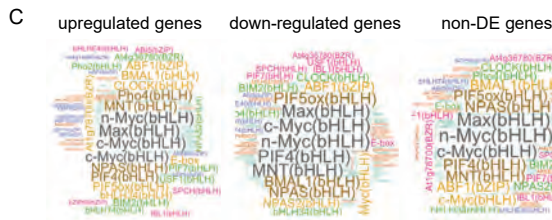
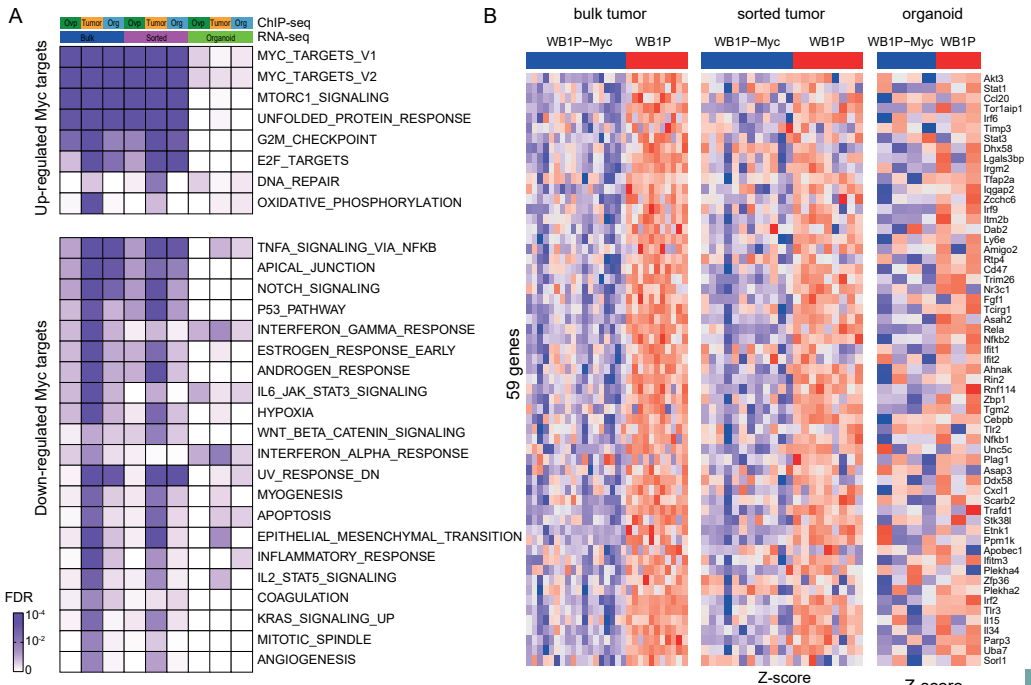


Supplementary Figure 6. Inducing MYC in existing tumors leads to expulsion of immune infiltrate.

A) WB1P organoids with a MycERT2 vector are orthotopically transplanted into mammary glands. Transplanted mice are treated with vehicle or Tamoxifen and resulting tumors assessed for CD3⁺ cell infiltration (IHC, CD3 in brown), quantification in right panel, n=5 mice/group, 5 windows/tumor counted, unpaired t-test, p=0.001. **B)** Kaplan-Meier curves of LentiCreMycERT2 injected mice with

and without Tamoxifen. **C**) Relative tumor growth (left) of intraductally injected WB1P mice with Lenti-Cre MycERT2. Tamoxifen administration and immunostaining for CD3 (right) in selected mice with (*) showing that concomitant MYC de-activation and slower tumor progression is paired with loss of infiltrating lymphocytes and complete tumor regression (CR) in one of the mice. **D**) Growth curves of WB1P-MycERT2 tumors with (black), without (green) and with Tamoxifen from tumor size of 3x3 mm (red). Representative micrographs of CD3 IHC in tumors with and without Tamoxifen are shown (right).

Supplementary Figure 7. Integration of ChIP and RNA seq of murine tumors and organoids. **A**) Gene ontology analysis of differentially expressed genes in WB1P vs WB1P-Myc tumors, sorted epithelial tumor cells and organoids overlapped with MYC ChIP-seq peaks. **B**) Heat maps of the 59 differentially expressed genes with a peak called in tumor and/or organoid ChIP-seq. **C**) JASPAR binding site analysis of the sequences bound by MYC in the ChIP-seq in up-regulated, down-regulated and not transcriptionally affected genes. **D**) ChIP seq tracks of IRF9 and STAT3, two examples of genes with peaks in the promoter region in both tumor and organoid samples. **E**) Constructed co-functionality network of genes upregulated by MYC (n=430) retrieved from overlapping MYC-ChIP-seq peaks with RNA sequencing data of WB1P and WB1P-Myc tumors and organoids. Genes share strong predicted co-functionality ($r > 0.5$) within network that was enriched with genes predicted to be involved in e.g. DNA repair and RNA processing.



Therapeutic targeting and patient selection for cancers with homologous recombination defects

Francien Talens¹, Mathilde Jalving¹, Jourik A. Gietema¹ & Marcel A.T.M. van Vugt¹

¹Department of Medical Oncology, University Medical Center Groningen, University of Groningen, Groningen, The Netherlands.

Expert opinion on drug discovery (2017) 12(6):565-581

Abstract

Introduction: DNA double-strand breaks (DSBs) are toxic DNA lesions that can be repaired by nonhomologous end-joining (NHEJ) or homologous recombination (HR). Mutations in HR genes elicit a predisposition to cancer; yet, they also result in increased sensitivity to certain DNA damaging agents and poly (ADP-ribose) polymerase (PARP) inhibitors. To optimally implement PARP inhibitor treatment, patients with HR-deficient tumors must be adequately selected.

Areas covered: Herein, the authors describe the HR pathway mechanistically and review the treatment of HR-deficient cancers, with a specific focus on PARP inhibition for BRCA1/2-mutated breast and ovarian cancer. In addition, mechanisms of acquired PARP inhibitor resistance are discussed. Furthermore, combination therapies with PARP inhibitors are reviewed, in the context of both HR-deficient and HR-proficient tumors, and methods for proper patient selection are also discussed.

Expert opinion: Currently, only patients with germline or somatic BRCA1/2 mutations are eligible for PARP inhibitor treatment and only a proportion of patients respond. Patients with HR-deficient tumors caused by other (epi)genetic events may also benefit from PARP inhibitor treatment. Ideally, the selection of eligible patients for PARP inhibitor treatment includes a functional HR read-out, in which cancer cells are interrogated for their ability to perform HR repair and maintain replication fork stability.

1. Introduction

DNA continuously encounters multiple different DNA lesions from endogenous sources (e.g. radical species as byproducts from cellular metabolism) as well as exogenous sources (e.g. ultraviolet radiation and pharmaceutical agents). To preserve genomic stability, cells are equipped with a tightly regulated signaling network that detects and repairs DNA lesions, collectively called the 'DNA damage response' (DDR)¹. To facilitate DNA repair, the DDR activates cell cycle checkpoints to arrest ongoing cell cycle progression. Furthermore, if the number of DNA lesions exceeds the amount that can be managed by the DDR, cells will be cleared from the proliferative compartment by programmed cell death through apoptosis or induction of senescence.

The response to DNA damage is not a linear pathway, and its activation does not lead to fixed phenotypic outcomes. Rather, the DDR consists of multiple parallel pathways that display extensive feedback and cross talk. DDR signaling has a widespread influence on cellular homeostasis, as underscored by the observation that the upstream DDR kinases ATM and ATR phosphorylate >700 substrates in various pathways in response to DNA damage². Conversely, DDR pathways receive input from multiple cellular cues, including pro-survival and pro-death signals, which ultimately influence cell fate decisions to promote cell survival or cell death in response to DNA damage.

Genetic defects in DNA repair pathway components or cell cycle checkpoints are associated with a range of clinical phenotypes, including neurodegeneration and cancer predisposition¹. These observations illustrate the relevance and complexity of genome maintenance pathways. Interestingly, research over the last decades has demonstrated that cancer-associated DNA repair defects not only lie at the basis of tumor development but also give rise to vulnerabilities that can be exploited therapeutically.

1.1 Induction of double-strand breaks

DNA double-strand breaks (DSBs) are potentially highly toxic DNA lesions. DSBs can arise as a consequence of multiple mechanisms. First, DSBs are induced under physiological circumstances during maturation of B- and T-cells during V(D)J recombination, the mechanism that randomly assembles DNA segments to generate diversity in immunoglobulins and T-cell

receptors³. Specifically, RAG-1 and RAG-2 introduce DSBs that are randomly joined together to shuffle genomic areas and create sequence variation⁴. Second, DSBs arise non-physiologically. Most aberrant DSBs appear to be associated with replication. These breaks can result from unrepaired DNA single-strand breaks (SSBs) that are converted into DSBs during replication. Alternatively, nucleotide depletion, interstrand DNA cross-links, or collisions between the replication and transcription machinery may stall replication forks, which as a result thereof can collapse and lead to single-ended DSBs⁵. Notably, many anticancer therapeutics, including platinum-containing agents and topoisomerase inhibitors, exert their cytostatic effects through interfering with DNA replication and thus cause DSBs. Of note, other anticancer treatments (e.g. irradiation or chemotherapeutic agents such as bleomycin) also cause DSBs in nonreplicating cells, by directly assaulting DNA.

1.2. Repair of DNA DSBs

Repair of DSBs is governed by two fundamentally different pathways: non-homologous end-joining (NHEJ) and homologous recombination (HR). DSBs are repaired by either of these pathways, and the choice between these types of DSB repair depends largely on the cell cycle phase, although additional factors such as chromatin context appear to play a role⁶.

1.2.1. Non-homologous end-joining

Classical NHEJ is a very efficient DNA repair pathway that acts throughout the cell cycle and directly ligates DNA ends⁷. NHEJ is present in both eukaryotes and prokaryotes and operates through a largely conserved pathway⁸. In mammalian cells, most DSBs are repaired by NHEJ, since this repair type is active throughout interphase. An important characteristic of NHEJ is that it can ligate breaks with different chemical ends. In the process of NHEJ, DSBs are recognized and bound by Ku70–Ku80 heterodimers, which activate the DNA–PKcs kinase (**Figure 1A**, right panel). Subsequently, the XRCC4:DNA ligase-IV complex is recruited, together with nucleases and polymerases, to complete DNA-end joining⁹. NHEJ works in a sequence-independent fashion and, since DNA ends may have been damaged and require processing prior to ligation, NHEJ is error-prone and can induce mutations¹⁰. In contrast to classical NHEJ, alternative NHEJ (alt-NHEJ) involves different players and creates deletions at the repair junction¹¹.

1.2.2. Homologous recombination

In contrast to NHEJ, HR uses a DNA template to repair DSBs, for which the sister chromatid is usually employed. The use of a template makes HR conservative when it comes to DNA sequence and remarkably error-free when compared to NHEJ¹². Of note, single-strand annealing, an independent DNA repair pathway, also requires extensive homology but results in annealing of homologous single-strand DNA ends, which induces deletions¹³. The requirement of a template restricts HR to S and G2 phases of the cell cycle when DNA replication has occurred (**Figure 1B**)¹⁴. Although a genome-wide template for HR becomes available upon DNA replication, only a subset of DSBs is repaired by HR in S/G2. The mechanisms that underlie the usage of HR versus NHEJ in S/G2 cells remain largely unclear, although chromatin composition appears to influence the choice of repair type⁶. In contrast, repair of replication fork-associated DSBs is completely dependent on HR, since these DSBs are single-ended and therefore require template-mediated resolution.

HR is a complex pathway and involves many components (**Figure 1A**, middle panel). DSBs are recognized by the MRN complex, which consists of MRE11, RAD50, and NBS1. The MRN complex tethers DNA ends and promotes activation and recruitment of ATM to sites of DSBs. Reciprocally, ATM phosphorylates and activates all members of the MRN complex^{15,16}. A critical step in the commitment to repair DSB through HR is the formation of ssDNA overhangs at the sites of DNA ends. This process, called DNA-end resection, is initiated by the MRN complex in conjunction with CtIP and BRCA1¹⁷ (**Figure 1A**). MRE11, as part of the MRN complex, has

endonuclease activity and can initiate DNA-end resection in 5' to 3' direction and starts ≈200–300 nucleotides away from the DSB site¹⁸. In doing so, the MRN complex creates relatively short ssDNA overhang at DSB sites, which function as an entry site for the EXO1 and DNA2 helicase/exonuclease enzymes that generate extensive ssDNA stretches^{19,20}. Following end resection, the ssDNA is coated with replication protein A (RPA) protein complexes to stabilize ssDNA structures. In parallel, BRCA2 is recruited in a BRCA1- and PALB2-dependent fashion to ultimately recruit RAD51 to the ssDNA overhangs. RAD51 replaces RPA and forms nucleoprotein filaments on the ssDNA, which will invade the homolog sister chromatid to search for sequence homology and initiate strand exchange²¹. Multiple additional factors are involved in controlling HR. For instance, five paralogs of RAD51 exist (i.e. RAD51B, RAD51C, RAD51D, XRCC2, and XRCC3) that appear to support HR. All RAD51 paralogs are essential genes, as deletion of these genes in mice results in embryonic lethality²². The recruitment of RAD51 to DSBs is dependent on RAD51 paralogs as well as on RAD52, deficiency of which aggravates the phenotype of BRCA1, BRCA2, or PALB2 deletion²³. In this context, the RAD51C paralog appears to play the most prominent role. Mechanistically, it was shown to delay the progression of the cell cycle during DNA damage by promoting CHK2 phosphorylation during initiation of DDR signaling²⁴. Conversely, the HR component RAD54, a protein of the SWI2/SNF2 complex, has ATPase activity which requires the presence of dsDNA²⁵. RAD54 interacts with RAD51 to stabilize RAD51 filaments and is involved in strand invasion and, eventually, the formation of Holliday junctions²⁶.

As described above, the loading of RAD51 onto ssDNA is a key step in completing DSB repair by HR. It has been shown that TOPBP1, in conjunction with PLK1, is required for phosphorylation and loading of RAD51. In line with these findings, a siRNA screen identified TOPBP1 as being synthetically lethal with olaparib, which was explained by impaired RAD51 foci formation upon TOPBP1 depletion²⁷.

Cells that are deficient in HR, for example, due to loss of BRCA1/2, are dependent on alternative pathways to repair DSBs. This includes classical or alternative NHEJ. Indeed, error-prone NHEJ was shown to generate increased genomic instability when HR is defective²⁸. The alt-NHEJ pathway requires DNA polymerase θ (Pol θ), which prevents RAD51 loading onto ssDNA²⁹. When compared to other NHEJ polymerases, Pol θ was shown to preferably bind a 5'-terminal phosphate and use the opposite overhang to anneal DNA strands and therefore produce highly mutagenic DNA junctions³⁰.

1.3. Balancing between HR and NHEJ

DNA-end resection is a point-of-no-return and marks the ultimate decision to repair DSBs through HR (**Figure 1A**). This switch is governed in large part by cell cycle-dependent phosphorylation of CtIP by cyclin-dependent kinases (CDKs), which promotes endonuclease activity of MRE11 within the MRN complex to initiate DNA-end resection^{17,31}. CtIP is predominantly recruited to DSBs during S and G2, in complex with BRCA1³². Since the activity of CDKs increases when DNA recombination commences, this mechanism ensures the restriction of DNA end-resection to cell cycle phases where template DNA is available. The switch between HR and NHEJ is also regulated by additional mechanisms. Specifically, DNA-end resection is negatively regulated by 53BP1 and RIF1, which are both substrates of ATM. RIF1 binds to 53BP1 and ultimately promotes NHEJ³³. 53BP1 interferes with BRCA1 function and thereby prevents DNA-end resection whereas, conversely, BRCA1 promotes dephosphorylation of 53BP1 to stimulate DNA-end resection³⁴. In recent years, multiple other factors have been identified that regulate DNA-end resection and thereby control HR initiation and poly (ADP-ribose) polymerase (PARP) inhibitor sensitivity. For example, REV7 is recruited to sites of DSBs in a 53BP1-dependent fashion and blocks DNA-end resection^{35,36}. Also, the DNA helicase HELB and the demethylase JMJD1C affect chromatin responses to DNA breaks and ensuing DNA-end resection and thereby control RAD51 recruitment to sites of DNA breaks^{37,38}. Finally,

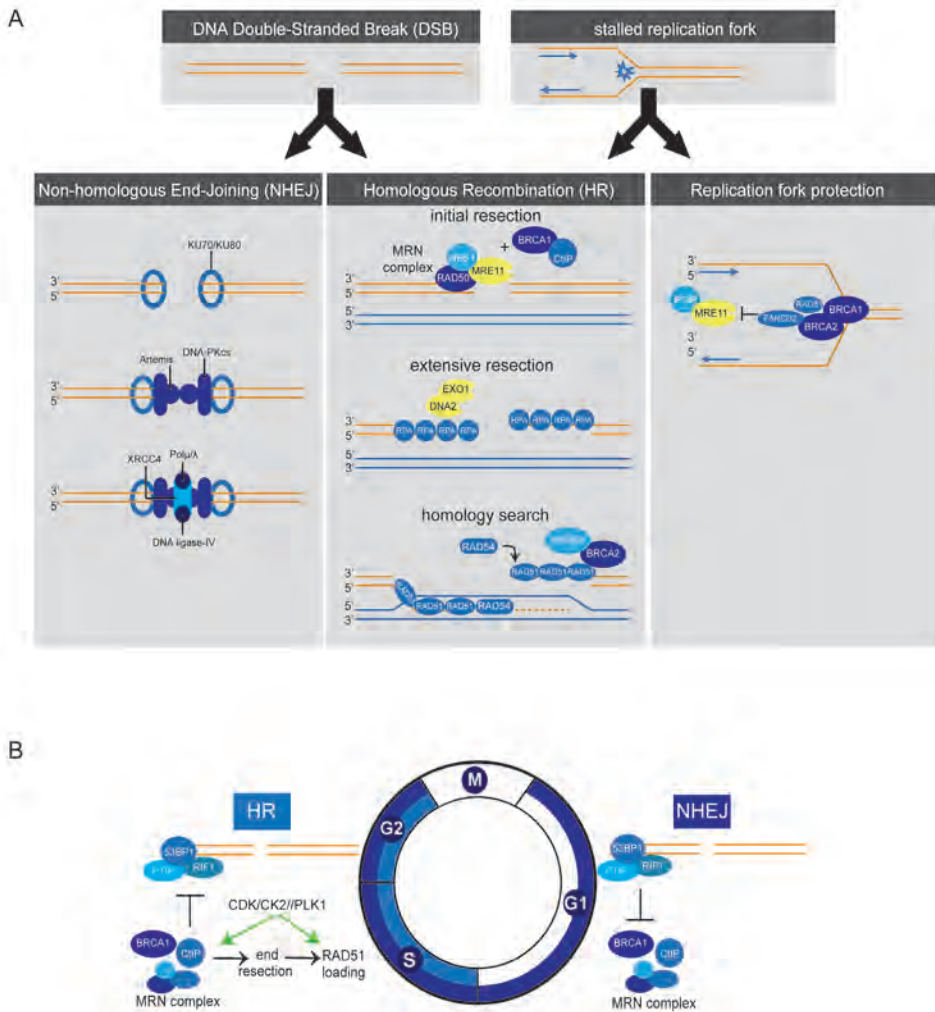


Figure 1. A) Schematic representation of double-strand break repair and protection of stalled replication forks. **Left panel:** For repair of DSBs by NHEJ, breaks are recognized and bound by Ku70-Ku80 heterodimers which activate DNA-PKcs. XRCC4, DNA ligase-IV, and polymerases (μ/λ) are recruited to complete DNA end joining. **Middle panel:** During HR repair, DSBs are recognized by the MRN complex, which initiates DNA-end resection in conjunction with CtIP and BRCA1. EXO1 and DNA2 generate extensive ssDNA stretches, which are coated with RPA. In a PALB2-dependent fashion, BRCA2 is recruited, which loads RAD51 onto the ssDNA to invade the sister chromatid and to find sequence homology. **Right panel:** In response to stalled replication forks, BRCA1, BRCA2, FANCD2, and RAD51 protect nascent DNA for MRE11-dependent degradation. **B)** Cell cycle-dependent switch between HR and NHEJ. HR only occurs in the S and G2 phases of the cell cycle. The switch between HR and NHEJ depends on the activity of S-phase CDKs, which phosphorylate CtIP to activate the MRN complex and stimulate DNA-end resection. DNA-end resection is negatively regulated by 53BP1 and RIF1, which thereby promote NHEJ. Other cell cycle kinases also control HR, including Plk1 and CK2 which control RAD51 recruitment.

53BP1 recruitment was shown to be regulated by ring finger protein 168 (RNF168), an altered abundance of which induced toxic NHEJ, genomic instability, and differential sensitivity towards PARP inhibitors³⁹. Exactly how the opposing effects of CtIP/BRCA1 and 53BP1/RIF1/REV7/HELB/JMJD1C operate at the molecular level remain incompletely clear. It has been shown, however, that the repositioning of 53BP1 and end-resection activity depend on ubiquitin ligase activity of BRCA1 together with BARD1 and the subsequent chromatin remodeling by SMARCD1⁴⁰.

Also, other cell cycle regulators have been shown to impact on DSB repair. For example, RAD51 is phosphorylated by polo-like kinase-1 (Plk1) and casein kinase-2 (CK2), which is followed by binding to the MRN component NBS1, which facilitate recruitment to DNA breaks⁴². Although not all molecular mechanisms have been elucidated and novel regulators will likely be identified, it is becoming increasingly clear that the switch between HR and NHEJ not only requires CDK activity but involves multiple stimulatory and inhibitory factors of DNA-end resection and homology search.

1.4. Replication fork stability

Independent of their role in the repair of DSBs, HR proteins such as BRCA2 and RAD51 paralogs are involved in the protection of stalled replication forks, thereby preventing chromosomal instability (**Figure 1A**, right panel). BRCA2, as well as BRCA1 and FANCD2, prevents degradation of nascent DNA at stalled replication forks by stabilizing RAD51 filaments. This pathway is independent of the role of BRCA1/2 in loading RAD51 onto ssDNA during HR^{42,43}. In line with these findings, Somyajit et al. showed that complexes of RAD51 paralogs bind to nascent DNA at stalled replication forks to prevent the formation of DSBs by protecting forks against MRE11 activity⁴⁴. The capacity to stabilize stalled replication forks appears very relevant in the context of PARP inhibition. Specifically, trapping of PARP enzymes onto DNA was shown to stall replication forks⁴⁵, and PARP trapping lies at the basis of PARP inhibitor-induced cytotoxicity⁴⁶. Conversely, the degree to which cells can maintain replication fork stability was reported to determine PARP inhibitor sensitivity⁴⁷.

2. HR-deficient cancers

2.1. HR gene mutations

Germline BRCA1/2 mutations are predominantly linked to the development of breast and ovarian cancer, but they are also associated with an elevated risk for other cancer types, including pancreatic, prostate, and endometrial cancer⁵³⁻⁵⁵. Tumor onset in BRCA1/2 mutation carriers invariably involves loss of the remaining wild-type (wt) allele through somatic inactivation or loss-of-heterozygosity (LOH) and results in tumor cells that are HR defective⁵⁶. Besides mutation, epigenetic silencing of HR genes has also been shown to underpin defective HR in tumors. Specifically, the BRCA1 promoter is frequently hypermethylated in breast and ovarian cancer^{57,58}.

Importantly, not only germline BRCA1/2 mutations underlie HR deficiency in tumors, but somatic BRCA1/2 mutations have also been described⁵⁹. Also, mutations in other HR genes, such as PALB2^{60,61}, RAD51 paralogs⁶², or ATM⁶³, predispose to cancer development and may result in HR-defective tumors. In a cohort of patients with uterine serous carcinoma, different germline HR genes were found to be mutated⁶⁴. Furthermore, HR genes were shown to be mutated in lung, breast, intestinal, and skin cancer⁶⁵. Also, mutations in the cell cycle checkpoint gene CHEK2 were identified in breast cancer patients without a BRCA1/2 mutation (5.1%) when compared to healthy controls (1.1%)^{66,67}. CHK2 is involved in BRCA1 phosphorylation upon DNA damage and has been implicated in controlling HR^{68,69}. Whether the impact of the commonly occurring CHEK2 1100delC variant is strong enough to impact on HR repair and has therapeutic consequences needs to be established.

2.2. BRCA1/2 mutations in breast and ovarian cancer

Mutations in BRCA1 result in a ~65% lifetime risk for breast cancer development by the age of 70 years and a ~30–40% lifetime risk for ovarian cancer. For BRCA2 mutation carriers, the lifetime risk for breast cancer is around 50% at age 70 and ~10–15% for ovarian cancer⁷⁰⁻⁷². The risk of cancer development depends on multiple factors, including the exact position of the mutation for both genes. Furthermore, somatic mutations in other genes such as TP53⁷³ or PTEN⁷⁴ were suggested to influence BRCA1/2-related carcinogenesis.

Most breast cancers caused by BRCA1 mutations are ‘triple-negative’ breast cancers (TNBCs), which entails that they do not overexpress the estrogen receptor (ER), progesterone receptor, or the human epidermal growth factor receptor-2. TNBCs are characterized by aggressive growth and very limited targeted treatment options. In contrast, BRCA2-mutant breast cancers are mainly low-grade ER+ luminal tumors, which grow more slowly, and inhibition of signaling through the ER is one of the treatment options^{75,76}.

Ovarian tumors arising in BRCA1/2 mutation carriers are mainly high-grade serous carcinomas (HGSOCs)⁷⁷. Notably, when RNA expression profiles were examined, high levels of similarity were observed between BRCA1/2-related and non-BRCA1/2-related HGSOC, indicating that this subgroup is characterized by a high degree of genomic instability⁷⁵. Importantly, these observations suggest that inactivation of DNA repair is a common feature of serous ovarian cancer tumorigenesis. Indeed, genomic analysis by The Cancer Genome Atlas suggests that around half of HGSOCs are HR deficient, based on mutations in BRCA1/2 or mutations in other HR genes such as RAD51, ATM, CHEK2, PALB2, and MRE11⁷⁸.

2.3. Tumorigenesis and HR deficiency

BRCA1/2 genes have a tumor-suppressive function; heterozygous germline mutations in BRCA1 or BRCA2 predispose to cancer, in which cancer cells have lost the remaining wt allele and are fully HR defective. In apparent contradiction with this notion, HR deficiency caused by homozygous genetic inactivation of *Brca1*^{79,80}, *Brca2*^{81,82}, or *Rad51*^{82,83} causes early embryonic lethality in vivo, showing that HR is required for cell survival and development. The requirement for BRCA1 and BRCA2 extends beyond development since *Brca1* or *Brca2* knock-out mouse embryonic fibroblasts and blastocysts also display compromised viability in vitro^{80,84}. Apparently, tumor cells that arise due to defective HR have developed mechanisms to cope with increased genomic instability. How these tumor cells survive and proliferate in the absence of HR is incompletely understood and was coined the ‘BRCA paradox’⁸⁵.

The enhanced rate of genomic aberrations induced by HR deficiency allows the accumulation of multiple secondary mutations, which support the survival of HR-deficient cells. Indeed, loss of HR leads to DNA damage accumulation and instigates a DDR, including transcriptional activation of p53⁸⁶, suggesting that the p53 signaling axis may preclude the survival of HR-deficient cells. The observation that tumorigenesis in a *Brca1* conditional mouse model was significantly accelerated by introducing a *Tp53*^{-/-} mutation underscores the important role of p53 in BRCA1/2-associated tumors⁸⁷. Furthermore, a conditional mouse model with a CK14-driven Cre-mediated somatic loss of *Brca1* and *Tp53* resulted in a high incidence of mammary tumors that resemble human basal-like BRCA1 breast cancer⁸⁸. These data are in line with the human situation, in which TP53 is mutated in ~66% of BRCA1/2-related breast tumors⁸⁹. Combined, these observations explain the early embryonic death upon BRCA1/2 loss and show that HR-deficient cells cannot survive without a concomitant mutation in other genes, such as TP53. Interestingly, co-mutation of *Tp53* only partially rescued the viability of cell cultures and mice lacking *Brca1/2*⁹⁰. This suggests that other factors exist that promote BRCA1/2-related tumorigenesis and lead to the survival of BRCA1/2-deficient tumor cells.

3. Therapeutic targeting of HR-deficient cancers

HR deficiency drives tumorigenesis but simultaneously provides an Achilles' heel that can be exploited therapeutically. The absence of HR components is often correlated with improved therapeutic outcome¹. HR-deficient tumors are generally more sensitive to DNA damage that requires HR for repair, including platinum-induced DNA replication lesions.

3.1. Cross-linking agents and effectiveness

Different compounds can induce inter- or intra-strand cross-links (ICLs) which interfere with DNA replication. These drugs, including platinum-containing cytostatics, are widely used in various treatment settings for numerous cancer types including ovarian cancer. ICLs prevent separation of the DNA strands during replication and transcription and thus lead to stalled replication forks and stalled transcription⁹¹. Besides template-based repair of DSBs, HR is also involved in the protection and restart of stalled replication forks and repair of ICLs (**Figure 1A**, right panel). This latter process is initiated by components of the Fanconi anemia (FA) pathway, which consists of multiple FA genes⁹². Significant overlap exists between the components that function in HR and the FA pathways, including BRCA2 (FANCD1)⁹³ and BRCA1 (FANC-S)⁹⁴. Germline mutations in FA genes lead to the FA syndrome, a very rare inherited disease. These patients are often diagnosed with cancer at an early age due to increased chromosomal instability⁹⁵. Of note, and in line with the repair function of FA genes, this syndrome is characterized by increased sensitivity to ICLs.

In epithelial ovarian carcinoma, both somatic and germline mutations in BRCA1 and BRCA2 are positively correlated with response to platinum-based treatment. A total of 14.9% of patients with a BRCA1/2 mutation had progressive disease within 6 months after primary treatment with platinum-based chemotherapy compared to 31.7% of patients with BRCA1/2 wt tumors⁹⁶. Also, BRCA1/2 deficiency (either through mutation or loss of expression) is associated with improved progression-free survival (PFS) after platinum-based chemotherapy in serous ovarian cancer⁹⁷. Regardless of mutational status, decreased expression of BRCA1 was also positively correlated with response to cisplatin plus paclitaxel treatment⁹⁸. The increased response to chemotherapy in BRCA1/2-deficient ovarian cancers may underlie the fact that patients with germline BRCA1/2-mutated tumors have a better outcome in general (improved response rates and overall survival)⁹⁹.

Whereas standard treatment of HGSOE is based on surgery and primary platinum-based chemotherapy, TNBCs in the past years were not consistently treated with platinum-based chemotherapy. A significant proportion of TNBCs are HR deficient, e.g. through BRCA1/2 mutations, and BRCA1/2-associated breast tumors have common characteristics with TNBCs in general¹⁰⁰. Rottenberg et al. have shown that spontaneous mammary mouse tumors induced by combined Brca1 and Tp53 inactivation resembled human BRCA1-associated breast cancer in humans¹⁰¹. These Brca1^{-/-}; Tp53^{-/-} mouse tumors responded very well to cisplatin therapy and did not acquire resistance after five relapses, even though tumors were not completely eradicated¹⁰¹. In a study with 190 TNBC patients, both the BRCA1/2 (16%) and the non-BRCA1/2-mutant tumors responded well to neo-adjuvant combination therapy of carboplatin and docetaxel with pathologic complete responses in 59% and 56% of the cases, respectively¹⁰².

Low BRCA1 mRNA expression was found to be associated with increased cisplatin sensitivity in patients with TNBC¹⁰³. Finally, stage III breast cancer patients with a tumor of which the genomic pattern resembled BRCA1/2-mutated breast cancers and was thus classified as BRCA-like showed improved overall survival after high-dose platinum-containing chemotherapy (cyclophosphamide–thiotepa–carboplatin) compared to conventional 5-fluorouracil–epirubicin–cyclophosphamide (FE90C) therapy in a randomized controlled trial¹⁰⁴. These combined results have resulted in platinum-containing agents being increasingly included in standard chemotherapy regimens of TNBCs.

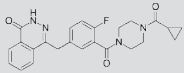
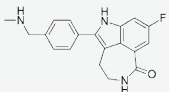
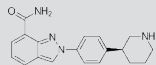
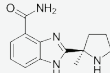
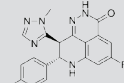
PARP inhibitor	trade name	status	structure	Ki	relative trapping capacity
olaparib/AZD-2281	Lynparza	2014: FDA/EMA approved		PARP1: 5 nM PARP2: 1 nM	+++
rucaparib/AG-014699	Rubraca	2016: FDA approved		PARP1: 1.4 nM	+++
niraparib/MK-4827	Zejula	2017: FDA approved		PARP1: 3.2 nM PARP2: 4.0 nM	++++
veliparib/ABT-888		2016: FDA Orphan Drug Designation		PARP1: 5.2 nM PARP2: 2.9 nM	+
talazoparib/BMN-673		phase 3 testing		PARP1: 1.2 nM PARP2: 0.9 nM	+++++

Figure 2. Overview of PARP inhibitors in clinical development. For each PARP inhibitor, various characteristics are indicated, including trade name, status in clinical development, chemical structure, dissociation constant (Ki) reflecting PARP1 catalytic inhibition, and capacity to trap PARP onto DNA.

3.2. PARP inhibition

Based on the principle of synthetic lethality, new molecularly targeted therapeutic strategies have been developed for HR-deficient tumors, which interfere with remaining DNA repair pathways in the tumor^{105,106}. PARP is an enzyme involved in base-excision repair (BER) which is used to repair SSBs¹⁰⁷. The first PARP inhibitor was developed in 1980 and was initially used to sensitize tumors to chemotherapy¹⁰⁸. In 2005, two seminal studies showed that BRCA1/2-mutated tumor cells were extremely sensitive to PARP inhibition, in contrast to BRCA1/2 heterozygote or wt cells due to synthetic lethality^{109,110}. The developed small-molecule PARP inhibitors (KU0058684 and KU0058948) formed the basis for the first FDA-approved PARP inhibitor olaparib (AZD-2281, trade name: Lynparza, AstraZeneca Rubraca, Clovis Oncology Zejula, Tesaro)^{111,112}. Very recently, two other PARP inhibitors were FDA approved, namely rucaparib (AG-014699, trade name: Rubraca) and niraparib (MK-4827, trade name: Zejula)¹¹³ (**Figure 2**).

3.2.1. Mechanisms of PARP inhibitor-induced cell death in HR-deficient tumor cells

Inhibition of the PARP enzyme results in insufficient repair and ensuring the accumulation of SSBs, which are converted into DSBs during replication. Normal cells in BRCA1/2 mutation carriers still have a remaining BRCA1/2 allele and are therefore HR proficient. These cells can effectively repair DSBs and are only marginally affected by PARP inhibition. In contrast, tumor cells in which the remaining BRCA1/2 allele is lost are HR deficient and unable to effectively repair the DSBs induced by PARP inhibition and will ultimately undergo cell death. For this reason, the tumor specificity of PARP inhibitors is favorable when compared to traditional chemotherapeutic agents which target all dividing cells. Nevertheless, the adverse side effects of PARP inhibition have been reported^{114,115}.

Recently, additional mechanisms of PARP inhibitor-induced cell death have been described. Besides interfering with SSB repair through inhibition of BER, PARP inhibitors can also trap the PARP enzyme onto the DNA to form protein:DNA complexes. These complexes behave like DNA inter-strand cross-links that interfere with DNA replication and require repair by the Fanconi pathway and HR machinery^{46,116}. Again, for this mechanism to effectively induce cell death, lack of HR is required.

These studies also explain the observations that PARP inhibitors are most effective when PARP itself is abundantly present and that chemical PARP inhibition is more effective than removing PARP genetically⁴⁵. Many different PARP inhibitors have been described, all of which inactivates the PARP enzyme catalytically to a high degree (**Figure 2**). However, these inhibitors differ in their capability to trap PARP onto DNA (**Figure 2**). Notably, the cytotoxicity of the different PARP inhibitors is related to their trapping potential¹¹⁷. Currently, the PARP inhibitor with the highest trapping activity used in clinical studies is talazoparib (BMN-673), and this agent also has the highest single agent toxicity. The PARP trapping ability of talazoparib is a 100-fold higher than that of olaparib^{116,118}.

Of note, PARP1 was also shown to interact with NHEJ components. Specifically, PARP1 can bind to the NHEJ proteins Ku70/80 and DNA-PKcs and competes with Ku80 for the repair of DSBs through an alternative NHEJ pathway^{119,120}. In line with these observations, Patel et al. demonstrated that PARP inhibition leads to phosphorylation of DNA-PK substrates, thereby enhancing NHEJ activity in BRCA2-deficient cells¹²¹. In the same study, inhibition of NHEJ through knockdown of Ku80 could increase the cell survival of BRCA2-deficient cells to PARP inhibition, suggesting that NHEJ repair of PARP inhibitor-induced DNA lesions contributes to the toxicity of PARP inhibitors. In line with this notion, inhibition of DNA-PK decreased the sensitivity of ATM- and BRCA1-deficient cancer cells to PARP inhibition¹²¹.

3.2.2. PARP inhibition in the clinic

In a phase I trial, only BRCA1/2 mutation carriers (n = 22) with different tumor types, including ovarian, breast, and prostate cancer, showed antitumor activity in response to olaparib monotherapy (63%) compared to non-mutation carriers¹¹². In the same study, adverse effects of olaparib monotherapy were observed that were mainly categorized as grade 1 or 2 and were, in general, less severe than those of classical chemotherapy. The observed presence of grade 3 adverse effects, such as myelosuppression and anemia, might be explained by long cancer history or pretreatment with chemotherapy regimens and be manageable by dose reduction or treatment interruption¹²².

A phase II trial included HGSOC patients who had received two or more platinum-based chemotherapy regimens and had a platinum-sensitive relapse¹²³. Patients were randomly assigned to olaparib monotherapy (n = 136) or placebo (n = 129), and PFS was significantly longer in the olaparib-treated group (median: 8.4 months) compared to patients treated with placebo (median: 4.8 months)¹²³. Most clinical trials with olaparib concern combination therapies with chemotherapeutic agents. For instance, in a randomized phase II trial, it was shown that olaparib combined with carboplatin and paclitaxel followed by olaparib monotherapy improves PFS in recurrent, platinum-sensitive HGSOC patients (median: 12.2 versus 9.6 months in chemotherapy alone), especially in patients with a BRCA1/2 mutation (hazard ratio (HR): 0.21)¹²⁴. Maintenance monotherapy with olaparib significantly prolonged PFS versus placebo in patients with platinum-sensitive recurrent serous ovarian cancer, especially in patients with a BRCA1/2 mutation¹²⁵. Maintenance olaparib monotherapy in patients with BRCA1/2-mutated breast, ovarian, or fallopian tube tumors (n = 21) after combination chemotherapy with carboplatin and paclitaxel was well tolerated¹²⁶ and has been approved by the European Medicines Agency (EMA) for this indication. In advanced, heavily pretreated, platinum-resistant

ovarian cancer patients (n = 193), of whom 80% had germline BRCA1/2 mutations, olaparib monotherapy resulted in an objective response rate of 34%¹²⁷, and this trial resulted in the FDA approval in this setting. Furthermore, in a multicenter phase II trial, heavily pretreated patients with a germline BRCA1/2 mutation (n = 298) were treated with olaparib monotherapy. This resulted in stable disease up to 8 weeks in 42% of the patients and an overall tumor response rate of 31.1%¹²². Although olaparib showed responses as monotherapy, especially in BRCA1/2-mutant tumors, various studies have suggested that combination therapies are required to improve response rates¹²⁸, likely at the cost of increased toxicity. In this context, numerous studies are ongoing.

3.2.3. Increasing the sensitivity for PARP inhibition

PARP inhibition is selectively cytotoxic in HR-deficient tumors. An approach to extend PARP eligibility to other HR-proficient tumors is to therapeutically induce temporary defects in HR. For instance, it was shown that HR is suppressed in multiple cancer cell lines under hypoxic conditions through the downregulation of RAD51¹²⁹. Also, inhibition of vascular endothelial growth factor receptor 3 (VEGFR3) resulted in decreased expression of BRCA1 and BRCA2 in ovarian cancer cells¹³⁰. These data suggest that inhibiting angiogenesis can be used to enforce HR deficiency and improve responses to PARP inhibition. Indeed, when olaparib was combined with cediranib, a drug that targets the VEGFRs, improved PFS was observed in patients with platinum-sensitive recurrent ovarian, fallopian tube, or peritoneal tumors¹³¹. Adverse effects of this combination therapy, however, were also increased when compared to olaparib treatment alone. Nevertheless, these adverse effects do not prevent current ongoing clinical trials.

Another family of enzymes involved in maintaining HR is phosphoinositide 3-kinases (PI3Ks), which are activated upon receptor signaling and have distinct functions in signal transduction pathways¹³². The isoform PI3K β is found to be important for DSB sensing as it regulates recruitment of NBS1, a subunit of the MRN complex, to sites of DNA breaks¹³³. In line with these observations, Juvekar et al. showed that the PI3K and mitogen-activated protein kinase pathway were activated in a Brca1-mutated breast cancer mouse model, as judged by increased AKT and ERK phosphorylation¹³⁴. Conversely, PI3K class I inhibition using BKM-120 led to increased DNA damage and in combination with olaparib delayed *in vivo* tumor growth¹³⁴. Subsequently, PI3K inhibition in patients with BKM120 resulted in increased DNA damage in tumors, decreased levels of BRCA1 and BRCA2, and increased sensitivity of TNBCs to olaparib, even in tumors without a BRCA1/2 mutation¹³⁵. This combination may be valuable in other tumor types, as it also showed synergistic effects in human prostate cancer cell lines and Pten/Tp53-mutated mouse prostate tumors¹³⁶. Currently, an ongoing clinical trial combines BKM-120 with olaparib in TNBC and HGSOC patients (NCT01623349).

Another class of kinases that is essential for HR is CDKs. HR is strictly cell cycle-regulated, which is governed by S and G2 CDKs, as explained above. In line with this notion, inhibition of CDK1 activity was shown to impair HR and to sensitize otherwise HR-proficient tumor cell lines for PARP inhibition¹³⁷. Furthermore, inhibition of multiple CDKs simultaneously using dinaciclib could overcome PARPi resistance in BRCA1/2-mutated TNBC cell lines and xenograft models by blocking the restored HR function¹³⁸. Dinaciclib is currently being assessed in combination with the PARP inhibitor veliparib in solid tumors (NCT01434316). Surprisingly, also a G1/S cyclin-CDK complex was found to be involved in HR regulation. Specifically, cyclin D, the non-catalytic partner of CDK4 and CDK6, appeared essential for HR, and this finding may open up additional possibilities to potentiate PARP inhibitor sensitivity¹³⁹.

Finally, DNA repair through HR is inactivated in response to hyperthermia. The inhibition of HR shifts repair of DSBs to error-prone NHEJ and thereby sensitizes tumor cells to DNA damaging agents¹⁴⁰. Upon transient hyperthermia to 42.5°C, it was shown that BRCA2 is degraded in a proteasome-dependent fashion. Loss of BRCA2 lasts for several hours and

functionally impairs HR. Consequently, tumor cells become sensitive to cisplatin, doxorubicin as well as PARP inhibitors in vitro and in vivo¹⁴¹. This concept is currently being tested in a range of clinical trials, including a trial in head and neck cancer patients, testing the effects of hyperthermia on responses to the PARP inhibitor olaparib (Dutch Trial registry: NTR5842).

3.2.4. Resistance to PARP inhibitors

As with many molecularly targeted agents, resistance to PARP inhibitors is a clinical problem. Currently, different mechanisms underlying resistance to PARP inhibitor treatment have been described (**Figure 3**).

Secondary mutations or translocations may arise within the mutated BRCA1 or BRCA2 gene, restoring the reading frame of the affected gene. This was firstly described in breast and pancreatic cell lines in which secondary BRCA2 mutations restored the BRCA2 reading frame and resulted in cisplatin and PARP inhibitor resistance¹⁴². The same research group reported that secondary mutations of BRCA1 also occur in platinum-resistant ovarian cancer with a BRCA1 mutation¹⁴³. In germline BRCA1/2-mutated ovarian cancer patients, secondary somatic mutations that restore BRCA1/2 were correlated with resistance to platinum-based chemotherapy¹⁴⁴. A mechanistically unrelated resistance mechanism was described for BRCA1-hypermethylated breast patient-derived xenograft (PDX) tumors, in which BRCA1 expression was restored through the rearrangement of the BRCA1 locus, resulting in expression of BRCA1 from a different promoter¹⁴⁵. The loss of BRCA1 promoter methylation has already been described in chemotherapy-resistant ovarian cancer patients¹⁴⁶.

The function of HR can also be restored by mutations in other genes. An important finding by Cao and coworkers described that loss of 53BP1 prevented the senescence and cell death induced by BRCA1 deficiency, both in vitro and in vivo¹⁴⁷. 53BP1 was originally identified as an activator of p53 in the DDRs¹⁴⁸ and was later shown to promote NHEJ¹⁴⁹. Notably, 53BP1 inactivation partially restored HR in mouse embryonic stem cells with a conditional *Brca1* knockout¹⁵⁰. Through this mechanism, loss of 53BP1 reversed the sensitivity of BRCA1-deficient cells to PARP inhibition^{150,151}. Although these experiments were executed in mouse models, loss of 53BP1 may be a resistance mechanism to PARP inhibition in patients with BRCA1-mutant tumors¹⁵². Indeed, altered expression of 53BP1 is commonly observed in BRCA1-mutated breast cancers.

Comparable observations were done for other NHEJ-promoting genes Rif1 and REV7 (also called Mad2L2). Mutation of these genes also rescued HR defects, promoted the cellular viability, and reversed PARP inhibitor sensitivity in BRCA1-deficient cells^{36,153}. Additionally, it was shown that ubiquitylation and recruitment to DSBs of BRCA1, but not 53BP1, are regulated by the demethylase JMJD1C. Knockdown of JMJD1C resulted in increased RPA phosphorylation and accelerated formation of RAD51 foci upon irradiation. In BRCA1-depleted cells, knockdown of JMJD1C resulted in decreased sensitivity to PARP inhibition by olaparib and restored RAD51 foci formation³⁷. Furthermore, reduced expression of JMJD1C was found in a subset of invasive human breast cancers (26%), which suggests that JMJD1C is another player in PARP inhibitor resistance similar to 53BP1 and its cofactors.

Most of the above-described mechanisms reversed PARP inhibitor sensitivity and HR in BRCA1-mutant cancers, but not in BRCA2-mutant cancers. This probably reflects the upstream function of BRCA1 within the HR pathway, at the level of DNA-end resection initiation. BRCA2, by contrast, functions in RAD51 recruitment beyond the step of DNA-end resection. Recently, loss of PTIP (also known as PAX-interacting protein 1, encoded by the *PAXIP1* gene) was described to rescue the lethality of *Brca2*-mutated embryonic mouse stem cells and caused PARP inhibitor resistance. However, PTIP inactivation did not restore HR, but rather lead to the protection of replication forks through prevention of MRE11 recruitment to stalled replication forks⁴⁷. These data suggest that besides HR functionality, replication fork protection is critically involved in sensitivity to PARP inhibitors in BRCA2-deficient cancers.

As the cytotoxicity of PARP inhibition is dependent on the presence of its target PARP-1, it is suggested that decreased levels or activity of PARP-1 may interfere with the PARP inhibitor response. The levels of PARP-1 were decreased in PARP inhibitor-resistant cell lines and increased activity of PARP-1 (as measured by PARylation) correlated to PARP inhibitor sensitivity^{154,155}. Small nucleotide polymorphisms (SNPs) in the PARP1 gene may alter its function and activity and thereby influence the response to PARP inhibition¹⁵⁶.

4. Patient selection for PARP inhibitor treatment

Currently, only serous ovarian cancer patients with proven germline or somatic BRCA1/2 mutations are eligible for treatment with olaparib or rucaparib (**Figure 4**). In 2006, it was already suggested that PARP inhibition might be effective not only in tumors with BRCA1/2 mutations but also in tumors with loss of other HR components and tumors beyond breast and ovarian cancer¹⁵⁷. Very recently, niraparib has also been approved by the FDA for treatment of recurrent fallopian tube or primary peritoneal cancer. Below, various techniques are described that can be used to facilitate patient selection for PARP inhibitor treatment.

4.1. Mutation analysis

BRCA1/2 mutational status and BRCA1 promoter methylation analysis of tumors will identify patients, likely to benefit from PARP inhibition. However, mutations in other HR genes might also result in HR deficiency and thus PARP inhibitor sensitivity, although these mutations are less frequently observed. Extending the panel of genes for mutational analysis might increase the selection of HR-deficient tumors, but for each of these genes, variants of unknown significance (VUS) occur which challenge clinical decision-making. In a study by Easton et al., 1433 VUS alleles in BRCA1 and BRCA2 were classified, of which the majority appeared to be of no significance in relation to cancer development¹⁴⁴. It was suggested that family history should play an important role in decision-making and prediction of cancer risk in patients with VUS alleles¹⁵⁸. Systemic approaches and combining big data sets are required to optimally classify the thousands of VUS alleles in BRCA1/2 and other HR genes to predict if these mutations predispose to cancer. In parallel, experimental models have been developed in which VUS alleles can be tested for functionality¹⁵⁹. Members of the global Evidence-based Network for the Interpretation of Germline Mutant Alleles (ENIGMA) consortium collaborate to better implement information on VUS alleles into clinical decision-making¹⁶⁰.

Furthermore, secondary mutations either within the mutant BRCA1/2 alleles or in secondary genes that restore HR function have been described and may underlie resistance to platinum-based chemotherapy and PARP inhibitors¹⁶¹. Profiling all these genes for mutations will make genetic screening increasingly complex.

4.2. Genomic scar analysis

Different approaches have been developed to discriminate between HR-proficient and HR-deficient tumors based on the landscape of the genomic tumor aberrations, referred to as a 'genomic scar' (**Figure 4**).

To detect breast cancer tumors without BRCA1/2 mutations, but with a similar phenotype, a classifier was developed based on tumor profiles with array-comparative genomic hybridization (CGH) using a set of BRCA1-mutated breast tumors as well as control breast tumors¹⁶². In a group of 48 patients from families with hereditary breast and ovarian cancer, two tumors with a 'BRCA1-like' array-CGH profile but without BRCA1/2 germline mutation were detected. Furthermore, this classifier predicted response to genotoxic agents with improved outcomes of 'BRCA1-like' tumors (based on the array-CGH profile) to platinum-based chemotherapy in stage III breast cancer patients¹⁶³. Of note, this technique might not only

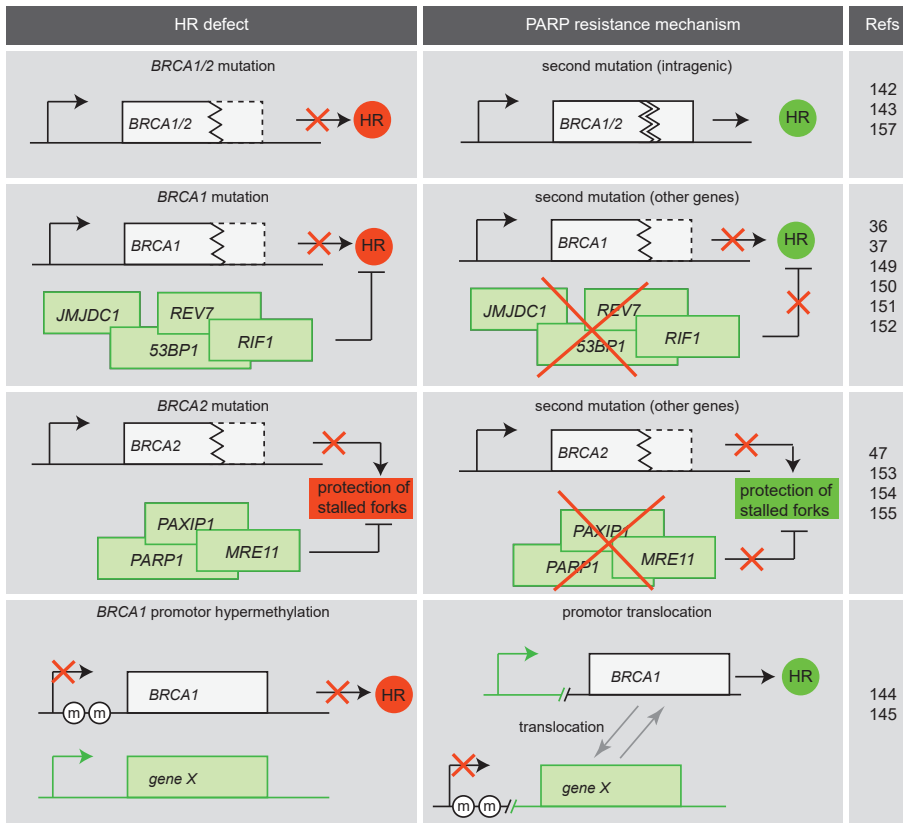


Figure 3. PARP inhibitor resistance mechanisms. Various mechanisms for PARP inhibitor resistance are described. Secondary intragenic mutations (*BRCA1/2*), secondary mutations in other genes in *BRCA1*-mutant cancer cells, or promotor translocations in *BRCA1* may restore HR function. Secondary mutations in other genes may restore the protection of stalled replication forks caused by *BRCA2* inactivation.

be useful for prediction but also to give insight into the significance of certain VUS alleles and identify compensatory genomic alterations that facilitate cellular survival in the absence of HR.

In a recent study by Davies et al., whole-genome profiling was applied to 24 breast tumors with a germline *BRCA1/2* mutation, and results were compared to sporadic breast cancer samples to develop an algorithm that can differentiate between these groups¹⁶⁴. Included parameters were based on indels, base-substitutions, and rearrangements. In different additional cohorts of breast, pancreatic, and ovarian cancer, tumors with a *BRCA1/2* deficiency were identified when the developed algorithm (named 'HRDetect') was applied. These tumors harbored either biallelic germline or somatic mutations in *BRCA1* or *BRCA2* or promotor hypermethylation of *BRCA1* combined with a loss of the second allele. Importantly, also tumors without genetic alterations in *BRCA1/2* were identified, illustrating that sequence analysis for *BRCA1/2* alone is insufficient to detect all tumors with an HR-deficient phenotype¹⁶⁴.

Myriad Genetics has developed a homologous recombination deficiency (HRD) test to identify patients that could benefit from PARP inhibitor treatment (termed 'MyChoice' test). This test includes genetic and phenotypic analysis of formalin-fixed, paraffin-embedded tumor tissue collected by biopsy or surgery. Genes associated with HR deficiency are sequenced, including *BRCA1/2* as well as others¹⁶⁵. As this analysis cannot identify tumors with epigenetically

silenced HR genes and other yet unknown causes of HR deficiency, tumor tissue is also analyzed at a phenotypic level for three features of genomic instability. These characteristics include large-scale transitions, clustering of LOH, and assessing the telomeric allelic imbalance rates (reviewed in ¹⁶⁶). The tumors are assigned a combined HRD score based on these three characteristics. It has been shown that this phenotypic HRD score strongly correlates with a BRCA1/2 deficiency in different types of breast tumors¹⁶⁷. The combination of mutational analysis and HRD score gives a better prediction of HR compared to mutational status alone. Currently, based on clinical trials, the MyChoice test identifies twice as many patients that may benefit from PARP inhibitor treatment and platinum-based chemotherapy compared to selection by BRCA1/2 mutational analyses alone for both breast and ovarian cancer (NCT01847274)¹⁶⁸. Included patients without BRCA1/2 mutations but with high HRD score appear to show a favorable response to platinum-based therapy in TNBC¹⁶⁹. However, not all HR-deficient tumors based on mutational analysis or genomic scarring will be sensitive to PARP inhibition. These tumors are highly genomically unstable and may, therefore, develop secondary mutations that restore HR function or result in PARP inhibitor resistance as described above.

Genomic scar analysis is performed on tumor specimens taken prior to treatment. The disadvantage of this approach is that it provides a historic representation of the genetic aberrations in the tumor, but does not reflect current HR deficiency as influenced by secondary mutations. Additional biomarkers or functional assays to determine whether HR is still defective or possibly restored will, therefore, provide better insight.

4.3. Functional HR read-out – RAD51 foci formation

The essential last step in HR repair is RAD51 loading, and its functionality can be visualized by foci formation analysis¹⁷⁰. Mechanistically, BRCA2 is required for RAD51 foci formation upon DSBs induced by ionizing radiation (IR)¹⁷¹. As RAD51 is the effector in HR, lack of BRCA2, but also upstream HR defects in components such as BRCA1 or PALB2, results in the absence of RAD51 foci formation. The formation of RAD51 foci is, therefore, a functional read-out for HR deficiency (**Figure 4**).

To determine the ability of cells to repair DSBs by HR, different *in vitro* or *ex vivo* models have been used to assess the formation of irradiation-induced RAD51 foci. In ovarian cancer cell lines and PDX models from omental tumors, *ex vivo* assessed irradiation-induced RAD51 foci correlated with response to the PARP inhibitor veliparib (ABT-888)¹⁷². In primary cultures of ascites from patients with epithelial ovarian cancer, a correlation was found between the response to PARP inhibition (AG14699) and decreased RAD51 foci formation, although in this study RAD51 foci formation was determined at 24 h after treatment with AG14699, rather than at short-term interval upon IR¹⁷³.

It is important to consider that different sources of DSBs, such as IR versus chemical compounds, may lead to a different time frame in which RAD51 foci appear. It has been shown that efficient DNA repair, and thus the formation of RAD51 foci, in response to irradiation is optimal after 2 h¹⁷⁴. Counting RAD51 foci at 24 h after treatment may, therefore, lead to an overestimation of tumors that are HR deficient. Furthermore, both studies did not discriminate between cells in different phases of the cell cycle^{172,173}. Since HR only occurs in S and G2 of the cell cycle, RAD51 foci will only appear in a subset of tumor cells. If RAD51 foci are counted in cells regardless of the cell cycle phase, it may result in false-negative results, for instance in tumor samples that contain a high percentage of non-proliferating cells. The appearance of false negatives was indeed the case in Mukhopadhyay et al. To reliably determine HR functionality, a cell cycle or proliferation markers should be included. Geminin, for instance, is a nuclear protein that is present during the S and G2 phase to coordinate replication and can, therefore, be used as cell cycle marker¹⁷⁵. Taking geminin into account as a cell cycle marker provides an additional check to determine whether the *ex vivo* cultures are still proliferating. Naipal et al. determined the presence of RAD51 foci upon irradiation in

geminin-positive cells of ex vivo breast cancer tissue samples. In this study, 11% of samples were HR deficient, and defective RAD51 foci formation correlated with TNBC status¹⁷⁶.

In another study with fresh tumor samples of breast cancer patients, ex vivo RAD51 foci formation was assessed, and 22% of tumors were found to be RAD51 deficient and thus HR defective. Subsequently, biallelic inactivation of different HR genes was detected by sequencing and could explain almost 90% of the RAD51-foci devoid of tumors¹⁷⁷.

Graeser et al. assessed RAD51 foci formation in biopsies of patients taken at 24 h after neoadjuvant chemotherapy. RAD51 foci were assessed in geminin-positive cells, and HR deficiency was found in 26% of the tumors, which were again enriched for TNBC status¹⁷⁸. Also, low levels of RAD51 foci correlated with pathologic complete response to anthracycline-based chemotherapy (33%), when compared to tumors that were HR proficient (3%). Different approaches to counting RAD51 foci in multiple studies, such as the time point after irradiation, may explain the variation in percentages of HR-deficient tumors.

5. Conclusion

Repair of DNA DSBs and collapsed replication forks depends on HR for efficient resolution. Defective HR, such as caused by cancer-associated mutations in BRCA1, BRCA2, or related HR genes, leads to genomic instability and facilitates tumor progression. Yet, HR defects come with acquired sensitivity to DNA damaging agents, including PARP inhibitors. Current patient inclusion is largely based on BRCA1/2 mutational analysis. However, BRCA1/2 mutational analysis is likely not sufficient to include all HR-deficient tumors, and conversely, some BRCA1/2 mutant cancers may be HR proficient, due to secondary mutations. The restoration of HR underlies one of the mechanisms by which tumors become resistant to PARP inhibition, especially in BRCA1-mutant tumors. Restoration of replication fork stability appears to be another mechanism of PARP inhibitor resistance, especially in BRCA2-deficient tumors. The development of functional HR deficiency tests may more reliably identify patients who may benefit from PARP inhibition. Functional assays in preclinical testing have correlated RAD51 foci formation with clinical parameters and response to DNA damaging agents¹⁷⁸. A clinical trial designed to determine whether ex vivo RAD51 foci formation can predict responses to PARP inhibition in multiple tumor types (NCT03044795) is due to commence soon. Additionally, functional testing at the time of resistance to PARP inhibitor therapy may aid in yielding a better understanding of the mechanisms of acquired PARP resistance.

6. Expert opinion

PARP inhibition in HR-deficient cancers is the prototypical example of personalized medicine, based on synthetic lethality. Currently, three PARP inhibitors have been approved by the FDA, and olaparib has been approved by the EMA for BRCA1/2-mutated ovarian cancer. Several other PARP inhibitors are in clinical development. Increasingly, it appears that the ability to trap the PARP enzyme onto DNA is important for cytotoxic effects, in addition to their ability to catalytically inhibit PARP.

To optimally implement PARP inhibitors in cancer treatment, the selection of patients with most suitable tumors is key. Genetic testing for BRCA1/2 mutation remains a powerful approach but might miss a significant number of HR-deficient tumors, harboring BRCA1 promoter hypermethylation or mutations in other HR genes. Identification of such tumors is challenged by the multitude of genes involved in HR and by our limited understanding of the contribution of each of these genes.

Ideally, the selection of eligible patients for PARP inhibitor treatment involves a test that measures downstream consequences of defective HR. Existing tests are based on genomic platforms such as array-CGH, SNP arrays, or deep sequencing-based analysis and display genomic

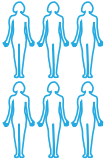

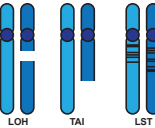
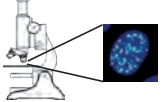
		PROS	CONS
Patient selection: HR deficient tumor 	BRCA1/2 mutation analysis 	-easy and fast -can be performed on archived material	-no information on other HR genes -secondary mutations (e.g. <i>TP53BP1</i>) remain undetected -'variants of unknown significance (VUS)' complicate analysis
	Genomic 'scar' analysis (eg: aCGH, SNP array) 	-tests consequences of HR deficiency -also detects 'BRCA-like' mutations -can be performed on archived material -provides additional genome-wide data -performance likely increases with increasing numbers of samples	-historic scar may not represent functional HR defect
	Functional HR read-out 	-allows detection of functional HR defect -includes all causes of HR deficiency	-requires 'wet' lab work -requires fresh tumor material -requires vulnerable reagents (antibodies)

Figure 4. Patient selection for PARP inhibitor treatment. Currently, patients are selected for PARP inhibitor treatment based on BRCA1/2 mutation analysis. Additional techniques such as genomic scar analysis (e.g. array-CGH or DNA sequencing-based) or a functional HR read-out are being developed and could be included to better select patients with HR-deficient tumors. The advantages (PROS) and disadvantages (CONS) of each method are indicated.

'scars' induced by HR deficiency. Using algorithms, genomic scars can be identified that resemble those of BRCA1/2-mutant cancers and predict HR deficiency, regardless of the underlying gene mutation. These assays will grow increasingly reliable, with growing numbers of samples analyzed.

As with other targeted anticancer agents, acquired resistance to PARP inhibitors occurs. Increasingly, the genetic events that may underlie resistance are uncovered and could be included in decision-making for PARP inhibitor treatment. Over the last years, multiple genetic alterations have been described that can rescue defective HR and thereby render tumor cells insensitive to PARP inhibitors. Importantly, genomic scars represent historic events and may not reflect current HR deficiency when such secondary mutations have occurred.

To address this issue, assays are required that functionally interrogate HR functionality. In this context, fresh tumor samples can be prepared and analyzed for their ability to induce focus formation of the HR component RAD51 or related downstream HR components. Although these assays are technically feasible and require fresh tumor material, they theoretically would be able to include all HR-deficient tumors, beyond breast and ovarian cancer. Most of the tumor tissue in studies that assess RAD51 foci formation is irradiated as a model to induce DSBs. In an ideal situation, PARP inhibitors are employed instead of irradiation, as they instigate the most relevant type of DNA lesions and activate the relevant DNA repair pathway. Furthermore, some tumors contain a small portion of actively proliferating cells. Since RAD51 foci formation can only be functional in proliferating cells, it may turn out to be challenging to assess sufficient amounts of cycling tumor cells. Finally, different approaches may need to be tested to keep tumor tissues viable for the duration of the ex vivo procedure.

Recent insight has also shown that PARP inhibitor sensitivity is associated with the ability of tumors to stabilize stalled replication forks, a mechanism that also involves HR components. The ideal functional assay to test PARP inhibitor eligibility therefore not only includes RAD51 foci formation but also involves the ability of cancer cells to maintain replication fork stability. Various technical hurdles will need to be overcome to implement such functional assays clinically.

Combined, PARP inhibitors may provide clinical benefit for various cancers, beyond BRCA1/2-mutant ovarian cancers. To facilitate patient selection for PARP inhibitors, additional tests beyond BRCA1/2 mutational analysis should be employed, ranging from genetic analysis to functional assays in fresh tumor tissue. In the coming years, accurate ways to select patients for PARP inhibitor treatment will be assessed in the context of clinical trials. As more PARP inhibitor resistance mechanisms are being discovered, it is important to be able to detect if resistance mechanisms are active in the tumor to efficiently adapt the treatment with other treatment regimens, such as immunotherapies.

Acknowledgments

We thank Dik van Gent, Titia Meijer, Agnes Jager, Maaike Vreeswijk, Jos Jonkers for fruitful discussions.

References

1. Jackson SP, Bartek J. The DNA-damage response in human biology and disease. *Nature*. 2009 Oct 22;461(7267):1071–1078.
2. Matsuoka S, Ballif BA, Smogorzewska A, et al. ATM and ATR substrate analysis reveals extensive protein networks responsive to DNA damage. *Science*. 2007 May 25;316(5828):1160–1166.
3. Bassing CH, Swat W, Alt FW. The mechanism and regulation of chromosomal V(D)J recombination. *Cell*. 2002 Apr;109(Suppl): S45–55.
4. Fugmann SD, Lee AI, Shockett PE, et al. The RAG proteins and V(D)J recombination: complexes, ends, and transposition. *Annu Rev Immunol*. 2000;18:495–527.
5. Zeman MK, Cimprich KA. Causes and consequences of replication stress. *Nat Cell Biol*. 2014 Jan;16(1):2–9.
6. Aymard F, Bugler B, Schmidt CK, et al. Transcriptionally active chromatin recruits homologous recombination at DNA double-strand breaks. *Nat Struct Mol Biol*. 2014 Apr;21(4):366–374.
7. Lieber MR. The mechanism of human nonhomologous DNA end joining. *J Biol Chem*. 2008 Jan 4;283(1):1–5.
8. Pitcher RS, Wilson TE, Doherty AJ. New insights into NHEJ repair processes in prokaryotes. *Cell Cycle*. 2005 May;4(5):675–678.
9. Ma Y, Lu H, Schwarz K, et al. Repair of double-strand DNA breaks by the human nonhomologous DNA end joining pathway: the iterative processing model. *Cell Cycle*. 2005 Sep;4(9):1193–1200.
10. Radhakrishnan SK, Jette N, Lees-Miller SP. Non-homologous end joining: emerging themes and unanswered questions. *DNA Repair (Amst)*. 2014 May;17:2–8.
11. Bennardo N, Cheng A, Huang N, et al. Alternative-NHEJ is a mechanistically distinct pathway of mammalian chromosome break repair. *Plos Genet*. 2008 Jun 27;4(6):e1000110.
12. Moynahan ME, Jasin M. Mitotic homologous recombination maintains genomic stability and suppresses tumorigenesis. *Nat Rev Mol Cell Biol*. 2010 Mar;11(3):196–207.
13. Wyman C, Kanaar R. DNA double-strand break repair: all's well that ends well. *Annu Rev Genet*. 2006;40:363–383.
14. Johnson RD, Jasin M. Sister chromatid gene conversion is a prominent double-strand break repair pathway in mammalian cells. *Embo J*. 2000 Jul 3;19(13):3398–3407.
15. Wu X, Ranganathan V, Weisman DS, et al. ATM phosphorylation of Nijmegen breakage syndrome protein is required in a DNA damage response. *Nature*. 2000 May 25;405(6785):477–482.
16. Zhao S, Weng YC, Yuan SS, et al. Functional link between ataxiatelangiectasia and Nijmegen breakage syndrome gene products. *Nature*. 2000 May 25;405(6785):473–477.
17. Anand R, Ranjha L, Cannavo E, et al. Phosphorylated CtIP functions as a co-factor of the MRE11-RAD50-NBS1 endonuclease in DNA end resection. *Mol Cell*. 2016 Dec 1;64(5):940–950.
18. Garcia V, Phelps SE, Gray S, et al. Bidirectional resection of DNA double-strand breaks by Mre11 and Exo1. *Nature*. 2011 Oct 16;479(7372):241–244.
19. Nimmonkar AV, Genschel J, Kinoshita E, et al. BLM-DNA2-RPA-MRN and EXO1-BLM-RPA-MRN constitute two DNA end resection machineries for human DNA break repair. *Genes Dev*. 2011 Feb 15;25(4):350–362.

20. Sturzenegger A, Burdova K, Kanagaraj R, et al. DNA2 cooperates with the WRN and BLM RecQ helicases to mediate long-range DNA end resection in human cells. *J Biol Chem*. 2014 Sep 26;289(39):27314–27326.
21. Gudmundsdottir K, Ashworth A. The roles of BRCA1 and BRCA2 and associated proteins in the maintenance of genomic stability. *Oncogene*. 2006 Sep 25;25(43):5864–5874.
22. Suwaki N, Klare K, Tarsounas M. RAD51 paralogs: roles in DNA damage signalling, recombinational repair and tumorigenesis. *Semin Cell Dev Biol*. 2011 Oct;22(8):898–905.
23. Lok BH, Carley AC, Tchang B, et al. RAD52 inactivation is synthetically lethal with deficiencies in BRCA1 and PALB2 in addition to BRCA2 through RAD51-mediated homologous recombination. *Oncogene*. 2013 Jul 25;32(30):3552–3558.
24. Badie S, Liao C, Thanasoula M, et al. RAD51C facilitates checkpoint signaling by promoting CHK2 phosphorylation. *J Cell Biol*. 2009 May 18;185(4):587–600.
25. Swagemakers SM, Essers J, De Wit J, et al. The human RAD54 recombinational DNA repair protein is a double-stranded DNA-dependent ATPase. *J Biol Chem*. 1998 Oct 23;273(43):28292–28297.
26. Bugreev DV, Mazina OM, Mazin AV. Rad54 protein promotes branch migration of Holliday junctions. *Nature*. 2006 Aug 3;442(7102):590–593.
27. Moudry P, Watanabe K, Wolanin KM, et al. TOPBP1 regulates RAD51 phosphorylation and chromatin loading and determines PARP inhibitor sensitivity. *J Cell Biol*. 2016 Feb 1;212(3):281–288.
28. Pace P, Mosedale G, Hodskinson MR, et al. Ku70 corrupts DNA repair in the absence of the Fanconi anemia pathway. *Science*. 2010 Jul 9; 329(5988):219–223.
29. Ceccaldi R, Liu JC, Amunugama R, et al. Homologous-recombination-deficient tumours are dependent on poltheta-mediated repair. *Nature*. 2015 Feb 12;518(7538):258–262.
30. Kent T, Chandramouly G, McDevitt SM, et al. Mechanism of microhomology-mediated end-joining promoted by human DNA polymerase theta. *Nat Struct Mol Biol*. 2015 Mar;22(3):230–237.
31. Sartori AA, Lukas C, Coates J, et al. Human CtIP promotes DNA end resection. *Nature*. 2007 Nov 22;450(7169):509–514.
32. Yu X, Chen J. DNA damage-induced cell cycle checkpoint control requires CtIP, a phosphorylation-dependent binding partner of BRCA1 C-terminal domains. *Mol Cell Biol*. 2004 Nov;24(21):9478–9486.
33. Escribano-Diaz C, Orthwein A, Fradet-Turcotte A, et al. A cell cycle-dependent regulatory circuit composed of 53BP1-RIF1 and BRCA1-CtIP controls DNA repair pathway choice. *Mol Cell*. 2013 Mar 7;49(5):872–883.
34. Isono M, Niimi A, Oike T, et al. BRCA1 directs the repair pathway to homologous recombination by promoting 53BP1 dephosphorylation. *Cell Rep*. 2017 Jan 10;18(2):520–532.
35. Boersma V, Moatti N, Segura-Bayona S, et al. MAD2L2 controls DNA repair at telomeres and DNA breaks by inhibiting 5' end resection. *Nature*. 2015 May 28;521(7553):537–540.
36. Xu G, Chapman JR, Brandsma I, et al. REV7 counteracts DNA double-strand break resection and affects PARP inhibition. *Nature*. 2015 May 28;521(7553):541–544.
37. Watanabe S, Watanabe K, Akimov V, et al. JMJD1C demethylates MDC1 to regulate the RNF8 and BRCA1-mediated chromatin response to DNA breaks. *Nat Struct Mol Biol*. 2013 Dec;20(12):1425–1433.
38. Tkac J, Xu G, Adhikary H, et al. HELB is a feedback inhibitor of DNA end resection. *Mol Cell*. 2016 Feb 4;61(3):405–418.
39. Chroma K, Mistrik M, Moudry P, et al. Tumors overexpressing RNF168 show altered DNA repair and responses to genotoxic treatments, genomic instability and resistance to proteotoxic stress. *Oncogene*. 2016 Nov 14.
40. Densham RM, Garvin AJ, Stone HR, et al. Human BRCA1-BARD1 ubiquitin ligase activity counteracts chromatin barriers to DNA resection. *Nat Struct Mol Biol*. 2016 Jul;23(7):647–655.
41. Yata K, Lloyd J, Maslen S, et al. Plk1 and CK2 act in concert to regulate Rad51 during DNA double strand break repair. *Mol Cell*. 2012 Feb 10;45(3):371–383.
42. Schlacher K, Christ N, Siaud N, et al. Double-strand break repair-independent role for BRCA2 in blocking stalled replication fork degradation by MRE11. *Cell*. 2011 May 13; 145(4):529–542.
43. Schlacher K, Wu H, Jasin M. A distinct replication fork protection pathway connects Fanconi anemia tumor suppressors to RAD51- BRCA1/2. *Cancer Cell*. 2012 Jul 10;22(1):106–116.
44. Somyajit K, Saxena S, Babu S, et al. Mammalian RAD51 paralogs protect nascent DNA at stalled forks and mediate replication restart. *Nucleic Acids Res*. 2015 Nov 16;43(20):9835–9855.
45. Strom CE, Johansson F, Uhlen M, et al. Poly (ADP-ribose) polymerase (PARP) is not involved in base excision repair but PARP inhibition traps a single-strand intermediate. *Nucleic Acids Res*. 2011

- Apr;39(8):3166–3175.
46. Murai J, Huang SY, Das BB, et al. Trapping of PARP1 and PARP2 by clinical PARP inhibitors. *Cancer Res.* 2012 Nov 1;72(21):5588–5599.
 47. Ray Chaudhuri A, Callen E, Ding X, et al. Replication fork stability confers chemoresistance in BRCA-deficient cells. *Nature.* 2016 Jul 20;535(7612):382–387.
 48. Hanahan D, Weinberg RA. Hallmarks of cancer: the next generation. *Cell.* 2011 Mar 4;144(5):646–674.
 49. Futreal PA, Liu Q, Shattuck-Eidens D, et al. BRCA1 mutations in primary breast and ovarian carcinomas. *Science.* 1994 Oct 7;266(5182):120–122.
 50. Miki Y, Swensen J, Shattuck-Eidens D, et al. A strong candidate for the breast and ovarian cancer susceptibility gene BRCA1. *Science.* 1994 Oct 7;266(5182):66–71.
 51. Tavtigian SV, Simard J, Rommens J, et al. The complete BRCA2 gene and mutations in chromosome 13q-linked kindreds. *Nat Genet.* 1996 Mar;12(3):333–337.
 52. Wooster R, Bignell G, Lancaster J, et al. Identification of the breast cancer susceptibility gene BRCA2. *Nature.* 1995 Dec 21-28;378(6559):789–792.
 53. Iqbal J, Ragone A, Lubinski J, et al. The incidence of pancreatic cancer in BRCA1 and BRCA2 mutation carriers. *Br J Cancer.* 2012 Dec 4;107(12):2005–2009.
 54. Thompson D, Easton DF. Breast cancer linkage consortium. Cancer incidence in BRCA1 mutation carriers. *J Natl Cancer Inst.* 2002 Sep 18;94(18):1358–1365.
 55. Mersch J, Jackson M, Park M, et al. Cancers associated with BRCA1 and BRCA2 mutations other than breast and ovarian. *Cancer.* 2015 Jul 15;121(14):2474–2475.
 56. Osorio A, De La Hoya M, Rodriguez-Lopez R, et al. Loss of heterozygosity analysis at the BRCA loci in tumor samples from patients with familial breast cancer. *Int J Cancer.* 2002 May 10;99(2):305–309.
 57. Esteller M, Silva JM, Dominguez G, et al. Promoter hypermethylation and BRCA1 inactivation in sporadic breast and ovarian tumors. *J Natl Cancer Inst.* 2000 Apr 5;92(7):564–569.
 58. Cancer Genome Atlas Research Network. Integrated genomic analyses of ovarian carcinoma. *Nature.* 2011 Jun 29;474(7353):609–615.
 59. Moschetta M, George A, Kaye SB, et al. BRCA somatic mutations and epigenetic BRCA modifications in serous ovarian cancer. *Ann Oncol.* 2016 Aug;27(8):1449–1455.
 60. Ramus SJ, Song H, Dicks E, et al. Germline mutations in the BRIP1, BARD1, PALB2, and NBN genes in women with ovarian cancer. *J Natl Cancer Inst.* 2015 Aug 27;107(11). Print 2015 Nov. doi:10.1093/jnci/djv214.
 61. Antoniou AC, Casadei S, Heikkinen T, et al. Breast-cancer risk in families with mutations in PALB2. *N Engl J Med.* 2014 Aug 7;371(6):497–506.
 62. Song H, Dicks E, Ramus SJ, et al. Contribution of germline mutations in the RAD51B, RAD51C, and RAD51D genes to ovarian cancer in the population. *J Clin Oncol.* 2015 Sep 10;33(26):2901–2907.
 63. Minion LE, Dolinsky JS, Chase DM, et al. Hereditary predisposition to ovarian cancer, looking beyond BRCA1/BRCA2. *Gynecol Oncol.* 2015 Apr;137(1):86–92.
 64. Frimer M, Levano KS, Rodriguez-Gabin A, et al. Germline mutations of the DNA repair pathways in uterine serous carcinoma. *Gynecol Oncol.* 2016 Apr;141(1):101–107.
 65. Chae YK, Anker JF, Carneiro BA, et al. Genomic landscape of DNA repair genes in cancer. *Oncotarget.* 2016 Apr 26;7(17):23312–23321.
 66. Meijers-Heijboer H, Van Den Ouweland A, Klijn J, et al. Low-penetrance susceptibility to breast cancer due to CHEK2(*)1100delC in noncarriers of BRCA1 or BRCA2 mutations. *Nat Genet.* 2002 May;31(1):55–59.
 67. Vahteristo P, Bartkova J, Eerola H, et al. A CHEK2 genetic variant contributing to a substantial fraction of familial breast cancer. *Am J Hum Genet.* 2002 Aug;71(2):432–438.
 68. Lee JS, Collins KM, Brown AL, et al. hCds1-mediated phosphorylation of BRCA1 regulates the DNA damage response. *Nature.* 2000 Mar 9;404(6774):201–204.
 69. Zhang J, Willers H, Feng Z, et al. Chk2 phosphorylation of BRCA1 regulates DNA double-strand break repair. *Mol Cell Biol.* 2004 Jan;24(2):708–718.
 70. Antoniou A, Pharoah PD, Narod S, et al. Average risks of breast and ovarian cancer associated with BRCA1 or BRCA2 mutations detected in case series unselected for family history: a combined analysis of 22 studies. *Am J Hum Genet.* 2003 May;72(5):1117–1130.
 71. Easton DF, Ford D, Bishop DT. Breast and ovarian cancer incidence in BRCA1-mutation carriers. Breast Cancer Linkage Consortium. *Am J Hum Genet.* 1995 Jan;56(1):265–271.
 72. Mavaddat N, Peock S, Frost D, et al. Cancer risks for BRCA1 and BRCA2 mutation carriers: results

- from prospective analysis of EMBRACE. *J Natl Cancer Inst.* 2013 Jun 5;105(11):812–822.
73. Shive HR, West RR, Embree LJ, et al. BRCA2 and TP53 collaborate in tumorigenesis in zebrafish. *Plos One.* 2014 Jan 29;9(1):e87177.
 74. van der Groep P, van der Wall E, van Diest PJ. Pathology of hereditary breast cancer. *Cell Oncol (Dordr).* 2011 Apr;34(2):71–88.
 75. Jazaeri AA, Yee CJ, Sotiriou C, et al. Gene expression profiles of BRCA1-linked, BRCA2-linked, and sporadic ovarian cancers. *J Natl Cancer Inst.* 2002 Jul 3;94(13):990–1000.
 76. Lakhani SR, van de Vijver MJ, Jacquemier J, et al. The pathology of familial breast cancer: predictive value of immunohistochemical markers estrogen receptor, progesterone receptor, HER-2, and p53 in patients with mutations in BRCA1 and BRCA2. *J Clin Oncol.* 2002 May 1;20(9):2310–2318.
 77. Moslehi R, Chu W, Karlan B, et al. BRCA1 and BRCA2 mutation analysis of 208 Ashkenazi Jewish women with ovarian cancer. *Am J Hum Genet.* 2000 Apr;66(4):1259–1272.
 78. Helleday T, Petermann E, Lundin C, et al. DNA repair pathways as targets for cancer therapy. *Nat Rev Cancer.* 2008 Mar;8(3):193–204.
 79. Gowen LC, Johnson BL, Latour AM, et al. Brca1 deficiency results in early embryonic lethality characterized by neuroepithelial abnormalities. *Nat Genet.* 1996 Feb;12(2):191–194.
 80. Hakem R, De La Pompa JL, Sirard C, et al. The tumor suppressor gene Brca1 is required for embryonic cellular proliferation in the mouse. *Cell.* 1996 Jun 28;85(7):1009–1023.
 81. Suzuki A, De La Pompa JL, Hakem R, et al. Brca2 is required for embryonic cellular proliferation in the mouse. *Genes Dev.* 1997 May 15;11(10):1242–1252.
 82. Sharan SK, Morimatsu M, Albrecht U, et al. Embryonic lethality and radiation hypersensitivity mediated by Rad51 in mice lacking Brca2. *Nature.* 1997 Apr 24;386(6627):804–810.
 83. Ludwig T, Chapman DL, Papaioannou VE, et al. Targeted mutations of breast cancer susceptibility gene homologs in mice: lethal phenotypes of Brca1, Brca2, Brca1/Brca2, Brca1/p53, and Brca2/p53 nullizygous embryos. *Genes Dev.* 1997 May 15;11(10):1226–1241.
 84. Patel KJ, Yu VP, Lee H, et al. Involvement of Brca2 in DNA repair. *Mol Cell.* 1998 Feb;1(3):347–357.
 85. Elledge SJ, Amon A. The BRCA1 suppressor hypothesis: an explanation for the tissue-specific tumor development in BRCA1 patients. *Cancer Cell.* 2002 Mar;1(2):129–132.
 86. Hirao A, Kong YY, Matsuoka S, et al. DNA damage-induced activation of p53 by the checkpoint kinase Chk2. *Science.* 2000 Mar 10;287(5459):1824–1827.
 87. Brodie SG, Xu X, Qiao W, et al. Multiple genetic changes are associated with mammary tumorigenesis in Brca1 conditional knockout mice. *Oncogene.* 2001 Nov 8;20(51):7514–7523.
 88. Liu X, Holstege H, van der Gulden H, et al. Somatic loss of BRCA1 and p53 in mice induces mammary tumors with features of human BRCA1-mutated basal-like breast cancer. *Proc Natl Acad Sci U S A.* 2007 Jul 17;104(29):12111–12116.
 89. Crook T, Brooks LA, Crossland S, et al. p53 mutation with frequent novel condons but not a mutator phenotype in BRCA1- and BRCA2-associated breast tumours. *Oncogene.* 1998 Oct 1;17(13):1681–1689.
 90. Evers B, Jonkers J. Mouse models of BRCA1 and BRCA2 deficiency: past lessons, current understanding and future prospects. *Oncogene.* 2006 Sep 25;25(43):5885–5897.
 91. Deans AJ, West SC. DNA interstrand crosslink repair and cancer. *Nat Rev Cancer.* 2011 Jun 24;11(7):467–480.
 92. Kee Y, D'Andrea AD. Expanded roles of the Fanconi anemia pathway in preserving genomic stability. *Genes Dev.* 2010 Aug 15;24(16):1680–1694.
 93. Howlett NG, Taniguchi T, Olson S, et al. Biallelic inactivation of BRCA2 in Fanconi anemia. *Science.* 2002 Jul 26;297(5581):606–609.
 94. Sawyer SL, Tian L, Kahkonen M, et al.; University of Washington Centre for Mendelian Genomics. Biallelic mutations in BRCA1 cause a new Fanconi anemia subtype. *Cancer Discov.* 2015 Feb;5(2):135–142.
 95. Niedernhofer LJ, Lalai AS, Hoeijmakers JH. Fanconi anemia (cross) linked to DNA repair. *Cell.* 2005 Dec 29;123(7):1191–1198.
 96. Alsop K, Fereday S, Meldrum C, et al. BRCA mutation frequency and patterns of treatment response in BRCA mutation-positive women with ovarian cancer: a report from the Australian Ovarian Cancer Study Group. *J Clin Oncol.* 2012 Jul 20;30(21):2654–2663.
 97. Hennessy BT, Timms KM, Carey MS, et al. Somatic mutations in BRCA1 and BRCA2 could expand the number of patients that benefit from poly (ADP ribose) polymerase inhibitors in ovarian cancer. *J Clin Oncol.* 2010 Aug 1;28(22):3570–3576.
 98. Lesnock JL, Darcy KM, Tian C, et al. BRCA1 expression and improved survival in ovarian cancer

- patients treated with intraperitoneal cisplatin and paclitaxel: a gynecologic oncology group study. *Br J Cancer*. 2013 Apr 2;108(6):1231–1237.
99. Tan DS, Rothermundt C, Thomas K, et al. “BRCAness” syndrome in ovarian cancer: a case-control study describing the clinical features and outcome of patients with epithelial ovarian cancer associated with BRCA1 and BRCA2 mutations. *J Clin Oncol*. 2008 Dec 1;26 (34):5530–5536.
 100. Cancer Genome Atlas Network. Comprehensive molecular portraits of human breast tumours. *Nature*. 2012 Oct 4;490(7418):61–70.
 101. Rottenberg S, Nygren AO, Pajic M, et al. Selective induction of chemotherapy resistance of mammary tumors in a conditional mouse model for hereditary breast cancer. *Proc Natl Acad Sci U S A*. 2007 Jul 17;104(29):12117–12122.
 102. Sharma P, Lopez-Tarruella S, Garcia-Saenz JA, et al. Efficacy of neoadjuvant carboplatin plus docetaxel in triple-negative breast cancer: combined analysis of two cohorts. *Clin Cancer Res*. 2017 Feb 1;23(3):649–657.
 103. Silver DP, Richardson AL, Eklund AC, et al. Efficacy of neoadjuvant cisplatin in triple-negative breast cancer. *J Clin Oncol*. 2010 Mar 1;28(7):1145–1153.
 104. Vollebbergh MA, Lips EH, Nederlof PM, et al. Genomic patterns resembling BRCA1- and BRCA2-mutated breast cancers predict benefit of intensified carboplatin-based chemotherapy. *Breast Cancer Res*. 2014 May 15;16(3):R47.
 105. Lucchesi JC. Synthetic lethality and semi-lethality among functionally related mutants of *Drosophila melanogaster*. *Genetics*. 1968 May;59(1):37–44.
 106. Hartwell LH, Szankasi P, Roberts CJ, et al. Integrating genetic approaches into the discovery of anticancer drugs. *Science*. 1997 Nov 7;278(5340):1064–1068.
 107. Hegde ML, Hazra TK, Mitra S. Early steps in the DNA base excision/ single-strand interruption repair pathway in mammalian cells. *Cell Res*. 2008 Jan;18(1):27–47.
 108. Purnell MR, Whish WJ. Novel inhibitors of poly(ADP-ribose) synthetase. *Biochem J*. 1980 Mar 1;185(3):775–777.
 109. Farmer H, McCabe N, Lord CJ, et al. Targeting the DNA repair defect in BRCA mutant cells as a therapeutic strategy. *Nature*. 2005 Apr 14;434(7035):917–921.
 110. Bryant HE, Schultz N, Thomas HD, et al. Specific killing of BRCA2- deficient tumours with inhibitors of poly(ADP-ribose) polymerase. *Nature*. 2005 Apr 14;434(7035):913–917.
 111. Gelmon KA, Tischkowitz M, Mackay H, et al. Olaparib in patients with recurrent high-grade serous or poorly differentiated ovarian carcinoma or triple-negative breast cancer: a phase 2, multicentre, open-label, non-randomised study. *Lancet Oncol*. 2011 Sep;12 (9):852–861.
 112. Fong PC, Boss DS, Yap TA, et al. Inhibition of poly(ADP-ribose) polymerase in tumors from BRCA mutation carriers. *N Engl J Med*. 2009 Jul 9;361(2):123–134.
 113. Mirza MR, Monk BJ, Herrstedt J, et al. Niraparib maintenance therapy in platinum-sensitive, recurrent ovarian cancer. *N Engl J Med*. 2016 Dec 1;375(22):2154–2164.
 114. Lord CJ, Ashworth A. PARP inhibitors: synthetic lethality in the clinic. *Science*. 2017 Mar 17;355(6330):1152–1158.
 115. Brown JS, Kaye SB, Yap TA. PARP inhibitors: the race is on. *Br J Cancer*. 2016 Mar 29;114(7):713–715.
 116. Murai J, Huang SY, Renaud A, et al. Stereospecific PARP trapping by BMN 673 and comparison with olaparib and rucaparib. *Mol Cancer Ther*. 2014 Feb;13(2):433–443.
 117. Pommier Y, O’Connor MJ, De Bono J. Laying a trap to kill cancer cells: PARP inhibitors and their mechanisms of action. *Sci Transl Med*. 2016 Oct 26;8(362):362ps17.
 118. Shen Y, Rehman FL, Feng Y, et al. BMN 673, a novel and highly potent PARP1/2 inhibitor for the treatment of human cancers with DNA repair deficiency. *Clin Cancer Res*. 2013 Sep 15;19(18):5003–5015.
 119. Wang M, Wu W, Wu W, et al. PARP-1 and ku compete for repair of DNA double strand breaks by distinct NHEJ pathways. *Nucleic Acids Res*. 2006;34(21):6170–6182.
 120. Li B, Navarro S, Kasahara N, et al. Identification and biochemical characterization of a Werner’s syndrome protein complex with Ku70/80 and poly(ADP-ribose) polymerase-1. *J Biol Chem*. 2004 Apr 2;279(14):13659–13667.
 121. Patel AG, Sarkaria JN, Kaufmann SH. Nonhomologous end joining drives poly(ADP-ribose) polymerase (PARP) inhibitor lethality in homologous recombination-deficient cells. *Proc Natl Acad Sci U S A*. 2011 Feb 22; 108(8):3406–3411.
 122. Kaufman B, Shapira-Frommer R, Schmutzler RK, et al. Olaparib monotherapy in patients with advanced cancer and a germline BRCA1/2 mutation. *J Clin Oncol*. 2015 Jan 20;33(3):244–250.
 123. Ledermann J, Harter P, Gourley C, et al. Olaparib maintenance therapy in platinum-sensitive

- relapsed ovarian cancer. *N Engl J Med*. 2012 Apr 12;366(15):1382–1392.
124. Oza AM, Cibula D, Benzaquen AO, et al. Olaparib combined with chemotherapy for recurrent platinum-sensitive ovarian cancer: a randomised phase 2 trial. *Lancet Oncol*. 2015 Jan;16(1):87–97.
 125. Ledermann J, Harter P, Gourley C, et al. Olaparib maintenance therapy in patients with platinum-sensitive relapsed serous ovarian cancer: a preplanned retrospective analysis of outcomes by BRCA status in a randomised phase 2 trial. *Lancet Oncol*. 2014 Jul;15 (8):852–861.
 126. Van Der Noll R, Marchetti S, Steeghs N, et al. Long-term safety and anti-tumour activity of olaparib monotherapy after combination with carboplatin and paclitaxel in patients with advanced breast, ovarian or fallopian tube cancer. *Br J Cancer*. 2015 Jul 28;113 (3):396–402.
 127. Domchek SM, Aghajanian C, Shapira-Frommer R, et al. Efficacy and safety of olaparib monotherapy in germline BRCA1/2 mutation carriers with advanced ovarian cancer and three or more lines of prior therapy. *Gynecol Oncol*. 2016 Feb;140(2):199–203.
 128. Lee JM, Hays JL, Annunziata CM, et al. Phase I/Ib study of olaparib and carboplatin in BRCA1 or BRCA2 mutation-associated breast or ovarian cancer with biomarker analyses. *J Natl Cancer Inst*. 2014 May 19;106(6):dju089.
 129. Bindra RS, Schaffer PJ, Meng A, et al. Down-regulation of Rad51 and decreased homologous recombination in hypoxic cancer cells. *Mol Cell Biol*. 2004 Oct;24(19):8504–8518.
 130. Lim JJ, Yang K, Taylor-Harding B, et al. VEGFR3 inhibition chemosensitizes ovarian cancer stemlike cells through downregulation of BRCA1 and BRCA2. *Neoplasia*. 2014 Apr;16(4):343,53. e1-2.
 131. Liu JF, Barry WT, Birrer M, et al. Combination cediranib and olaparib versus olaparib alone for women with recurrent platinum-sensitive ovarian cancer: a randomised phase 2 study. *Lancet Oncol*. 2014 Oct;15(11):1207–1214.
 132. Engelman JA, Luo J, Cantley LC. The evolution of phosphatidylinositol 3-kinases as regulators of growth and metabolism. *Nat Rev Genet*. 2006 Aug;7(8):606–619.
 133. Kumar A, Fernandez-Capetillo O, Carrera AC. Nuclear phosphoinositide 3-kinase beta controls double-strand break DNA repair. *Proc Natl Acad Sci U S A*. 2010 Apr 20;107(16):7491–7496.
 134. Juvekar A, Burga LN, Hu H, et al. Combining a PI3K inhibitor with a PARP inhibitor provides an effective therapy for BRCA1-related breast cancer. *Cancer Discov*. 2012 Nov;2(11):1048–1063.
 135. Ibrahim YH, Garcia-Garcia C, Serra V, et al. PI3K inhibition impairs BRCA1/2 expression and sensitizes BRCA-proficient triple-negative breast cancer to PARP inhibition. *Cancer Discov*. 2012 Nov;2 (11):1036–1047.
 136. Gonzalez-Billalabeitia E, Seitzer N, Song SJ, et al. Vulnerabilities of PTEN-TP53-deficient prostate cancers to compound PARP-PI3K inhibition. *Cancer Discov*. 2014 Aug;4(8):896–904.
 137. Johnson N, Li YC, Walton ZE, et al. Compromised CDK1 activity sensitizes BRCA-proficient cancers to PARP inhibition. *Nat Med*. 2011 Jun 26;17(7):875–882.
 138. Johnson SF, Cruz C, Greifenberg AK, et al. CDK12 inhibition reverses de novo and acquired PARP inhibitor resistance in BRCA wild-type and mutated models of triple-negative breast cancer. *Cell Rep*. 2016 Nov 22;17(9):2367–2381.
 139. Jirawatnotai S, Hu Y, Michowski W, et al. A function for cyclin D1 in DNA repair uncovered by protein interactome analyses in human cancers. *Nature*. 2011 Jun 8;474(7350):230–234.
 140. Bergs JW, Krawczyk PM, Borovski T, et al. Inhibition of homologous recombination by hyperthermia shunts early double strand break repair to non-homologous end-joining. *DNA Repair (Amst)*. 2013 Jan 1;12(1):38–45.
 141. Krawczyk PM, Eppink B, Essers J, et al. Mild hyperthermia inhibits homologous recombination, induces BRCA2 degradation, and sensitizes cancer cells to poly (ADP-ribose) polymerase-1 inhibition. *Proc Natl Acad Sci U S A*. 2011 Jun 14;108(24):9851–9856.
 142. Sakai W, Swisher EM, Karlan BY, et al. Secondary mutations as a mechanism of cisplatin resistance in BRCA2-mutated cancers. *Nature*. 2008 Feb 28;451(7182):1116–1120.
 143. Swisher EM, Sakai W, Karlan BY, et al. Secondary BRCA1 mutations in BRCA1-mutated ovarian carcinomas with platinum resistance. *Cancer Res*. 2008 Apr 15; 68(8):2581–2586.
 144. Easton DF, Deffenbaugh AM, Pruss D, et al. A systematic genetic assessment of 1,433 sequence variants of unknown clinical significance in the BRCA1 and BRCA2 breast cancer-predisposition genes. *Am J Hum Genet*. 2007 Nov;81(5):873–883.
 145. Ter Brugge P, Kristel P, Van Der Burg E, et al. Mechanisms of therapy resistance in patient-derived xenograft models of BRCA1- deficient breast cancer. *J Natl Cancer Inst*. 2016 Jul 5;108(11). Print 2016 Nov. doi:10.1093/jnci/djw148.
 146. Patch AM, Christie EL, Etemadmoghadam D, et al. Whole-genome characterization of

- chemoresistant ovarian cancer. *Nature*. 2015 May 28;521(7553):489–494.
147. Cao L, Xu X, Bunting SF, et al. A selective requirement for 53BP1 in the biological response to genomic instability induced by Brca1 deficiency. *Mol Cell*. 2009 Aug 28;35(4):534–541.
 148. Iwabuchi K, Bartel PL, Li B, et al. Two cellular proteins that bind to wild-type but not mutant p53. *Proc Natl Acad Sci U S A*. 1994 Jun 21;91(13):6098–6102.
 149. Wang B, Matsuoka S, Carpenter PB, et al. 53BP1, a mediator of the DNA damage checkpoint. *Science*. 2002 Nov 15;298(5597):1435–1438.
 150. Bouwman P, Aly A, Escandell JM, et al. 53BP1 loss rescues BRCA1 deficiency and is associated with triple-negative and BRCAmutated breast cancers. *Nat Struct Mol Biol*. 2010 Jun;17(6):688–695.
 151. Bunting SF, Callen E, Wong N, et al. 53BP1 inhibits homologous recombination in Brca1-deficient cells by blocking resection of DNA breaks. *Cell*. 2010 Apr 16;141(2):243–254.
 152. Kass EM, Moynahan ME, Jasin M. Loss of 53BP1 is a gain for BRCA1 mutant cells. *Cancer Cell*. 2010 May 18;17(5):423–425.
 153. Chapman JR, Barral P, Vannier JB, et al. RIF1 is essential for 53BP1-dependent nonhomologous end joining and suppression of DNA double-strand break resection. *Mol Cell*. 2013 Mar 7;49(5):858–871.
 154. Gottipati P, Vischioni B, Schultz N, et al. Poly(ADP-ribose) polymerase is hyperactivated in homologous recombination-defective cells. *Cancer Res*. 2010 Jul 1;70(13):5389–5398.
 155. Liu X, Han EK, Anderson M, et al. Acquired resistance to combination treatment with temozolomide and ABT-888 is mediated by both base excision repair and homologous recombination DNA repair pathways. *Mol Cancer Res*. 2009 Oct;7(10):1686–1692.
 156. Zaremba T, Ketzner P, Cole M, et al. Poly(ADP-ribose) polymerase-1 polymorphisms, expression and activity in selected human tumour cell lines. *Br J Cancer*. 2009 Jul 21;101(2):256–262.
 157. McCabe N, Turner NC, Lord CJ, et al. Deficiency in the repair of DNA damage by homologous recombination and sensitivity to poly (ADP-ribose) polymerase inhibition. *Cancer Res*. 2006 Aug 15;66(16):8109–8115.
 158. Moghadasi S, Hofland N, Wouts JN, et al. Variants of uncertain significance in BRCA1 and BRCA2 assessment of in silico analysis and a proposal for communication in genetic counselling. *J Med Genet*. 2013 Feb;50(2):74–79.
 159. Bouwman P, Van Der Gulden H, Van Der Heijden I, et al. A highthroughput functional complementation assay for classification of BRCA1 missense variants. *Cancer Discov*. 2013 Oct;3(10):1142–1155.
 160. Eccles DM, Mitchell G, Monteiro AN, et al. BRCA1 and BRCA2 genetic testing-pitfalls and recommendations for managing variants of uncertain clinical significance. *Ann Oncol*. 2015 Oct;26(10):2057–2065.
 161. Norquist B, Wurz KA, Pennil CC, et al. Secondary somatic mutations restoring BRCA1/2 predict chemotherapy resistance in hereditary ovarian carcinomas. *J Clin Oncol*. 2011 Aug 1;29(22):3008–3015.
 162. Joosse SA, van Beers EH, Tielen IH, et al. Prediction of BRCA1- association in hereditary non-BRCA1/2 breast carcinomas with array-CGH. *Breast Cancer Res Treat*. 2009 Aug;116(3):479–489.
 163. Vollebbergh MA, Lips EH, Nederlof PM, et al. An aCGH classifier derived from BRCA1-mutated breast cancer and benefit of highdose platinum-based chemotherapy in HER2-negative breast cancer patients. *Ann Oncol*. 2011 Jul;22(7):1561–1570.
 164. Davies H, Glodzik D, Morganella S, et al. HRDetect is a predictor of BRCA1 and BRCA2 deficiency based on mutational signatures. *Nat Med*. 2017 Apr;23(4):517–525.
 165. Norquist BM, Harrell MI, Brady MF, et al. Inherited mutations in women with ovarian carcinoma. *JAMA Oncol*. 2016 Apr;2(4):482–490.
 166. Watkins JA, Irshad S, Grigoriadis A, et al. Genomic scars as biomarkers of homologous recombination deficiency and drug response in breast and ovarian cancers. *Breast Cancer Res*. 2014 Jun 3;16(3):211.
 167. Timms KM, Abkevich V, Hughes E, et al. Association of BRCA1/2 defects with genomic scores predictive of DNA damage repair deficiency among breast cancer subtypes. *Breast Cancer Res*. 2014 Dec 5;16(6):475,014-0475-x.
 168. Patel J, Sehoul J, Timms K, et al. Characteristics of homologous recombination deficiency (HRD) in paired primary and recurrent high-grade serous ovarian cancer (HGSOC). *Ann Oncol*. 2016;27(suppl_6):113
 169. Telli ML, Timms KM, Reid J, et al. Homologous recombination deficiency (HRD) score predicts response to platinum-containing neoadjuvant chemotherapy in patients with triple-negative

- breast cancer. *Clin Cancer Res.* 2016 Aug 1;22(15):3764–3773.
170. Haaf T, Golub EI, Reddy G, et al. Nuclear foci of mammalian Rad51 recombination protein in somatic cells after DNA damage and its localization in synaptonemal complexes. *Proc Natl Acad Sci U S A.* 1995 Mar 14;92(6):2298–2302.
 171. Yuan SS, Lee SY, Chen G, et al. BRCA2 is required for ionizing radiation-induced assembly of Rad51 complex in vivo. *Cancer Res.* 1999 Aug 1;59(15):3547–3551.
 172. Shah MM, Dobbin ZC, Nowsheen S, et al. An ex vivo assay of XRT-induced Rad51 foci formation predicts response to PARP-inhibition in ovarian cancer. *Gynecol Oncol.* 2014 Aug;134(2):331–337.
 173. Mukhopadhyay A, Elattar A, Cerbinskaite A, et al. Development of a functional assay for homologous recombination status in primary cultures of epithelial ovarian tumor and correlation with sensitivity to poly(ADP-ribose) polymerase inhibitors. *Clin Cancer Res.* 2010 Apr 15;16(8):2344–2351.
 174. van Veelen LR, Essers J, van de Rakt MW, et al. Ionizing radiation-induced foci formation of mammalian Rad51 and Rad54 depends on the Rad51 paralogs, but not on Rad52. *Mutat Res.* 2005 Jul 1;574 (1–2):34–49.
 175. Wohlschlegel JA, Kutok JL, Weng AP, et al. Expression of geminin as a marker of cell proliferation in normal tissues and malignancies. *Am J Pathol.* 2002 Jul;161(1):267–273.
 176. Naipal KA, Verkaik NS, Ameziane N, et al. Functional ex vivo assay to select homologous recombination-deficient breast tumors for PARP inhibitor treatment. *Clin Cancer Res.* 2014 Sep 15;20(18):4816–4826.
 177. Mutter RW, Riaz N, Ng CK, et al. Bi-allelic alterations in DNA repair genes underpin homologous recombination DNA repair defects in breast cancer. *J Pathol.* 2017 Mar 15. doi:10.1002/path.4890.
 178. Graeser M, McCarthy A, Lord CJ, et al. A marker of homologous recombination predicts pathologic complete response to neoadjuvant chemotherapy in primary breast cancer. *Clin Cancer Res.* 2010 Dec 15;16(24):6159–6168.

Functional RAD51 based assay predicts in vivo PARP inhibitor response in ovarian cancer models beyond BRCA

Francien Talens¹, Vivian O.N. Teixeira¹, Efraim H. Rosenberg², Petra M. Nederlof², Rashmie D. Debipersad², Marketa Janatova³, Petra Zemankova³, Zdenek Kleibl³, Evelien W. Duiker⁴, G. Bea A. Wisman⁵, Steven de Jong¹ & Marcel A.T.M. van Vugt¹

¹ Department of Medical Oncology, University Medical Center Groningen, University of Groningen, Groningen, The Netherlands.

² Department of Pathology, Netherlands Cancer Institute, Amsterdam, The Netherlands.

³ Institute of Biochemistry and Experimental Oncology, First Faculty of Medicine, Charles University, Prague, Czech Republic.

⁴ Department of Pathology and Medical Biology, University Medical Center Groningen, University of Groningen, Groningen, The Netherlands.

⁵ Department of Gynecologic Oncology, University Medical Center Groningen, University of Groningen, Groningen, The Netherlands.

Abstract

Purpose: A majority of ovarian cancers, especially within the high-grade serous (HGSOC) subtype, is thought to be defective in homologous recombination (HR) and might therefore benefit from PARP inhibitor treatment. Currently, only patients with proven BRCA1/2 mutations are included for PARP inhibitor treatment. In this study, we aim to correlate genomic features, ex-vivo functionality of HR, and replication fork stability to *in vivo* PARP inhibitor response of ovarian cancer patient-derived xenograft (PDX) models.

Experimental design: BRCA1/2 mutation status, BRCA1 promoter methylation, and copy-number variations (CNVs) were analyzed in a cohort of ovarian cancer PDX models. 15 PDX models were assessed for *in vivo* PARP inhibitor (olaparib) sensitivity. In parallel, freshly isolated *ex vivo* tumor tissue was used for the detection of irradiation-induced RAD51 foci formation and replication fork stability, using single DNA fiber analyses. Targeted panel sequencing was applied to olaparib-sensitive models, lacking BRCA1/2 alterations.

Results: In our cohort, 22.6% (7/31) harbored a BRCA1/2 alteration and 48.3% (15/31) was considered genomically unstable, based on CNV profiles. 5 BRCA1/2-altered PDX models were included for *in vivo* olaparib sensitivity from which 4 responded. 8 out of 12 included genomically unstable PDX models responded to *in vivo* olaparib of which 4 did not have a BRCA1/2 alteration. Replication fork protection or replication speed in *ex vivo* tumor tissue did not correlate to *in vivo* olaparib responses, whereas the RAD51-based RECAP assay identified all models that responded to olaparib *in vivo*, including the 4 models without BRCA1/2 alterations. Genomic sequence analysis of a panel of DNA repair-associated genes revealed mutations as a possible underlying cause of HR deficiency.

Conclusions: The *ex vivo* RECAP assay effectively predicts *in vivo* olaparib response and identified a subset of PARP inhibitor sensitive, HR-deficient ovarian cancer PDX tumors, lacking a BRCA1/2 alteration. Assessment of HR functionality in the clinic is warranted to select patients for PARP inhibitor treatment.

Introduction

Ovarian cancer is the 8th most common cancer type among women worldwide and survival rates have hardly improved over the last decades¹. High grade serous ovarian cancer (HGSOC) is the most common subtype of ovarian cancer (~70%). It is frequently diagnosed in an advanced stage (60% diagnosed with stage III) with a 5-year relative survival rate of 30%². The current treatment of HGSOC consists of surgery combined with (neo)adjuvant platinum-based chemotherapy.

Approximately 15-20% of HGSOC are characterized by BRCA1/2 mutations or BRCA1 promoter hypermethylation³. BRCA1 and BRCA2 function in homologous recombination (HR), an error-free pathway to repair toxic DNA double-stranded breaks (DSBs)⁴. HR proteins, such as BRCA1 and BRCA2, have additional functions in preventing chromosomal instability as they prevent degradation of nascent DNA at stalled replication forks^{5,6}.

Patients carrying a germline BRCA1 or BRCA2 mutation have a highly increased lifetime risk to develop breast and/or ovarian cancer^{7,8}. Tumor cells that lack efficient HR are sensitive to treatment with inhibitors of the Poly(ADP-ribose) polymerase (PARP) enzyme, which functions in single-strand break (SSB) repair^{9,10}. The cytotoxic effect of PARP inhibition in HR defective cells is caused by impairment of SSB repair and trapping of the PARP enzyme onto the DNA, which results in the stalling and subsequent collapse of replication forks^{11,12}. Several PARP inhibitors, including olaparib, niraparib, and rucaparib, have been clinically evaluated and showed improved progression-free survival in BRCA1/2 mutated ovarian cancer and therefore resulted in FDA approval¹³⁻¹⁷.

Currently, PARP inhibitors are approved for use in BRCA1/2 mutant ovarian and BRCA1/2 mutant HER2-negative metastatic breast cancers¹⁸. However, PARP inhibitor treatment might

be efficient beyond tumors with a proven BRCA1/2 mutation. It was suggested that up to 50% of HGSOV is HR-deficient, caused for example by mutation or epigenetic silencing of other HR genes, including PALB2, CHEK1/2, RAD51C, RAD51D, and ATM^{3,19–21}. In line with this notion, several clinical trials have shown proven efficacy of PARP inhibitors beyond BRCA1/2-mutated ovarian cancer^{14,22}. Using the current patient selection strategy, only patients with a proven BRCA1/2 mutation are eligible for treatment with PARP inhibitors, and patients with HR-deficient tumors without BRCA1/2 mutations are excluded from PARP inhibitor treatment.

Conversely, several mechanisms have been described by which HR-defective tumors become resistant to PARP inhibitor treatment²³. For instance, inactivation of TP53BP1^{24,25}, REV7²⁶, and Shieldin complex genes^{27,28} were shown to restore HR in BRCA1 mutant cancer cells and lead to PARP inhibitor resistance in experimental models. Similarly, mutations in the CST genes rescue HR in BRCA1 mutant cancer cells and lead to PARP inhibitor insensitivity²⁹. Also for BRCA2 mutant cells, mechanisms were described to restore DNA repair. Specifically, mutations in PAXIP2, which rescues replication fork stability in BRCA2-mutant cells, were shown to determine PARP inhibitor sensitivity³⁰. Tumor cells with such secondary genetic events would not respond to PARP inhibitor treatment, despite a mutant BRCA1/2 status.

Several HR deficiency (HRD) tests have been developed to select patients for treatment with PARP inhibitors³¹. For example, the myChoice HRD test combines BRCA1/2 mutation status with different measurements of genomic instability in tumor cells, including loss-of-heterozygosity (LOH), telomeric imbalance, and large-scale state transitions, and has demonstrated varying results in predicting platinum response in triple-negative breast cancer (TNBC)^{32,33}. Unfortunately, it did not predict response to PARP inhibitors in platinum-sensitive ovarian cancer¹⁴. In a different approach, algorithms were developed on whole-genome sequencing profiles to distinguish BRCA1/2-mutated breast cancers from sporadic breast cancer^{34,35}. Of these, the HRDetect algorithm was able to detect HR-deficient tumors without BRCA1/2 mutations in different cancer types and HRDetect scores were associated with response to platinum-based chemotherapy in advanced breast cancer, independently of BRCA1/2 mutation status³⁶.

Since both BRCA1/2 mutation analysis and analysis of genomic features associated with HR deficiency do not per se reflect actual HR functionality, these assays may therefore not be adequate in the proper selection of patients that benefit from PARP inhibitor treatment. Therefore, an ex vivo functional test for HR pathway proficiency was developed, which assesses the foci formation of the RAD51 recombinase³⁷. The loading of RAD51 onto ssDNA at DSBs is the final and crucial step in HR and can be visualized with immunofluorescence³⁸. Although this approach does not take into account all functions of HR proteins, including replication fork protection, this assay successfully identified breast cancers that did not have BRCA1/2 mutations, but was not able to recruit RAD51 foci and was therefore considered HR deficient^{39,40}. Also, functional HR testing could predict platinum sensitivity in ovarian cancer patients⁴¹. Furthermore, the formation of RAD51 foci correlated to PARP inhibitor resistance in BRCA1/2 mutant breast cancer models, regardless of the underlying resistance mechanism^{42,43}. In primary cultures derived from ascitic fluid from ovarian cancer patients, RAD51 foci formation correlated to in vitro PARP inhibition⁴⁴. However, it remains unclear whether responses to PARP inhibition can be predicted in vivo using functional HR assays in ovarian cancer models.

In this study, we used genomic analysis and functional assays to study HR deficiency and predict olaparib response in a cohort of patient-derived xenograft (PDX) ovarian cancer models. To this end, BRCA1/2 mutation status, BRCA1 promoter methylation, and copy-number variations (CNVs) were determined as a readout for genomic instability. Also, RAD51 foci formation and replication fork stability were assessed in ex vivo tumor tissues. Finally,

Table 1. Tumor characteristics of PDX models included in the study. Highlighted models were included for *in vivo* PARP inhibitor sensitivity

PDX #	Tumor type	Grade	Stage	Tissue origin	Follow up
30	Serous cystadenocarcinoma	High	IIIC	Diagnostic laparotomy	Relapse after 24 months, deceased
37	Serous cystadenocarcinoma	High	IIIC	Diagnostic laparotomy	No signs of recurrence (2015)
56	Serous cystadenocarcinoma	High	IIIC	Interval debulking	No signs of recurrence (2015)
60	Serous cystadenocarcinoma	High	IIA	Diagnostic laparotomy	Deceased, 17 months
61	Mucinous adenocarcinoma	Undifferentiated	IV	Diagnostic laparotomy	Deceased
67	Serous cystadenocarcinoma	High	IIIC	Diagnostic laparotomy	No signs of recurrence (2015)
68	Ovarian carcinosarcoma	High	IIC	Diagnostic laparotomy	Recurrence 29 months after last chemo. Re-debulkin. Deceased 40 months
70	Serous adenocarcinoma with partial oxyfile clearcell component	High	IIIA	Diagnostic laparotomy	Deceased
79	Serous cystadenocarcinoma	Low	IIIC	Diagnostic laparotomy	Bad response: Palliative situation
81	Endometrioid adenocarcinoma	Moderate	IC	Diagnostic laparotomy	No signs of recurrence
84	Serous cystadenocarcinoma	High	IV	Diagnostic laparotomy	No signs of recurrence (2015)
102	Unknown			Diagnostic laparotomy	Unknown
112	Endometrioid adenocarcinoma	High	IIIC	Diagnostic laparotomy	No signs of recurrence
130	Serous cystadenocarcinoma	High	IIIB	Diagnostic laparotomy	No signs of recurrence
143	Serous cystadenocarcinoma	High	IIIC	Interval debulking	Deceased 11 months
157	Endometrioid adenocarcinoma	High	IV	Diagnostic laparotomy	Deceased 6 months
167	Endometrioid adenocarcinoma	Moderate	IA	Interval debulking	Recurrence 50 months
171	Serous cystadenocarcinoma	High	III	Recurrence 2010	Recurrence 38 months, deceased 51
174	Serous cystadenocarcinoma	High	IV	Interval debulking	Good response
176	Serous cystadenocarcinoma		IIIC	Diagnostic laparotomy	No signs of recurrence. Deceased 9 months
177	Serous cystadenocarcinoma with partial clear cell differentiation	High	IIC	Diagnostic laparotomy	
179	Serous cystadenocarcinoma	High	IIIC	Interval debulking	Interval: good clinical response, deceased 9 months
187	Serous cystadenocarcinoma	High	IIIC	Interval debulking	Interval: good response
188	Serous cystadenocarcinoma	High	IIIC	Primary debulking	Progression within 6 months after chemotherapy (deceased)
189	Endometrioid adenocarcinoma	High	IC	Diagnostic laparotomy	Disease free at last follow-up (10 months)
191	Ovarian carcinosarcoma		IIIC	Primary debulking	Recurrence 20 months
193	Serous cystadenocarcinoma	High	IIIC	Diagnostic laparotomy	Adjuvant chemotherapy
195	Serous cystadenocarcinoma	High	IV	Diagnostic laparotomy	Complete debulking, adjuvant chemotherapy
203	Serous cystadenocarcinoma	High	IIIC	Primary debulking	Disease-free at last follow-up (25 months)
207	Serous cystadenocarcinoma	High	IIIC	Diagnostic laparotomy	Disease-free at last follow-up (36 months)
208	Endometrioid adenocarcinoma	Low	IIB	Diagnostic laparotomy	Disease-free at last follow-up (18 months)

functional assays and genomic features were related to *in vivo* olaparib responses and showed that *ex vivo* RAD51 foci formation most effectively predicted olaparib response, and identified a subset of HR-deficient HGSOC PDX tumors not harboring a BRCA1/2 alteration, that responded to PARP inhibition.

Results

Characterization and selection of ovarian cancer PDX models

To study the response of ovarian cancer towards the PARP inhibitor olaparib, we studied 31 pre-established ovarian PDX models⁴⁵. Based on retrieved pathology reports, 21 out of 31 PDX models represented HGSOC, whereas other models represented carcinosarcoma, mucinous- or endometrioid adenocarcinoma (**Table 1**). Genomic DNA from first generation (F1) PDX tumor pieces was extracted and was used to analyze BRCA1/2 alterations. Out of 31 PDX models, 7 models harbored a pathogenic BRCA1 or BRCA2 alteration (**Table 1**). Of these models, only PDX177 and PDX203 had a BRCA2 deletion with an allele frequency above 50%, suggesting that the other BRCA1/2 alterations can be considered heterozygous, without loss of heterozygosity (LOH). In addition to the observed genomic alterations, PDX84 showed BRCA1 promoter hypermethylation, which results in BRCA1 gene silencing.

As a readout for genomic instability, levels of CNVs were determined based on

PDX #	BRCA1 mutation	BRCA2 mutation	BRCA1 promoter methylation	CNV profile	MSI status	BRCA1 classifier
30				D	stable	
37				E	stable	yes
56				D	stable	yes
60				C	stable	
61				C	stable	
67				E	stable	
68				A	stable	
70				E	stable	
79				B	stable	
81	Deletion c.1823delA: p.K608fs in exon 11 of 50%			A	MSI-high	
84			BRCA1 promoter methylation	E	stable	yes
102				A	stable	
112				A	stable	
130				C	stable	
143				E	stable	yes
157				B	stable	
167				B	stable	
171				A	stable	
174				D	stable	
176				D	stable	
177		Deletion c.1457delA: p.Q486fs in exon 10 of 97%		D	stable	
179				B	stable	
187				D	stable	
188				C	stable	
189		Deletion c.9097delA: p.T3033fs in exon 23 of 51%		B	MSI-high	
191				D	stable	
193	Exon 3 duplication			E	stable	
195	Deletion c.5542del: p.Q1848fs in exon 24 of 51%			D	stable	yes
203		Deletion c.7007_7007+1delinsTT, a splice mutation in exon 13 of 75%		D	stable	yes
207				A	stable	
208				A	stable	

CNVseq profiles obtained by low-coverage whole-genome sequencing of F1 tumor DNA (**Supplementary Figure 1A**). PDX models were classified into 5 categories ranging from a ‘flatline’ category that contained very few CNVs (category A) towards genomically unstable categories with high amounts of CNVs (category E). In total, 15 models were considered genomically unstable, based on a CNV category D or E. Notably, not all PDX models with BRCA1/2 alterations showed high levels of CNVs (i.e. PDX81, PDX189), in line with these models not representing HGSOE but endometrioid tumors, and not having homozygous BRCA1/2 alterations (**Table 1, Supplementary Figure 1B**). Additionally, analysis of microsatellite instability (MSI) status was performed on all PDX models and identified both BRCA1/2-mutated endometrioid models (PDX81, PDX189) with an MSI-high profile (**Table 1**).

As BRCAness correlates with high levels of genomic instability and is associated with PARP inhibitor response, all tumor models with D or E CNV categories were included for in vivo assessment of olaparib sensitivity³⁴. Additionally, two PDX models without BRCA1/2 alterations and considered genomically stable (category A; PDX68 and PDX112) were included for reference (**Supplementary Figure 1B**). Furthermore, all models that harbored a BRCA1/2 alteration were included, regardless of their CNVs category. From 19 selected PDX models included for in vivo PARP inhibitor response assessment, four could not be analyzed due to limited tissue availability (PDX203), no tumor development after re-implantation (PDX70, PDX189), or absence of human tumor cells (PDX30). Ultimately, 15 PDX models were included

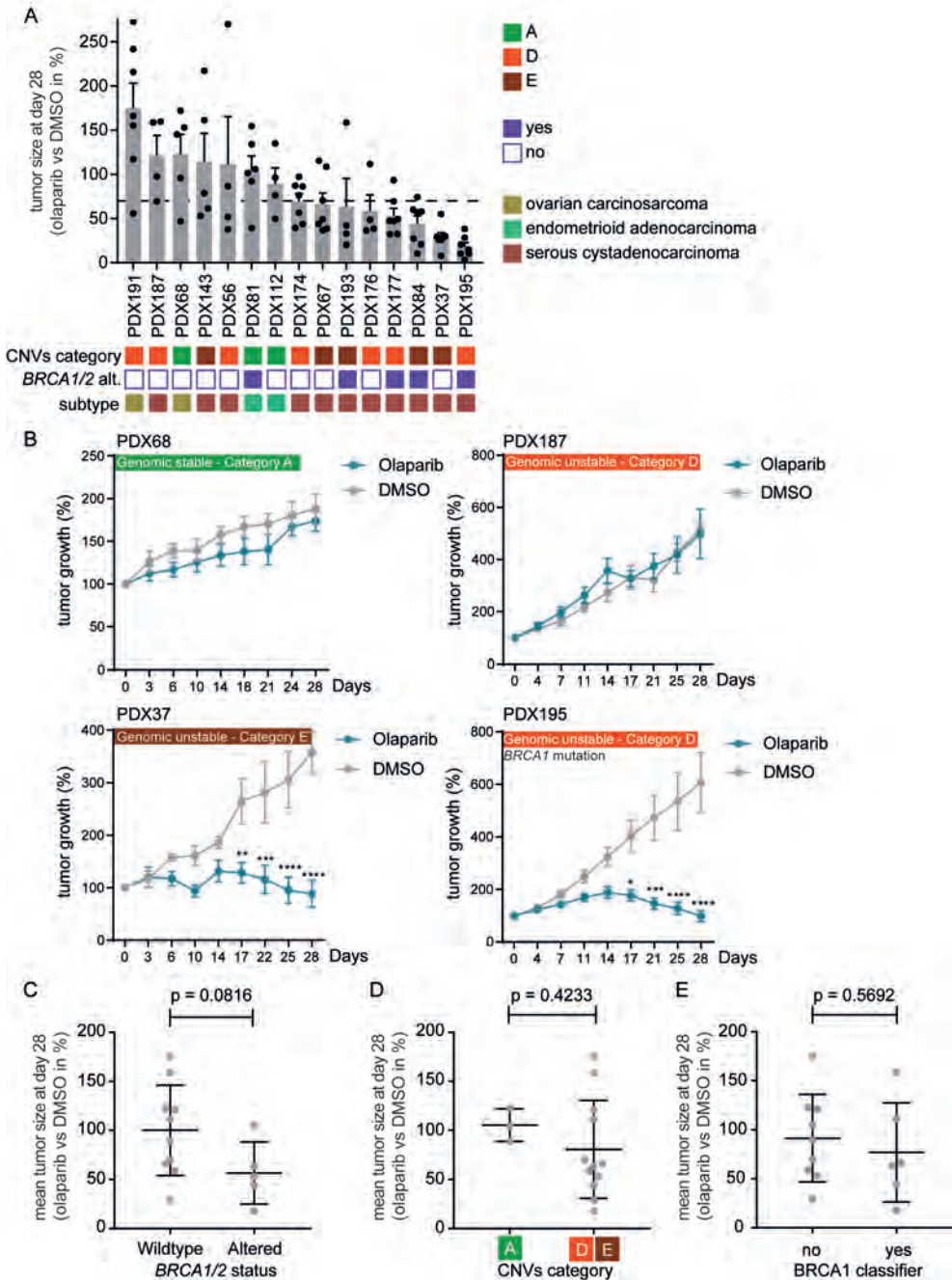


Figure 1. Response to olaparib in BRCA1/2-altered or genomically unstable ovarian PDX models. **A)** Mice were treated for 28 days with olaparib or solvent (DMSO). Bars show the mean tumor size at day 28 in the olaparib-treated group relative to the mean tumor size at day 28 in the solvent-treated group. Each dot represents one olaparib-treated mouse ($n \geq 4$). Data are shown as mean \pm SEM of olaparib-treated mice. A decrease in at least 30% of tumor size (partial response) is marked by a

for in vivo determination of PARP inhibitor sensitivity and further ex vivo analyses (highlighted in **Table 1**).

PARP inhibitor response in relation to BRCA1/2 status or levels of genomic instability

The selected 15 ovarian cancer PDX models were treated for 28 days with olaparib or a solvent control treatment. In total, 8 out of 15 models showed a response to olaparib, as assessed by a decrease of at least 30% (partial response, RECIST criteria) in mean tumor growth at the end of treatment in the olaparib-treated group versus the mean tumor growth in the control-treated group (**Figure 1A**). As expected, both PDX models in CNV category A and lacking BRCA1/2 alterations (PDX68 and PDX112), did not respond to olaparib (**Figure 1A, B**). For models categorized as genomically unstable (CNVs category D, E), 8 did respond to olaparib whereas 4 did not (**Figure 1A, B**). Of the 5 PDX models with BRCA1/2 alterations, 1 model (PDX81) did not respond to olaparib, likely explained by the lack of LOH, corresponding low level of genomic instability (CNVs category A), and an endometrioid tumor type. Tumor growth curves, final tumor growth percentages, and tumor weights upon olaparib or control treatment for individual PDX models can be found in **Supplementary Figure 2** and **3**.

Previously, BRCA1/2 mutational status was shown to be associated with olaparib response in breast cancer and ovarian cancer patients^{16,18}. Analysis of tumor responses to olaparib versus BRCA1/2 mutation status showed that BRCA1/2 mutational status alone was not sufficient to predict responses to olaparib in this specific ovarian cancer cohort (**Figure 1C**), with some BRCA1/2 mutant models not responding to treatment (i.e. PDX81), whereas olaparib-sensitive models also included BRCA1/2 wt tumors (PDX37, PDX176, PDX67, PDX174) (**Figure 1C**). We next assessed if the level of genomic instability was associated with response to olaparib. Whereas all 3 PDX models in category A did not respond to olaparib, 8/12 models in CNVs category D or E responded to olaparib (**Figure 1D**), underscoring that CNVs categories are not sufficient to separate olaparib-sensitive from olaparib-insensitive models (**Figure 1D**). For diagnostic purposes in breast cancer, a BRCA1 classifier was developed to identify tumors with a 'BRCA1-like' phenotype⁴⁹. Application of a modified version of the breast cancer BRCA1 classifier to our selected ovarian PDX models, identified 6 out of 15 models as a 'BRCA1-like' tumors (**Table 1**, last column). However, 2 of these 6 models did not respond to olaparib, whereas 4 PDX models were not identified as 'BRCA1-like' but did respond to olaparib (**Figure 1E**). Combined, these data show that the presence of genomic BRCA1/2 alterations, nor levels of CNVs or BRCA1 classifier scores predicted response to olaparib in this cohort of ovarian cancer models.

*dashed line at 70%. Boxes show characteristics of each PDX model. First row represents CNVs category A (green), D (orange) or E (brown). Purple boxes represent the presence of a BRCA1/2 mutation or BRCA1 hypermethylation. Last row represents ovarian cancer subtypes for the primary tumor origin. B) Representative tumor growth curves of individual PDX models treated with olaparib (blue) or solvent (grey). Percentages of tumor growth were calculated as tumor volume at day x compared to tumor volume at day 0. Data are shown as mean \pm SEM of at least 4 mice per group. P values were calculated using two-way ANOVA with Bonferroni correction. * $P < 0.05$, ** $P < 0.01$ and *** $P < 0.001$. C) Mean tumor size at day 28 in olaparib-treated mice was normalized to mean tumor size in solvent-treated mice as a measure of olaparib response (<100%). Every dot represents mean response one PDX model. BRCA1/2 wt PDX models were separated from PDX models with a BRCA1/2 alteration. Data are shown as mean \pm SD of individual PDX models. P value was calculated using a two-tailed Student's t-test. D) Olaparib response was calculated as described for panel C. Each dot represents one PDX model. PDX models in CNVs category A were separated from PDX models in CNVs category D or E. Data are shown as mean \pm SD of different PDX models. P value was calculated using two-tailed Student's t-test. E) Olaparib response was calculated as described for panel C. Each dot represents one PDX model. PDX models classified as 'BRCA1-like' were separated from non-'BRCA1-like' tumors based on BRCA1-classifier outcome. Data are shown as mean \pm SD of different PDX models. P value was calculated using a two-tailed Student's t-test.*

Functional assessment of DNA repair in relation to olaparib response in ovarian cancer PDX models.

To test whether the functionality of DNA repair is associated with a response to olaparib, we analyzed two genome maintenance functions that have been attributed to BRCA1 and BRCA2, specifically the ability to recruit RAD51 to sites of DNA damage³⁷, and the ability to protect stalled replication forks^{5,6}.

Firstly, we conducted the RECAP assay, in which the ability of cells to recruit the downstream HR repair component RAD51 to irradiation-induced DNA damage foci is assessed^{37,39}. To this end, freshly isolated PDX tumor tissue from 15 models was irradiated *ex vivo* and the formation of RAD51 foci was subsequently visualized using immunofluorescence (**Figure 2A,B**). Because HR is only employed in proliferating cells, the cell cycle-regulated protein geminin was included as a marker for S/G2 cells. 8 out of 15 PDX models showed RECAP positivity, as judged by at least 20% of geminin-positive cells showing RAD51 foci (**Figure 2C**). When RECAP positivity was related to response to olaparib, we observed a statistically significant difference, with RECAP-negative tumors showing a decrease in tumor size upon treatment ($p = <0.0001$, **Figure 2D**). Also, when percentages of RAD51-positive tumor cells were used as a continuous variable, a strong correlation was observed between HR repair capacity and response to olaparib ($r = 0.8247$, $p = 0.0002$, **Figure 2E**).

The ability of cells to protect their replication forks is also relevant for PARP inhibitor sensitivity, as trapping of PARP onto the DNA by PARP inhibition results in replication fork stalling⁵⁰. Therefore, we analyzed the ability of tumor cells to protect stalled replication forks, which has been shown to depend on various HR proteins and was reported to be related to olaparib response^{5,30}.

The replication and the ability of cells to protect stalled replication forks can be assessed with the fiber technique⁵¹. To this end, we performed *ex vivo* DNA fiber analysis on freshly isolated tumor tissue which was successful for 13 PDX models. Tumor tissue was dissociated into single cells and subsequently incubated with synthetic nucleotides CldU and IdU (**Figure 3A**). To deplete the nucleotide pool and to stall replication forks, cells were then treated with a high dose of hydroxyurea (HU). Finally, DNA was isolated, stretched, fixed onto glass slides, and incorporated synthetic nucleotides were visualized to quantify the length of DNA fibers. To confirm that measured fibers were originating from tumor cells, dissociated cells used for fiber analysis were simultaneously incubated with EdU and afterward stained for both EdU and cytokeratin to count replicating tumor cells for 10 PDX models (**Supplementary Figure 4A, B**). As a readout for the ability of tumor cells to protect replication forks from HU-induced degradation, IdU/CldU ratios in HU-treated cells were normalized to the untreated setting. A large variety was observed between the models and their ability to protect their replication forks, which is similar to a ratio of 1 (**Figure 3B**). All individual IdU/CldU ratio's in -HU and +HU conditions can be found in **Supplementary Figure 4C**.

Surprisingly, PDX81 showed the lowest degree of replication fork protection, but had a heterozygous BRCA1 deletion and was classified as genomically stable (CNV category A) (**Figure 3B**). When normalized IdU/CldU ratios were used as a continuous variable, no significant correlation between replication fork protection and response to olaparib was observed ($r = -0.3872$, $p = 0.1911$, **Figure 3C**). As an additional readout for replication stress, we calculated the overall replication speed (**Figure 3C**). Similar to normalized IdU/CldU ratios, analysis of overall replication speed showed large variation between PDX models and did not show an association with CNVs categories or BRCA1/2 mutation status (**Figure 3D**). Also, when overall replication speed was used as a continuous variable, no statistically significant correlation was found with the response to olaparib ($r = -0.1980$, $p = 0.5167$, **Figure 3E**).

Despite the low number of PDX models compared to clinical studies, receiver operating characteristic (ROC) curves from genomic (**Supplementary Figure 4D**) and

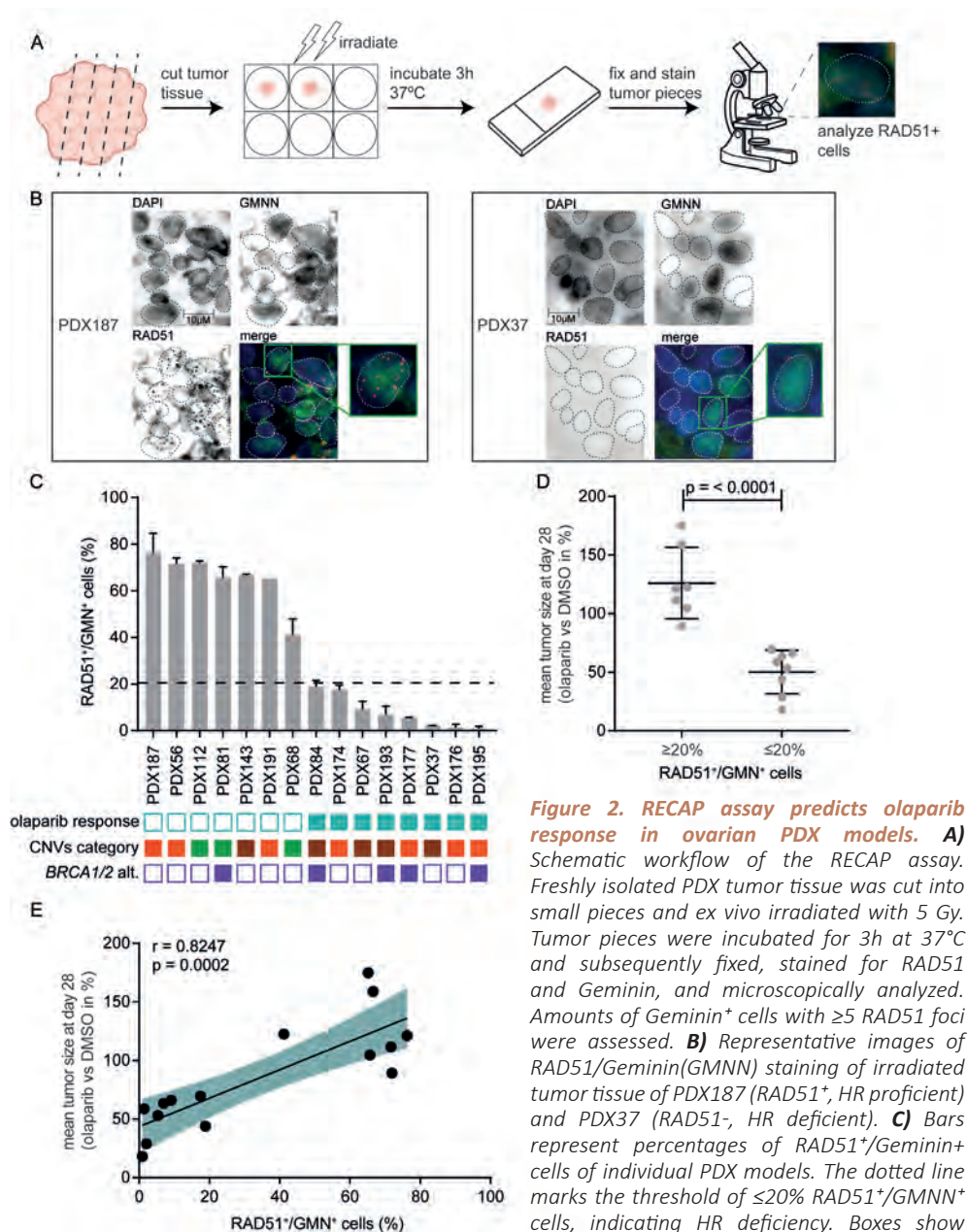


Figure 2. RECAP assay predicts olaparib response in ovarian PDX models.

A) Schematic workflow of the RECAP assay. Freshly isolated PDX tumor tissue was cut into small pieces and ex vivo irradiated with 5 Gy. Tumor pieces were incubated for 3h at 37°C and subsequently fixed, stained for RAD51 and Geminin, and microscopically analyzed. Amounts of Geminin⁺ cells with ≥ 5 RAD51 foci were assessed. **B)** Representative images of RAD51/Geminin (GMNN) staining of irradiated tumor tissue of PDX187 (RAD51⁺, HR proficient) and PDX37 (RAD51⁻, HR deficient). **C)** Bars represent percentages of RAD51⁺/Geminin⁺ cells of individual PDX models. The dotted line marks the threshold of $\leq 20\%$ RAD51⁺/GMNN⁺ cells, indicating HR deficiency. Boxes show

different characteristics of each PDX model. First row represents CNVs category A (green), D (orange) or E (brown). Purple boxes represent the presence of a BRCA1/2 mutation or BRCA1 hypermethylation. Data are shown as mean \pm SEM of at least 3 different tissue slides. **D)** Olaparib response was plotted as mean tumor size at day 28 in olaparib-treated mice normalized to mean tumor size in solvent-treated mice. Each dot represents one PDX model. HR proficient ($>20\%$ RAD51⁺/Geminin⁺ cells) PDX models were separated from HR deficient ($\leq 20\%$ RAD51⁺/Geminin⁺ cells) PDX models. Data are shown as mean \pm SD of different PDX models. P value was calculated using two-tailed Student's t-test. **E)** Percentages of RAD51⁺/Geminin⁺ cells and mean percentages of tumor growth from olaparib-treated mice vs solvent-treated mice were plotted. Each dot represents one PDX model. Correlation coefficients were calculated using Pearson, and linear regression was plotted.

functional analyses (**Supplementary Figure 4E**), demonstrated that the RECAP assay could predict in vivo olaparib response with an area under the curve (AUC) of 1. Additionally, the optimal cut-off value of the RECAP result (< 29.82 %) determined by the ROC curve, confirms our 20% cut-off used that was previously determined³⁷. Thus, in contrast to replication fork protection or replication speed, a functional read-out of HR repair capacity based on RAD51 recruitment was associated with response to olaparib in this cohort of ovarian cancer PDX models.

Mutations in olaparib-sensitive PDX model

Since several PDX models showed a response to olaparib that could not be explained by BRCA1/2 alterations, we analyzed a panel of 226 genes that were previously demonstrated to be involved in DNA repair (**Supplementary Table 1**). Panel sequencing was performed on 10 PDX models, including PDX models with BRCA1/2 mutations and olaparib sensitive models without BRCA1/2 alterations. Candidate variants were filtered for germline variant frequencies found in patients and controls. Concordant with our first genomic DNA analyses, all BRCA1/2 deletions were found in PDX81, PDX177, PDX189, and PDX195 (**Table 2**). Besides the variants in BRCA1/2, 19 additional interesting variants were found in olaparib sensitive models (**Table 2**). Furthermore, 6/10 models showed homozygous mutated TP53 (all from HGSOC subtype), and 2/3 TP53 wt samples had inactivated PTEN and mutated MSH2/3 (data not shown). PDX112 had none of these alterations and was also sequenced as a wt control endometrioid model in CNVs category A.

One particular variant caught our attention in PDX37, which is a nonsynonymous substitution in MUS81 altering the Arginine on position 496 to Glutamine (highlighted in **Table 2**). It is a homozygous mutation and considered to be located in a highly conserved region close to its ERCC4 binding domain and within a predicted Hef domain (**Figure 4A**). Furthermore, it is described that MUS81 is a highly confident hit in genome-wide CRISPR screens for olaparib sensitivity and is shown to cause olaparib sensitivity when depleted in ovarian cancer cell lines^{52,53}. Future research is needed to unravel the role of MUS81 depletion and the specific mutation found in PARP inhibitor sensitivity.

Discussion

In this study, we associated in vivo olaparib responses to genomic features related to HR deficiency, functional HR assessment, and replication fork stability in a cohort of ovarian cancer PDX models. The presence of BRCA1/2 alterations, including BRCA1 promoter methylation, did not fully predict in vivo olaparib response in the included PDX models. Also, only a subset of genomically unstable tumors, as assessed by CNVs analysis, responded to olaparib. These findings underscored the need for additional selection methods for PARP inhibitor eligibility. Functional testing of replication fork stability or replication speed using DNA fiber analysis on freshly isolated tumor tissue did not correlate to in vivo olaparib responses. In contrast, the RECAP assay, which tests HR functionality as determined by the formation of RAD51 foci in ex vivo tumor tissue, fully predicted in vivo olaparib response. Several PDX models were identified that did not harbor BRCA1/2 alterations. These results further support this method to identify patients that may benefit from PARP inhibitors, beyond those with BRCA1/2 mutant tumors.

Clinical trials previously demonstrated that PARP inhibitors can be beneficial in patients with breast or ovarian cancers lacking BRCA1/2 mutations^{14,22}, and other cancer types⁵⁴. So, there is a clear need for a robust biomarker of HR functionality that correlates with the PARP inhibitor response. To this end, various HR deficiency tests have been developed, focused mostly on genomic features. The myChoice HRD test combines BRCA1/2 mutation status with different measurements of genomic instability but was unable to

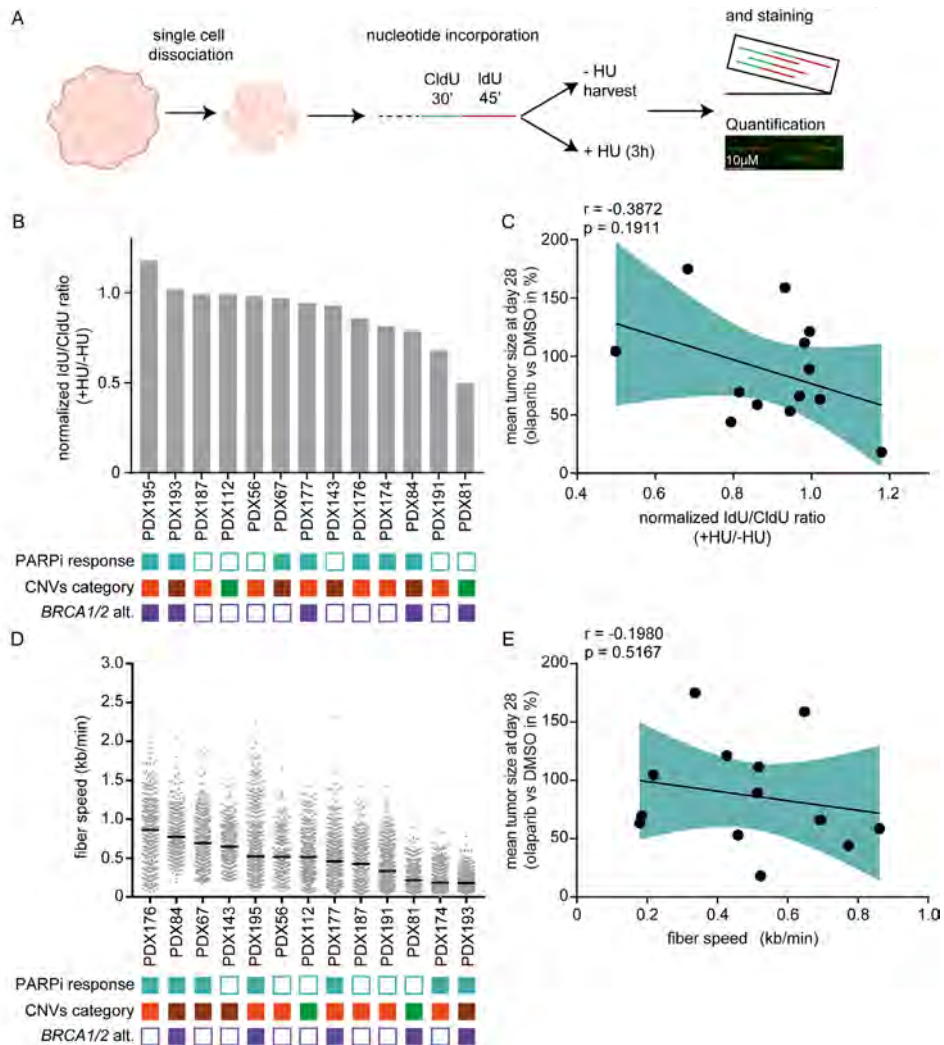


Figure 3. Analysis of replication fork stability and replication speed does not correlate with olaparib responses in ovarian PDX models. **A)** Schematic workflow of ex vivo DNA fiber analysis. Freshly isolated tumor tissue was dissociated into single cells and incubated with synthetic nucleotides CldU and IdU. Cells were subsequently treated with or without HU to stall replication forks. DNA was then isolated, stretched and fixed onto glass slides. Incorporated synthetic nucleotides were visualized, and the length of DNA fibers was quantified. **B)** The ratio of IdU/CldU fiber lengths upon HU treatment was normalized to the untreated condition. Bars represent normalized ratios per PDX model. A ratio of <math><1</math> represents replication fork degradation. Boxes indicate different characteristics of each PDX model. First row represents CNVs category A (brown), D (light green) or E (dark green). Purple boxes represent the presence of a BRCA1/2 mutation or BRCA1 hypermethylation. **C)** Normalized IdU/CldU ratios and mean percentages of tumor growth from olaparib-treated mice vs solvent-treated mice were plotted. Each dot represents one PDX model. Correlation coefficients were calculated using Pearson and linear regression was plotted. **D)** Fiber speed (kb/min) of CldU fibers was calculated as mentioned in the methods. Data are shown as median of all measured fibers per PDX. Each dot represents one fiber. Boxes indicate different characteristics of each PDX model as for panel B. **E)** Median fiber speed and mean percentages of tumor growth from olaparib-treated mice vs solvent-treated mice were plotted. Each dot represents one PDX model. Correlation coefficients were calculated using Pearson and linear regression was plotted.

Table 2. Variants found with panel sequencing in PARPi sensitive PDX models.

PDX #	Chromosome	Gene	Alteration	het/hom	Exogenic function
193	chr16	AXIN1	AXIN1:NM_003502:exon2:c.833C>T;p.P278L	het	nonsynonymous SNV
81	chr17	BRCA1	BRCA1:NM_007294:exon10:c.1823delA;p.K608fs	het	frameshift deletion
195	chr17	BRCA1	BRCA1:NM_007294:exon23:c.5542delC;p.Q1848fs	het	frameshift deletion
177	chr13	BRCA2	BRCA2:NM_000059:exon10:c.1457delA;p.Q486fs	hom	frameshift deletion
189	chr13	BRCA2	BRCA2:NM_000059:exon23:c.9090delA;p.T3030fs	het	frameshift deletion
176	chr11	CDKN1C	CDKN1C:NM_000076:exon1:c.549_554del;p.183_185del	hom	nonframeshift deletion
174	chr11	CWF19L2	CWF19L2:NM_152434:exon3:c.273delA;p.K91fs	het	frameshift deletion
37	chr10	DMBT1	DMBT1:NM_007329:exon17:c.1975C>T;p.Q659X	hom	stopgain SNV
174	chr10	DMBT1	DMBT1:NM_007329:exon26:c.2975C>T;p.A992V	het	nonsynonymous SNV
67	chr7	EGFR	EGFR:NM_201284:exon16:c.2060G>A;p.S687N	het	nonsynonymous SNV
193	chr13	ERCC5	ERCC5:NM_000123:exon15:c.3356C>T;p.A1119V	het	nonsynonymous SNV
176	chr10	FAM175B	FAM175B:NM_032182:exon9:c.1120G>A;p.D374N	het	nonsynonymous SNV
37	chr11	MUS81	MUS81:NM_025128:exon14:c.1487G>A;p.R496Q	hom	nonsynonymous SNV
67	chr8	PREX2	PREX2:NM_024870:exon17:c.1876G>A;p.E626K	het	nonsynonymous SNV
37	chr5	TERT	TERT:NM_198253:exon2:c.1171C>T;p.P391S	het	nonsynonymous SNV
37	chr9	TLR4	TLR4:NM_138554:exon2:c.T197A;p.L66Q;TLR4:NM_003266:exon3:c.T77A;p.L26Q	het	nonsynonymous SNV
174	chr9	TLR4	TLR4:NM_003266:exon4:c.1402C>A;p.L468M	het	nonsynonymous SNV
37	chr17	TP53	TP53:NM_000546:exon7:c.742C>T;p.R248W	hom	nonsynonymous SNV
67	chr17	TP53	TP53:NM_000546:exon8:c.844C>T;p.R282W	hom	nonsynonymous SNV
174	chr17	TP53	TP53:NM_000546:exon9:c.972dupT;p.G325fs	hom	frameshift insertion
176	chr17	TP53	TP53:NM_000546:exon5:c.488A>G;p.Y163C	hom	nonsynonymous SNV
193	chr17	TP53	TP53:NM_000546:exon7:c.737T>C;p.M246T	hom	nonsynonymous SNV
177	chr17	TP53	TP53:NM_000546:exon8:c.817C>T;p.R273C	hom	nonsynonymous SNV
37	chr10	ZNF365	ZNF365:NM_014951:exon5:c.1093G>A;p.E365K	het	nonsynonymous SNV

predict responses to the PARP inhibitor Niraparib in ovarian cancer¹⁴. HRDetect is based on algorithms on whole-genome sequencing profiles from BRCA1/2-mutated breast cancers and was able to detect HR deficient tumors that responded to platinum-based chemotherapy³⁴. Studies that use HRDetect to predict responses to PARP inhibitors are still lacking.

Although these genomic analyses are relatively easily applicable in the clinic, they do not reflect HR functionality at the time of treatment decision making. This is relevant because the functionality of the HR pathway can be restored in BRCA1/2 mutant tumors through secondary mutations which cause PARP inhibitor resistance^{19,31}. Such mutations can appear due to previous treatments with DNA damaging agents such as chemotherapy or during PARP inhibitor treatment⁵⁵.

Our findings are in line with other reports, in which functional testing of HR by RAD51 foci formation can detect HR deficiency in breast cancer³⁹. The RECAP assay was used in an extensive cohort of primary breast cancer tissues (n=148) and identified 19% of these samples to be HR deficient, of which 7 samples were non-BRCA related³⁹. In this study, however, correlation with clinical treatment response was lacking. Despite the relatively low number of PDX models used in our study compared to clinical studies, ROC curves of our distinct analyses demonstrated that the RECAP assay might predict PARP inhibitor responses with very high sensitivity and specificity in ovarian cancer.

The relevance of assessing HR functionality by detection of RAD51 foci was underscored in BRCA1/2-mutated breast cancer PDX models, in which HR function was restored and therefore caused PARP inhibitor resistance⁴². Importantly, the RECAP assay was able to identify HR restoration, despite various underlying mechanisms. Also, the RECAP assay was able to detect restoration of HR in BRCA1 mutant metastatic breast cancer upon treatment with platinum-based and PARP inhibitor treatment⁴³.

In the RECAP assay, the formation of RAD51 foci is assessed by immunofluorescence upon ex vivo irradiation. Although this creates a good dynamic window to detect HR defects, this does come with logistic challenges, including the processing of fresh tumor tissue and the availability of a radiation source. Interestingly, recent studies analyzed endogenous RAD51 foci in untreated paraffin-embedded samples. In this approach, RAD51 assessment was successful in identifying olaparib-sensitive breast cancer PDX models, beyond BRCA1/2 mutated tumors⁴⁰. Whether this approach is also feasible for ovarian cancer tissues remains unclear.

Of note, PARP inhibitor resistance might also occur independently of HR restoration, involving restored replication fork protection^{30,56}. However, the role of BRCA2 in HR was primarily associated with cell viability and prevention of replication stress and not its role in replication fork protection⁵⁷. Importantly, the capability of tumor cells to protect replication forks did not correlate to in vivo olaparib response in our PDX cohort.

Interestingly, two of our PDX models (PDX81, PDX189) with a BRCA1 and BRCA2 mutation respectively, were classified as genomically stable based on CNVs categories (category A and B). Furthermore, PDX81 did not respond to olaparib in vivo. The fact that they do not behave as BRCAness tumors, might partially be explained by these tumors being derived from primary endometrioid tumors. Furthermore, the BRCA1/2 mutations found had an allele frequency of only 50%, which suggests the presence of a heterozygous mutation without loss of heterozygosity (LOH). Finally, both tumors were classified as MSI-high, caused by MLH1 methylation in 1 model (PDX189), and might have resulted in the presence of a heterozygous BRCA1/2 mutation without the suspected BRCAness phenotype. MSI and chromosomal instability (high CNVs) are mainly considered two distinct subtypes to classify tumors that do often not coexist⁵⁸.

We finally aimed to find the underlying cause of HR deficiency in PDX models sensitive to olaparib without harboring a BRCA1/2 alteration (n=4). We identified several interesting homozygous mutations in olaparib sensitive PDX models as possible HR deficient mechanisms. Future research should reveal whether these mutations play an important role in HR deficiency.

In summary, we showed for the first time that functional testing of HR with the RECAP assay correlates to in vivo olaparib response in a big cohort of ovarian cancer PDX models. Surprisingly, the presence of BRCA1/2 alterations, CNVs category, or ex vivo assessed replication fork protection did not correlate to in vivo olaparib response in ovarian cancer PDX models. Several PDX models were identified as HR deficient and PARP inhibitor sensitive without carrying a BRCA1/2 alteration. The RECAP assay warrants further investigation in clinical trials to assess its predictive potential for in vivo response to PARP inhibitor therapy to increase the population of patients that might benefit from PARP inhibitor therapy.

Materials and methods

Patient-derived tumor xenograft (PDX) mouse models

Tumor pieces used for PDX models were derived from ovarian cancer patients with different subtypes that were operated in the UMCG (Groningen, the Netherlands). Clinicopathological and follow-up data have been registered in an anonymous database. All patients gave informed consent. Cryopreserved tumor pieces from previously established PDX models were thawed for implantation into 6–10 weeks old female NOD.Cg-Prkdcscid Il2rgtm1Wjl/SzJ (NSG) mice (internal breed, Central Animal Facility, University of Groningen). Typically, one tumor piece was subcutaneously implanted on one side of the flank and surgery was performed as previously described⁴⁵. Mice received sterilized food and water ad libitum and were kept under pathogen-free conditions in the Central Animal Facility at the University Medical Center Groningen. Animal experiments were approved by the Institutional Animal Care and Use Committee of the University of Groningen and followed the EU Guideline on Animal Experiments. Mouse experiments were divided into two phases: an expansion phase and a treatment phase. For the expansion phase, two mice were implanted with F1 or F2 ovarian cancer specimens. When tumors reached a volume of approximately 1000 mm³, mice were terminated and tumors were used for implantation into 14 recipient mice for the treatment phase. In parallel to implantation for treatment studies, tumor pieces were used

for ex vivo DNA fiber assay analysis and the RECAP (REpair CAPacity) assay.

Analysis of copy-number variations (CNVs) and genomic status of BRCA1/2

PDX models were analyzed for CNVs and BRCA1/2 status. Frozen tissue slices (10 μm) were cut from F1 tumor material that was stored at -80°C . Tissue slices were stained for hematoxylin and eosin (H&E), and were analyzed by a gynecologic pathologist to determine tumor cell percentage. Genomic DNA was isolated using the QIAamp DNA mini kit (Qiagen) according to manufacturer's protocol. For BRCA1/2 mutational analysis, samples were sequenced using Multiplicom BRCA MASTR for NGS. To determine BRCA1 promoter methylation, MS-MLPA (SALSA MLPA Probemix ME001, MRC Holland) was performed according to manufacturer's instructions and as previously described⁴⁶. Cartagenia Bench was used for variant calling and results were compared with (inter)national mutation repositories. Library preparation for CNV sequencing analysis was performed with KAPA Hyper Prep Kit according to manufacturer's instructions. In brief, ~ 60 ng DNA was fragmented, followed by end repair, A-tailing, adaptor ligation and library amplification. The library pool was analyzed on an MiSeq or HiSeq NGS sequencer (Illumina). Based on CNVs categories, models were classified by visual interpretation into 5 categories (A-E), ranging from a 'flatliner' category containing no CNVs (category A), few aberrations (categories B, C) and categories with many aberrations and intrachromosomal rearrangements (categories D, E). Classification of categories was done 'blind', without knowledge about other tumor characteristics, such as gene alterations, ovarian cancer tumor type etc. Examples of CNV categories can be found in Supplementary **Figure 1**.

Microsatellite instability (MSI) analysis

MSI was tested by multiplex PCR of five mononucleotide repeat markers (BAT25, BAT26, NR21, NR24 and NR27) followed by fragment analysis on a 3500XL genetic analyzer Thermo Fisher Scientific). Microsatellite unstable is defined by at least 2 markers showing an aberrant pattern of allelic size variation.

In vivo evaluation of PARP inhibitor response

Mice were closely observed, weighed and tumor size was measured at least once a week. Tumor size was measured using a caliper, and volume was calculated using the following formula: $(\text{width}^2 \times \text{length})/2$. When tumors reached a volume of approximately 200 mm^3 , mice were distributed into a vehicle treatment group (10% dimethyl sulfoxide (DMSO), 10% 2-hydroxypropyl-beta-cyclodextrin (HPBCD) in phosphate saline buffer (PBS)) or olaparib treatment group (100 mg/kg diluted in 10% DMSO, 10% HPBCD in PBS). In general, mice were divided into 7 mice per treatment group based on tumor size to maintain a comparable mean tumor size in both groups at start of treatment. Treatment was administered using intraperitoneal injections for 6 times a week. After 28 days, mice were terminated by cervical dislocation under isoflurane anesthesia. Tumors were harvested, weighed and cut into two pieces: one piece was snap-frozen and kept in -80°C whereas the other piece was stored in formalin. Following the guidelines of animal experimentation, the following humane endpoints were applied to avoid unnecessary suffering of animals: tumor size $>1500 \text{ cm}^3$, weight loss $>15\%$, ulceration of tumors, observation of hunched posture or altered behavior. Tumor growth (%) during treatment was calculated by comparing the tumor volume at the end of treatment to tumor volume at day 0. The response to olaparib for each PDX model was calculated by comparing the mean tumor growth in the olaparib-treated group at day 28 with the mean tumor growth in the DMSO-treated group at day 28. Adapted Response Evaluation Criteria in Solid Tumors (RECIST) guidelines were used to classify PDX models as responders to olaparib⁴⁷. A model was considered sensitive when a decrease of at least 30% (partial

response, RECIST) in mean tumor growth upon olaparib treatment was observed compared to DMSO treatment.

RECAP assay

The RECAP assay, a functional assay to assess RAD51 foci formation in tumor tissue after *ex vivo* irradiation, was performed as described previously³⁷. Fresh PDX tumor tissue harvested from mice was cut into 2-3 mm pieces and placed in 6 wells plates with Roswell Park Memorial Institute (RPMI) medium, supplemented with 10% fetal calf serum (FCS) and 1% penicillin/streptomycin (P/S) within 4 hours after resection. After irradiation using a Cesium¹³⁷ source (5 Gy, IBL 637 Cesium¹³⁷ gamma-ray machine), tumor pieces were incubated for 3 hours at 37°C. Tumor pieces were then put in formalin overnight and embedded in paraffin. Tissue sections were deparaffinized with xylene and hydrated with decreasing concentrations of ethanol. For antigen retrieval, sections were microwaved for 12 minutes at 100°C in retrieval solution (DAKO, #S2367). Sections were cooled down for 20 minutes, permeabilized with 0.2% Triton-X-100 in PBS for 20 minutes at room temperature, washed once with PBS and incubated with DNase I (1000 U/mL, Roche, #04536282001) for 1 hour at 37°C in an incubator. Slides were incubated in blocking buffer (1% BSA, 2% FCS in PBS) for at least 30 minutes. Primary antibodies were diluted in blocking buffer and incubated at room temperature for 1 hour. Primary antibodies used were mouse anti-human RAD51 (1:200; Genetex, #gtx70230 clone 14B4) and rabbit anti-human Geminin (1:400, Protein Tech, #10802). Secondary antibodies AlexaFluor 594-conjugated goat anti-mouse (1:1000, Invitrogen, #A11005) and AlexaFluor 488-conjugated goat anti-rabbit (1:1000, Invitrogen, #A11034) were diluted in blocking buffer and incubated for 1 hour at room temperature. Sections were air-dried in the dark for 30 minutes and mounted with ProLong Diamond Antifade Mountant reagent with DAPI (Invitrogen, #P36966) and stored overnight at 4°C. RAD51 staining was quantified by scoring the percentage of geminin-positive cells with ≥ 5 foci/cell. At least 30 geminin-positive cells were analyzed on at least two different slides. Immunofluorescence images were acquired on a Leica DM-6000RXA microscope using LAS X software.

DNA fiber assay

Fresh tumor material harvested from mice was cut into pieces of approximately 2-3 mm each, while kept in RPMI medium supplemental with 10% FCS and 1% P/S. Tumors were dissociated into single-cell suspensions using the Human Tumor Dissociation Kit according to manufacturer's instructions (Macs Miltenyi Biotec, #130-095-929). Human cells were enriched from the cell pool using the Mouse Cell Depletion Kit (Macs Miltenyi Biotec, #130-104-694). After isolation, tumor cells were incubated in 6 wells plates and resuspended in RPMI medium supplemented with 10% FCS and 1% P/S, containing CldU (25 μ M) for 30 minutes at 37°C. After extensive washing with medium, cells were incubated in medium supplemented with IdU (250 μ M) for 45 minutes at 37°C. If indicated, IdU was washed away after 45 minutes and cells were then treated with hydroxyurea (HU, 5 mM) for 3 hours at 37°C. Cells were subsequently lysed on glass slides in lysis buffer (200 mM Tris-HCl pH 7.4, 50 mM EDTA, 0.5% SDS) and DNA fibers were spread by tilting the glass slides approximately 15 degrees. At least 3 slides of each condition were made. Fibers were fixed with methanol/acetic acid (3:1) for 10 minutes, and then stored at 4°C. Prior to immunolabeling, slides were washed with water and incubated with 2.5 M HCl for 75 minutes to denature the DNA. Slides were then washed with PBS and incubated with blocking solution (1% bovine serum albumin, 0.1% Tween-20 in PBS) for 30 minutes. Next, slides were incubated with primary antibodies rat-anti-BrdU (1:1000, Abcam #ab6326) and mouse-anti-BrdU (1:250, BD Biosciences #347580) for 1 hour, followed by incubation with secondary antibodies AlexaFluor 488-conjugated goat anti-rat (1:500, Invitrogen #A11006) and AlexaFluor 594-conjugated goat anti-mouse

(1:500, Invitrogen #A11005) for 90 minutes. Immunofluorescence images were acquired on a Leica CTR6000 microscope using LAS X software (Leica Application Suite X). Fiber length was measured using ImageJ software.

EdU/Cytokeratin immunofluorescence staining

Single-dissociated cells used for DNA fiber analyses were incubated with EdU for 1 hour at 37°C. Cells were harvested and cytopinned on glass slides. Cells were fixed with 3.7% formaldehyde in PBS for 15 minutes at room temperature. Until staining, slides were stored in -80°C. For EdU staining, cells were permeabilized with 0.5% Triton-X-100 in PBS for 20 minutes. Subsequently, cells were incubated with a reaction cocktail for 30 minutes in the dark consisting of 116.3 mM Tris-HCl pH 8.5, 100 mM CuSO₄, Alexa fluor azide (0.24 uL per reaction) and 100 mM ascorbic acid in H₂O. Washing steps were performed with 3% BSA in PBS. For further staining, cells were washed with PBS and permeabilized with 0.1% Triton-X-100 in PBS for 5 minutes. Blocking was performed in 2.5% BSA-0.05% Tween-20 in PBS for 1 hour. Slides were incubated with primary antibody anti-pan cytokeratin (1:50, AE1AE3, DAKO) in 0.05% Tween-20 in PBS overnight at 4°C followed by secondary Alexa-conjugated antibodies for 1 hour at room temperature. Immunofluorescence images were acquired on a Leica CTR6000 microscope using LAS X software (Leica Application Suite X).

Targeted DNA sequencing

Multi-gene panel sequencing of DNA from F1 PDX tumor material was performed using the CZECANCA panel⁴⁸. The procedure was performed as described previously with the following minor modifications. The CZECANCA panel version 1.2 was used, which targets 226 genes instead of 219 genes. The list of targeted genes included in CZECANCA panel version 1.2 can be found in **Supplementary Table 1**. Sequencing was performed on the Illumina NextSeq platform. Coverages exceeded 500x for the majority of targeted sequences. In total, 39,341 variants were called and the following filters were applied: sequencing errors/low quality variants (quality <150 from GATK software pipeline), frequent variants (MAF>0.05 in 1000 Genomes project and ESP6500), variants with difficult interpretation (extragenic, intronic (except splicing alterations), UTR), variants described in ClinVar as benign or likely benign, mouse tissue contamination or presence in non-cancer and general population controls. Remaining 22 variants were validated using the Integrative genomics viewer (IGV) and are listed in **Table 2**.

Statistical analysis

All statistical tests were performed using GraphPad Prism version 7.0. Parametric data were analyzed using unpaired t tests (two-tailed), one-way ANOVA or two-way ANOVA. Non-parametric data were analyzed using Mann-Whitney tests. Data are presented as means or median with standard error of the mean (SEM). Correlations were calculated using Pearson or nonparametric Spearman tests.

Acknowledgments

We thank members from the Medical Oncology lab (UMCG) and from the Alpe d'Huzes consortium for helpful discussions. This work was financially supported by the Dutch Cancer Society/Alpe d'HuZes (Grant EMCR2014-7048 to M.A.T.M.v.V.). We thank Marieke Everts for technical assistance. Furthermore, we want to thank Frans B.L. Hogervorst and Rob J. Plug for their help with the genomic analyses.

Author contributions

M.A.T.M.v.V. and F.T. conceived and initiated the project. F.T. and V.O.N.T. performed in vivo and ex vivo experiments. E.H.R., P.M.N and R.D.D. performed genomic BRCA1/2 and CNV analyses.

M.J., P.Z. and Z.K performed targeted DNA sequencing. E.W.D. analyzed H&E stainings from PDX tumors. S.d.J and G.B.A.W. established and provided PDX models. F.T., V.O.N.T., E.H.R., P.M.N., M.J., P.Z., Z.K. and M.A.T.M. analyzed data. F.T. and M.A.T.M.v.V. wrote the manuscript. All authors provided feedback on the manuscript before submission.

References

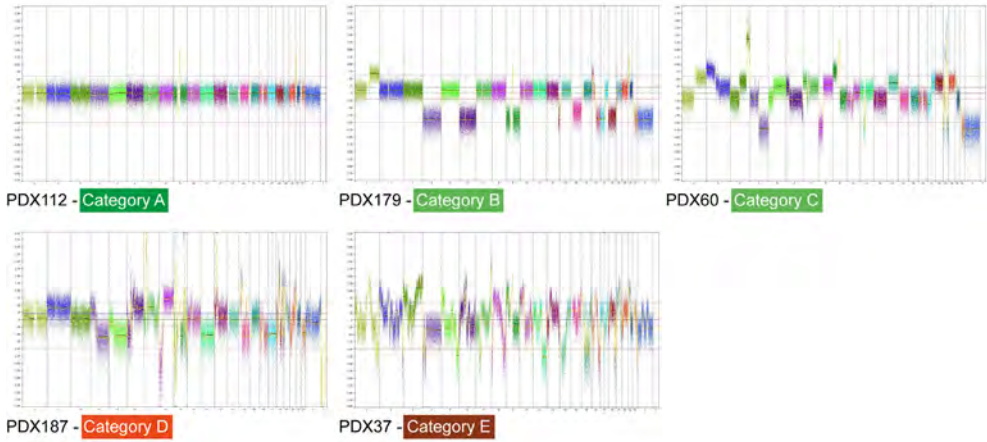
1. Bray, F. et al. Global cancer statistics 2018: GLOBOCAN estimates of incidence and mortality worldwide for 36 cancers in 185 countries. *CA. Cancer J. Clin.* 68, 394–424 (2018).
2. Ovarian Cancer Survival Rates | Ovarian Cancer Prognosis. <https://www.cancer.org/cancer/ovarian-cancer/detection-diagnosis-staging/survival-rates.html#references>.
3. Bell, D. et al. Integrated genomic analyses of ovarian carcinoma. *Nature* 474, 609–615 (2011).
4. Moynahan, M. E. & Jasin, M. Mitotic homologous recombination maintains genomic stability. *Nat Rev Mol Cell Biol.* 11, 196–207 (2010).
5. Schlacher, K., Wu, H. & Jasin, M. A distinct replication fork protection pathway connects Fanconi anemia tumor suppressors to RAD51-BRCA1/2. *Cancer Cell* 22, 106–16 (2012).
6. Schlacher, K. et al. Double-strand break repair-independent role for BRCA2 in blocking stalled replication fork degradation by MRE11. *Cell* 145, 529–542 (2011).
7. Antoniou, A. et al. Average Risks of Breast and Ovarian Cancer Associated with BRCA1 or BRCA2 Mutations Detected in Case Series Unselected for Family History: A Combined Analysis of 22 Studies. *Am. J. Hum. Genet.* 72, 1117–1130 (2003).
8. Kuchenbaecker, K. B. et al. Risks of breast, ovarian, and contralateral breast cancer for BRCA1 and BRCA2 mutation carriers. *JAMA- J. Am. Med. Assoc.* 317, 2402–2416 (2017).
9. Bryant, H. E. et al. Specific killing of BRCA2-deficient tumours with inhibitors of poly(ADP-ribose) polymerase. *Nature* 434, 913–917 (2005).
10. Farmer, H. et al. Targeting the DNA repair defect in BRCA mutant cells as a therapeutic strategy. *Nature* 434, 917–921 (2005).
11. Murai, J. et al. Trapping of PARP1 and PARP2 by clinical PARP inhibitors. *Cancer Res.* 72, 5588–5599 (2012).
12. Pommier, Y., O'Connor, M. J. & De Bono, J. Laying a trap to kill cancer cells: PARP inhibitors and their mechanisms of action. *Science Translational Medicine* vol. 8 362ps17 (2016).
13. Pujade-Lauraine, E. et al. Olaparib tablets as maintenance therapy in patients with platinum-sensitive, relapsed ovarian cancer and a BRCA1/2 mutation (SOLO2/ENGOT-Ov21): a double-blind, randomised, placebo-controlled, phase 3 trial. *Lancet. Oncol.* 18, 1274–1284 (2017).
14. Mirza, M. R. et al. Niraparib maintenance therapy in platinum-sensitive, recurrent ovarian cancer. *N. Engl. J. Med.* 375, 2154–2164 (2016).
15. Fong, P. C. et al. Poly(ADP)-ribose polymerase inhibition: frequent durable responses in BRCA carrier ovarian cancer correlating with platinum-free interval. *J. Clin. Oncol.* 28, 2512–9 (2010).
16. Kaufman, B. et al. Olaparib monotherapy in patients with advanced cancer and a germline BRCA1/2 mutation. *J. Clin. Oncol.* 33, 244–250 (2015).
17. Fong, P. C. et al. Inhibition of poly(ADP-ribose) polymerase in tumors from BRCA mutation carriers. *N. Engl. J. Med.* 361, 123–134 (2009).
18. Robson, M. et al. Olaparib for metastatic breast cancer in patients with a germline BRCA mutation. *N. Engl. J. Med.* 377, 523–533 (2017).
19. Konstantinopoulos, P. A., Ceccaldi, R., Shapiro, G. I. & D'Andrea, A. D. Homologous Recombination Deficiency: Exploiting the Fundamental Vulnerability of Ovarian Cancer. *Cancer Discov.* 5, 1137–54 (2015).
20. Takaya, H., Nakai, H., Takamatsu, S., Mandai, M. & Matsumura, N. Homologous recombination deficiency status-based classification of high-grade serous ovarian carcinoma. *Sci. Rep.* 10, 1–8 (2020).
21. Pennington, K. P. et al. Germline and somatic mutations in homologous recombination genes predict platinum response and survival in ovarian, fallopian tube, and peritoneal carcinomas. *Clin. Cancer Res.* 20, 764–775 (2014).
22. Coleman, R. L. et al. Rucaparib maintenance treatment for recurrent ovarian carcinoma after

- response to platinum therapy (ARIEL3): a randomised, double-blind, placebo-controlled, phase 3 trial. *Lancet* (London, England) 390, 1949–1961 (2017).
23. Norquist, B. et al. Secondary somatic mutations restoring BRCA1/2 predict chemotherapy resistance in hereditary ovarian carcinomas. *J. Clin. Oncol.* 29, 3008–15 (2011).
 24. Bouwman, P. et al. 53BP1 loss rescues BRCA1 deficiency and is associated with triple-negative and BRCA-mutated breast cancers. *Nat. Struct. Mol. Biol.* 17, 688–695 (2010).
 25. Bunting, S. F. et al. 53BP1 inhibits homologous recombination in *brca1*-deficient cells by blocking resection of DNA breaks. *Cell* 141, 243–254 (2010).
 26. Xu, G. et al. REV7 counteracts DNA double-strand break resection and affects PARP inhibition. *Nature* 521, 541–544 (2015).
 27. Dev, H. et al. Shieldin complex promotes DNA end-joining and counters homologous recombination in BRCA1-null cells. *Nat. Cell Biol.* 20, 954–965 (2018).
 28. Noordermeer, S. M. et al. The shieldin complex mediates 53BP1-dependent DNA repair. *Nature* vol. 560 117–121 (2018).
 29. Barazas, M. et al. The CST Complex Mediates End Protection at Double-Strand Breaks and Promotes PARP Inhibitor Sensitivity in BRCA1-Deficient Cells. *Cell Rep.* 23, 2107–2118 (2018).
 30. Chaudhuri, A. R. et al. Replication fork stability confers chemoresistance in BRCA-deficient cells. *Nature* 535, 382–387 (2016).
 31. Talens, F., Jalving, M., Gietema, J. A. & Van Vugt, M. A. Therapeutic targeting and patient selection for cancers with homologous recombination defects. *Expert Opin. Drug Discov.* 12, 565–581 (2017).
 32. Telli, M. L. et al. Homologous Recombination Deficiency (HRD) Score Predicts Response to Platinum-Containing Neoadjuvant Chemotherapy in Patients with Triple-Negative Breast Cancer. *Clin. Cancer Res.* 22, 3764–73 (2016).
 33. Tutt, A. et al. Carboplatin in BRCA1/2-mutated and triple-negative breast cancer BRCAness subgroups: The TNT Trial. *Nat. Med.* 24, 628–637 (2018).
 34. Davies, H. et al. HRDetect is a predictor of BRCA1 and BRCA2 deficiency based on mutational signatures. *Nat. Med.* 23, 517–525 (2017).
 35. Angus, L. et al. The genomic landscape of metastatic breast cancer highlights changes in mutation and signature frequencies. *Nat. Genet.* 51, 1450–1458 (2019).
 36. Zhao, E. Y. et al. Homologous recombination deficiency and platinum-based therapy outcomes in advanced breast cancer. *Clin. Cancer Res.* 23, 7521–7530 (2017).
 37. Naipal, K. A. T. et al. Functional Ex vivo assay to select homologous recombination-deficient breast tumors for PARP inhibitor treatment. *Clin. Cancer Res.* 20, 4816–4826 (2014).
 38. Haaf, T., Golub, E. I., Reddy, G., Radding, C. M. & Ward, D. C. Nuclear foci of mammalian Rad51 recombination protein in somatic cells after DNA damage and its localization in synaptonemal complexes. *Proc. Natl. Acad. Sci. U. S. A.* 92, 2298–302 (1995).
 39. Meijer, T. G. et al. Functional ex vivo assay reveals homologous recombination deficiency in breast cancer beyond BRCA gene defects. *Clin. Cancer Res.* 24, 6277–6287 (2018).
 40. Castroviejo-Bermejo, M. et al. A RAD 51 assay feasible in routine tumor samples calls PARP inhibitor response beyond BRCA mutation. *EMBO Mol. Med.* 10, (2018).
 41. Tumiat, M. et al. A functional homologous recombination assay predicts primary chemotherapy response and long-term survival in ovarian cancer patients. *Clin. Cancer Res.* 24, 4482–4493 (2018).
 42. Cruz, C. et al. RAD51 foci as a functional biomarker of homologous recombination repair and PARP inhibitor resistance in germline BRCA-mutated breast cancer. *Ann. Oncol.* 29, 1203–1210 (2018).
 43. Meijer, T. G. et al. Direct Ex Vivo Observation of Homologous Recombination Defect Reversal After DNA-Damaging Chemotherapy in Patients With Metastatic Breast Cancer. *JCO Precis. Oncol.* 1–12 (2019) doi:10.1200/po.18.00268.
 44. Mukhopadhyay, A. et al. Development of a functional assay for homologous recombination status in primary cultures of epithelial ovarian tumor and correlation with sensitivity to poly(ADP-ribose) polymerase inhibitors. *Clin. Cancer Res.* 16, 2344–2351 (2010).
 45. Alkema, N. G. et al. Biobanking of patient and patient-derived xenograft ovarian tumour tissue: Efficient preservation with low and high fetal calf serum based methods. *Sci. Rep.* 5, (2015).
 46. Gross, E. et al. Identification of BRCA1-like triple-negative breast cancers by quantitative multiplex-

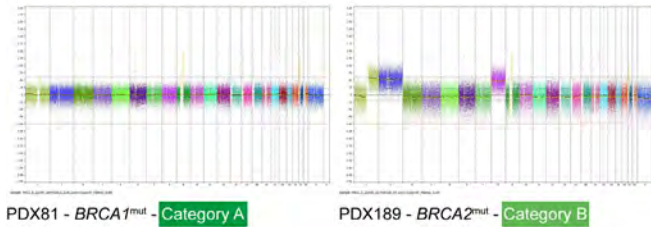
- ligation-dependent probe amplification (MLPA) analysis of BRCA1-associated chromosomal regions: A validation study. *BMC Cancer* 16, (2016).
47. Eisenhauer, E. A. et al. New response evaluation criteria in solid tumours: Revised RECIST guideline (version 1.1). *Eur. J. Cancer* 45, 228–247 (2008).
 48. Soukupova, J. et al. Validation of CZECA (CZEch CAncer paNel for Clinical Application) for targeted NGS-based analysis of hereditary cancer syndromes. *PLoS One* 13, e0195761 (2018).
 49. Vollebbergh, M. A. et al. Genomic patterns resembling BRCA1- and BRCA2-mutated breast cancers predict benefit of intensified carboplatin-based chemotherapy. *Breast Cancer Res.* 16, (2014).
 50. Ström, C. E. et al. Poly (ADP-ribose) polymerase (PARP) is not involved in base excision repair but PARP inhibition traps a single-strand intermediate. *Nucleic Acids Res.* 39, 3166–75 (2011).
 51. Nieminuszczy, J., Schwab, R. A. & Niedzwiedz, W. The DNA fibre technique – tracking helicases at work. *Methods* vol. 108 92–98 (2016).
 52. Zhong, A. et al. Inhibition of MUS81 improves the chemical sensitivity of olaparib by regulating MCM2 in epithelial ovarian cancer. *Oncol. Rep.* 39, 1747–1756 (2018).
 53. Zimmermann, M. et al. CRISPR screens identify genomic ribonucleotides as a source of PARP-trapping lesions. *Nature* 559, 285–289 (2018).
 54. Mateo, J. et al. DNA-repair defects and olaparib in metastatic prostate cancer. *N. Engl. J. Med.* 373, 1697–1708 (2015).
 55. Lheureux, S. et al. Somatic BRCA1/2 recovery as a resistance mechanism after exceptional response to poly (ADP-ribose) polymerase inhibition. *J. Clin. Oncol.* 35, 1240–1249 (2017).
 56. Kais, Z. et al. FANCD2 Maintains Fork Stability in BRCA1/2-Deficient Tumors and Promotes Alternative End-Joining DNA Repair. *Cell Rep.* 15, 2488–99 (2016).
 57. Feng, W. & Jasin, M. BRCA2 suppresses replication stress-induced mitotic and G1 abnormalities through homologous recombination. *Nat. Commun.* 8, (2017).
 58. Trautmann, K. et al. Chromosomal instability in microsatellite-unstable and stable colon cancer. *Clin. Cancer Res.* 12, 6379–6385 (2006).

Supplementary Figures

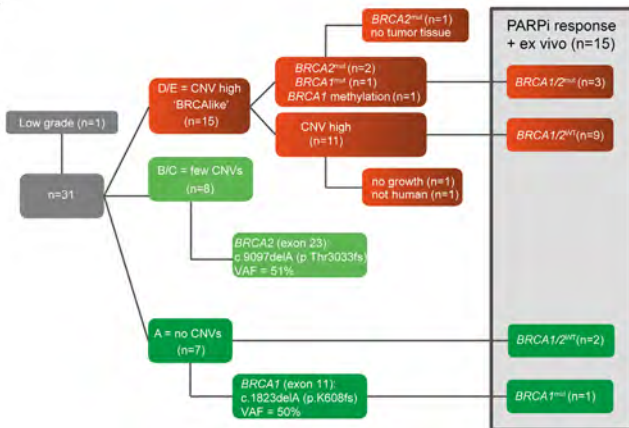
A



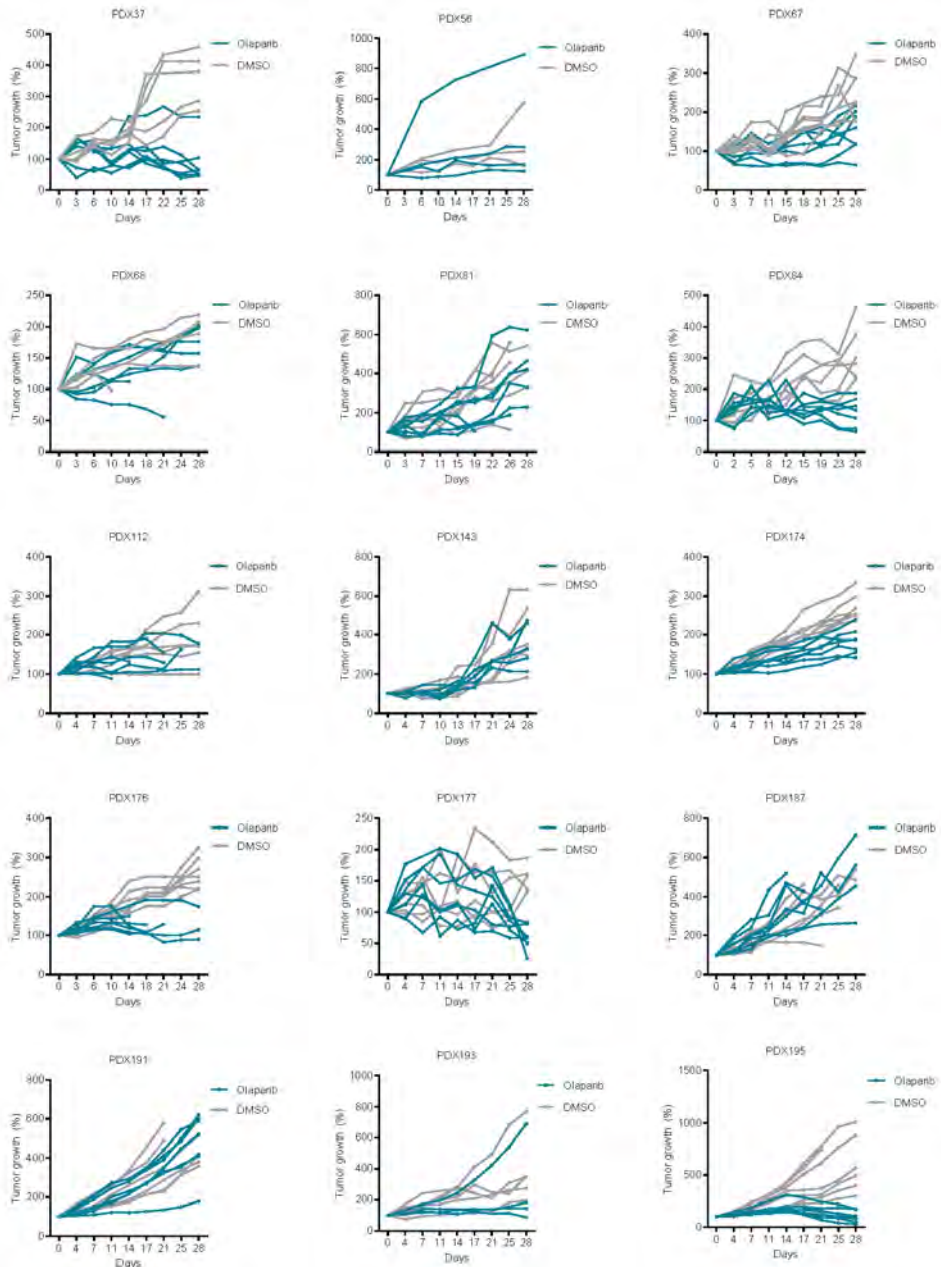
B



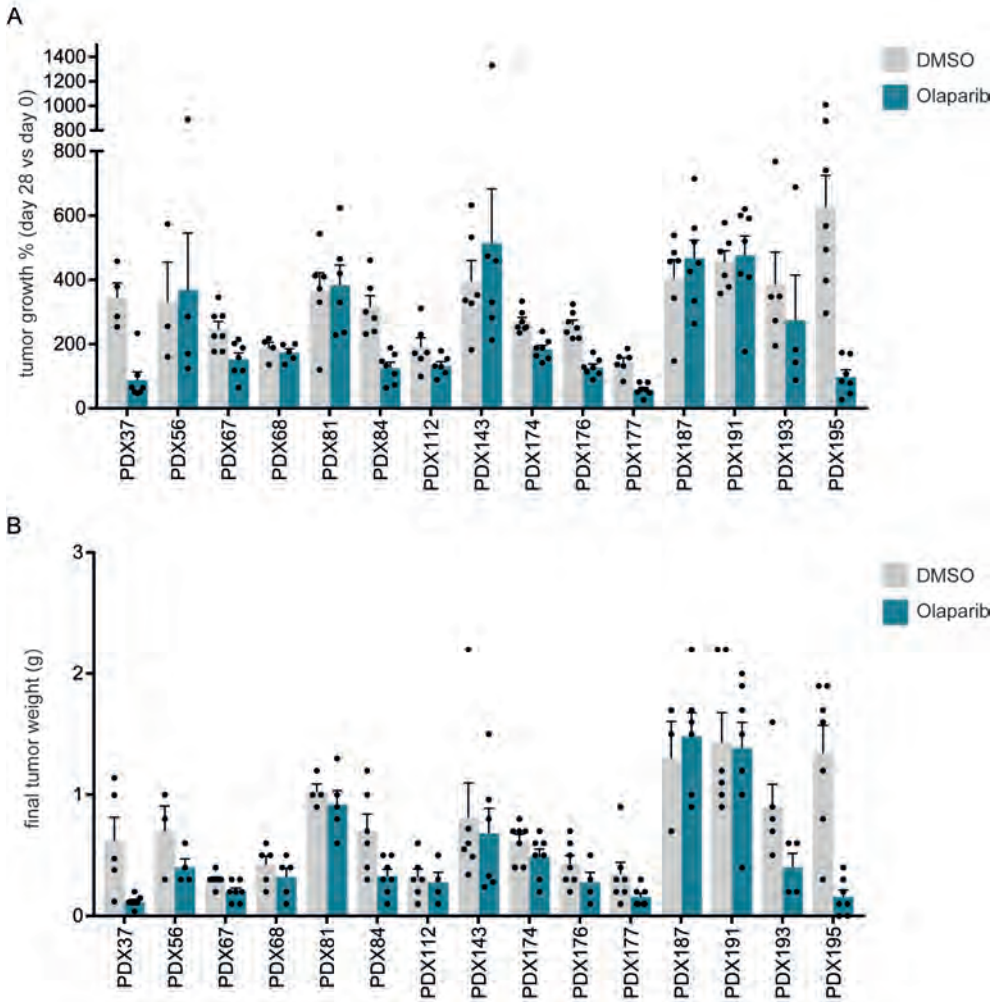
C



Supplementary figure 1. CNV categories and PDX model inclusion for in vivo analyses. A) Representative examples of CNV categories representing different levels of genomic instability, ranging from a 'flatliner' category that contain very few CNVs (category A) towards genomically unstable categories with high amounts of CNVs (category D or E). **B)** CNV categories from BRCA1/2-mutated models PDX81 (category A) and PDX189 (category B). **C)** Decision tree for selection of PDX models for in vivo analysis of olaparib sensitivity and additional ex vivo analyses. In total, 15 models were included for in vivo olaparib treatment.

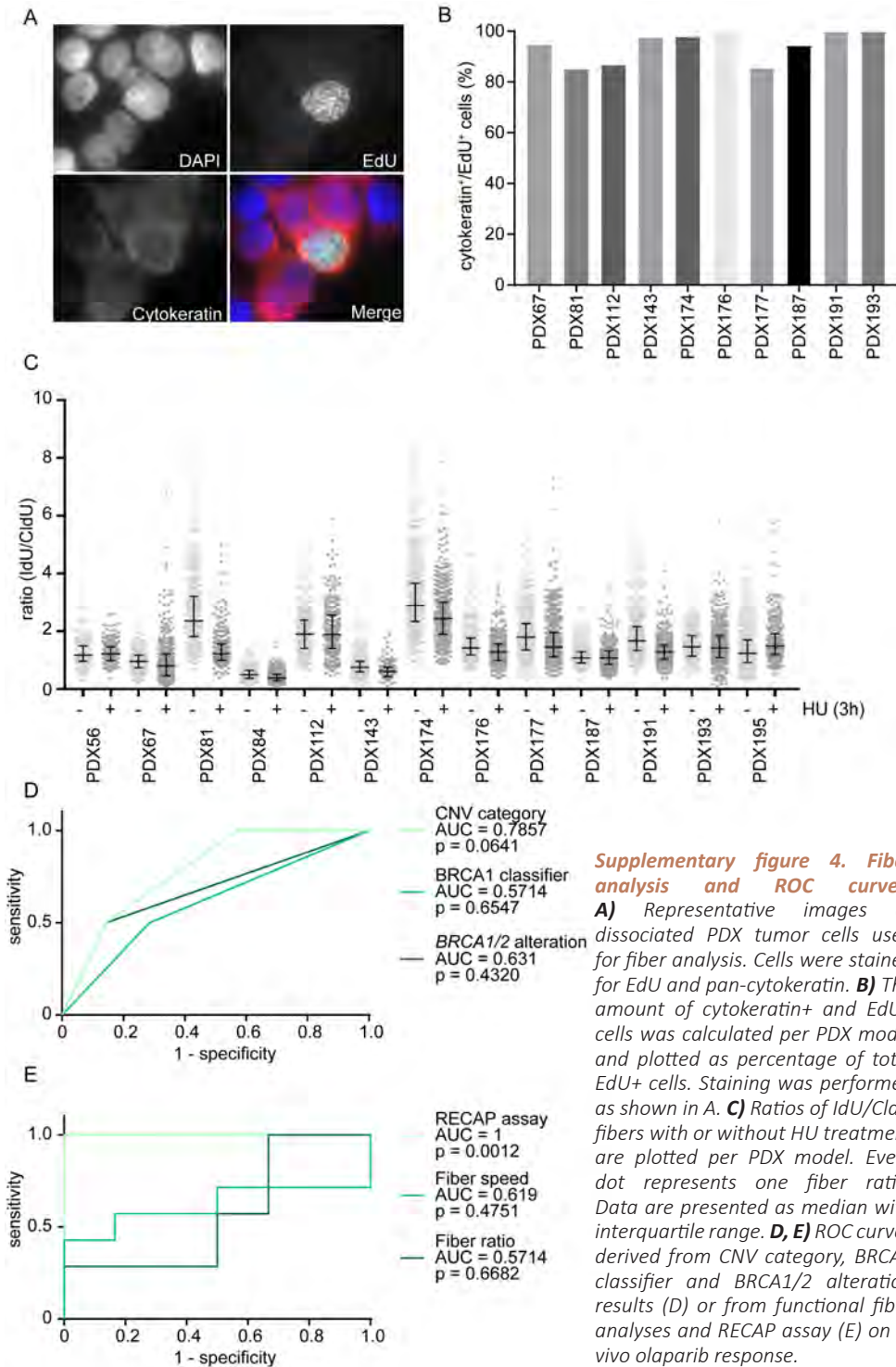


Supplementary figure 2. Tumor growth curves of individual PDX models. Every graph represents tumor growth curves per PDX model, treated with olaparib (blue) or solvent (grey). Tumor growth was calculated as tumor volume at day x compared to tumor volume at day 0. Each line represents one tumor.



Supplementary figure 3. Final tumor growth and tumor weight of PDX models at end of treatment.

A) Bars represent mean tumor growth at day 28 of treatment with olaparib (blue) or solvent (grey). Tumor growth was calculated as tumor volume at day 28 compared to tumor volume at day 0. Each dot represents one tumor. Data is presented as mean \pm SEM of at least 4 mice per treatment group. **B)** Bars represent mean tumor weight harvested at day 28 of treatment with olaparib (blue) or solvent (grey). Each dot represents one tumor. Data are presented as mean \pm SEM of at least 4 mice per treatment group.



Supplementary table 1. List of 226 targeted genes in CZECANCA panel version 1.2.

Gene			
AIP	FANCI	PTCH1	XRCC6
ALK	FANCL	PTTG2	ZNF350
APC	FANCM	RAD1	ZNF365
APEX1	FBXW7	RAD17	DIS3L2
ATM	FH	RAD18	DMBT1
ATMIN	FLCN	RAD23B	PMS2
ATR	GADD45A	RAD50	SBDS
ATRIP	GATA2	RAD51	SDHA
AURKA	GPC3	RAD51AP1	SDHC
AXIN1	GRB7	RAD51B	SDHD
BABAM1	HELQ	RAD51C	
BAP1	HNF1A	RAD51D	
BARD1	HOXB13	RAD52	
BLM	HRAS	RAD54B	
BMPR1A	HUS1	RAD54L	
BRAP	CHEK1	RAD9A	
BRCA1	CHEK2	RB1	
BRCA2	KAT5	RBBP8	
BRCC3	KCNJ5	RECQL	
BRE	KIT	RECQL4	
BRIP1	LIG1	RECQL5	
BUB1B	LIG3	RET	
EMSY	LIG4	RFC1	
FAAP24	LMO1	RFC2	
CASP8	LRIG1	RFC4	
CCND1	MAX	RHBDF2	
CDC73	MCPH1	RNF146	
CDH1	MDC1	RNF168	
CDK4	MDM2	RNF8	
CDKN1B	MDM4	RPA1	
CDKN1C	MEN1	RUNX1	
CDKN2A	MET	SDHAF2	
CEBPA	MGMT	SDHB	
CEP57	MLH1	SETBP1	
CLSPN	MLH3	SETX	
CSNK1D	MMP8	SHPRH	
CSNK1E	MPL	SLX4	
CWF19L2	MRE11A	SMAD4	
CYLD	MSH2	SMARCA4	
DCLRE1C	MSH3	SMARCB1	
DDB2	MSH5	SMARCE1	
DHFR	MSH6	STK11	
DICER1	MSR1	SUFU	
DMC1	MUS81	TCL1A	
DNAJC21	MUTYH	TELO2	
DPYD	NAT1	TERF2	
EGFR	NBN	TERT	
EPCAM	NCAM1	TLR2	

Summary, discussion and future perspectives

Summary

A very toxic type of DNA lesion that needs to be repaired to maintain genomic integrity and cellular viability, is the DNA double-stranded break (DSB). Homologous recombination (HR) is a tightly regulated pathway that can faithfully repair DSBs in S- or G2-phase of the cell cycle. Mutations in HR genes cause a predisposition to cancer; yet, HR defects also result in increased sensitivity to poly(ADP-ribose) polymerase (PARP) inhibitors due to induced synthetic lethality^{1,2}.

Mutations in *BRCA1* or *BRCA2*, two core HR genes, lead to an increased risk to develop high-grade serous ovarian cancer (HGSOC) and breast cancer. For patients with ovarian or breast cancers with confirmed *BRCA1/2* mutations, PARP inhibitors have become available for treatment. Unfortunately, acquired or intrinsic resistance to PARP inhibitors occurs, underscoring the need to improve patient selection and improve PARP inhibitor sensitivity to prevent acquired resistance. To this end, it is necessary to further increase our knowledge of the exact working mechanisms of PARP inhibition. Furthermore, it is important to understand the cellular and molecular consequences of BRCA defects in cancer cells to improve tolerable and effective combination therapies.

Genomic instability, which is a hallmark of HR-deficient cancer cells, has increasingly been associated with anti-tumor immune responses, while it has also been coined as a cell-intrinsic mechanism to evade clearance by the immune system. A better understanding of the involvement of the immune system in HR-deficient cancers might further improve effective combination therapies including immune checkpoint inhibitors.

PARP inhibitors are currently approved to treat *BRCA1/2*-mutated ovarian and breast cancer, while HR deficiency can also be caused by mutations in other DNA repair genes. Patients with HR-defective cancers caused by a non-*BRCA1/2* mutation are currently not eligible for PARP inhibitor treatment. To increase the patient population that might benefit from PARP inhibitor treatment, a way to adequately select patients with HR-deficient tumors is needed. In this thesis, we aimed to dissect the molecular mechanisms and cellular consequences of HR-deficient cancer cells to improve and select patients for whom PARP inhibitor treatment may be beneficial.

To assess the relationship between genomic instability and the immune system, a literature study was performed in **chapter 2**, to describe the multiple ways by which genomic instability leads to cGAS/STING-mediated inflammatory signaling. We described that activation of cGAS/STING signaling has consequences on tumor development and leads to both tumor-promoting and anti-tumor responses in the microenvironment. Genomically unstable tumor cells may have evolved to escape immune surveillance mechanisms that are triggered by cGAS/STING signaling. Possible immune-evasion mechanisms involve the upregulation of immune-checkpoint components, expression of oncogenes, upregulation of autophagy, somatic copy number alterations (CNAs), and activation of cytoplasmic nucleases to lower the amount of cytoplasmic DNA and subsequent interferon (IFN) responses. Finally, cGAS/STING-mediated signaling might be an important determinant of anti-cancer therapy responses and this pathway could be therapeutically targeted, for example using STING agonists, to improve responses to immune-checkpoint blockade or DNA-damaging agents.

In **chapter 3**, we aimed to better understand the underlying mechanisms of cell death induced by PARP inhibitor treatment in HR-deficient cancer cells. We observed that DNA lesions induced by PARP inhibitor treatment in *BRCA2*-depleted cells were transmitted into mitosis. The observed replication lesions, as detected by FANCD2 foci, resulted in increased numbers of chromatin bridges and lagging chromosomes during anaphase and telophase. A similar observation was seen for several human and murine cell lines depleted for *BRCA1* or *RAD51* and treated with PARP inhibitor. Using live-cell imaging, we showed that

the unresolved chromatin bridges are associated with micronucleation and cell death. Mechanistically, the trapping of PARP during S-phase appeared required for the induction of mitotic chromosome bridges. Finally, we observed that the cytotoxicity of PARP inhibition could be rescued by the depletion of EME1, which led to a mitotic bypass. These data add to the knowledge of how PARP inhibition is cytotoxic in HR-deficient cancer cells. These insights could be further exploited to potentiate PARP inhibitor treatment with combination strategies.

Surprisingly, loss of HR genes such as BRCA2 is tolerated in cancer cells, whereas these genes are essential in normal cells. This phenomenon is called the ‘BRCA paradox’. It was suggested that BRCA-deficient cells undergo specific alterations to be able to survive in the presence of genomic instability. In **chapter 4**, we performed a genome-wide genetic screen to identify genes of which a loss of function rescued BRCA2 inactivation. Among the most significant gene mutations, we identified components from the TNF α receptor complex, namely *TNFRSF1A* (encoding TNFR1) and *KHDRBS1* (encoding SAM68), to rescue cell death induced by BRCA2 inactivation in KBM-7 cells. We showed that loss of TNFR1 and SAM68 conferred a survival advantage in several human cancer cell lines depleted for BRCA2. The relation between BRCA2 inactivation and TNF α signaling was shown by the observation that BRCA2 depletion resulted in increased TNF α secretion, activation of downstream TNFR1 signaling kinases JNK and p38, and enhanced sensitivity towards TNF α treatment. The enhanced sensitivity towards TNF α treatment was rescued by depletion of TNFR1 or SAM68 and was not restricted to BRCA2 depletion, as BRCA1 or FANCD2 depletion or low-dose hydroxyurea treatment also sensitized cells to TNF α treatment. Proteomic and transcriptomic analysis revealed the upregulation of IFN-related pathways upon BRCA2 depletion. Finally, we showed that the observed IFN pathway activation upon BRCA2 inactivation is triggered by the formation of micronuclei, which instigates a cGAS/STING-dependent inflammatory response. In conclusion, our data revealed that micronuclei induced by loss of BRCA2 instigate a cGAS/STING-mediated IFN response, which resulted in re-wired TNF α signaling and enhanced TNF α sensitivity.

One of the mechanisms described in chapter 2 that could underlie the observation that genomic unstable tumor cells can escape immune surveillance triggered by cGAS/STING signaling, is oncogene overexpression. In **chapter 5**, we explored whether overexpression of MYC influenced immune responses in murine and human triple-negative breast cancer (TNBC) models in a *BRCA1/2* deficient context. Using two human TNBC cell lines, we found that several overexpressed oncogenes were capable of downregulating immune-related signatures based on RNA sequencing data. We focused on MYC, as MYC is the most frequently overexpressed oncogene in *BRCA*-mutant breast cancer and TNBC. Gene set enrichment analysis (GSEA) on The Cancer Genome Atlas (TCGA) data confirmed that TNBC samples with amplified *MYC* have downregulated immune-related mRNA expression signatures. In a *Brca1*-mutant TNBC mouse model, MYC overexpression resulted in a dramatic loss of lymphocytic infiltration and resulted in decreased tumor latency. Using tumor-derived organoids and *BRCA1/2*-depleted human TNBC cell lines, we showed that MYC overexpression altered several IFN-related responses, including decreased cytokine secretion, reduced expression of IFN-stimulated genes, and decreased phosphorylation of Interferon regulatory factor 3 (IRF3) and Signal transducer and activator of transcription 1 (STAT1). Furthermore, MYC overexpression directly decreased the migration and activation of lymphocytes *in vitro*. Finally, using chromatin immunoprecipitation (ChIP) followed by whole genome sequencing, we found that MYC directly controlled the expression of cytosolic nucleic acid-sensing factors as a possible mechanism to downregulate IFN signaling in a *Brca1*-depleted context. Combined, we uncovered a potential role of MYC overexpression in the immune evasion of *BRCA1/2*-defective TNBC through inhibition of STING-mediated IFN responses.

In **chapter 6**, we reviewed the recent literature on how the HR pathway is mechanistically wired and described current treatment options for HR-deficient cancers with a focus on PARP inhibitors. Resistance to PARP inhibition in the clinic is common and we elaborated on the currently known resistance mechanisms, including secondary mutations within the *BRCA1/2* genes that restore their function, mutations in other repair genes such as *TP53BP1*, *REV7*, or *RIF1* to restore HR function, or alterations in *PAXIP* or *PARP1* to restore protection of replication forks. We elaborated on several patient selection methods, such as mutation analyses, genomic ‘scar’ analyses, or functional HR read-outs, to properly select patients eligible for PARP inhibitor treatment.

Currently, only patients with germline or somatic *BRCA1/2* mutations are eligible for PARP inhibitor treatment, while it is suggested that up to 50% of all HGSOCS are HR-deficient but do not harbor a *BRCA1/2* mutation. In **chapter 7**, we correlated genomic features and *ex vivo* assessed HR functionality and replication fork stability with *in vivo* olaparib responses in a cohort of HGSOCS patient-derived xenograft (PDX) models. Based on CNVs profiles and *BRCA1/2* mutations, a subset of PDX models was selected for *in vivo* olaparib sensitivity and *ex vivo* assays. We found that *BRCA1/2* alterations or genomic instability profiles did not correlate significantly to *in vivo* olaparib response, because not all *BRCA1/2*-mutated or genomic unstable models responded to PARP inhibition. We assessed the capability of tumor cells to form RAD51 foci upon irradiation as a read-out for HR functionality using the *ex vivo* RECAP assay. As HR genes are also involved in the protection of replication forks, we additionally assessed the capability of tumor cells to protect stalled replication forks using an *ex vivo* fiber analysis. Replication fork protection or replication speed in *ex vivo* tumor tissue did not correlate to *in vivo* olaparib responses, whereas the RAD51-based RECAP assay identified all PDX models that responded to *in vivo* olaparib, and also detected PARP inhibitor-sensitive models lacking a *BRCA1/2* alteration. Genomic sequence analysis of a panel of DNA repair-associated genes revealed several mutations as a possible underlying cause of HR deficiency which needs further investigation.

Discussion and future perspectives

Mechanisms of cytotoxicity of PARP inhibitors

In chapter 3 we aimed to further elucidate the mechanism-of-action underlying PARP inhibitor cytotoxicity to possibly improve combined treatment strategies and overcome resistance. The initially proposed mechanism of PARP inhibitor sensitivity was based on the role of PARP in single-stranded break (SSB) repair and the increased formation of DSBs during replication, if SSBs are not properly repaired upon PARP inhibition. However, we found that levels of DSBs upon PARP inhibitor treatment in interphase as measured γH2AX foci were only marginal present. Surprisingly, we observed high levels of replication stress upon PARP inhibition and increased levels of unresolved DNA lesions in mitosis resulting in chromatin bridge formation and lagging chromosomes in HR deficient cancer cells. The observed mitotic aberrancies subsequently resulted in multinucleation or cell death. A few years earlier, it was demonstrated that the mechanism of action of PARP inhibitors also involved trapping of PARP onto damaged DNA, resulting in collapsed replication forks^{3,4}. Indeed, we showed that genetic inactivation of *PARP1* was not as effective as chemical PARP inhibition, highlighting the importance of the presence of PARP itself. Additionally, we uncovered that progression through mitosis is important for the PARP inhibitor-induced cytotoxicity. Combined, our data highlight that drugs that promote mitotic entry might potentiate the cytotoxic effects of PARP inhibition. These combination strategies could improve PARP inhibitor responses and might also be used to address resistance to PARP inhibition, which is commonly observed in the clinic.

Potentiating PARP inhibitors

We showed that PARP inhibition leads to more mitotic aberrancies and longer mitosis. Furthermore, PARP inhibition slows down the G2 phase of the cell cycle. This cell cycle delay may give cells more time to repair the damage, which might contribute to PARP inhibitor resistance⁵. Therefore, potentially effective therapy may involve a combination of PARP inhibitors with drugs that accelerate mitotic entry, including cell cycle checkpoint inhibitors, such as WEE1, CHK1, or ATR inhibitors. Treatment with these inhibitors inactivates the G2/M checkpoint and thereby forces cells into mitosis while preventing repair of DNA lesions. Indeed, induced mitotic entry upon ATR inhibition increased the cytotoxicity of PARP inhibition in BRCA2-deficient cells⁶. Additionally, PARP inhibition combined with ATR or CHK1 inhibition resulted in premature mitotic entry and increased cell death in *BRCA1/2* mutant ovarian cancer cells⁷. Several clinical studies are currently ongoing that combine PARP inhibitors with ATR inhibitors, predominantly in patients with advanced prostate- and ovarian cancer.

These combination therapies could also be used to treat patients with tumors that are PARP inhibitor-resistant through mechanisms that are independent of accelerated mitotic entry. Indeed, PARP inhibitor resistance was reversed by ATR inhibition as inhibition of ATR disrupts BRCA1-independent loading of RAD51 onto DSBs and stalled replication forks^{8,9}. In line with this model, data demonstrated that ATR inhibition suppressed HR and synergized with PARP inhibition in HR-proficient cells¹⁰. Indeed, ATR inhibition impaired the loading of RAD51, and DNA end resection, resulting in an HR-deficient phenotype¹¹. These data suggest that combining ATR inhibitors with PARP inhibition might also be effective beyond *BRCA*-mutated cancers. The combination of PARP inhibitors and cell cycle checkpoint inhibitors could also be synergistic due to the roles of cell cycle checkpoint kinases in the protection of stalled replication forks. For example, ATR protects ssDNA at stalled replication forks by providing RPA¹² and phosphorylation of SMARCAL1¹³, while WEE1 negatively regulates MUS81-mediated fork degradation¹⁴. Through these mechanisms, inhibition of cell cycle checkpoint inhibitors may target two possible PARP inhibitor resistance mechanisms at the same time; a cell cycle arrest in the G2 phase and repair/processing of stalled replication forks. In line with this notion, combination therapies of PARP inhibitors with inhibitors of the WEE1 or ATR kinases have shown efficacy in PARP inhibitor-resistant HR-deficient TNBC and ovarian PDX models. This combination therapy resulted in increased levels of replication stress, including pRPA32 and γ -H2AX¹⁵. Several clinical studies are currently investigating the combination of PARP inhibitors with ATR inhibitors. The combination treatment of PARP inhibitors with cell cycle checkpoint inhibitors might be effective in both HR-deficient and HR-proficient cancer cells.

PARP inhibitors are currently also being combined with other molecularly targeted drugs including inhibitors of mTOR and EGFR and anti-angiogenics^{16,17}. The rationale behind combinations with molecularly targeted drugs is to induce an HR deficiency phenotype (also called 'BRCAness') by suppression of HR genes. However, many of these targets are involved in MAPK signaling, which governs cell cycle control at the G1/S transition. If these agents result in a G1/S arrest¹⁸, it could result in diminished effectiveness of PARP inhibition, especially as we have shown that cell cycle progression and mitosis are necessary for PARP inhibitor cytotoxicity (chapter 3).

Inflammatory signaling in HR-deficient cancer cells

It is still largely unknown how cancer cells can survive in the absence of functional HR. Most of the HR genes belong to the human 'essentialome', which lists genes that are essential for the viability of cells¹⁹⁻²¹. This observation also suggests that the previously described 'BRCA paradox' could be regarded as an 'HR paradox'. To address this paradox, in chapter 4 we performed a genome-wide genetic screen and found TNF α signaling as a determinant of cell viability upon BRCA2 depletion. Previously, inactivation of BRCA2 in

human cancer cells was shown to increase sensitivity towards death receptor-mediated apoptosis with compounds activating the TRAIL receptor, which activates pathways similar to those activated by TNF α ²². Treatment with TRAIL receptor agonists did not result in a cell cycle arrest but induced an early apoptotic event, which supports our findings that BRCA2-depleted cells display intrinsic activation of TNF α -related apoptotic markers. Furthermore, the presence of germline *BRCA1* mutations was associated with decreased TNF α production and lower expression of TNF α -induced ICAM-1 expression on monocytes²³. Combined with our data, this suggests that *BRCA1* or *BRCA2* mutant tumors are sensitive to autocrine or paracrine TNF α or TRAIL, and therefore need to downregulate TNF α to maintain viability. Also, these findings support the exploration of agents that activate TNF α or TRAIL receptors to induce apoptosis in *BRCA1* or *BRCA2* mutant tumor cells²².

Activation of TNF α signaling and secretion of TNF α in our cell lines appeared to be part of a broader interferon response triggered by cGAS/STING signaling upon micronuclei formation. cGAS/STING signaling has recently been found to be an important determinant of anti-tumor immune-responses which further supports the importance of whole-genome screening methods to find unexpected players upon DNA damage responses, including TNF α signaling. As a result of BRCA2 deficiency, mitotic aberrancies can result in the formation of micronuclei in the cytoplasm that are recognized by cytoplasmic DNA sensors such as cGAS that subsequently activate a STING-induced interferon response²⁴. Both TNF α signaling and interferon signaling, as described in chapter 2, can have pro- and anti-tumor effects²⁵. In general, activation of STING-induced interferon signaling serves as a cell-intrinsic innate immune response to trigger cell clearance²⁶. Surprisingly, genomic instability induced by e.g. HR deficiency is a common feature of cancer which is associated with increased levels of cytoplasmic DNA. This notion is supported by our observations that the amounts of micronuclei were increased upon BRCA1 or BRCA2 depletion. In line with our data, chromosomally unstable cancer cells, derived from metastatic tumor models, were characterized by a high frequency of chromosome missegregation resulting in elevated levels of cytosolic DNA and an increased inflammatory phenotype²⁷. Interestingly, cGAS/STING activation in response to cytoplasmic DNA in these chromosomally unstable cells did not result in previously described interferon signaling^{24,28} but instead resulted in non-canonical NF- κ B activation²⁷. It remains unclear how genomically unstable cancer cells deal with the constant presence of cytoplasmic DNA. A shift towards non-canonical NF- κ B signaling might be a mechanism to suppress the anti-tumor immune responses downstream of cGAS/STING activation in favor of a metastatic inflammatory phenotype. Additionally, breast cancers defined by a DNA-damage response deficient profile were associated with lymphocyte infiltration, increased cytosolic DNA, cGAS/STING pathway activation, and cytokine secretion²⁹. However, the underlying S-phase damage also resulted in a STING-dependent upregulation of the immune-checkpoint PD-L1, which might explain the lack of immune-mediated cytotoxicity in these tumors²⁹. Also, treatment with chemotherapeutic agents was shown to induce PD-L1 expression in ovarian cancer via NF- κ B signaling³⁰. In line with these data, we also observed the upregulation of PD-L1 expression upon BRCA2 depletion in our TNBC cell lines (unpublished data). Further research is warranted to investigate if the upregulation of non-canonical NF- κ B signaling in *BRCA*-mutated cancer cells is responsible for immune evasion despite the continuous presence of cytoplasmic DNA and cGAS/STING activation.

Patient selection for PARP inhibitor treatment

Currently, patients are selected for PARP inhibitor therapy based on *BRCA1/2* mutational status and *BRCA1* promoter methylation. However, mutations in other HR genes have also been reported in multiple cancer types, including *PALB2*, *CHEK2*, or *ATM* mutations^{31–33}. Although these mutations are less frequently observed in the clinic ($\leq 2\%$), they might still

account for a significant patient population that might benefit from PARP inhibitor treatment. Therefore, identifying patients with HR-deficient tumors is important, as has been shown that PARP inhibitors can be effective in patients beyond *BRCA1/2* mutations^{34–36}.

A challenge in the clinic is that resistance to PARP inhibition is common, which further highlights the importance of patient selection. Several resistance mechanisms have been discovered that were described in chapter 6. For the majority of PARP inhibitor resistance mechanisms, there is a clear difference for *BRCA1* or *BRCA2* mutant cells as *BRCA1* and *BRCA2* serve distinct roles in HR. For *BRCA1* mutant cells, PARP inhibitor resistance occurs if factors are inactivated that inhibit end resection at DSBs and promote NHEJ, including 53BP1, REV7, Shieldin complex or CST complex genes. Inactivation of these genes results in the restoration of HR in *BRCA1* mutant cells^{37–40}. However, *BRCA2* functions downstream of end resection in the loading of RAD51, and thus HR cannot be restored in the absence of *BRCA2* through modulation of end resection factors⁴¹. In *BRCA2* mutant cells, inactivation of EZH2/MUS81 and PTIP was shown to restore fork protection, which may underly PARP inhibitor resistance^{42,43}. Interestingly, the protection of stalled replication forks from MRE11-mediated degradation was demonstrated to only play a minor role in the viability of *BRCA2*-deficient cells⁴⁴. These data also suggested that the protection of replication forks is therefore not an important factor in PARP inhibition resistance. It could be that restoration of fork protection in *BRCA2*-deficient cancer cells, is sufficient to deal with replication stress induced by PARP inhibitors, but is not sufficient to explain the ‘*BRCA2* paradox’. Furthermore, in chapter 7 we demonstrated that PARP inhibitor sensitivity in HGSOc PDX models was not associated with the ability of tumor cells to protect stalled replication forks.

Current knowledge points towards (independent) functions in the protection of replication forks by many of the HR genes. Up to now, PARP inhibitor resistance in the clinic mainly occurs through the restoration of HR by reverse mutations that restore the reading frame of the mutant allele, suggesting that the function of HR is dominant in determining PARP inhibitor sensitivity^{45,46}.

Many of the PARP inhibitor resistance mechanisms in a *BRCA1/2*-deficient context have been discovered in cell line or mouse models to explain the biology underlying possible resistance mechanisms, but have not yet been frequently assessed in the clinic. In metastatic breast cancer tissue used for PDX experiments, *TP53BP1* mutations and RAD51 amplification were found to cause PARP inhibitor resistance in *BRCA1*-mutant tumors⁴⁷. Furthermore, decreased 53BP1 levels were associated with decreased anti-tumor efficacy of the PARP inhibitor ABT-767 in HR-deficient ovarian cancer biopsies⁴⁸. As the patient population that is being treated with PARP inhibitors is increasing, resistance will more often occur and will lead to increased insight in which resistance mechanisms are clinically relevant. In parallel, organoids and primary cultures derived from PARP inhibitor-resistant patients followed in time could serve to gain further insight into the sensitivity and resistance mechanisms to PARP inhibitors.

As described previously, secondary mutations within the mutant HR gene or in other additional genes can restore HR function or replication fork stability. Additionally, there are large numbers of ‘variants of unknown significance’ (VUS) within HR genes for which it is currently unclear if they have pathogenic potential⁴⁹. Therefore, genetic testing is complicated by the large numbers of VUS alleles and possible mutational combinations that restore HR function need to be included. A proper patient selection tool should aim to identify tumors that capture HR deficiency on a genomic or functional level, which is also known as the ‘BRCAness’ phenotype.

Various HR deficiency tests have been developed that mainly focus on genomic tumor features. The myChoice HRD test was unable to predict responses to the PARP inhibitor Niraparib in ovarian cancer³⁵. HRDetect, based on whole-genome sequencing profiles from

BRCA1/2-mutated breast cancers, was able to detect HR deficient tumors that responded to platinum-based chemotherapy⁵⁰. However, studies that use HRDetect to predict responses to PARP inhibitors are currently lacking. Importantly, these genomic analyses do not reflect the current HR functionality, which is required at the time of treatment decision making.

The importance of functional HR testing at the time of treatment initiation was demonstrated in *BRCA1/2*-mutated breast cancer PDX models in which restoration of HR occurred and caused PARP inhibitor resistance⁴⁷. Specifically, secondary mutations that cause PARP inhibitor resistance, can arise during treatment with DNA damaging agents such as chemotherapy or PARP inhibitor treatment. Indeed, a majority of the PARP inhibitor-resistant models in this manuscript were originally derived from metastatic *BRCA1*-mutant breast cancer patients that were pre-treated with chemotherapy regimens or olaparib, but in which the *BRCA1* mutation was still present in the harvested tumor tissue for PDX development⁴⁷. Two of the resistant models were shown to have somatic mutations in *TP53BP1* resulting in 53BP1 loss, which was previously been described to be an important PARP inhibitor resistance mechanism in a *BRCA1*-mutated context^{39,51,52}. In a different study, three metastatic breast cancer patients with a germline *BRCA1* or *BRCA2* mutation were identified as HR deficient initially but became HR-proficient after treatment with several DSB-inducing agents, including carboplatin with or without PARP inhibition⁵³. In the described studies, restoration of HR could be detected with a functional RAD51-based assay^{47,53}. Patients with TNBC or HGSOc are, both in the current setting and in clinical trials, often pre-treated with (platinum-based) chemotherapy prior to PARP inhibitor treatment, possibly inducing resistance. As platinum-based chemotherapy and PARP inhibitor sensitivity often co-exist due to similar underlying DNA repair deficiencies, a functional HR test will probably predict platinum response initially and subsequent PARP inhibitor response in consecutive treatment regimes. However, it should be noted that only 53.8% of a cohort of patients with HR-deficient ovarian cancer responded to platinum chemotherapy⁵⁴. Also, PARP inhibitor resistance can occur in platinum-sensitive tumors and vice versa^{40,55}. Of note in this context, *TP53BP1* mutations were shown to cause resistance to PARP inhibition but not cisplatin resistance in *BRCA1* mutant mouse models³⁹. It is important to develop patient selection tools for both PARP inhibition and platinum chemotherapy separately.

Many studies that report on the effectiveness of functional testing of HR were performed in breast cancer and studies to correlate functional HR to *in vivo* PARP inhibitor response are lacking in ovarian cancer. In chapter 7, we performed a functional RAD51-based assay called the RECAP (REpair CAPacity) assay in ovarian PDX models. From several functional and genomic features, the RECAP assay effectively predicted *in vivo* olaparib response and identified a subset of PARP inhibitor-sensitive, HR-deficient PDX tumors lacking a *BRCA1/2* alteration. Within our consortium, the RECAP test was compared to two genomic scar based HR deficiency tests, a *BRCA1/2*-like classifier⁵⁶ and Classifier of HOMologous Recombination Deficiency (CHORD)⁵⁷, in a cohort of 71 breast tumors⁵⁸. These different tests could not identify the same population of breast cancer patients as HR deficient (60-70% concordance). Using the *BRCA1*-classifier in our panel of PDX models, we identified 6 models of which 5 responded to *in vivo* olaparib and were also HR deficient based on the RECAP assay. More importantly, additional PDX models were identified by the RECAP assay in our PDX cohort that responded to *in vivo* olaparib but were not identified by the *BRCA1*-classifier (false negatives using the *BRCA1*-classifier). Multiple HR deficiency tests, both functional and genomic, should be included in clinical trials to determine which one predicts best for *in vivo* PARP inhibitor response. Until now, RAD51-based assays have shown promising results in identifying HR-deficient tumors and in predicting *in vivo* response in several models for breast cancer or ovarian cancer⁵⁹⁻⁶². Surprisingly, one report suggested that diminished RAD51 foci failed to predict response to the PARP inhibitor Niraparib in a few HGSOc PDX models⁶³. However, in

this specific study, the RAD51 foci assay was conducted in a completely different set-up, in which dissociated PDX cells were used, at different time points post-irradiation and using a higher irradiation dose. Also, proper controls were lacking to discriminate HR-proficient from HR-deficient cells.

The next step in the development of PARP inhibitor patient selection tools is to design proper prospective clinical trials to validate the predictive value of the RECAP assay in patients treated with PARP inhibitors. Although the RECAP assay appears a very effective test in predicting response, it comes with some logistic and functional challenges. Firstly, the RECAP test requires the processing of fresh tumor tissue, the availability of a radiation source, and three days of physical labor. Also, the assay requires the use of an antibody, which is considered an unstable reagent. Furthermore, the use of the RECAP assay in ovarian tissue seems challenging as only 40% of patient samples resulted in a successful RECAP result (manuscript in preparation). In the UMCG, we encountered similar challenges in performing the RECAP assay in ovarian tissue due to pre-treated biopsies with chemotherapy and the use of eosin during the process for pathology diagnosis, which interferes with immunofluorescence analysis (unpublished data). Also, a relatively low frequency of HR-deficient samples was detected in the ovarian cancer patient cohort (20%), which might be explained by the high percentage of these patients receiving neoadjuvant treatment, whereby patients who respond to platinum due to an HR deficiency were not included for further analysis (in preparation, LUMC). Eventually, a good functional test should be designed to be applicable in all hospitals and on several tumor types. Transforming the RECAP assay to a RAD51 foci staining on paraffin-embedded material with immunohistochemistry on unirradiated tissue should be of great value and has already been demonstrated to be effective in archived breast tumor samples⁶¹.

Besides the challenges that have to be overcome in performing the RECAP test, the RECAP test is restricted to a selected feature (RAD51 recruitment) of one specific pathway. The test thereby excludes possible unknown functions of HR genes that might also be of importance in PARP inhibitor sensitivity. Namely, impaired ribonucleotide excision repair caused by mutations in ribonuclease H2 was shown to induce PARP inhibitor sensitivity, which is independent of HR function⁶⁴. It is currently unknown how relevant ribonucleotide excision repair deficiency is in cancer.

It is still not entirely clear if the ability of cells to protect replication forks is of importance for PARP inhibitor sensitivity and resistance. Interestingly, organoids derived from a germline *BRCA2* mutant ovarian cancer patients and positive for a genomic HR-deficient signature, appeared to PARP inhibitor-resistant but sensitive to carboplatin and ATR inhibition, suggesting an underlying fork protection defect and not an HR defect⁶⁵. Unfortunately, functional RAD51 foci formation could not be assessed in these organoids to determine HR status. This observation underscores the need to determine how important functional pathways, including replication fork protection, are for PARP inhibitor sensitivity in clinical samples. However, using separation-of-function mutations, replication fork protection was shown to be of minor importance for PARP inhibitor sensitivity in *BRCA2* deficient cells⁴⁴. In our HGSOC PDX cohort, replication fork protection also did not correlate to *in vivo* olaparib response as shown in chapter 7.

Silencing inflammatory signaling by oncogene expression

Many cancer types, including TNBC and HGSOC, are characterized by high levels of genomic instability as well as overexpression of a variety of oncogenes. In chapter 5 we aimed to unravel the role of oncogene overexpression in the tumor-cell intrinsic inflammatory response and found that overexpression of several oncogenes in breast cancer is associated with silenced immune-related signatures. We demonstrated that *MYC* overexpression diminished anti-tumor

immune responses in BRCA-deficient TNBC models. MYC was previously shown to regulate immune signaling, through modulation of the expression of immune checkpoint proteins CD47 and PD-L1^{66,67}. Furthermore, preliminary data suggested that MYC, in complex with MIZ1, prevents activation of type I interferon response induced by genomic instability⁶⁸. Recently, and in line with our data, MYC-MIZ1 complexes were shown to bind directly to promoters of IFN regulators, including IRFs and STAT1. Thereby, MYC suppressed IFN signaling and NK cell-mediated immune responses in pancreatic cancer models⁶⁹. Important to note in this context is that overexpression of MYC did not rescue cell death induced by depletion of BRCA1 or BRCA2 in our panel of TNBC cell line models. The possible role of MYC in altering immune responses, therefore, does not appear to be related to directly resolving the ‘BRCA paradox’.

In vivo, we demonstrated that MYC overexpression completely abolished the presence of immune cells in the tumor microenvironment. Interestingly, TNBC and HGSOc patients are often characterized by high amounts of tumor-infiltrating lymphocytes (TILs)⁵⁹ and it has been shown that responses to immune checkpoint inhibitors strongly depend on the composition and activity of immune cells in the tumor⁷⁰. Interestingly, improved immunogenicity was observed in *BRCA1* mutant ovarian cancer, as judged by infiltration of T cells, which was triggered by interferon signaling and could be augmented by PARP inhibitor treatment (unpublished data, Coukos et al.). Unfortunately, clinical responses to immune checkpoint inhibitor monotherapies have been disappointing in patients with TNBC and HGSOc^{71,72}. In contrast to some literature, the decreased amounts of TILs observed in our *Brca1*-mutant mouse model might be caused by the high levels of amplified MYC in our models (~8-fold) compared to patient tumors, in which MYC expression is generally considered an amplification with an average of >2,46 copy number amplification. Furthermore, MYC overexpression is the only altered factor in our mouse model, while a patient tumor harbors many more alterations besides an MYC amplification making the mouse model a very clean but also somewhat extreme situation. In line with our data, elevated expression of MYC in *KRAS* mutant lung and pancreatic cancer models resulted in immune-suppressive tumor microenvironments by altered CCL9/IL-23 signaling and repression of IFN regulators^{67,69}. These data demonstrated that overexpression of MYC also altered the immune micro-environment of the tumor cells extrinsically. We additionally estimated immune cell type fractions in complex TCGA breast cancer samples using CIBERSORT analyses and showed that high MYC expression correlated to lower fractions of CD8⁺ T cells. However, caution should be taken when drawing conclusions based on TCGA data, as these samples contain complex biopsies that are often taken at the edge of the tumor in which cell populations might not exactly reflect the situation within the tumor. It would be interesting to perform retrospective sub-analyses on breast cancer samples to find correlations between high MYC expression and TILs using immunohistochemistry. A key experiment to confirm the role of MYC in the infiltration of immune cells *in vivo* is the use of mice without an adaptive immune system to verify if the effects of MYC on earlier tumor development depend on the suppression of an adaptive immune response.

We demonstrated that MYC overexpression not only diminished immune cell recruitment but also lowered the activity of T cells *in vitro*. Interestingly, high amounts of CNAs were also associated with decreased CD8⁺ T cell activity in the tumor microenvironment^{73,74} whereas high MYC levels were associated with decreased CNAs in the *Brca1*-mutant mouse model that we used⁷⁵. Future research should aim to uncover if overexpression of MYC not only diminishes the presence and activation of immune cells *in vivo* but also if MYC amplification is associated to the level of CNAs and are together responsible for shaping the tumor microenvironment.

MYC was previously described as a master regulator that targets a large part of the transcriptome⁷⁶. Recent literature suggests that MYC targets multiple regulators of the IFN pathway simultaneously⁶⁹. We ultimately identified an immune-related co-functionality

network consisting of genes that were downregulated upon direct binding and expression of MYC and could explain in the diminished inflammatory responses. One of the identified downregulated genes was *DDX58*, the gene encoding RIG-I, which was shown to be a cytoplasmic sensor of RNA, instead of DNA⁷⁷. Recently, mitochondrial DNA damage was demonstrated to result in elevated levels of cytoplasmic RNA that triggered an interferon response via RIG-I and was independent of cGAS⁷⁸. However, it remains unclear if the depletion of BRCA1/2 also results in cytoplasmic RNA release. Also, it has been suggested that RIG-I indirectly can trigger interferon signaling in response to cytoplasmic DNA⁷⁹. The role of mitochondrial damage and the release of RNA in the cytoplasm should be further studied in the context of cancer. Importantly, it is not excluded that there is overlap in the recognition of DNA and RNA by several pattern recognition receptors, including cGAS and RIG-I, to trigger interferon signaling in response to cytoplasmic nucleic acids. Interestingly, systemic RIG-I activation enhanced the sensitivity to anti-PD-1 checkpoint inhibition in an acute myeloid leukemia model via interferon signaling and increased numbers of T cells⁸⁰.

Technically, for future research regarding MYC overexpression, it is advised that experiments should be performed using multiple monoclonal cell lines, as the selection of clones from a heterogeneous population will probably result in clones that have significant biological differences due to different levels of MYC expression. Additionally, the use of an inducible plasmid might also be an alternative to the use of multiple clones per cell line and thereby resembling a more polyclonal *in vivo* situation. Also, the cell line models that we used were not completely compatible with the *in vivo* models, as tumor development cannot be followed in cell lines. Yet, these cell line models reflect relatively clean genetic models, which we used to demonstrate that MYC overexpression diminished the interferon response upon acute BRCA depletion *in vitro*. In an *in vivo* setting, this could allow BRCA1/2-depleted cells to elongate their viability and remain under the radar of the immune system longer, and thereby obtain enough time to acquire properties to survive BRCA depletion.

Targeting oncogene expression and interferon signaling in genomic unstable cancer

The recruitment and activity of immune cells, together with NF- κ B and interferon- γ signaling, determine responses to immunotherapy^{81,82}. In chapters 2, 4, and 5 we demonstrated that these pathways are increased upon BRCA1/2 inactivation and are potentially decreased by oncogene overexpression. These observations highlight the importance of understanding the exact consequences of HR deficiency on the tumor environment to improve treatment regimes. Important follow-up questions in this context are: Can we further trigger interferon signaling to increase sensitivity towards immune therapies? And: Can we target the upstream mechanism that is responsible for the downregulation of interferon signaling in HR-deficient tumors, such as MYC overexpression?

MYC has been studied extensively in the past, but it never resulted in direct targeting of MYC using specific inhibitors⁸³. Recently, inhibition of cyclin-dependent kinase (CDK) 7 and CDK12/13 by THZ1 was demonstrated to target transcriptional addiction in cancer cells⁸⁴, including cellular addiction to MYC. Specifically, THZ1 treatment decreased MYC expression and was effective in ovarian cancer PDX models⁸⁵. Furthermore, CDK7 inhibition caused DNA damage, micronuclei formation, and interferon signaling which was suggested to be independent of cGAS/STING signaling, although an alternative mechanism is lacking⁸⁶. Dinaciclib, a CDK1/2/5/9 inhibitor, was synthetic lethal with MYC expression in TNBC^{87,88}. Interestingly, combined treatment of dinaciclib with niraparib, a PARP inhibitor, increased DNA damage levels and downregulated HR resulting in synthetic lethality in TNBC models⁸⁷. Additionally, the expression of MYC determined the sensitivity to combined treatment of olaparib with Palbociclib (CDK4/6 inhibitor) in ovarian cancer⁸⁹. These data suggest possible combination strategies with CDK inhibitors to target tumors with overexpressed MYC.

Furthermore, Bromo- and Extra-Terminal domain (BET) bromodomain inhibitors, often used in the setting of acute leukemia and multiple myeloma, were demonstrated to downregulate transcription and expression of MYC and MYC-dependent target genes^{90,91}. Several studies already reported the effective combination of bromodomain inhibitors with PARP inhibitors in HR-proficient cancer cells, based on the downregulation of genes involved in HR by bromodomain inhibitors^{92,93}. Future research is needed to investigate if bromodomain inhibitors might also be effective in *BRCA*-mutant cancer cells, that depend on overexpression of MYC for evading clearance by the immune system.

Of note, it was demonstrated that activation of the STING pathway is required for the olaparib response in *BRCA1*-deficient ovarian tumors⁹⁴. In contrast to acute inactivation of *BRCA* in cell line models, a constitutive *BRCA1* defect in itself did not result in an increased interferon response in this *in vivo* model⁹⁴ as these cancer cells might already be adapted to evade the immune system. However, PARP inhibition might trigger interferon signaling in these tumors as these signaling cascades are probably suppressed in established tumors. The combination of olaparib with a STING inhibitor or blocking antibody against Interferon Alpha And Beta Receptor Subunit 1 (IFNAR1), both attenuated the antitumor activity of olaparib indicating that caution should be taken by combining PARP inhibitors with agents that inhibit STING or IFN responses⁹⁴. Additionally, tumor cells lacking IFNAR failed to respond to chemotherapy, highlighting the importance of interferon signaling in tumor cells towards DNA damaging agents⁹⁵.

One of the approaches to trigger interferon signaling in tumors is through the administration of STING agonists, including 2'3'-Cyclic GMP-AMP (cGAMP). cGAMP is a second messenger that is produced by cGAS in response to cytosolic double-stranded DNA, which subsequently activates STING. Notably, cGAMP can also be excreted and taken up by neighboring cells, to activate e.g. NK cells⁹⁶⁻⁹⁸. STING agonists were shown to be able to promote radiation-induced anti-cancer immunity and showed promising effects *in vivo*⁹⁹⁻¹⁰¹. However, poor results in clinical studies were obtained so far due to instability and high polarity of the drugs or due to poor STING agonist capacity¹⁰². cGAMP treatment in combination with immune checkpoint therapies or DNA damaging agents is suggested to be more effective than cGAMP treatment alone. Specifically, activation of STING by cGAMP alone resulted in immune cells with low cross-priming activity¹⁰³. Currently, several new synthetic cGAMP compounds are being investigated in clinical trials in combination with immune checkpoint inhibitors (e.g. NCT03010176, NCT02675439, NCT03172936). However, caution should be taken regarding cGAMP treatment in tumors that are not chromosomally unstable, as it has been shown that cGAMP increases invasion and migration of cells with low chromosomal instability, probably due to the tumor-promoting effects of non-canonical NF- κ B activation^{27,104}.

The above-mentioned STING agonists are currently not being tested in *BRCA* mutant cancers specifically. However, the described effects of cGAS/STING pathway activation in *BRCA*-deficient cells on innate immune responses suggest a prominent role for immune checkpoint inhibition in genomically unstable tumors. Indeed, cGAS and STING protein levels correlated to PD-L1 expression in ovarian cancer cell lines that could be further enhanced by cGAMP treatment¹⁰⁵. Furthermore, PD-L1 levels are increased upon induction of DSBs and upon loss of DNA repair proteins¹⁰⁶, thereby supporting the rationale of combining DNA damaging agents, including PARP inhibitors, with immune checkpoint inhibitors^{107,108}. A phase I study combining pamiparib with tislelizumab in solid tumors showed promising results¹⁰⁹. Also, combining niraparib with pembrolizumab in patients with recurrent ovarian carcinoma was tolerable and showed better responses than monotherapy of both agents, also in patients without a *BRCA* mutation¹¹⁰. Currently, approximately 10 clinical trials are ongoing in which PARP inhibitors are combined with immune checkpoint inhibitors (e.g. NCT02734004, NCT02571725) illustrating the high expectations of targeting DNA damage responses and immune responses simultaneously.

Concluding remarks

Unraveling the mechanisms and consequences of HR deficiency in cancer cells has led to important new insights into the links between DNA damage and immune responses. Future research should aim to investigate how genomic unstable cancer types can suppress the anti-tumor immune responses and investigate how these mechanisms could be targeted to improve the outcome of immune checkpoint inhibitor therapies. It appears of key importance to target HR-deficient tumors at three levels, specifically; induction of DNA damage, triggering cGAS/STING signaling and interferon signaling, and targeting immune checkpoints. For the selection of patients for PARP inhibitor treatment, it is important to perform prospective clinical studies to compare several functional and genomic HR deficiency tests.

References

- Farmer, H. et al. Targeting the DNA repair defect in BRCA mutant cells as a therapeutic strategy. *Nature* 434, 917–921 (2005).
- Bryant, H. E. et al. Specific killing of BRCA2-deficient tumours with inhibitors of poly(ADP-ribose) polymerase. *Nature* 434, 913–917 (2005).
- Pommier, Y., O'Connor, M. J. & De Bono, J. Laying a trap to kill cancer cells: PARP inhibitors and their mechanisms of action. *Science Translational Medicine* vol. 8 362ps17 (2016).
- Murai, J. et al. Trapping of PARP1 and PARP2 by clinical PARP inhibitors. *Cancer Res.* 72, 5588–5599 (2012).
- Rein, I. D., Landsverk, K. S., Micci, F., Patzke, S. & Stokke, T. Replication-induced DNA damage after PARP inhibition causes G2 delay, and cell line-dependent apoptosis, necrosis and multinucleation. *Cell Cycle* 14, 3248–3260 (2015).
- Schoonen, P. M. et al. Premature mitotic entry induced by ATR inhibition potentiates olaparib inhibition-mediated genomic instability, inflammatory signaling, and cytotoxicity in BRCA2-deficient cancer cells. *Mol. Oncol.* 13, 2422–2440 (2019).
- Kim, H. et al. Targeting the ATR/CHK1 axis with PARP inhibition results in tumor regression in BRCA-mutant ovarian cancer models. *Clin. Cancer Res.* 23, 3097–3108 (2017).
- Yazinski, S. A. et al. ATR inhibition disrupts rewired homologous recombination and fork protection pathways in PARP inhibitor-resistant BRCA-deficient cancer cells. *Genes Dev.* 31, 318–332 (2017).
- Haynes, B., Murai, J. & Lee, J. M. Restored replication fork stabilization, a mechanism of PARP inhibitor resistance, can be overcome by cell cycle checkpoint inhibition. *Cancer Treatment Reviews* vol. 71 1–7 (2018).
- Ning, J. F. et al. Myc targeted CDK18 promotes ATR and homologous recombination to mediate PARP inhibitor resistance in glioblastoma. *Nat. Commun.* 10, 1–18 (2019).
- Dibitetto, D. et al. ATR Inhibitors as Potent Modulators of DNA End Resection Capacity. doi:10.1101/2020.01.13.905059.
- Toledo, L. I. et al. XATR prohibits replication catastrophe by preventing global exhaustion of RPA. *Cell* 155, 1088 (2013).
- Couch, F. B. et al. ATR phosphorylates SMARCAL1 to prevent replication fork collapse. *Genes Dev.* 27, 1610–1623 (2013).
- Domínguez-Kelly, R. et al. Wee1 controls genomic stability during replication by regulating the Mus81-Eme1 endonuclease. *J. Cell Biol.* 194, 567–579 (2011).
- O'Connor, M. J. et al. Abstract 932: Reversing PARP inhibitor resistance by targeting the replication stress response. in *Cancer Research* vol. 79 932–932 (American Association for Cancer Research (AACR), 2019).
- Ibrahim, Y. H. et al. PI3K inhibition impairs BRCA1/2 expression and sensitizes BRCA-proficient triple-negative breast cancer to PARP inhibition. *Cancer Discov.* 2, 1036–1047 (2012).
- Pilié, P. G., Tang, C., Mills, G. B. & Yap, T. A. State-of-the-art strategies for targeting the DNA damage response in cancer. *Nature Reviews Clinical Oncology* vol. 16 81–104 (2019).
- Russo, M. et al. Adaptive mutability of colorectal cancers in response to targeted therapies. *Science* (80-.). 366, 1473–1480 (2019).
- Blomen, V. A. et al. Gene essentiality and synthetic lethality in haploid human cells. *Science* (80-.).

-). 350, 1092–1096 (2015).
20. Wang, T. et al. Identification and characterization of essential genes in the human genome. *Science* (80-.). 350, 1096–1101 (2015).
 21. Hart, T. et al. High-Resolution CRISPR Screens Reveal Fitness Genes and Genotype-Specific Cancer Liabilities. *Cell* 163, 1515–1526 (2015).
 22. De Toni, E. N. et al. Inactivation of BRCA2 in human cancer cells identifies a subset of tumors with enhanced sensitivity towards death receptormediated apoptosis. *Oncotarget* 7, 9477–9490 (2016).
 23. Zielinski, C. C. et al. Defect of tumour necrosis factor-alpha (TNF-alpha) production and TNF-alpha-induced ICAM-1-expression in BRCA1 mutations carriers. *Breast Cancer Res. Treat.* 81, 99–105 (2003).
 24. Harding, S. M. et al. Mitotic progression following DNA damage enables pattern recognition within micronuclei. *Nature* 548, 466–470 (2017).
 25. Montfort, A. et al. The TNF paradox in cancer progression and immunotherapy. *Frontiers in Immunology* vol. 10 (2019).
 26. Ishikawa, H., Ma, Z. & Barber, G. N. STING regulates intracellular DNA-mediated, type I interferon-dependent innate immunity. *Nature* 461, 788–92 (2009).
 27. Bakhoum, S. F. et al. Chromosomal instability drives metastasis through a cytosolic DNA response. *Nature* 553, 467–472 (2018).
 28. Dou, Z. et al. Cytoplasmic chromatin triggers inflammation in senescence and cancer. *Nature* 550, 402–406 (2017).
 29. Parkes, E. E. et al. Activation of STING-Dependent Innate Immune Signaling By S-Phase-Specific DNA Damage in Breast Cancer. *J. Natl. Cancer Inst.* 109, djw199 (2017).
 30. Peng, J. et al. Microenvironment and Immunology Chemotherapy Induces Programmed Cell Death-Ligand 1 Overexpression via the Nuclear Factor-kB to Foster an Immunosuppressive Tumor Microenvironment in Ovarian Cancer. (2015) doi:10.1158/0008-5472.CAN-14-3098.
 31. Heeke, A. L. et al. Prevalence of Homologous Recombination-Related Gene Mutations Across Multiple Cancer Types. *JCO Precis. Oncol.* 2018, 1–13 (2018).
 32. Minion, L. E. et al. Hereditary predisposition to ovarian cancer, looking beyond BRCA1/BRCA2. *Gynecol. Oncol.* 137, 86–92 (2015).
 33. Buys, S. S. et al. A study of over 35,000 women with breast cancer tested with a 25-gene panel of hereditary cancer genes. *Cancer* 123, 1721–1730 (2017).
 34. Coleman, R. L. et al. Rucaparib maintenance treatment for recurrent ovarian carcinoma after response to platinum therapy (ARIEL3): a randomised, double-blind, placebo-controlled, phase 3 trial. *Lancet* (London, England) 390, 1949–1961 (2017).
 35. Mirza, M. R. et al. Niraparib maintenance therapy in platinum-sensitive, recurrent ovarian cancer. *N. Engl. J. Med.* 375, 2154–2164 (2016).
 36. Mateo, J. et al. DNA-repair defects and olaparib in metastatic prostate cancer. *N. Engl. J. Med.* 373, 1697–1708 (2015).
 37. Dev, H. et al. Shieldin complex promotes DNA end-joining and counters homologous recombination in BRCA1-null cells. *Nat. Cell Biol.* 20, 954–965 (2018).
 38. Barazas, M. et al. The CST Complex Mediates End Protection at Double-Strand Breaks and Promotes PARP Inhibitor Sensitivity in BRCA1-Deficient Cells. *Cell Rep.* 23, 2107–2118 (2018).
 39. Bouwman, P. et al. 53BP1 loss rescues BRCA1 deficiency and is associated with triple-negative and BRCA-mutated breast cancers. *Nat. Struct. Mol. Biol.* 17, 688–695 (2010).
 40. Xu, G. et al. REV7 counteracts DNA double-strand break resection and affects PARP inhibition. *Nature* 521, 541–544 (2015).
 41. Gogola, E., Rottenberg, S. & Jonkers, J. Resistance to PARP Inhibitors: Lessons from Preclinical Models of BRCA-Associated Cancer. *Annu. Rev. Cancer Biol.* 3, 235–254 (2019).
 42. Rondinelli, B. et al. EZH2 promotes degradation of stalled replication forks by recruiting MUS81 through histone H3 trimethylation. *Nat. Cell Biol.* 19, 1371–1378 (2017).
 43. Chaudhuri, A. R. et al. Replication fork stability confers chemoresistance in BRCA-deficient cells. *Nature* 535, 382–387 (2016).
 44. Feng, W. & Jasin, M. BRCA2 suppresses replication stress-induced mitotic and G1 abnormalities through homologous recombination. *Nat. Commun.* 8, (2017).

45. Lord, C. J. & Ashworth, A. PARP inhibitors: Synthetic lethality in the clinic. *Science* (80-). 355, 1152–1158 (2017).
46. Kondrashova, O. et al. Secondary Somatic Mutations Restoring RAD51C and RAD51D Associated with Acquired Resistance to the PARP Inhibitor Rucaparib in High-Grade Ovarian Carcinoma. *Cancer Discov.* 7, 984–998 (2017).
47. Cruz, C. et al. RAD51 foci as a functional biomarker of homologous recombination repair and PARP inhibitor resistance in germline BRCA-mutated breast cancer. *Ann. Oncol.* 29, 1203–1210 (2018).
48. Hurley, R. M. et al. 53BP1 as a potential predictor of response in PARP inhibitor-treated homologous recombination-deficient ovarian cancer. *Gynecol. Oncol.* 153, 127–134 (2019).
49. Easton, D. F. et al. A systematic genetic assessment of 1,433 sequence variants of unknown clinical significance in the BRCA1 and BRCA2 breast cancer-predisposition genes. *Am. J. Hum. Genet.* 81, 873–883 (2007).
50. Davies, H. et al. HRDetect is a predictor of BRCA1 and BRCA2 deficiency based on mutational signatures. *Nat. Med.* 23, 517–525 (2017).
51. Bunting, S. F. et al. 53BP1 inhibits homologous recombination in brca1-deficient cells by blocking resection of DNA breaks. *Cell* 141, 243–254 (2010).
52. Noordermeer, S. M. et al. The shieldin complex mediates 53BP1-dependent DNA repair. *Nature* vol. 560 117–121 (2018).
53. Meijer, T. G. et al. Direct Ex Vivo Observation of Homologous Recombination Defect Reversal After DNA-Damaging Chemotherapy in Patients With Metastatic Breast Cancer. *JCO Precis. Oncol.* 1–12 (2019) doi:10.1200/po.18.00268.
54. Mukhopadhyay, A. et al. Clinicopathological features of homologous recombination-deficient epithelial ovarian cancers: Sensitivity to PARP inhibitors, platinum, and survival. *Cancer Res.* 72, 5675–5682 (2012).
55. Ceccaldi, R. et al. A unique subset of epithelial ovarian cancers with platinum sensitivity and PARP inhibitor resistance. *Cancer Res.* 75, 628–634 (2015).
56. Schouten, P. C. et al. Robust BRCA1-like classification of copy number profiles of samples repeated across different datasets and platforms. *Mol. Oncol.* 9, 1274–1286 (2015).
57. Nguyen, L., Martens, J., Hoeck, A. van & Cuppen, E. Pan-cancer landscape of homologous recombination deficiency. *bioRxiv* 2020.01.13.905026 (2020) doi:10.1101/2020.01.13.905026.
58. Meijer, T. G. et al. RECAP identifies BRCAness samples undetected by DNA-based homologous recombination deficiency tests. (Erasmus MC, 2020).
59. Meijer, T. G. et al. Functional ex vivo assay reveals homologous recombination deficiency in breast cancer beyond BRCA gene defects. *Clin. Cancer Res.* 24, 6277–6287 (2018).
60. Naipal, K. A. T. et al. Functional Ex vivo assay to select homologous recombination-deficient breast tumors for PARP inhibitor treatment. *Clin. Cancer Res.* 20, 4816–4826 (2014).
61. Castroviejo-Bermejo, M. et al. A RAD 51 assay feasible in routine tumor samples calls PARP inhibitor response beyond BRCA mutation. *EMBO Mol. Med.* 10, (2018).
62. Mukhopadhyay, A. et al. Development of a functional assay for homologous recombination status in primary cultures of epithelial ovarian tumor and correlation with sensitivity to poly(ADP-ribose) polymerase inhibitors. *Clin. Cancer Res.* 16, 2344–2351 (2010).
63. AlHilli, M. M. et al. In vivo anti-tumor activity of the PARP inhibitor niraparib in homologous recombination deficient and proficient ovarian carcinoma. *Gynecol. Oncol.* 143, 379–388 (2016).
64. Zimmermann, M. et al. CRISPR screens identify genomic ribonucleotides as a source of PARP-trapping lesions. *Nature* 559, 285–289 (2018).
65. Hill, S. J. et al. Prediction of DNA repair inhibitor response in short-term patient-derived ovarian cancer organoids. *Cancer Discov.* 8, 1404–1421 (2018).
66. Casey, S. C. et al. MYC regulates the antitumor immune response through CD47 and PD-L1. *Science* 352, 227–31 (2016).
67. Kortlever, R. M. et al. Myc Cooperates with Ras by Programming Inflammation and Immune Suppression. *Cell* 171, 1301–1315.e14 (2017).
68. Krenz, B. et al. MYC suppresses genomic-instability-induced innate immune signalling. (2019).
69. Muthalagu, N. et al. Repression of the Type I Interferon pathway underlies MYC & KRAS-dependent evasion of NK & B cells in Pancreatic Ductal Adenocarcinoma. *Cancer Discov.* CD-19-0620 (2020) doi:10.1158/2159-8290.cd-19-0620.

70. Binnewies, M. et al. Understanding the tumor immune microenvironment (TIME) for effective therapy. *Nat. Med.* 24, 541–550 (2018).
71. Voorwerk, L. et al. Immune induction strategies in metastatic triple-negative breast cancer to enhance the sensitivity to PD-1 blockade: the TONIC trial. *Nature Medicine* vol. 25 920–928 (2019).
72. Hamanishi, J., Mandai, M. & Konishi, I. Immune checkpoint inhibition in ovarian cancer. doi:10.1093/intimm/dxw020.
73. Davoli, T., Uno, H., Wooten, E. C. & Elledge, S. J. Tumor aneuploidy correlates with markers of immune evasion and with reduced response to immunotherapy. *Science* (80-.). 355, (2017).
74. Rooney, M. S., Shukla, S. A., Wu, C. J., Getz, G. & Hacohen, N. Molecular and genetic properties of tumors associated with local immune cytolytic activity. *Cell* 160, 48–61 (2015).
75. Annunziato, S., Barazas, M., Rottenberg, S. & Jonkers, J. Genetic Dissection of Cancer Development, Therapy Response, and Resistance in Mouse Models of Breast Cancer. doi:10.1101/sqb.2016.81.030924.
76. Kress, T. R., Sabò, A. & Amati, B. MYC: Connecting selective transcriptional control to global RNA production. *Nature Reviews Cancer* vol. 15 593–607 (2015).
77. Zhao, Y., Ye, X., Dunker, W., Song, Y. & Karjoolich, J. RIG-I like receptor sensing of host RNAs facilitates the cell-intrinsic immune response to KSHV infection. *Nat. Commun.* 9, 4841 (2018).
78. Tigano, M., Vargas, D. C., Fu, Y., Tremblay-Belzile, S. & Sfeir, A. Nuclear sensing of mitochondrial DNA breaks enhances immune surveillance. *bioRxiv* 2020.01.31.929075 (2020) doi:10.1101/2020.01.31.929075.
79. Chiu, Y. H., MacMillan, J. B. & Chen, Z. J. RNA Polymerase III Detects Cytosolic DNA and Induces Type I Interferons through the RIG-I Pathway. *Cell* 138, 576–591 (2009).
80. Ruzicka, M. et al. RIG-I-based immunotherapy enhances survival in preclinical AML models and sensitizes AML cells to checkpoint blockade. *Leukemia* 34, 1017–1026 (2020).
81. Patel, S. J. et al. Identification of essential genes for cancer immunotherapy. *Nature* 548, 537–542 (2017).
82. Manguso, R. T. et al. In vivo CRISPR screening identifies Ptpn2 as a cancer immunotherapy target. *Nature* 547, 413–418 (2017).
83. Chen, H., Liu, H. & Qing, G. Targeting oncogenic Myc as a strategy for cancer treatment. *Signal Transduction and Targeted Therapy* vol. 3 (2018).
84. Christensen, C. L. et al. Targeting Transcriptional Addictions in Small Cell Lung Cancer with a Covalent CDK7 Inhibitor. *Cancer Cell* 26, 909–922 (2014).
85. Zeng, M. et al. Targeting MYC dependency in ovarian cancer through inhibition of CDK7 and CDK12/13. *Elife* 7, 1–20 (2018).
86. Zhang, H. et al. CDK7 Inhibition Potentiates Genome Instability Triggering Anti-tumor Immunity in Small Cell Lung Cancer. *Cancer Cell* 37, 37-54.e9 (2020).
87. Carey, J. P. W. et al. Synthetic lethality of PARP inhibitors in combination with MYC blockade is independent of BRCA status in triple-negative breast cancer. *Cancer Res.* 78, 742–757 (2018).
88. Horiuchi, D. et al. MYC pathway activation in triple-negative breast cancer is synthetic lethal with CDK inhibition. *J. Exp. Med.* 209, 679–96 (2012).
89. Yi, J. et al. MYC status as a determinant of synergistic response to Olaparib and Palbociclib in ovarian cancer. *EBioMedicine* 43, 225–237 (2019).
90. Delmore, J. E. et al. BET bromodomain inhibition as a therapeutic strategy to target c-Myc. *Cell* 146, 904–917 (2011).
91. Mertz, J. A. et al. Targeting MYC dependence in cancer by inhibiting BET bromodomains. *Proc. Natl. Acad. Sci. U. S. A.* 108, 16669–16674 (2011).
92. Sun, C. et al. BRD4 Inhibition Is Synthetic Lethal with PARP Inhibitors through the Induction of Homologous Recombination Deficiency. *Cancer Cell* 33, 401-416.e8 (2018).
93. Karakashev, S. et al. BET Bromodomain Inhibition Synergizes with PARP Inhibitor in Epithelial Ovarian Cancer. *Cell Rep.* 21, 3398–3405 (2017).
94. Ding, L. et al. PARP Inhibition Elicits STING-Dependent Antitumor Immunity in Brca1-Deficient Ovarian Cancer. *Cell Rep.* 25, 2972-2980.e5 (2018).
95. Sistigu, A. et al. Cancer cell–autonomous contribution of type I interferon signaling to the efficacy of chemotherapy. *Nat. Med.* 20, 1301–1309 (2014).
96. Wu, J. et al. Cyclic GMP-AMP Is an Endogenous Second Messenger in Innate Immune Signaling by

- Cytosolic DNA. *Science* (80-.). 339, 826–830 (2013).
97. Ablasser, A. et al. Cell intrinsic immunity spreads to bystander cells via the intercellular transfer of cGAMP. *Nature* 503, 530–4 (2013).
 98. Marcus, A. et al. Tumor-Derived cGAMP Triggers a STING-Mediated Interferon Response in Non-tumor Cells to Activate the NK Cell Response. *Immunity* 49, 754-763.e4 (2018).
 99. Carozza, J. A. et al. Extracellular cGAMP is a cancer-cell-produced immunotransmitter involved in radiation-induced anticancer immunity. *Nat. Cancer* 1, 184–196 (2020).
 100. Cheng, N. et al. A nanoparticle-incorporated STING activator enhances antitumor immunity in PD-L1–insensitive models of triple-negative breast cancer. *JCI Insight* 3, (2018).
 101. Ohkuri, T. et al. Intratumoral administration of cGAMP transiently accumulates potent macrophages for anti-tumor immunity at a mouse tumor site. *Cancer Immunol. Immunother.* 66, 705–716 (2017).
 102. Marloye, M., Lawler, S. E. & Berger, G. Current patent and clinical status of stimulator of interferon genes (STING) agonists for cancer immunotherapy. *Pharm. Pat. Anal.* 8, 87–90 (2019).
 103. Deng, L. et al. STING-dependent cytosolic DNA sensing promotes radiation-induced type I interferon-dependent antitumor immunity in immunogenic tumors. *Immunity* 41, 843–852 (2014).
 104. Wang, J., Yi, S., Zhou, J., Zhang, Y. & Guo, F. The NF- κ B subunit RelB regulates the migration and invasion abilities and the radio-sensitivity of prostate cancer cells. *Int. J. Oncol.* 49, 381–92 (2016).
 105. Grabosch, S. et al. Cisplatin-induced immune modulation in ovarian cancer mouse models with distinct inflammation profiles. *Oncogene* 1 (2018) doi:10.1038/s41388-018-0581-9.
 106. Sato, H. et al. DNA double-strand break repair pathway regulates PD-L1 expression in cancer cells. *Nat. Commun.* 8, 1751 (2017).
 107. Higuchi, T. et al. CTLA-4 Blockade Synergizes Therapeutically with PARP Inhibition in BRCA1-Deficient Ovarian Cancer. *Cancer Immunol. Res.* 3, 1257–1268 (2015).
 108. Jiao, S. et al. PARP Inhibitor Upregulates PD-L1 Expression and Enhances Cancer-Associated Immunosuppression. *Clin. Cancer Res.* 23, 3711–3720 (2017).
 109. Friedlander, M. et al. Pamiparib in combination with tislelizumab in patients with advanced solid tumours: results from the dose-escalation stage of a multicentre, open-label, phase 1a/b trial. *Lancet Oncol.* 20, 1306–1315 (2019).
 110. Konstantinopoulos, P. A. et al. Single-Arm Phases 1 and 2 Trial of Niraparib in Combination with Pembrolizumab in Patients with Recurrent Platinum-Resistant Ovarian Carcinoma. *JAMA Oncol.* 5, 1141–1149 (2019).

Nederlandse samenvatting

Over de auteur

Dankwoord

Appendices

Nederlandse samenvatting

Reparatie van DNA-schade in cellen

Bijna alle cellen in ons lichaam bevatten dezelfde 46 chromosomen, bestaande uit DNA waarin alle genetische informatie ligt opgeslagen. Met behulp van kleine stukjes DNA (genen) kunnen cellen eiwitten maken die nodig zijn voor de cel om te leven en functioneren, afhankelijk van het celtype. Om cellen te laten prolifereren (ofwel delen), moet al het DNA in een cel foutloos worden gekopieerd en vervolgens over twee nieuwe dochtercellen worden verdeeld. Het kopiëren van DNA wordt ook wel replicatie genoemd. Het DNA in onze cellen krijgt echter voortdurend te maken met verschillende soorten schade, hetzij van factoren buiten (bijv. UV stralen in zonlicht) of binnen het lichaam (bijv. schadelijke bijproducten die vrijkomen bij de stofwisseling of fouten die optreden tijdens het kopiëren van het DNA). Om te zorgen dat deze schade niet leidt tot blijvende veranderingen in het DNA, zijn cellen uitgerust met een breed scala aan mechanismen die deze schade kunnen detecteren en herstellen. Deze mechanismen tezamen wordt 'de DNA-schade-respons (DDR)' genoemd.

Een zeer toxisch type DNA-schade dat moet worden gerepareerd om het DNA intact te houden en om te zorgen dat cellen blijven leven, zijn DNA dubbelstrengs breuken (DSBs). Cellen hebben twee hoofdmechanismen om DSBs te repareren, namelijk 'non-homologous end joining' (NHEJ) en 'homologous recombination' (HR). Hoewel NHEJ zeer efficiënt is, is het ook een foutgevoelige manier van breuk reparatie en kan het zelfs mutaties (veranderingen in het DNA) veroorzaken. HR is daarentegen een foutloos reparatiemechanisme dat DSBs alleen in bepaalde fasen van de celcyclus kan repareren. HR is alleen actief in de S- en G2-fase van de celcyclus, omdat dit de fasen zijn waarin al het DNA al gekopieerd is en de cel zich voorbereid om te gaan delen. HR maakt gebruik van het DNA dat al foutloos gekopieerd is om daarmee de breuk te herstellen. Een heel belangrijk eiwit aan het einde van het HR-proces is RAD51. RAD51 vormt zich rondom de breuk die gerepareerd moet worden en zal vervolgens in het al nieuw gekopieerde DNA op zoek gaan naar het juiste stukje DNA om de breuk te kopiëren en herstellen. De aanwezigheid van RAD51 rondom DNA-breuken kan gebruik worden om te kijken of een cel beschikt over functionele HR. Als DNA-schade niet goed kan worden gerepareerd in een cel, bijvoorbeeld als gevolg van defecten in de DNA-reparatie mechanismen, kan dit leiden tot structurele veranderingen in het DNA die gevolgen hebben voor het functioneren van een cel.

Verlies van DNA-schade mechanismen in kanker

Erfelijke defecten in DNA-schade reparatie mechanismen, door het hebben van een mutatie in een gen dat heel belangrijk is in een dergelijk mechanisme, kan leiden tot een toename van DNA-schade in een cel. Verschillende erfelijke mutaties in deze DNA-schade reparatie mechanismen worden in verband gebracht met een reeks ziektebeelden, waaronder neurologische aandoeningen, versnelde veroudering en ze spelen ook een belangrijke rol bij de ontwikkeling van kanker¹. Er is beschreven dat een aanzienlijk deel van alle kankers defecten heeft in DNA-schade reparatie mechanismen, waaronder in HR. Deze kankers worden 'HR deficiënt' genoemd. Defecten in DNA-schade reparatie mechanismen en de resulterende fouten in het genoom zijn daarom ook beschreven als een belangrijk kenmerk van kanker². Een verband tussen defecten in DNA-schade reparatie mechanismen en kanker werd voor het eerst vastgesteld toen in de jaren '90 specifieke mutaties werden ontdekt die ten grondslag lagen aan het krijgen van erfelijke borstkanker. De genen waarin deze mutaties voorkwamen werden hier vervolgens ook naar vernoemd, namelijk 'breast cancer early onset-1' (BRCA1) en 'breast cancer early onset-2' (BRCA2). Personen met een erfelijke mutatie in het *BRCA1* of *BRCA2* gen hebben een verhoogd risico tot 70% om borstkanker te

ontwikkelen. Bovendien worden *BRCA1/2* mutaties ook geassocieerd met een verhoogd risico op het ontwikkelen van eierstokkanker en een reeks andere kankertypes³. In de decennia die volgden op de ontdekking van de *BRCA1/2* genen, zijn talrijke mutaties in andere HR-genen ook geassocieerd met het ontwikkelen van kanker.

In een poging om kankers te bestuderen die geassocieerd zijn met *BRCA1/2* mutaties, bleken beide *BRCA*-genen essentieel te zijn voor de ontwikkeling van muis embryo's, wat betekent dat deze genen en daarmee ook HR een essentieel proces is voor de proliferatie van normale cellen^{4,5}. Bovendien vervullen *BRCA1* en *BRCA2* belangrijke functies bij de bescherming van vastgelopen replicatievorken, de structuur waarin DNA wordt opengebrouwen om het te kunnen repliceren. Deze waarnemingen vormden een duidelijk contrast met het idee dat kankercellen juist levensvatbaar zijn bij gebrek aan functionele HR door een *BRCA1* of *BRCA2* mutatie. Hoe deze kankercellen overleven in de afwezigheid van *BRCA1/2* is nog niet volledig begrepen en wordt de 'BRCA-paradox' genoemd⁶. Steeds meer onderzoek suggereert dat er secundaire gebeurtenissen hebben plaatsgevonden, zoals mutaties of verhoogde expressie van andere genen, die deze kankercellen in staat zouden kunnen stellen te overleven in de context van HR-deficiëntie. Bovendien wordt steeds meer erkend dat het immuunsysteem ook een belangrijke rol speelt bij de overleving en groei van HR-deficiënte kankercellen.

Behandeling van HR-deficiënte kanker

Als kanker nog gelokaliseerd is, wordt deze bij voorkeur chirurgisch verwijderd. Als een operatie niet mogelijk is, worden de meeste kankersoorten behandeld met radiotherapie, chemotherapie of met een combinatie van beide. Radiotherapie en de meeste chemotherapie veroorzaken hoge niveaus van DNA-schade, die daarmee de snel delende kankercellen doodt, maar daardoor ook schadelijk is voor normale cellen. Bovendien hebben veel kankercellen, net als normale cellen, nog steeds de capaciteit om de DNA-schade te repareren en zijn ze niet gevoelig genoeg voor deze behandelingsopties of worden ze resistent.

Om de effectiviteit van kankerbehandeling te vergroten, zijn strategieën nodig die specifiek gericht zijn op kenmerken die uniek zijn voor kankercellen. Deze behandelstrategie wordt 'gerichte therapie' genoemd. Een specifiek type gerichte therapie is gebaseerd op het principe 'synthetische letaliteit'. Een combinatie van genen wordt synthetisch letaal genoemd, wanneer in beide genen een defect voorkomt (bijv. gelijktijdig verlies van gen A en gen B) en daardoor resulteert in celdood. Verlies van slechts één van deze genen is dus niet voldoende. Het principe van synthetische letaliteit kan worden toegepast in kankertherapie, wanneer in kankercellen met een mutatie in gen A, vervolgens gen B therapeutisch wordt uitgeschakeld. Een bekend voorbeeld is de synthetische letaliteit tussen *BRCA1/2* en het gen *PARP1*. Dit leidde tot de bevinding dat kankers die HR-deficiënt zijn (door een *BRCA1/2* mutatie), kunnen worden behandeld met PARP-remmers^{7,8}. Gezonde cellen hebben nog steeds functionele HR en zullen daarom minder gevoelig zijn voor PARP-remmers. In 2014 werd de eerste PARP-remmer olaparib (Lynparza) door de 'Food and Drug Administration' (FDA) goedgekeurd voor de behandeling van patiënten met vergespreide eierstokkanker en een *BRCA1/2* mutatie. In 2016 werden de PARP-remmers rucaparib en niraparib ook goedgekeurd voor de behandeling van patiënten met terugkerende *BRCA1/2*-gemuteerde eierstokkanker. Recentelijk is olaparib ook goedgekeurd voor de behandeling van *BRCA1/2*-gemuteerde uitgezaaide borstkanker.

Helaas ontwikkelen veel kankers uiteindelijk resistentie tegen de behandeling met PARP-remmers. Resistentie kan optreden zodra kankercellen de functie van HR herstellen door genen uit te schakelen die normaal gesproken HR remmen (suppressie genen). Dit is een resistentie mechanisme dat vooral is aangetoond in *BRCA1*-mutante cellen. Bovendien kan

de oorspronkelijke mutatie verloren gaan of zorgt een nieuwe secundaire mutatie in *BRCA1* of *BRCA2* ervoor dat de functie van het gen hersteld wordt. Tot slot kan extra bescherming van vastgelopen replicatievorken in een *BRCA2*-mutante achtergrond ook leiden tot PARP-resistentie. Om resistentie te voorkomen, is het belangrijk om onze kennis over de exacte werkingsmechanismen van PARP-remmers te vergroten en hun werkzaamheid te verbeteren door combinatiestrategieën met andere geneesmiddelen te ontwikkelen. Combinatieonderzoeken waren tot dusver gericht op het combineren van PARP-remmers met chemotherapie, angiogenese-remmers (voorkomt de vorming van nieuwe bloedvaten) en meer recent met immuuntherapie. Helaas wordt toxiciteit vaak waargenomen in onderzoeken die chemotherapie combineren met PARP-remmers. Om tolereerbare en effectieve combinatietherapieën te ontwikkelen, is het ook noodzakelijk om de cellulaire en moleculaire gevolgen van BRCA-defecten in kankercellen te begrijpen. In deze context wordt de combinatie van PARP-remmers met immuuntherapie in toenemende mate bestudeerd, aangezien recentelijk wordt gesuggereerd dat de rol van het immuunsysteem een belangrijke rol speelt bij het overleven van HR-deficiënte kankercellen.

Terwijl PARP-remmers momenteel zijn goedgekeurd voor de behandeling van *BRCA1/2*-gemuteerde eierstokkanker en borstkanker, kan HR-deficiëntie in kanker ook worden veroorzaakt door mutaties in andere DNA-reparatiegenen, buiten *BRCA1* of *BRCA2*. Deze patiënten komen momenteel niet in aanmerking voor behandeling met PARP-remmers, maar kunnen wel baat hebben bij deze behandeling, zoals reeds is aangetoond in klinische onderzoeken. Daarom is selectie van patiënten die baat zouden kunnen hebben bij PARP-remmers, naast patiënten met een *BRCA1/2*-mutatie, nodig en de hulpmiddelen om dit te doen zijn nog niet optimaal. Dergelijke hulpmiddelen voor patiëntselectie zullen waarschijnlijk ook relevant zijn voor het identificeren van kankercellen die mogelijk resistent zijn geworden tegen PARP-remmers, om zo onnodige behandeling te voorkomen.

Doel van dit proefschrift

Het algemene doel van dit proefschrift is om de moleculaire mechanismen en cellulaire gevolgen van HR-deficiënte kankercellen te identificeren om de effectiviteit van behandelingen en patiëntselectie voor PARP-remmers te verbeteren.

Samenvatting van de hoofdstukken

In **hoofdstuk 1** wordt een algemene introductie gegeven voor dit proefschrift en wordt beschreven wat er in de verschillende hoofdstukken onderzocht is.

Veranderingen in het vermogen van cellen om hun DNA te herstellen, kunnen leiden tot een instabiel genoom, wat vaak voorkomt bij kanker. Normaal gesproken hoort al het DNA in de kern van een cel te zitten, maar als gevolg van ongeprepareerde DNA-schade kan er DNA in het cytoplasma buiten de kern van cellen terecht komen. DNA in het cytoplasma wordt herkend via cGAS/STING signalering en veroorzaakt een cel-intrinsieke inflammatoire (ontsteking) en immuunrespons. In **hoofdstuk 2** van dit proefschrift worden verschillende mechanismen beschreven waarmee een instabiel genoom leidt tot cGAS/STING-gemedieerde inflammatoire signalering en hoe dit de kankercellen en hun omgeving positief en negatief kan beïnvloeden. Kankercellen die worden gekenmerkt door een instabiel genoom, bijvoorbeeld door verlies van HR, zijn blijkbaar geëvolueerd om aan deze immuunreactie te ontsnappen om zo te voorkomen dat ze door het immuunsysteem worden opgeruimd. Mogelijke mechanismen waarmee kankercellen zich kunnen aanpassen aan deze inflammatoire signalering zijn: toename van immuun-belemmerende eiwitten (immuun checkpoint eiwitten), expressie van oncogenen en de activering van eiwitten die de hoeveelheid

cytoplasmatisch DNA en daaropvolgende responses kunnen verlagen. Ten slotte schetsen we hoe cGAS/STING-gemedieerde inflammatoire signalering therapeutisch aangepakt kan worden om behandeling te verbeteren. Er wordt onderzocht of toediening van cGAMP (een activator van cGAS/STING) of immuuntherapie de huidige behandelingen verbeterd.

PARP-remmers zijn op dit moment een gerichte behandelstrategie voor HR-deficiënte kanker. Echter, niet alle tumoren reageren op PARP-remmers en veel tumoren ontwikkelen uiteindelijk resistentie die resulteert in groei na een initiële respons. Meer inzichten in hoe PARP-remmers kankercellen met een HR-defect doden, is nodig om de therapierespons te verbeteren en nieuwe combinatiestrategieën te ontwikkelen. In hoofdstuk 3 hebben we daarom de mechanismen van PARP-remmers bestudeerd in verschillende HR-deficiënte kankermodellen. We hebben waargenomen dat de DNA-schade die veroorzaakt wordt door PARP-remmers in BRCA2 deficiënte cellen, resulteert in defecten gedurende de verdeling van chromosomen tijdens mitose, de laatste fase van de celdeling. Er is na behandeling met PARP-remmers een toename van zogenoemde chromatinebruggen en achterblijvende chromosomen te zien die niet goed verdeeld worden over de dochtercellen. Een soortgelijke waarneming werd gezien in verschillende humane en muis cellijnen die deficiënt waren voor BRCA1 of RAD51 en behandeld zijn met PARP-remmers. Met behulp van 'time-lapse' microscopie toonden we aan dat onopgeloste chromatinebruggen resulteren in cellen met meerdere kernen (micronucleatie) en uiteindelijk celdood. Ten slotte zagen we dat cellen niet meer doodgingen door PARP-remmers zodra het eiwit genaamd EME1 geremd werd, wat ervoor zorgde dat de gehele mitose werd overgeslagen. Deze waarnemingen dragen bij aan de kennis over hoe PARP remming in HR-deficiënte kankercellen werken. Deze inzichten kunnen verder worden benut om de behandeling met PARP-remmers te versterken en om ze te combineren met middelen die mitose bevorderen.

Verrassend genoeg wordt verlies van HR-genen zoals BRCA2 getolereerd in kankercellen, terwijl deze genen essentieel zijn in normale cellen. Dit fenomeen wordt de 'BRCA-paradox' genoemd. Er wordt gesuggereerd dat BRCA-deficiënte cellen specifieke veranderingen ondergaan om te kunnen overleven in afwezigheid van BRCA1 of BRCA2. In **hoofdstuk 4** hebben we een genetische screen uitgevoerd om genen te identificeren waarvan uitschakeling ervoor zorgt dat kankercellen overleven na verlies van BRCA2. We toonden aan dat verlies van de TNF α -receptor (TNFR1) en SAM68 voorkomt dat cellen doodgaan na inactivatie van BRCA2. De relatie tussen BRCA2-inactivering en TNF α -signalering werd aangetoond door de observatie dat BRCA2 inactivatie resulteerde in verhoogde TNF α productie, activering van TNFR1-signalering en verhoogde gevoeligheid voor TNF α -behandeling. De verhoogde gevoeligheid voor TNF α -behandeling werd vervolgens verminderd door inactivatie van TNFR1 of SAM68. Vergelijkbare resultaten werden gezien na inactivatie van andere HR-genen, zoals BRCA1 of FANCD2. Ten slotte toonden we aan dat inactivatie van BRCA2 resulteerde in activering van een interferon respons die veroorzaakt werd door de vorming van micronuclei (stukjes DNA in het cytoplasma) die vervolgens resulteert in een cGAS/STING-afhankelijke ontstekingsreactie. Concluderend toonden onze resultaten aan dat micronuclei veroorzaakt door verlies van BRCA2, een cGAS/STING-gemedieerde interferon respons veroorzaken, wat resulteerde in TNF α -signalering en TNF α -gevoeligheid.

In hoofdstuk 2 zijn meerdere mechanismen beschreven die ten grondslag zouden kunnen liggen aan de observatie dat genomisch instabiele kankercellen moeten ontsnappen aan de immuun surveillance, veroorzaakt door cGAS/STING signalering, om te kunnen overleven. Een van deze mechanismen is de verhoogde expressie van oncogenen, wat vaak wordt beschreven als mechanisme om proliferatie en andere routes te activeren die gunstig zijn voor de overleving van kankercellen. In het bijzonder wordt het MYC-oncogen vaak verhoogd tot expressie gebracht in genomisch instabiele tumoren, zoals in triple-

negatieve borstkanker (TNBC) en komt het vaak samen voor met een *BRCA1/2* mutatie. In **hoofdstuk 5** hebben we onderzocht of verhoogde expressie van MYC de immuunreacties, ofwel cGAS/STING-gemedieerde signalering, beïnvloedde in TNBC. Dit is voornamelijk onderzocht in de context van een *BRCA1/2* mutatie. Met behulp van twee humane cellijnen ontdekten we dat verschillende tot over expressie gebrachte oncogenen in staat waren om immuun gerelateerde signaturen te verminderen op basis van RNA-expressie. Analyse op basis van genexpressie in een grote database (TCGA) bevestigde dat TNBC-samples met over expressie van MYC een vermindering van immuun gerelateerde expressie signaturen vertoonden. In een *Brcr1*-mutant TNBC-muismodel, resulteerde MYC over expressie in een dramatisch verlies aan de infiltratie van lymfocyten en een verminderde tumorlatentie. Met behulp van een 3D kweekmodel en humane cellijnen, toonden we aan dat verhoogde MYC-expressie verschillende interferon-gerelateerde reacties veranderde, waaronder een verminderde cytokinesecretie, verminderde expressie van interferon-gestimuleerde genen en verminderde activatie van interferon-gereguleerde factoren (IRF3 en STAT1). Bovendien leidde een verhoogde MYC-expressie tot minder directe migratie en activatie van lymfocyten *in vitro*. Tenslotte, met behulp van chromatine immunoprecipitatie (ChIP) gevolgd door sequentie bepaling van het genoom, ontdekten we dat MYC direct de transcriptie van een netwerk aan immuun-gerelateerde genen verminderd. Concluderend ontdekten we een mogelijke rol van MYC-expressie in de ontduiking van *BRCA1/2*-gemuteerde TNBC voor het immuunsysteem door remming van interferon reacties.

In **hoofdstuk 6** hebben we de recente literatuur besproken over hoe HR mechanistisch in elkaar zit en wat de huidige behandelingsopties zijn voor HR-deficiënte kanker met een focus op PARP-remmers. Aangezien resistentie tegen PARP-remmers in de kliniek vaak voorkomt, zijn we uitgebreid ingegaan op de momenteel bekende resistentiemechanismen zoals: secundaire mutaties binnen de *BRCA1/2* genen die hun functie herstellen, mutaties in andere reparatiegenen zoals *TP53BP1*, *REV7* of *RIF1* om de HR-functie te herstellen of mutaties in *PAXIP* of *PARP1* om de bescherming van replicatievorken te herstellen. Om de behandeling met PARP-remmers in de kliniek optimaal uit te voeren, is het belangrijk dat patiënten met HR-deficiënte kanker adequaat worden geselecteerd. We hebben verschillende patiëntselectiemethoden uitgewerkt, zoals mutatieanalyses, genomische ‘scar’ analyses of het functioneel uitlezen van de HR-route, om mogelijk de juiste patiënten te kunnen selecteren die in aanmerking komen voor behandeling met PARP-remmers.

Aangenomen wordt dat een groot deel van de patiënten met eierstokkanker een HR-deficiënte kanker heeft, maar geen mutatie in *BRCA1/2* vertoont. Deze patiënten komen daarom niet in aanmerking voor behandeling met PARP-remmers, terwijl ze wel baat kunnen hebben bij deze behandeling. Om de patiëntselectie verder te verbeteren, hebben we in **hoofdstuk 7** genomische kenmerken bepaald, waaronder de *BRCA1/2*-mutatiestatus en een profiel op basis van genomische instabiliteit, in een cohort van 30 patiënt-afgeleide xenograft (PDX) muismodellen voor eierstokkanker. In een subset van de PDX-modellen beoordeelden we *ex vivo* HR-functionaliteit en replicatievorkstabiliteit en correleerden uiteindelijk alle genomische en functionele resultaten met de *in vivo* respons op de PARP remmer olaparib. We ontdekten dat veranderingen in *BRCA1/2* of genomische instabiliteitsprofielen niet volledig correleerden met de *in vivo* olaparib respons, omdat niet alle *BRCA1/2*-gemuteerde of genomische instabiele tumoren reageerden op PARP-remming. We beoordeelden het vermogen van tumorcellen om RAD51-foci te vormen bij bestraling met behulp van de *ex vivo* RECAP-assay wat diende als een uitlezing voor functionele HR. Aangezien HR-genen ook betrokken zijn bij de bescherming van replicatievorken, hebben we bovendien het vermogen van tumorcellen beoordeeld om vastgelopen replicatievorken te beschermen met behulp van een *ex vivo* ‘fiber’ analyse. De gemeten replicatievorkbescherming of replicatiesnelheid

correleerde niet met de olaparib response, terwijl de op RAD51 gebaseerde RECAP-assay alle PDX-modellen identificeerde die reageerden op *in vivo* olaparib. Tevens werden PDX-modellen geïdentificeerd zonder *BRCA1/2* mutatie, die wel reageerde op olaparib. Genomische sequentieanalyse in de PARP-remmer gevoelige modellen bracht verschillende mutaties aan het licht als mogelijke onderliggende oorzaak van HR-deficiëntie die nader onderzoek behoeven.

Referenties

1. Jackson, S. P. & Bartek, J. The DNA-damage response in human biology and disease. *Nature* vol. 461 1071–1078 (2009).
2. Hanahan, D. & Weinberg, R. A. Hallmarks of Cancer: The Next Generation. *Cell* 144, 646–674 (2011).
3. Kuchenbaecker, K. B. et al. Risks of breast, ovarian, and contralateral breast cancer for BRCA1 and BRCA2 mutation carriers. *JAMA- J. Am. Med. Assoc.* 317, 2402–2416 (2017).
4. Hakem, R. et al. The tumor suppressor gene *Brca1* is required for embryonic cellular proliferation in the mouse. *Cell* 85, 1009–23 (1996).
5. Suzuki, A. et al. *Brca2* is required for embryonic cellular proliferation in the mouse. *Genes Dev.* 11, 1242–1252 (1997).
6. Elledge, S. J. & Amon, A. The BRCA1 suppressor hypothesis: An explanation for the tissue-specific tumor development in BRCA1 patients. *Cancer Cell* vol. 1 129–132 (2002).
7. Bryant, H. E. et al. Specific killing of BRCA2-deficient tumours with inhibitors of poly(ADP-ribose) polymerase. *Nature* 434, 913–917 (2005).
8. Farmer, H. et al. Targeting the DNA repair defect in BRCA mutant cells as a therapeutic strategy. *Nature* 434, 917–921 (2005).

Over de auteur

Francien Gesina Talens werd geboren op 2 december 1990 in Groningen. Ze is opgegroeid in de gemeente Hoogezand-Sappemeer en heeft in 2009 haar VWO diploma behaald aan het dr. Aletta Jacobs College te Hoogezand.

Haar interesse in biologie, het menselijk lichaam en scheikunde leidde tot een studie Life, Science and Technology aan de Rijksuniversiteit te Groningen met als hoofdrichting Biomedische wetenschappen. De vrije keuze in het 3^e jaar werd gevuld met een minor 'Misdad en Straf' aan de Faculteit Rechtsgeleerdheid.

Na een tussenjaar, waarin ze een paar maanden in Zuid-Afrika heeft doorgebracht om vrijwilligerswerk te doen, is ze in het najaar van 2013 begonnen met de masteropleiding Biomedical Sciences in Groningen. De eerste onderzoeksstage tijdens deze master werd uitgevoerd bij de afdeling Medische Oncologie in het UMCG onder leiding van Prof. dr. Frank Kruyt, waarin stamcellen in slokdarmkanker werden bestudeerd. De tweede onderzoeksstage werd uitgevoerd bij de afdeling Medische Microbiologie in het UMCG onder leiding van Prof. dr. Toos Daemen. Tijdens deze stage werd onderzocht of een DNA-vaccin kon dienen als immuuntherapie bij HPV-gerelateerde baarmoederhalskanker.

Na haar master is ze in september 2015 begonnen aan een promotietraject bij de afdeling Medische Oncologie onder leiding van Prof. dr. Marcel van Vugt en Prof. dr. Jourik Gietema. De resultaten van het onderzoek tijdens dit promotietraject staan beschreven in dit proefschrift.

Tegenwoordig is ze werkzaam als docent aan de hogeschool van Hall Larenstein te Leeuwarden bij de opleiding Forensisch Laboratoriumonderzoek.

Dankwoord

Daar is eindelijk mijn proefschrift en ik ben er trots op. Dit proefschrift was niet tot stand gekomen zonder hulp van velen. Een aantal wil ik in het bijzonder bedanken.

Ten eerste wil ik mijn promotores, prof. dr. **Marcel van Vugt** en prof. dr. **Jourik Gietema**, bedanken voor hun begeleiding.

Beste **Marcel**, ik denk dat ik me geen betere promotor had kunnen wensen. Via Steven kwam ik bij jou in de groep solliciteren en ik heb er geen moment spijt van gehad. Je continue enthousiasme voor het onderzoek werkte erg aanstekelijk en ik kwam altijd positief en vol goede moed uit een van onze meetings. Manuscripten kwamen rood weer terug, maar ze werden altijd beter en scherper en dus had ik daar absoluut geen problemen mee. Bedankt voor de fijne samenwerking. Ik hoop dat je onderzoeksgroep zo goed en leuk zal blijven als dat hij nu is.

Beste **Jourik**, een klinische studie is er helaas (nog) niet van gekomen tijdens mijn promotie en daardoor ben je als arts wat minder betrokken geweest bij mijn projecten. Toch was je altijd geïnteresseerd en enthousiast op zowel werk- en persoonlijk vlak. Ik heb het heel fijn gevonden dat er altijd klinici over mijn schouders meekeken over hoe het onderzoek uiteindelijk toepasbaar kan zijn voor patiënten. Je staat aan het hoofd van een hele fijne afdeling. Dankjewel voor je begeleiding.

Ik wil de leden van de leescommissie, prof. dr. **Hans Nijman**, prof. dr. **Cor Calkhoven** en prof. dr. **John Martens** bedanken voor het lezen en beoordelen van mijn proefschrift.

Voor dit proefschrift is met veel mensen, afdelingen en onderzoeksgroepen samengewerkt. Ik wil daarom alle co-auteurs bedanken voor hun bijdrage aan diverse hoofdstukken. In het bijzonder wil ik de volgende mensen bedanken voor hun hulp.

Iedereen die betrokken was bij het **KWF/Alpe D'huzes consortium**, o.a. dr. Dik van Gent, dr. Maaïke Vreeswijk, prof. dr. Jos Jonkers, dr. Agnes Jager en Titia Meijer, wil ik bedanken voor de gezamenlijke bijeenkomsten en discussies die ik altijd erg leerzaam en enthousiasmerend heb gevonden. Nu is het tijd om de 'RECAP assay' verder de kliniek in te krijgen en ik wens iedereen die daarbij betrokken zal zijn heel veel succes met het vervolg.

Prof. dr. **Jos Jonkers**, **Chiara** and **Dario**, thank-you for the nice collaboration on the MYC manuscript. It wasn't an easy manuscript, but I think we combined our data into a very nice story in a relatively short time.

Prof. dr. **Zdenek Kleibl**, **Petra** and **Marketa**, thank-you for the sequencing you performed for our PDX study. Hopefully we can continue working on a gene mutation that we identified.

Beste prof. dr. **Steven de Jong** en dr. **Bea Wisman**, bedankt voor de samenwerking waarin we werkten aan de gevoeligheid van PARP-remmers in PDX-modellen. Deze biobank van PDX-modellen is heel erg waardevol voor de afdeling. Steven, bedankt voor de betrokkenheid die jij voor iedereen van de afdeling hebt en dat je ons gemotiveerd hield tijdens de maandelijkse journal club. Beste dr. **Marco de Bruyn**, relatief laat in mijn PhD traject begonnen we immuun-gerelateerde proeven te doen. Bedankt voor je bereidheid, met een goede portie enthousiasme en vrolijkheid, om ons altijd te helpen met vragen en ideeën voor deze proeven. Beste dr. **Rudolf Fehrmann**, bedankt voor de vele analyses die jij met je team voor onze groep en enkele van mijn hoofdstukken hebt gedaan. Ook dank voor je kritische en (vaak) terechte

opmerkingen tijdens onze meetings. Dat hield ons scherp.

Het liefste zou ik alle collega's van het **Medische Oncologie Laboratorium** afzonderlijk willen bedanken, want die hebben gezorgd voor een enorm fijne werksfeer. Iedereen buiten mijn werk om was altijd jaloers dat wij als collega's zoveel leuke dingen deden samen: borrels, bezoeken aan festivals, kroegtochten, wintersport, bowlen, etc. Die gezelligheid heeft er zeker voor gezorgd dat ik mijn PhD traject op een (toch best wel) ontspannen manier ben doorgekomen. Daarnaast wil ik de feestcommissies bedanken voor alle leuke activiteiten en labdagen die georganiseerd zijn. De commissie uit 2015-2016, bedankt dat jullie mij samen met Johannes in de nieuwe commissie hebben gestopt!

Al mijn **kantoorgenootjes** van F1.23 en G1.25 bedankt voor de gezelligheid, de vragen en discussies, de klaagmomentjes, de kopjes koffie, meegebrachte koekjes en pepernoten, het samen uitzitten van de hitte in de zomer zonder airco en het verzorgen van mijn plant.

Stijn en **Danique**, als mede-guppies uit de vissenkomp tijdens onze master hebben we samen heel wat jaartjes doorgebracht op de afdeling. Er zijn te veel leuke herinneringen om te noemen en er is een hechte vriendschap ontstaan. Hopelijk kunnen we snel onze etentjes weer voortzetten als Stijn ooit weer terug komt naar Nederland. Lieve Danique, het was vanaf het begin af aan overduidelijk dat jij mijn #1 paranimef zou zijn als goede vriendin! Daar ben ik super blij mee, dankjewel.

In het bijzonder wil ik enkele (ex)collega's van de '**DNA damage group**' bedanken, een hele leuke gevarieerde groep. We hadden elke week nuttige meetings en ik keek altijd erg uit naar onze tripjes naar Tsjechië of onze andere sociale activiteiten (forever second met bowlen...). Pepijn, Rolv, Colin, Sergi, Arko, Rico, Carlos, Stephanie & Audrey, ik vond het super gezellig met jullie. **Anne-Margriet**, jij hebt me in het begin van mijn promotietraject heel erg op weg geholpen en zorgde ervoor dat ik op de al rijdende, maar nog lange, trein van hoofdstuk 4 kon springen. Dat hebben we toch maar mooi samen geflikt en samenwerken met jou was prettig en lekker efficiënt. **Yannick**, bedankt dat jij je geworpen hebt op het maken van de mus81 mutatie uit hoofdstuk 7. Je brengt altijd sfeer en gezelligheid, waar je ook bent. Ik ga die gesprekjejes en vrolijkheid missen. **Maurits**, bedankt voor je hulp bij het analyseren van de RNA-sequencing data uit hoofdstuk 5. Je bent kritisch en dat maakt je een goede onderzoeker en collega. Succes met je eigen PDX studie. **Elles** en **Marieke**, dank voor alle ritjes naar de stikstof en jullie bereidheid om altijd te helpen als het nodig is. **Mengting**, thank you for your drive and work spirit to continue working on chapter 7. I wish you all the best during your PhD. **Vivian**, you were my lifesaver for chapter 7. Without you I wouldn't have been able to finish all the mice experiments and it became a very nice manuscript. Thank you for your help, home-made baking's and your 'gezelligheid' in the office. **Nathalie**, vanaf het moment dat je in onze groep kwam had ik door dat je een goede aanwinst en een leuk kantoorgenootje zou zijn. Ik spreek denk ik namens de hele groep dat jij als moederfiguur optreedt (ook al vind je dat misschien niet leuk om te horen), maar jij bent er altijd voor vragen, advies of een luisterend oor. Super leuk dat ook jij mijn paranimef wilde zijn! Dankjewel.

Buiten werk om hecht ik veel waarde aan mijn hobby's, andere activiteiten en gezelschap. Ik heb geprobeerd om daar zoveel mogelijk tijd voor vrij te maken tijdens mijn promotietraject. Dat betekent dat al mijn vrienden en nichtjes ook heel erg belangrijk zijn geweest en dat zij voor de goede afleiding zorgde wanneer dat nodig was.

Beste **Capriccio**, de zaterdagmorgen repetities (vrienden en collega's snappen nog steeds niets van die toewijding) zijn onmisbaar voor mij. Na inmiddels 20 jaar is dat een belangrijk moment van ontspanning en onderdeel van mijn wekelijkse routine. Altijd zal ik proberen om

zoveel mogelijk activiteiten met het orkest te blijven doen. Jullie zijn mijn tweede familie en het heeft me ook levenslange vriendschappen opgeleverd (klarinetchickies!). Ik hoop dat we nog heel lang samen muziek mogen maken.

Lieve **Jona**, ik ben zo trots dat ik het mooie schilderij van Hein heb mogen gebruiken voor de voorkant en ter inspiratie van mijn boekje. Bedankt dat jij en Irene dit ook een mooi en leuk idee vonden. En zoals we vaker zeggen: we hebben echt goede genen!

Je kunt mij gerust een familiemens noemen en daarom ben ik zo enorm blij met mijn lieve familie en schoonfamilie. **Jan** en **Sjouk**, bedankt voor jullie liefde en interesse die jullie altijd tonen in Johannes en mij. Het doet me altijd goed jullie weer te zien en hopelijk gaan we onze regelmatige etentjes nog lang voortzetten. **Piter** en **Yvonne**, we zien elkaar te weinig maar ik vind het altijd zo gezellig met jullie. Die 'cervicale dislocatie' van de muizen houdt jullie nog altijd bezig, maar ik vond het leuk dat jullie zo geïnteresseerd waren in wat ik nou allemaal deed op dat lab. **Henk-Jaap** en **Ingrid**, c'est très malheureux que vous vivez si loin et j'espère que nous pourrions vous rendre visite bientôt (sorry voor mijn Franse vertaling).

Lieve **pap** en **mam**, ha daar staan jullie dan! Het is te moeilijk om in een paar zinnen uit te drukken hoe dankbaar ik ben voor jullie steun, liefde, aanmoediging, interesse en goede zorgen. Met kerst werd altijd rekening gehouden met de locatie van het vakantiehuisje zodat ik nog naar het UMCG kon. Ik kijk er altijd naar uit om richting Kiel te komen om jullie weer te zien, bij te kletsen en te ontspannen. **Lucy** en **Dennis**, gelukkig zien we elkaar nog regelmatig, maar jullie wonen ook te ver weg! Ik geniet er altijd van als we met zijn allen compleet zijn. Luuc, bedankt voor je altijd nuchtere en relativerende blik.

Liefste **Johannes**, jij bent het belangrijkste geweest de afgelopen jaren en je bent echt mijn steun en toeverlaat. Tijdens de corona lockdown hebben we maandenlang samen aan de eettafel geschreven aan ons proefschrift en dat was super gezellig. Je kent me als geen ander en woorden zijn niet nodig. Daarnaast ben je slim en kritisch, waardoor je vaak heel relevante vragen kon stellen over mijn onderzoek of van die irritant slimme opmerkingen maakt in het algemeen. Het was fijn dat we elkaars werkzaamheden begrepen en het konden hebben over promotie struggles zo nu en dan. Ik weet zeker dat jij een mooie carrière tegemoet gaat en ik kijk heel erg uit naar onze toekomst.

Liefs,

Francien